AFRL-VA-WP-TR-1999-3018

AN EXPERIMENTAL INVESTIGATION OF TANGENTIAL BLOWING TO REDUCE BUFFET RESPONSE OF THE VERTICAL TAILS OF AN F-15 WIND TUNNEL MODEL

VOLUME 1 – TEST RESULTS, DISCUSSION AND CORRELATION

MARTY A. FERMAN, PH.D, P.E., CONSULTANT
CSA ENGINEERING
2850 BAYSHORE ROAD
PALO ALTO, CA 94303-8794

ELIJAH W. TURNER, P.E.
STRUCTURES DIVISION
DESIGN AND ANALYSIS BRANCH
WRIGHT-PATTERSON AFB, OH 45433-7542

JANUARY 1999

FINAL REPORT FOR 06/01/1996 – 12/31/1998

AIR VEHICLES DIRECTORATE
AIR FORCE RESEARCH LABORATORY
AIR FORCE MATERIEL COMMAND
WRIGHT-PATTERSON AIR FORCE BASE OH 45433-7542

NOTICE

When Government drawings, specifications, or other data are used for any purpose other than in connection with a definite Government-related procurement, the United States Government incurs no responsibility or any obligation whatsoever. The fact that the Government may have formulated or in any way supplied the said drawings, specification, or other data, is not to be regarded by implication, or otherwise in any manner construed, as licensing the holder, or any other person or corporation, or as conveying any rights or permission to manufacture, use, or sell any patented invention that may in any way be related thereto.

This report is releasable to the National Technical Information Service (NTIS). At NTIS, it will be available to the general public, including foreign nations.

This technical report has been reviewed and is approved for publication.

Elijah W. Turner
Elijah W. Turner
Project Engineer
Design and Analysis Branch

L J Huttsell
L. J. HUTTSELL
Leader, Unsteady Aerodynamics
Integrated Product Team

Nelson D. Wolf
NELSON D. WOLF
Chief, Design and Analysis Branch
Structures Division

If your address has changed, if you wish to be removed from our mailing list, or if the addressee is no longer employed by your organization, please notify AFRL/VASD Bldg. 45, 2130 Eighth Street, Suite 1, WPAFB OH 45433-7542 to help maintain a current mailing list.

Copies of this report should not be returned unless return is required by security consideration, contractual obligations, or notice on a specified document.

REPORT DOCUMENTATION PAGE

Form Approved
OMB No. 0704-0188

1. AGENCY USE ONLY *(Leave blank)*

2. REPORT DATE
JANUARY 1999

3. REPORT TYPE AND DATES COVERED
FINAL REPORT FOR 06/01/1996 - 12/31/1998

4. TITLE AND SUBTITLE
AN EXPERIMENTAL INVESTIGATION OF TANGENTIAL BLOWING TO REDUCE BUFFET RESPONSE OF THE VERTICAL TAILS OF AN F-15 WIND TUNNEL; VOLUME 1 - TEST RESULTS, DISCUSSION AND CORRELATION

5. FUNDING NUMBERS
C F33615-94-C-3200
TASK 3413-31
PE 62201
PR 2404
TA 49
WU 51

6. AUTHOR(S)
MARTY A FERMAN, PH.D., P.E., CONSULTANT FOR CSA ENGINEERING
ELIJAH W. TURNER, P.E., WRIGHT-PATTERSON AFB, OH

7. PERFORMING ORGANIZATION NAME(S) AND ADDRESS(ES)
CSA ENGINEERING
2850 BAYSHORE ROAD
PALO ALTO, CA 94303-8794

STRUCTURES DIVISION
DESIGN AND ANALYSIS BRANCH
WRIGHT-PATTERSON AFB, OH
45433-7542

8. PERFORMING ORGANIZATION REPORT NUMBER

9. SPONSORING/MONITORING AGENCY NAME(S) AND ADDRESS(ES)
AIR VEHICLES DIRECTORATE
AIR FORCE RESEARCH LABORATORY
AIR FORCE MATERIEL COMMAND
WRIGHT-PATTERSON AFB, OH 45433-7542
POC: ELIJAH W. TURNER, AFRL/VASD, 937-255-7229

10. SPONSORING/MONITORING AGENCY REPORT NUMBER
AFRL-VA-WP-TR-1999-3018

11. SUPPLEMENTARY NOTES

12a. DISTRIBUTION AVAILABILITY STATEMENT
APPROVED FOR PUBLIC RELEASE; DISTRIBUTION UNLIMITED

12b. DISTRIBUTION CODE

13. ABSTRACT *(Maximum 200 words)*
Tangential blowing was investigated as a means to reduce buffeting pressures and response on the tails of a 4.7% scale model of the F-15 Fighter Aircraft in the Subsonic Aerodynamic Research Laboratory (SARL) wind tunnel. Buffeting pressures, structural strains, and structural acceleration were measured and recorded for a range of angles of attack and angles of side slip, and for blowing at three locations on the model, both individually, in combinations, and without blowing. The test were conducted for two wind tunnel dynamic pressures. One vertical tail was rigid to permit buffet excitation pressures to be measured, and the other was flexible to permit buffet response pressures and structural response to be measured. Unsteady pressure data, strains and accelerations were reduced to PSD and RMS forms. This report contains a general description of the model, the test program, samples of the reduced data, an in depth analysis of the data, and conclusions with respect to the effectiveness of blowing to reduce buffeting of vertical tails.

14. SUBJECT TERMS
UNSTEADY AERODYNAMICS, PRESSURE MEASUREMENTS, BUFFETING FLOW, WIND TUNNEL TEST, EXPERIMENTAL DATA, PRESSURE TRANSDUCERS

15. NUMBER OF PAGES
223

16. PRICE CODE

17. SECURITY CLASSIFICATION OF REPORT	18. SECURITY CLASSIFICATION OF THIS PAGE	19. SECURITY CLASSIFICATION OF ABSTRACT	20. LIMITATION OF ABSTRACT
UNCLASSIFIED	UNCLASSIFIED	UNCLASSIFIED	SAR

Standard Form 298 (Rev. 2-89) (EG)
Prescribed by ANSI Std. 239.18
Designed using Perform Pro, WHS/DIOR, Oct 94

TABLE OF CONTENTS

TABLE OF CONTENTS (Concluded)

LIST OF FIGURES

LIST OF FIGURES (Continued)

LIST OF FIGURES (Continued)

LIST OF FIGURES (Continued)

LIST OF FIGURES (Continued)

LIST OF FIGURES (Continued)

LIST OF FIGURES (Continued)

LIST OF FIGURES (Continued)

LIST OF FIGURES (Continued)

LIST OF FIGURES (Concluded)

LIST OF TABLES

FOREWORD

This report was prepared by Dr. Marty Allen Ferman, Consultant for CSA Engineering of Palo Alto, California. The work was performed under Contract F33615-94-3200, Task 3413-31 for the Air Vehicles Directorate of the Air Force Research Laboratory, Wright-Patterson Air Force Base, Ohio. Mr. Elijah W. Turner was the Air Force Project Engineer. This effort was sponsored by the Unsteady Aerodynamics Integrated Product Team (IPT) of the Air Vehicles Directorate, Air Force Research Laboratory. Mr. Lawrence J. Huttsell was Chairman of the IPT.

The work by Dr. Ferman was conducted between 15 June 1996 and 15 October 1998 under job order number 24044951. The data presented in this report were reduced by Mr. Dansen Brown of the Acoustics and Sonic Fatigue Branch, Structures Division, Air Vehicles Directorate, Air Force Research Laboratory from the 4.7% F-15 Vertical Tail Buffet Test.

The Buffet Tests were conducted in the Subsonic Aerodynamics Research Laboratory (SARL) wind tunnel at Wright-Patterson Air Force Base in October and November of 1995. The Test Engineer was Mr. Jon Tinapple of the Aerodynamic Configuration Branch, Aeronautical Sciences Division, Air Vehicles Directorate, Air Force Research Laboratory.

This report was submitted in January 1999 for publication as an Air Force Research Laboratory Technical Report.

ACKNOWLEDGEMENTS

The Sr. Author wishes to express sincere thanks to Mr. Ken Juhl, a student at Parks College, St. Louis University, who gave tireless help with this work including making many graphs and figures. Similarly, the Sr. Author is deeply grateful to Mr. Dansen Brown, AFRL, WPAFB, OH for the dedicated data reduction effort and for making a multitude of graphs and tables which comprise a major part of this data. Sincere thanks to Mr. Jon Tinapple, AFRL, WPAFB, OH who made the wind tunnel effort succeed. Sincere thanks to Mr. Larry Huttsell and Mr. Elijah Turner, AFRL, WPAFB, OH for their steadfast support with the long term effort in this data reduction, analysis of data, conclusions, and in the preparation of the final report. A special thanks to Mr. Turner for acting as co-author to help with final preparations of this large report.

1. SUMMARY, BACKGROUND AND APPROACH

1.1 SUMMARY - A concept employing tangential blowing was investigated experimentally as a possible means for mitigating buffet response of empennage on fighter aircraft. Wind tunnel tests of a 4.7% scale model of the F-15 Fighter were run in the Subsonic Aerodynamics Research Laboratory (SARL), WPAFB, OH. Tangential blowing was introduced from three points: (a) the nose, (b) the wing root leading edge, and (c) the gun bump, with symmetric blowing being used from both sides of the model for each location. Blowing from the three individual locations was used, as were combinations; namely, wing/ gun, wing/ nose, and nose/ gun. Wing blowing pressures of 45 and 65 psi were used, while blowing pressures of 65 psi at the gun bump, and 87 psi at the nose were used. Baseline data without blowing was acquired as a reference from which blowing results were compared. The model was equipped with one flexible tail and one rigid tail, and instrumented so that oscillatory pressures could be measured on both tails for the various blowing cases. The flexible tail was further instrumented to allow measurement of vibratory root bending and torsion moments, and tip acceleration for the various blowing cases. Angles of attack from 0 to 32 degrees, and yaw angles of -4, 0, 4 degrees were investigated. Two dynamic pressures (Q) were employed, 30 and 56 psf, both to check on data scaling, and to assess the blowing effects at two Q's.

Generally, an influence of blowing could be seen in the response results and in the oscillatory pressures, but it is difficult to cite complete general trends in a simple statement. Most cases showed some reduction in response from blowing, though the broadband and narrowband results differed as to the degree and trend, especially bending response as compared to torsion, and especially depending on what yaw angle was considered. In some cases, blowing actually increased response slightly. The wing blowing position was the most effective, the gun position was the next most effective, while the nose was the least effective. This concept of tangential blowing appears to reflect a type of Coanda effect, since the blowing was injected well upstream of the empennage, but closely followed the model surfaces until reaching the tails. This blowing technique suggests further investigation and application.

This work was sponsored by the Air Force Research Laboratory (AFRL) under their Unsteady Aerodynamics Integrated Product Team (IPT) effort. The results of the tests regarding acquisition of basic buffet data for the wind tunnel model, and the effectivity of the blowing results for reducing buffet response are discussed here. A separate effort under this IPT will employ piezoelectric actuators and modern control methods as another means for mitigating buffet response on the empennage of this model.

1.2 BACKGROUND AND APPROACH - A number of modern fighter aircraft attain high angle-of-attack maneuvering capability through vortex lift. At the lower angles of attack, the vortex core is tightly wound and convects aftwards, producing an additional static (steady-state) lift effect, with little or no associated vibratory loading effects. At the higher angles of attack, these vortices exhibit what is called, breakdown, where a turbulent characteristic appears to be superimposed on the calmer vortex core. Thus, in

addition to the principal lifting effect, a strong vibratory loading characteristic, or buffeting, is now present. While the burst vortex still convects aftwards, it is wider and generally touches, or comes closer to the empennage than did the original vortex core. Thus, the buffeting pressures are able to induce strong excitation of the empennage, leading to severe structural strains occurring at frequencies whereby large numbers of cycles could be quickly accumulated, potentially causing overstress, cracking or foreshortened fatigue life. Several twin tailed aircraft, the F-14, F-15, and F/A-18, have experienced these buffeting loads and have had to consider these effects in their design approaches for safe flight operation. Techniques, ranging from using structural stiffening, to adding composite doublers, and to attaching leading edge extensions or wing vents, have been employed in the attempt to meet buffet requirements. A wide range of programs using piezoelectric dampers and other new concepts have been initiated by many investigators.

A concept considered herein attempted to alter these turbulent flows by employing airflow injected tangentially along the fuselage and wing, but upstream, of the empennage. These controlled airflows are often referred to as "blowing." Rather than starting with a full size airplane, it was decided to first evaluate the overall concept of tangential blowing with a wind tunnel model. Since the F-15 Fighter operates at high angles of attack, and since it has experienced these types of buffet from vortical flow breakdown, a wind tunnel model of the F-15 was selected for the investigation. This model was a 4.7% scale of the full sized F-15. It was used in the wind tunnel tests to evaluate this upstream, tangential blowing concept as a means of reducing buffet pressures on the model vertical tails at high angles of attack. A standard aerodynamic model was used with modifications for these tests. The model was altered to accommodate the blowing ports and tubing to provide the tangential blowing sources. Three blowing positions were employed in the tests; namely, the wing root location, the gun bump location, and the nose. The nominal tails used in aerodynamics tests were removed and replaced with special tails for this testing. The left hand tail was replaced by a scaled flexible tail, designed to replicate, at this scale, the first several natural vibration modes of the full size tail. This tail was instrumented with pressure transducers, root bending and torsion strain gauge bridges, and accelerometers at the tip. The other tail was replaced by a relatively rigid tail equipped with pressure transducers. The flexible tail instrumentation provided data on oscillatory root bending and torsion moments, tip acceleration, and pressures. The rigid tail instrumentation provided data on oscillatory pressures without the influence of tail flexibility and vibration. Tests were conducted in the Subsonic Aeronautical Research Laboratory (SARL) wind tunnel at Wright-Patterson Air Force Base during the Fall of 1995, and were sponsored by the Air Force Research Laboratory (AFRL) under their Unsteady Aerodynamics Integrated Product Team (IPT) effort. The subject report was prepared in support of the IPT, to cover the data reduction, data analysis, and synthesis to establish trends, and to make conclusions regarding the effectivity of the blowing approach. Flow visualization tests were run as well, and are partially documented in Reference 1. Some of the test results and some of the early data reduction results are also given in Reference 1.

Reduction of these oscillatory pressures from buffet can lead to the reduction of the normally large responses and associated stresses on the structure, and hence potentially extend the fatigue life of the vertical tails, both for the model size and full-scale. This blowing method did show some reduction of response and is thus promising. Successful wind tunnel test could lead to full-scale tests and application. Likewise, a potential application to other aircraft could follow this work. Some suggestions of a possible Coanda effect may be inferred from the data and may suggest further investigation of that effect as a means of reducing buffet response of fighter aircraft tails. A separate effort under this IPT will explore another approach for potentially mitigating buffet response on the empennage, where the use of piezoelectric actuators and modern control methods will be employed.

There are three volumes to the report; namely, (a) this volume, Volume 1-Test Results, Discussion, and Correlation, (b) Volume 2- Response Data, and (c) Volume 3 - Oscillatory Pressure Data. These volumes are in sequential report numbers, Volume 1 being this report, AFRL-VA-WP-TR-1999-3018 while Volumes 2 and 3 are respectively, AFRL-VA-WP-TR-1999-3019 and AFRL-VA-WP-1999-3020. A buffet bibliography, collected by AFRL, has been updated, and included to aid other investigators in finding information.

2. TEST SETUP

2.1 MODEL - A 4.7% scale model of the F-15 Fighter Aircraft was employed in these tests. The model was the standard aerodynamics model normally used in these types of wind tunnel tests, and thus essentially rigid in these speed ranges and dynamic pressures. Several figures and photos are shown here to give a perspective of the model and the instrumentation used. For the subject tests, however, the original model was modified. There were modifications to the model to accommodate the tangential blowing ports and tubing for pressure flow. The nominal vertical tails were removed and replaced. The vertical tail on the left hand side (LHS) was replaced by a scaled flexible tail which simulated at a 4.7% scale, the first several vibration modes of the full sized tail. The tail on the right hand side (RHS) was replaced by a tail that was relatively rigid, compared to the flexible tail. Figure 2.1.1 shows an overall planform sketch of the wind tunnel model. Figures 2.1.2 and 2.1.3 show photos of the complete model mounted on the tunnel sting. Figure 2.1.4 shows the detailed tail geometry, with and without the tip pod. Figures 2.1.5 and 2.1.6 detail the tail instrumentation, showing pressure pickups, accelerometers, and strain gauges. The flexible tail was equipped with bending and torsion strain gauge bridges, as shown in Figure 2.1.5, to measure root bending and root torsion moments, both static and oscillatory. Accelerometers were placed at the forward and aft areas of the tip of the vertical tail, as shown in Figure 2.1.5, to capture overall and bending and torsional motions at the tip. The flexible tail was also equipped to measure static and oscillatory pressures, with pressure transducers located identically to those on the rigid tail, as shown in Figure 2.1.6

The natural frequencies of the model flexible tail were measured by the model manufacturer, Dynamic Engineering Incorporated (DEI), and again by AFRL. These results are shown here along with finite element analysis (FEM) results from DEI.

	AFRL Test*	DEI Test**	DEI Analysis***	
	Hz	Hz.	Hz.	
MODE 1	39.8	37.5	36.8	First Bending
MODE 2	169.0	160.6	159.3	First Torsion
MODE 3	189.0	183.8	195.3	Second Bending

* Tail clamped to fixture
** Tail on model
*** Finite Element Analysis

The right hand tail (RHS), being relatively rigid compared to the flexible tail, was believed to enhance measurement of both static and oscillatory pressures from buffeting flows, ideally free of model elastic and vibratory effects. Conversely, the pressure pickups on the flexible tail (LHS) could show effects of structural motions induced on pressures.

Tangential blowing was done independently at the nose, gun bump and wing root locations, and in the combinations of nose/wing, nose/gun, and wing/gun locations. Data were also recorded for baseline conditions with no blowing. Blowing was done simultaneously on both sides of the model so as to maintain flow symmetry. The wing blowing pressures were 45 and 65 psi, the nose blowing pressure was 87 psi, and the gun bump blowing pressure was 65 psi. These injected flows were convected, effectively, back to the areas of the empennage, essentially similar to a Coanda-like effect.

2.2 TEST EQUIPMENT - The SARL is a modern wind tunnel with a high contraction ratio, open circuit, operation capable of Mach numbers up to 0.55. It is fully equipped for flutter, aerodynamics, buffet, and loads testing. The tunnel test section is approximately 10 ft. high by 7 ft. wide and 15 ft. in length, and has 2 ft. flats at the wall and side intersections so as to make an octagonal-type cross section. Relatively large models can be tested. A fully automated sting can be pitched and yawed rather quickly at a given elevation, and these rates are adjustable. The sting elevation can be varied. A large portion of the viewing wall area is high quality Plexiglas, that allows excellent viewing and facilitates the use of laser sheet illumination. Modern data acquisition equipment is available to capture the data being taken from a wide range of instrumentation. Data can be digitized, as taken, for rapid data reduction, both insitu and post test for user convenience. Online data are recorded through a MicoVAX III computer connected to a software controlled, 120 channel multiplexer and connected to a 13 bit 100,000 samples per second auto ranging AC to DC converter. Balance channel signals, discrete pressure transducer data, strain gauge signals, and accelerometer signals were fed through Dynamic brand amplifier/bridge conditioners. Additionally, a Metrum dynamic data recorder was used for the bending and torsion and acceleration data for the flexible tail. Added detail is given in Reference 1. A majority of the dynamic data taken was reduced post test by digital data reduction methods using a VAX 11780 computer for most of this work. Some specific data reduction and analysis was carried out with a Micron Super PC computer. Fast Fourier transform methods were used to develop PSD and rms results for the data taken from the wind tunnel tests. The digitized data were fed to these computer programs, and used anti-aliasing filters and noise filtering to produce high quality data. The anti-aliasing filter was a 4 pole Chebysev, low pass type, set at 625 Hz.

2.3 INSTRUMENTATION - Figures 2.1.5 and 2.1.6 illustrate the instrumentation on the two tails. The flexible tail has two accelerometers located at the forward and aft locations of the tip pod, and has bending and torsion strain gauge bridges near the root of the tail. There are pressure pickups on the tail at the locations shown, and installed on both faces so that a pressure difference, **ΔP**, across the tail could be obtained. Similarly, there are pressure pickups on the rigid tail as shown in the figures, and located identically to those on the flexible tail. Data acquired were digitized at a rate of 5k samples per second per channel, and higher rates were compared to insure accuracy. Data were recorded with a Metrum RSR512 Digital Tape Recorder, with 32 channels being recorded simultaneously.

2.4 DATA ACQUISITION/REDUCTION - The data acquired were generally directly digitized for subsequent reduction, however some on-line data were constantly monitored for check pointing to ensure that parameters were in range of anticipated values. Oscillatory pressures, root bending moment, and root torsion moments were acquired and developed into PSD format and rms summary format to aid in tracking buffet effects versus angle attack and yaw angle for two values of dynamic pressure, 30 and 56 psf, and for blowing at the three positions (nose, wing and gun bump) and for various blowing pressures. Some pressure CSD's were determined for a few conditions to indicate typical behavior. Some acceleration data in PSD and rms forms were also included in the report. The bulky data, consisting of many PSD plots, are in Volumes 2 and 3, while only a few typical PSD's are in this overview, Volume 1.

The rms summary plots are in this volume to enhance discussion. Dimensional and nondimensional forms of the data are shown to further enhance explanation of the behavior patterns as well as to provide additional data to the growing base of buffet data.

2.5 TEST RUN LOG - A run log for the wind tunnel tests conducted in these tests is given in Table 2.5.1. The run number, dynamic pressure, blowing pressure/location, angle of attack, yaw angle, and other information are shown.

3. RESULTS

Typical PSD plots are given to characterize behavior patterns for key effects, but the majority of these data are in Volumes 2 and 3 for the more detailed need. Volume 2 presents the response data, while Volume 3 presents the pressure data. Attention is given here to the trends of the rms data from the PSD plots because they show more comprehensive trends. The pattern followed in the data presentation reflects the systematic testing employed. This format of presentation is shown to aid the reader with the large volume of data to review. Angle of attack is the main variable, followed by yaw angles, for several blowing pressures from the nose (NBP), gun bump (GBP), and wing leading edge (WBP), and for two values of dynamic pressure, Q, of 30 and 56 psf. Trends for the flexible tail for oscillatory root bending and torsion responses, acceleration at the tail tip, bending moment from pressure integration, and pressures on the tail are included. Trends for the rigid tail are from pressure data only. The two values of dynamic pressure, 30 and 56 psf, were selected for this scaling to show adequate buffet response, without interference, or masking effects, caused by other aeroelastic responses, such as flutter.

Test Variable			
	Dynamic Pressure,	Q	30, 56 psf
	Angle of Attack (AOA)	Alpha	0-32 deg
	Yaw Angle	Beta	-4, 0, 4 deg
Blowing pressures			
	No Blowing (base cases)		
	Wing Blowing	WBP	45, 65 psi
	Gun Blowing	GBP	65 psi
	Nose Blowing	NBP	87 psi

Measurands
- Flexible Tail
  - Oscillatory Root Bending and Torsion Moments
  - Tip Acceleration
  - Bending Moment from Pressure Integration
  - Oscillatory Pressures*
- Rigid Tail
  - Oscillatory Pressures*

* Dimensional and nondimensional data forms

Note that yaw is defined as positive when the right wing moves forward when viewing down onto the aircraft. Pitch, or angle of attack (AOA), is defined as positive when pitching the nose upwards. A right hand vector rule at the c.g. applies to yaw and pitch herein. Only positive angles of attack were used in these tests.

3.1 FLEXIBLE TAIL RESPONSES: BENDING AND TORSION MOMENTS WITH AND WITHOUT BLOWING FOR TWO Q'S - These figures are generally

grouped first by Q=56 psf, then Q=30 psf, again grouped vs angle of attack, AOA, with yaw angles (β) of -4, 0, 4 deg noted. Blowing pressures are a group with those sets. The PSD plots are shown first, followed by the rms summary plots. The PSD plots show key response information for the root bending and torsion moments, and include overall rms values. The rms values from the PSD plots are plotted versus the major test variables to give a synoptic view of trends, and are only given in this volume, Volume 1. The overall rms values from broadband analyses, and those from narrowband analyses are given. The rms broadband analyses are given first for bending and torsion, and followed by graphs comparing the bending and torsion broadband rms values against those narrowband analyses surrounding the first bending, second bending, and torsion modal responses, as applicable. These comparisons help track modal response effects with the various blowing conditions versus yaw and dynamic pressures.

3.1.1 PSD DATA- Figures 3.1.1 to 3.3.7 show typical root bending and root torsion moment PSD's. Figure 3.1.1, Parts 1 and 2, show bending data for AOA's 0-8 and 20-24 deg. The PSD's from 0-8 deg are about the same, while above 20 deg there is a large increase in the response level, especially prominent is the bending mode range, near 50 Hz. at the higher angles. Note that bending response continued to grow with AOA up to 32 deg. Figure 3.1.2, Parts 1 and 2, show comparable results for torsion, with the torsion mode of around 200 Hz being prominent. Torsion at the lower AOA's, below 10 deg, shows about the same low levels of response, while it is highly responsive above 16 deg, and peaking about 24 deg. Figure 3.1.3 and Figure 3.1.4 show bending response at AOA of 32 deg for yaw's (Beta) of 4 and -4 deg, respectively, where WBP=0 and 45 psi are compared. Blowing effects are seen, though slight, and show that at 4 deg, response increases slightly, while for -4 deg, blowing shows a slight decrease. Similarly Figures 3.1.5 and 3.1.6 show torsion moment response at an AOA of 32 deg for Betas of 4 and -4 deg for WBP=0 and 45 psi. Figure 3.1.7 shows, in three parts, the bending and torsion responses in side by side comparison for AOA's of 22, 24, 28 and 32 deg for WBP=0, and one case of AOA=24 and 32 deg for WBP=45 psi. Here, some of the differences in responses in bending vs torsion can be seen.

3.1.2 RMS TRENDS- The rms trends help to show a summary pattern of effects of angle of attack and yaw on bending and torsion response. Likewise, the effects of blowing from the various positions are more easily tracked from this data as well, compared to PSD's. (Further interpretation is gained from the nondimensional data form in later sections). Figure 3.1.8 sets the pattern of the data, as rms bending and torsion (5-500 Hz) responses are shown vs angle of attack (AOA) from 0 to 32 deg for yaws (β) of -4, 0, and 4 deg. Note that the bending responses for all three yaw angles appear to increase with increasing AOA, and that the negative yaws tend to increase response compared to the other cases, except where the negative yaw effect has begun to peak and decrease slightly for AOA above 30 deg. This makes sense when considering that the vortex is outboard of the left tail (flex), and negative yaw moves the right wing back, or left wing forward, which pushes the left hand vortex into the left tail. Conversely, positive yaw pushes the left tail away from the left hand vortex. Torsional responses

appear to peak within the AOA range, with yaw effects similar to those in bending, while with the negative yaw effects peaking at AOA below those of the bending. This trend is a little more complex, suggesting that the negative yaw causes the vortex to move into the tail and probably displaces it up or down the tail compared to unyawed, or positive yaws. Studies were made to show that the data here are nearly identical (out to the third place) to the data analyzed from 0-1000 Hz. After these comparisons, data were only analyzed to the 500 Hz limit to conserve efforts and resources. Figures 3.1.9 and 3.1.10 compare narrowband data, surrounding the first bending (35-65 Hz) and second bending (210-240 Hz) modes, against the broadband bending data. These figures display response vs AOA and are grouped by yaw angle. Here, it is seen that the composition of the overall response is largely first bending, but second bending is a significant contributor. Figure 3.1.11 shows a comparison of the narrowband region of the torsion mode (180 -210 Hz) versus the broadband torsion response. Obviously, the narrowband chosen entraps the overall response nicely, with the trend of AOA and yaw closely matching the broadband data.

Figures 3.1.12 to 3.1.19 repeat the sequence just shown for the base case, except that the influence of wing blowing pressures of 45 and 65 psi were employed. One may compare the various cases to see the effects of blowing on broad and narrowband response. Figures 3.1.20 and 3.1.21 are a set of cross plots of the blowing pressures vs AOA for the three yaw values. It is difficult to explain the trends in one general statement, rather several comments are needed. Blowing tends to slightly increase the bending response at lower angles, while at the higher angles for a yaw of zero, blowing decreases response. For negative yaw where buffet is stronger, the effect of blowing tends to increase response up through larger AOAs, probably due to increased flow activity in general. For positive yaw where the vorticity on the tail is less, the blowing pressure of 45 tends to decrease response at the lower angles, but increases response at the higher angles. The blowing pressure of 65 shows a reduction in response at higher angles. Torsional responses are different, peaking around AOA's of 24-28 deg, with blowing showing buffet reduction below the peak and slightly increasing above the peak. Both bending and torsion suggest that the flow injection can move the vortex activity into or away from the tail as well as moving the vortex spanwise along the tail.

The data for Q=30 psf shows more of this effectivity of the effect of blowing. Though the volume of data is more limited, this information is important, since responses at different Q's are scalable. Figures 3.1.22 through 3.1.31 essentially repeat the data sequence shown above, but for WBP of only 0 and 45 psi. Though the responses here are reduced compared to those for the higher Q, they are not quite reduced by the Q ratios, i.e. 30/56 values, as would be expected, and as addressed later. Again, the data sequence shows that the modal distribution of overall response is similar, and trends with AOA and yaw are similar. However, the effect of WBP=45 is seen to show a response reduction in all cases. This might suggest that higher WBP should have been used for Q=56.

In Figures 3.1.32 - 3.1.37, the effects of gun blowing, GBP, of 65 psi are indicated for a Q=56 psf. An AOA sweep of 16-26 deg for several types of plots similar to those for

wing blowing are given. Here, the overall responses of bending and torsion (0-500 Hz) and those for the frequency bands around the bending, torsion, and second bending modes are shown. The gun bump blowing shows some effects, but slighter than those of wing blowing. Figures 3.1.38 to 3.1.43 show results for blowing from both the wing and gun bump, WBP=65 psi, GBP=65 psi. Generally, the combination of blowing is slightly more effective than the wing blowing only.

Figures 3.1.44 to 3.1.49 display the effects of blowing from the model nose, NBP, of 87 psi, noting that it required more blowing pressure to show a slight effect compared to the wing blowing, WBP, cases. This is seen in the data when comparing with the first block of plots in the Figures 3.1.8 - 3.1.14 series. Figures 3.1.50 to 3.1.55 summarize the rms trends for NBP=87 psi, and GBP=65 psi. Figures 3.1.56 to 3.1.61 summarize the rms bending and torsion again for broadband and narrowbands for NBP=87 psi and WBP=65 psi. Again, the wing blowing effect is the more dominating influence.

3.1.3 BENDING MOMENTS FROM PRESSURE INTEGRATION- Bending moments on both tails were computed from the rms pressures. This was done as follows: (a) The tails were divided into grids surrounding the pressure pick-ups, as shown in Figure 3.1.62. (b) A sketch of the rms pressures at each pressure pick-up was made for each tail at each angle of attack of interest. (c) The pressure data were made into surface-like distributions, with the spanwise distribution being defined by the spanwise pressure data, while the chordwise shape of the three chordwise pickups was used at all spanwise locations to complete the surface shape. The pressure distribution chordwise for the estimated cases employed the percent shift of the true chordwise distribution compared to the central pressure location at that spanwise case. The lower pickups on the rigid tail were not available, and thus the pressures along the inboard span were estimated from the extrapolation of the data from the outer area, as well as comparing the spanwise pressure shapes from the flexible tail. This was done manually and quite carefully so as to maintain good control and accuracy. As shown in Figure 3.1.62, the tail was divided spanwise by lines at 0, 25, 57 and 100% chord, and chordwise by lines at 0, 50, 69.5, 85.5 and 100% span. This provided the areas and grid from which the pressure surface points were developed at the centers of each area. The pressure value from the pressure surface at the center of each area was used with the area and location from the root, in order to generate bending moment, BM; i.e.

$$BM = \sum_j p_j r_j A_j \tag{1}$$

where p is the pressure, A is the area, and r is the distance from the area center to the root. This method of pressure surface fitting from a few well dispersed pressure pick-ups was developed and used in References 2-6, and was shown to provide a good description of pressure data, and hence excitation, in studies for predicting oscillatory response. These studies were shown to predict results that compared well with wind tunnel and flight test data. Thus, this approach was used here as a means to check the scaling of bending moment with Q variation. The values of these bending moments based on direct pressure

integration would be of course higher than those measured due to modal effects and due to the random combination of pressures, especially random phasing. The more accurate means would be to use the pressures in a dynamic response prediction. Though this was not done, these computed bending moments should display the bending moment trends with angle of attack, and should show the effect of dynamic pressure scaling, since pressures displayed this property.

BM data were computed for Q=56 and 30 psf, for AOA's of 8-32 deg, β=-4, 0, 4, and for WBP of 0, 45, 65 psi for both the rigid and flexible tails, as available. Figures 3.1.63 to 3.1.66 are presented from this effort, and show the proper trends with angle of attack as per the measured data, and they show a closer scaling with dynamic pressure, Q, than do the measured moments; namely, the calculated bending moments at the lower Q are proportionally smaller than those for the higher Q's by the Q ratios.

3.2 FLEXIBLE TAIL RESPONSE: ACCELERATION DATA -

3.2.1 EQUATIONS FOR BENDING AND TORSION ACCELERATIONS -

The general arrangement of the flexible tail and the positions of the accelerometers is shown in Figure 2.1.5 previously, but repeated here as Figure 3.2.1 for convenience, and with more detail as used in the analysis to define the bending and torsional motions of the tail during buffet excitation. Two accelerometers were placed on the tail in the tip pod, one at the forward end, and one at the aft end, and oriented so as to measure the lateral motions, Z's, normal to the tail surface. These motions can be converted to bending measured lateral to the tail surface at an assumed elastic axis, and again converted to torsion about this elastic axis. A schematic on Figure 3.2.1 shows the Z motions and the lever arms R's from the elastic axis, (E.A.). Assuming small amplitudes, then the lateral deflections at the forward and aft accelerometers are given in relation to bending, H, and torsion, α, as the following:

$$\begin{aligned} Z_F &= H - R_F\alpha \\ Z_A &= H + R_A\alpha \end{aligned} \qquad ..(2)$$

The torsional motion along the E.A. is found first from the Z's by the expression:

$$\alpha = \frac{Z_A - Z_F}{R_F + R_A} \qquad (3)$$

The torsional acceleration $\ddot{\alpha}$ is found from the second derivative of this expression, namely:

$$\ddot{\alpha} = \frac{\ddot{Z}_A - \ddot{Z}_F}{R_F + R_A} = \frac{A_A - A_F}{R_F + R_A} \qquad (4)$$

where the A's represent the measured accelerometer reading taken during the test.

The bending at the E.A at this spanwise point is given by:

$$H = \frac{1}{2}\left\{(Z_F + Z_A) + \frac{R_F - R_A}{R_F + R_A}(Z_A - Z_F)\right\} \qquad (5)$$

The acceleration $\ddot{H}$ follows from derivatives of H, and following the $\ddot{\alpha}$ equation above, and it is determined from the measured accelerations as:

$$\ddot{H} = \frac{1}{2}\left\{(A_F + A_A) + \frac{R_F - R_A}{R_F + R_A}(A_A - A_F)\right\} \tag{6}$$

3.2.2 PSD DATA - Several PSD plots of acceleration are shown here to typify those data, while the bulk is again in Volume 2. In Figure 3.2.2 and Figure 3.2.3 the forward and aft accelerometers are shown for an AOA of 32 deg with no blowing, for Q=56 and 30 psf respectively. Both figures clearly show the various modes of the tail correctly, and their overall rms values are in proper ratio to the Q's. Figure 3.2.4 and Figure 3.2.5 show the bending response for these same cases, again displaying the proper ratio as with Q ratio. Note that bending values are not the averages of the two linear acceleration readings, forward and aft, in these curves. Rather, the bending values are lower than the lowest of the linear groups, suggesting torsion is highly active at the higher AOA's, as is already known, but at least this is reconfirming.

3.2.3 RMS TRENDS - A number of plots of rms values of the acceleration PSD's are shown to display effects of AOA, yaw, and wing blowing. In these figures, rms acceleration trends with AOA are the main variables, with Beta's as a grouping. The forward, aft, and bending accelerations are grouped to show those trends in Figure 3.2.6 to 3.2.8 for WBP=0, 45, 65 psi, respectively. All of the accelerometer data tends to show a peaking at about 24 to 26 deg, rather than a continual growth with AOA as do the measured bending strains.

These show a slight increase in response of the forward and aft accelerometers due to blowing, more notable at the higher angles, but bending decreases slightly, indicating the torsion is more active. Similar plots are shown for a Q=30 PSF in the next two figures, Figures 3.2.9 and 3.2.10 for WBP=0, and 45 psi (no data for WBP=65 psi). The next three plots, Figures 3.2.11 to 3.2.13 show the forward, the aft, and the bending acceleration rms data, respectively, for AOA variation for Q=56 psf. In these graphs, the WBP cases are grouped at the top, center and bottom, while Beta cuts are called out in each group. These graphs show AOA peaking at 24-26 deg for the forward and aft accelerometers, while bending shows only a mild peaking. The negative yaw shows a stronger buffeting effect except at the highest AOA which is similar to what was found with the strain gauges. The last two figures in this group, Figure 3.2.14 and 3.2.15, summarize the effect of Q on bending, namely showing the bending acceleration data vs AOA with Beta cuts in top to bottom subfigures, where the Q=56 vs Q=30 psf curves are noted. The case for no blowing is in Figure 3.2.14 while the 45 psi case is in Figure 3.2.15. The two curves for the different Q's are proportioned reasonably well, with the blowing seemingly increasing response at the higher Q for yaws of 0 and 4 deg.

3.3 OSCILLATORY PRESSURES: FLEXIBLE AND RIGID TAILS - Oscillatory pressures were measured at a number of places along the tails, and across one span location on the tails. Figure 3.3.1 is a repeat of an earlier figure, but detailed as to the

pressure pick-up call-outs used on the tails. For the flexible tail, pick-ups were noted as locations A, B, C, and E in an outboard fashion (upward) along the 37 % chordline, respectively at 37, 61, 78, and 93 % span locations. There were two chordwise pick-ups, denoted as F and D along the 78 % span point, and placed at 13 and 77 % chord lines, respectively. For the rigid tail, pick-ups noted as G, H, and J, were used along the span, while K and I were placed chordwise at the 78 % span point. These pick-ups on the rigid tail were located identically to those on the flexible tail. Note that the lower pick-ups on the rigid tail were not used during the tests, and thus no letter location designations were given to them. Recall that there were pressure pick-ups on both the inner and outer surfaces of the tails, and thus reference to pressures measured at these locations means the pressure difference measured across each tail at each location. This method has been used successfully in several buffet pressure tests, see References 2 - 7 for example.

3.3.1 PSD DATA - The majority of the pressure PSD's are in Volume 3, while a few are shown here to give typical result. Since there are a large number of pressure data locations and test conditions, as well as two tails to review, the rms data of the PSD's are used to more readily explain trends. Figures 3.3.2 and 3.3.3 show pick-ups E, F on the flexible tail and close locations G, H on the rigid tail for a Q=56 psf for an AOA of 24 deg, Beta=0, where the first figure shows WBP=0, while the second shows WBP=65 psi. Note that while the general shapes of the PSD's are similar, there is some slight influence of the flexibility shown for pick-ups E and F on the flexible tail as opposed to G and H on the rigid tail, but the levels are comparable. If the exact locations were compared, i.e., say locations E, F were compared to J, K of the rigid tail, these same curve shape differences are there, but levels are slightly closer. Thus, while there are some differences, they are slight overall, with pressures in some bands being slightly more affected by flexibility. There have been pros and cons as to which pressures should be used in predicted response studies, with the Author leaning to use of the pressures from the rigid surface being more the reliable, since one should be able to use those with flexibility studies to show the pressures measured on the flexible tail.

3.3.2 RMS TRENDS - Graphs have been prepared to summarize the rms values of the pressure PSD's, and to display these in a manner similar to the bending and torsion moment data, and the acceleration data. In these figures, both the flexible tail and the rigid tail are shown, with all pick-ups on each displayed. The main trend is AOA effect, the next is the Beta value, and then the blowing location and pressure is traced. Figures 3.3.4 to 3.3.8 cover the Q=56 PSF with WBP=0, 45, and 65, and the case of WBP=65 psi with GBP=65 psi. The PSD's of the flexible and rigid tails show comparable levels generally. While the distributions are different, the flexible tail case shows a tendency to peak near the torsion mode at the higher AOA's. There is a complex pattern of influences seen, and it is difficult to precisely summarize, but there are definite influences of AOA, Beta, and blowing. Negative yaw, once again, seems to raise pressures as in the increased bending response noted earlier for negative Beta's. AOA peaking is consistent with the measured moments, and blowing tends to decrease some of the pressure overall, but it also seems to redistribute AOA and Beta influences. The next group of Figures 3.3.9 and 3.3.10 show comparable data for Q=30 psf, but lesser data exists to compare with the first

three figures. Some of the same trends are in this set as in the Q=56 data, and the overall levels are comparable to Q differences, as they should be. Some pressure and AOA effects are slightly different, but reasonably consistent. These pressures suggest that the bending moments should scale with Q, but the measured bending moments do not. The remaining figures, Figures 3.3.11 - 3.3.13 show the effects of (a) NBP=87 psi, (b) NBP=87 psi with GBP=65 psi, (c) NBP=87 psi with WBP=65 psi. These data are self-explanatory.

3.3.3 CSD, COHERENCE, AND CORRELATION COEFFICIENT DATA - To add some additional information for those interested, CSD's, Coherence Functions and Correlation Coefficients were computed for the pressure data. Some investigators include the CSD's in the response calculations, thus it is believed necessary to include some here for that purpose. Again, the bulky data for this information is in Volume 3, while a limited amount is in this volume for summary purposes. Figures 3.3.14 and 3.3.15 show CSD modulus and phase plots for pick-up locations K,I on the rigid tail. These were selected to show because they are in the fore-aft, or flow, direction and thus should show as strong a coupling as one would expect here. Here the data is for a Q=56 psf case where Beta=0, with no blowing. AOA's of 8, 20, 24, 32 deg are included in the sweep shown. The rms values of the CSD's moduli are in the range of the PSD's, indicating a strong convection across the tail. Not much can be said of phase, it is as shown. Table 3.3.1 shows a listing of the CSD modulus values for the rigid tail vs AOA for a Q=56 psf, for the three Betas, for WBP=0, 45, and 65 psi. Note, the reader can trace the behavior pattern of CSD's vs the main test conditions. The pattern seems to follow the trends of the pressures, and in some cases at the higher AOA's, the CSD's fall in level, suggesting their influence on calculations may be less there.

Also, there were Coherence Functions (CH) computed. These functions were computed in the frequency domain by the formula:

$$CH_{1,2} = \frac{\left(CSD_{1,2}\right)^2}{\left(PSD_1\right)\left(PSD_2\right)} \tag{7}$$

where the subscripts show either the two parameters used in the cross terms, or the single parameter in the PSD's. A typical case is shown in Figure 3.3.16 for pick-ups K, I. The coherence levels seem to peak around an AOA of 20 deg, with a large hump at the torsion frequency band. At the higher angles where buffet is more significant, the coherence level is seemly less again, suggesting that the CSD's may not influence calculations with these pick-ups.

Correlation Coefficients were calculated for a few cases to show the influence of the interaction between the pressure at different points. This function is based on the CSD modulus behavior and the rms of the two signals involved. The Correlation Coefficient, CC, is computed by the formula:

$$CC_{1,2} = \frac{\left(\bar{r}_{1,2}\right)^2}{\left(\bar{r}_1\right)\left(\bar{r}_2\right)} \tag{8}$$

where $\bar{r}_{1,2}$ is the rms values of the $CSD_{1,2}$, and r_1 and r_2 are the rms values of the PSD'S. Table 3.3.2 lists a few of these typical values showing strong correlation in pressures between several locations.

3.4 NONDIMENSIONAL DATA: BENDING AND TORSION MOMENTS

3.4.1 PSD DATA - These curves were developed from the dimensional data addressed in the earlier sections. The same grouping of data, test parameter, and test condition are shown here again, the difference is the scaling. Here the PSD of the bending and torsion moment coefficients were found by the following equations. The bending moment coefficient, C_M, is found by:

$$C_M = \frac{BM}{QS\tilde{c}} \tag{9}$$

where BM is the bending moment, Q is dynamic pressure, $S = 19.9\ in^2$ is the area, and $\tilde{c} = 3.77\ in$ is the mean aerodynamic chord. The torsion moment coefficient, C_T, is found from the same equation, by substituting the torsion moment TM for the BM. Two figures are shown here, while the reader is referred to Volume 2 for the remainder. Figures 3.4.1 and 3.4.2 show the bending and torsion moment coefficients for Q=56 psf, Beta=0, no blowing, for several Alphas.

3.4.2 RMS TRENDS - While this data is probably even more interesting than the earlier set because it is more readily compared to other data, the trends are the same, merely scaled differently. Thus, these figures, noted as Figures 3.4.3 to 3.4.56 present the nondimensional bending and torsion data as measured and scaled. These curves help to show blowing effects more obviously because every plotted value is bounded in a more controlled fashion. The reader is encouraged to scour this data for more information. Some of the earlier comments on blowing effectivity is further ramified here. Note that the nondimensional bending, C_M, for Q=56 psf and for Q=30 psf, as shown respectively in Figures 3.4.3 and 3.4.17 do not scale as closely for AOA's above 20 deg as they should. Note that the torsion moment coefficient, C_T, does however appear to scale properly in those figures. Likewise, with WBP=45 psi, a similar disparity is seen in comparing Figure 3.4.17 vs Figure 3.4.20, and it appears throughout the whole grouping. If there were one case where the disparity was not present, some hope would have existed to resolve this oddity. A thorough post-test review of all calibrations, recordings, and data reduction did not resolve this difference. No such difference appeared in the acceleration data, pressure data, nor BM from pressure integration.

3.5 NONDIMENSIONAL PRESSURE DATA: BOTH TAILS -

3.5.1 PSD DATA - Though it was intended to develop nondimensional pressure PSD's, i.e., PSD(p/Q), this was somehow omitted from the data reduction. However, the nondimensional rms values of the pressures were obtained and are included.

3.5.2 RMS TRENDS - Values of the rms pressure data from the pressure PSD's were scaled with Q, i.e., the rms pressures were divided by Q to provide something akin to a random pressure coefficient. These data are shown here as Figures 3.5.1 to 3.5.10, and display ranges the Author is used to seeing from many other buffet tests of fighter empennage. These pressures scale nicely with Q, see Figure 3.5.1 vs 3.5.9, where the Pressure Coefficient for Q=56 and Q=30 psf are quite close for both tails.

3.6 CORRELATION WITH OTHER TEST DATA - Figures 3.6.1 to 3.6.10 were prepared to show how this test data compare with other test data. Also, a recap of some of the test trends of bending and torsion moment coefficients are shown here in new format to indicate added behavior patterns. Figures 3.6.1 and 3.6.2 show the bending and torsion coefficients for Q=30, 56 psf vs AOA of range 0 to 32 deg, for the three yaws, while the next two figures, Figures 3.6.3 and 3.6.4 show the same data forWBP=45 psi. The Q=30 data show larger values than do the Q=56 data, and note the Q=30 data show a bending response reduction with blowing, while Q=56 data show a slight increase with blowing. The torsion data correlates with Q and shows a little reduction with blowing for both Q's. Figures 3.6.5 to 3.6.8 repeat these same figures in dimensional data for the reader. This group of data suggest lesser response for the lower Q, but not in the correct proportion. Thus, originally the Q differences from dimensional results appeared to be consistent, that is until the bending and torsion coefficients were evaluated, and then for some explanation of the bending scaling oddity was sought.

Correlation of the buffet response of the 4.7% F-15 model empennage with that of the F/A-18 empennage from Reference 4 is presented in Figures 3.6.9 and 3.6.10. The F/A-18 data includes model test and flight test data. Figure 3.6.9, Parts 1 and 2, shows the F-15 4.7% model data versus the F/A-18 vertical tail data, Part I shows correlation between the F-15 inboard bending and torsion moments versus the F/A-18 outboard bending and torsion moments, while Part 2 compares inboard bending and torsion moments for both tails. The outboard bending and torsion data for the F/A-18 is from Figure 20 in Reference 4. In Part 1, it is seen that the F-15 inboard bending data is larger than the F/A-18 outboard bending data, as is expected from much experience with these types of tests. Similarly, the torsions are fairly comparable, again as expected. Note that the F/A-18 data for both bending and torsion seem to peak in this AOA range, while the F-15 bending does not, though the F-15 torsion does. In Figure 3.6.9, Part 2, data for the F/A - 18 inboard bending and torsion were developed by ratioing the outboard moment data with limited data from Figure 19 in Reference 4, showing the calculated and measured data for a typical case comparing inboard to outboard moments. Note that the F-15 inboard bending moments correlate fairly well with the F/A-18 inboard moments, and that at the higher AOA's, the F-15 data for Q=56 are somewhat lower, while the F-15 data for Q=30 are somewhat higher. Again, the F/A-18 bending data seems to peak out in this AOA range, while the F-15 does not. The torsions are fairly comparable, with the ratioed F/A data being slightly larger, both sets seem to peak in this AOA range. Note also, that the F/A-18 data seem to be consistent between sets of the model and full scale, though the flight data have more scatter as would be expected.

Figure 3.6.10, Parts 1 and 2, shows correlation between the 4.7% F-15 model buffet response and that of the F/A-18 stabilator from Figure 18 of Reference 4. Part 1 of this figure shows the F-15 model inboard bending and torsion versus that for the F/A-18 outboard bending and torsion. Note that the F-15 data is considerably larger than the that for the stabilator, as is expected since not only are the two data groups at different locations, but the stabilator is much stiffer due to aeroelastic requirements (flutter). Part 2 compares the inboard bending and torsion for the F-15 tail and F/A-18 stabilator. Note that despite the larger stabilator stiffness, these two data sets are comparable in the ranges where both exist, with the F/A-18 tending to be somewhat lower as expected due to it greater stiffness. It should be noted that the nondimensional methods used in the two data sets are somewhat different in terms of the coefficient forms. However, before absolute application of these coefficients can be made exactly, the data from both aircraft must be put into more completely scaled equivalents where all dynamic, elastic, and geometric properties are completely included, See Reference 2. Such data were not available for this effort, thus the comparison made was as good as could be at this time. More could be done if the total data for both were available to the Author.

4. CONCLUSIONS

This test demonstrated that tangential blowing from the front portion of the model altered buffet response of the flexible tail. Tangential blowing was introduced at three places, symmetrically and simultaneously, on both sides of the model. Likewise, oscillatory pressures measured on the flexible tail and a relatively rigid tail showed pressures differences due to blowing. Brief conclusions are here, however, the reader is referred to the main body to draw his own added conclusions, due to the complex nature of the data from many parameters.

4.1 BENDING AND TORSION RESPONSES AS AFFECTED BY BLOWING - Bending and torsion responses reflect some effects of blowing, especially by modes within the overall response of bending and torsion themselves, because there are both relatively independent modes and rather highly coupled modes within the principal frequency ranges of maximum oscillatory pressure excitation from buffet. There are influences with AOA, yaw, and the blowing pressures from the three locations. A complicating factor was the seemingly disproportionate effect on bending at the two Q's. That is, the bending response coefficients for the two Q's did not match as well as from many other tests. Torsion did however. Basically, all responses increased with initial AOA above the vortex burst angle, where after torsion seemed to peak and fall off, after an AOA of 24 – 26 deg at all yaws and with all blowing. Bending seemed to show no peaking, and displayed larger response at negative yaws. Also, bending displayed slight increases in response from blowing at the negative yaws, much more at Q=56 than Q=30 where there was a small reduction. At positive yaws, the bending was less, and blowing tended to reduce response, especially for Q=56. When unyawed, the bending at Q=56 showed a slight increase, while that at a Q=30 showed a slight decrease, again one must track the individual modes to satisfy a trend. Blowing from the wing, 45 and 65 psi, was the most effective, that from the gun bump, 65 psi, was the next most effective, while blowing from the nose, 87 psi, was the least effective. The nose blowing pressure was raised to 87 psi to help, but did not make much effect. Acceleration data were also developed as another check on trends of bending and torsion. This data showed proper scaling with Q, and indicated similar effects and trends with blowing as the strain gauge data. AOA effects were more like those from torsion, indicating a peaking of response in the AOA range investigated, the more common shape the Author has seen in the past. Similarly, bending moments were computed from the rms pressure data to see what Q scaling would show, despite the fact that these moments would be much larger than the modalized and random versions measured. These data did show the Q scaling and a more anticipated shape with AOA than did the bending measurements.

4.2 PRESSURES AS AFFECTED BY BLOWING - The oscillatory pressures showed proper rms level shifts with Q, AOA, and yaw as they should, while retaining PSD shapes. Blowing pressures made some alterations to PSD shapes and levels. Again, this is too complex to summarize, and the reader is referred to the data in this report, in both Volumes 1 and 3, to reach his own conclusion.

4.3 TREND PATTERNS AS COMPARED TO OTHER DATA - This has been covered thoroughly already, but some comments are due here. Generally, the AOA effect in the range explored was to show a peak response below 32 deg for Vertical Tails, while some stabilators show a higher AOA peaking due to more forward locations on the fuselage. For the F-15, the Vertical tail response was generally expected to peak around 22 - 28 deg, again depending on whether one is considering bending or torsion, and again depending if modal vs broadband response is considered. These all tend to show slight differences. The data here generally followed that pattern, especially torsion, but bending, especially at Q=56 psf, at the higher angles did not fall of as much as expected. These levels were some what lower than those for Q=30 PSF, based on Q scaling.

4.4 EFFECTIVITY OF BLOWING - This is really covered throughout the report, but in essence, there was more of an effect than might be imagined when considering the relative distance from the injection points to the tails. However, the pressures did reach the tails because of flow convection in something akin to a Coanda effect. There were effects, some positive and some negative, from the blowing, but a much more in-depth application of the response data to structural fatigue of the tails needs to be examined before drawing further conclusions. Any response reduction is certainly helpful, and some were shown. Also, the AOA sequence, and duration at these AOA's in a true statistical definition of actual life cycles in projected life time of usage is required before making further judgments.

5. RECOMMENDATIONS

5.1 MODEL - Future tests could be run where the tangential blowing might be injected at different points along the body, aiming to deflect, but not to alter the effect of the vortical flow providing the desirable lift at high AOA's. Likewise, with the current setup, or with blowing from other places along the body, an investigation of blowing effectivity should be run where the blowing airflow is pulsed at a range of frequencies that might have some influence on the buffeting pressures at the tail. Again, these must not alter the lift at high AOA's. It is believed effective to inject airflow at close proximity of the tail, i.e., at the tail base, especially at the front of the tail so as to deflect, but not to significantly alter the lift at high AOA's. Similarly, there is a potential gain from pulsing these airflows at close proximity of the tails.

Another significant model improvement would be to develop the capability to pitch the model more rapidly, to simulate the transient maneuvering effect that exists from actual aircraft flight data. Past work has shown that response predictions based on wind tunnel model pressures scaled to full size, are a bit conservative (high) as compared to flight tests. A thesis by C. Dima, St. Louis University, Reference 8 was done to investigate some areas of this idea, using a generic wind tunnel model. Dima compared the response at slowly varying alphas (static) to response measured when pitching the model more rapidly. He showed some influences of various pitch rates in his results. This needs to be followed up, especially regarding the pressures, as Dima did not measure pressures. Similarly, the blowing method studied here should be reassessed when the model is pitched at various rates, since this is a better simulation of flight conditions than only considering static AOA's as done here.

5.2 INSTRUMENTATION - It is recommended that instrumentation be included to permit the continual, or at least intermittent, spot-checking of test parameters. Meters exist to measure and display data relatively quickly, for example, rms data, spectral properties, and statistical data. These devices can handle samples ranging from short data bursts to longer data bursts approaching steady state times. This type of checking should always be done to insure data quality, trends, and levels during testing.

5.3 DATA ACQUISITION/REDUCTION - This was done rather well, and little or no suggestions are needed, except that the on-line data could be saved to be compared with post- test analyses, to further ensure data accuracy.

5.4 TEST SETUP AND CONDUCT IN GENERAL - It is recommended that during the testing all major parameters and measurands be sampled in a pre-test, or trial run series, and all this data be compared with anticipated values to verify calibration, instrumentation, data recording and data reduction, before proceeding. Likewise, during the testing, some key variables should be monitored on-line at all times to witness accurate data collection and to insure that trends and levels are making sense compared to anticipated data. A fault of these tests was that only pressures were readily measured on-line, all of the other parameters relied heavily on pre test setup to provide only post test

results. Perhaps the bending moment scaling oddity would have been more readily found, and perhaps eliminated, if bending had been checked during the tests. Post-test re-checking of calibrations did not find any obvious errors anywhere in the entire setup, data system, or data reduction.

It may be possible that some vortex, eddy, turbulence or other tunnel flow oddity had an effect on the bending response of the model that resulted in the scaling oddity. This might be investigated to determine if there is something to be noted, or fixed in tunnel tests, so as to ensure that it does not occur again in these types of experiments.

Flow visualization tests were run after the response tests, due to scheduling conflicts, rather than beforehand. This is somewhat contrary to the Author's prior experience, where flow visualization was sometimes used to help select critical response testing conditions, and to fill-in points from pretest selected conditions. It is recommended that these be run beforehand in the future, even if nothing significant is altered, it simply adds confidence to pretest think and planning.

5.5 MISCELLANEOUS - There are several miscellaneous suggestions to perhaps aid in future work with this data. A NASTRAN model of the 4.7% Vertical tail was made under an earlier contract, and perhaps this could be used in a study to predict the behavior of the tail employing the methods of References 2 to 6. Also, other methods in those four References can be used, for example, the Rayleigh techniques based on the measured pressures, vibration data, and mass data from these model tests. It is possible that at the higher Q's, some damping value, say aerodynamic damping was disproportionately larger (or smaller, depending on the mode) than envisioned, due to flutter related damping changes. This needs to be studied closely to see if it were overlooked. Likewise, there is always the possibility, of an interaction between the vortical flows and the oscillatory pressures from nominal vibratory motions, especially as flutter is approached, i.e., some type of force coupling (or tuning). Similarly, there is always the subject blamed for anything not explainable otherwise....<u>nonlinearity</u>....this could be the oddity at the higher angles for bending at Q=56 seemingly being too small, (conversely the bending response at Q=30 seemingly being too large). If nothing else, the large amplitudes of vibration in these intense regions of excitation might require some nonlinear approximation to be made to adjust the linear case without doing a fully nonlinear analysis. The research could be directed to determine if the nonlinearity is structural, or aerodynamic, or both structural and aerodynamic. Another suggestion is to acquire as much buffet response data from the empennage of all fighters world wide, along with the basic vibration, generalized mass, test conditions (Mach Number, velocities, densities, altitude, etc.), geometry for these cases. Then the data should be completely nondimensionalized as per Reference 2 so that some type of generalized design chart could be constructed to aid future designers. This requires that the dimensional data first be scaled to the same equivalents before the same nondimensional parameters, such as a bending moment coefficient, can have full significance.

6. REFERENCES

1. Huttsell, L.J.,Tinapple, J. A., and Weyer, R.M., "Investigation of Buffet Load Alleviation on A Scaled F-15 Twin Tail Model," AGARD Report-R-822, AGARD SMP, Aalborg, Denmark, 14 - 15 Oct. 1997

2. Zimmerman, N. H., and Ferman, M. A., "Prediction of Tail Buffet Loads for Design Applications," USN Report, NADC 88043-60, July 1987

3. Zimmerman, N.H., Ferman, M.A., Yurkovich, R. N.,and Gerstenkorn, G., "Prediction of Tail Buffet Loads for Design Applications," 30 th SDM, Mobile, AL, 3-5 April 1989

4. Ferman, M. A., Patel, S., Zimmerman, N.H., And Gersternkorn, G., "A Unified Approach to Buffet Response of Fighter Aircraft Empennage," AGARD/NATO 70th SMP, Sorrento, Italy, 2-4 April 1990

5. Ferman, M.A., and Liguore, S. L., "Buffet Coupled Response of the HARV Thrust Vectoring Vane System," NASA High Angle of Attack Conference, Hampton, VA, Oct 1990

6. Washburn, A. E., Jenkins, L.N., and Ferman, M.A., "Experimental Investigation of Vortex-Fin Interaction," 31 Aersospaces Meeting, Reno, NV, 11-14 Jan 1993

7. Ferman, M.A., Liguore, S. L. Liguore, Colvin,B.L., Smith, C.M., "Composite Exoskin Doubler Extends F-15 Vertical Tail Fatigue Life," AIAA/ASME 34th SDM, La Jolla, CA, 19-21 April 1993

8. DIMA, C. "The Effects of Time Varying Maneuver Conditions on Empennage Buffet Response," MS Thesis, Parks College, St. Louis University, St. Louis, MO, Dec 1994

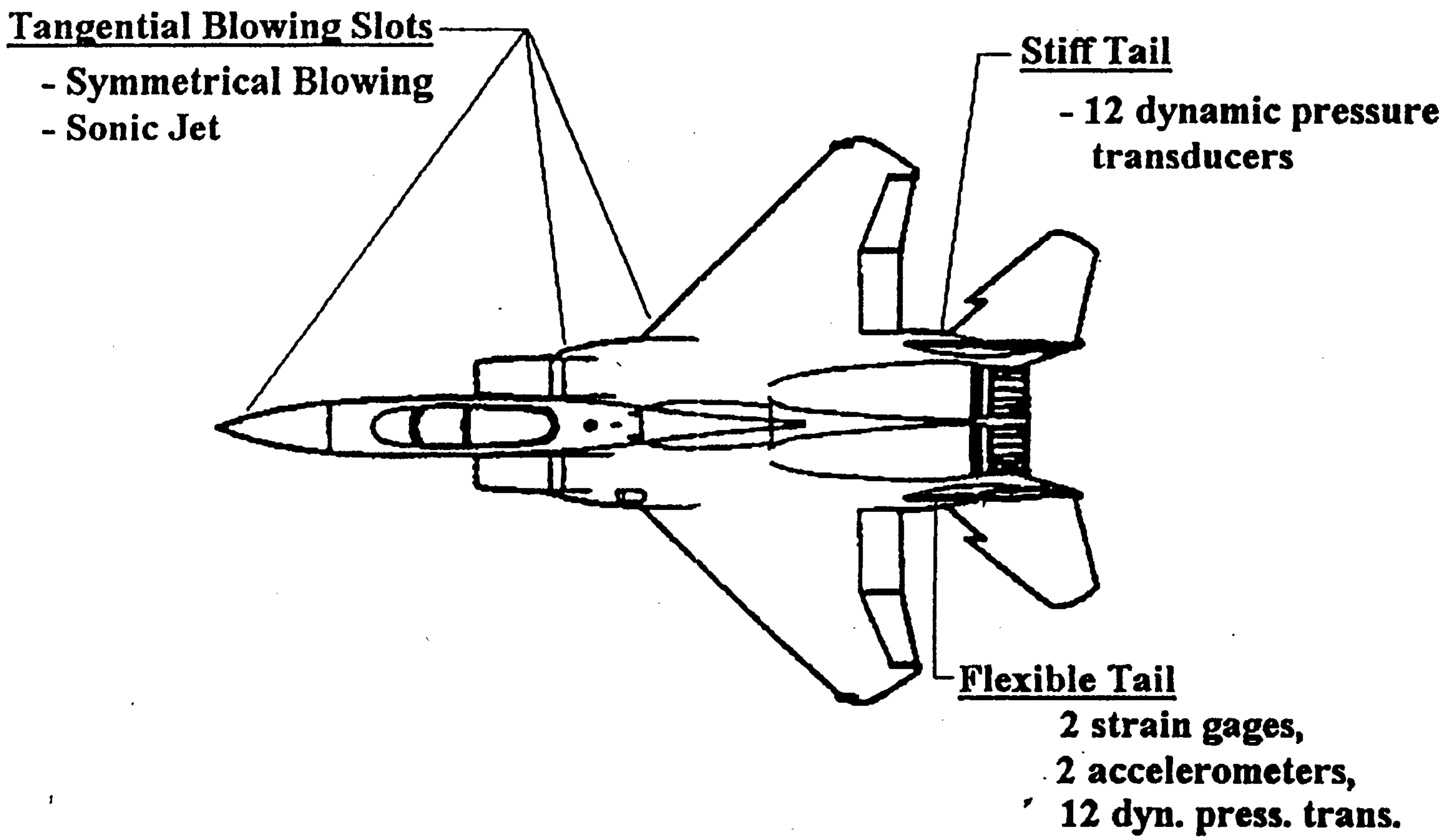

Figure 2.1.1 Planview of 4.7 % Wind Tunnel Model

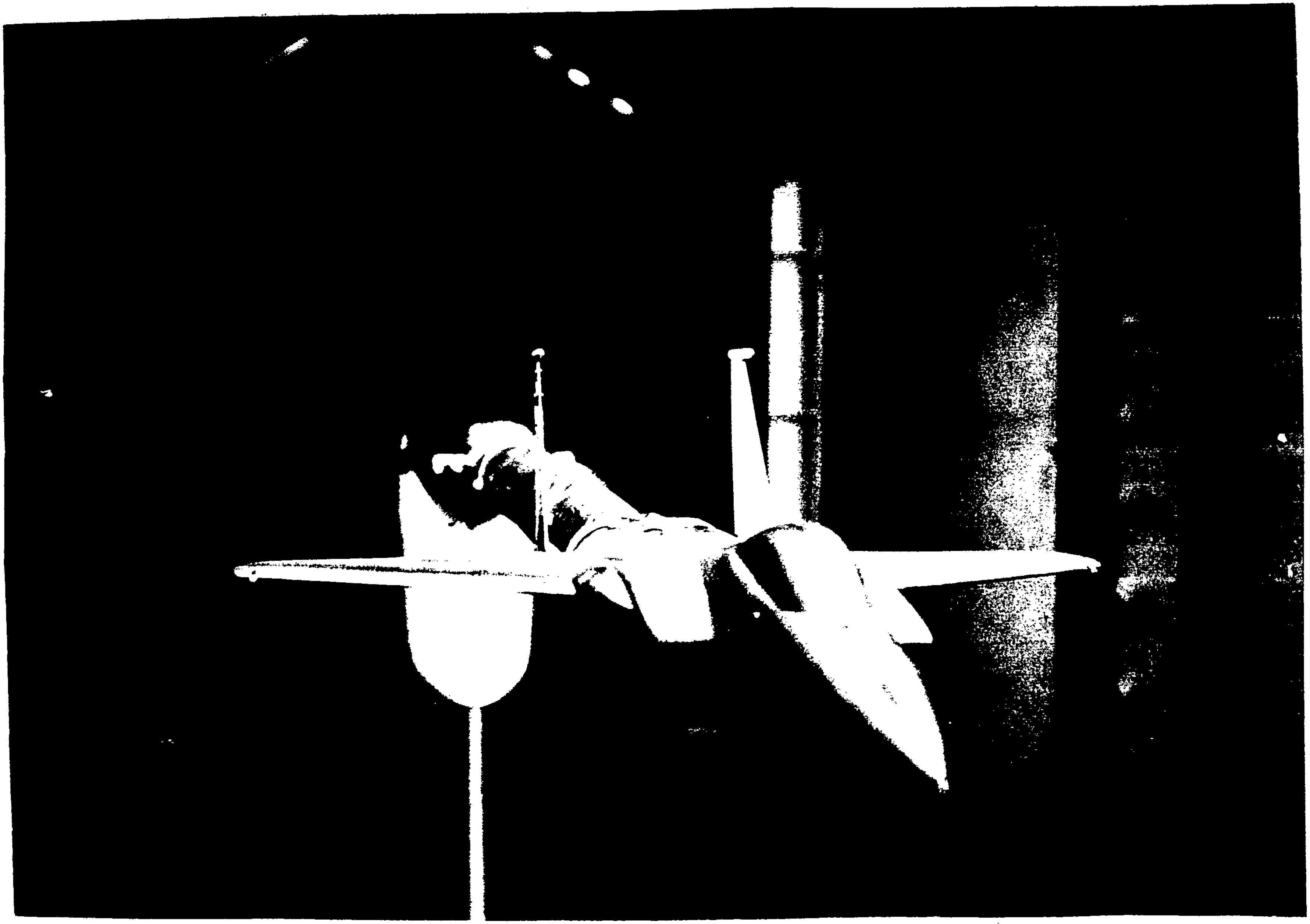

Figure 2.1.2 4.7 % Buffet Model in Wind Tunnel

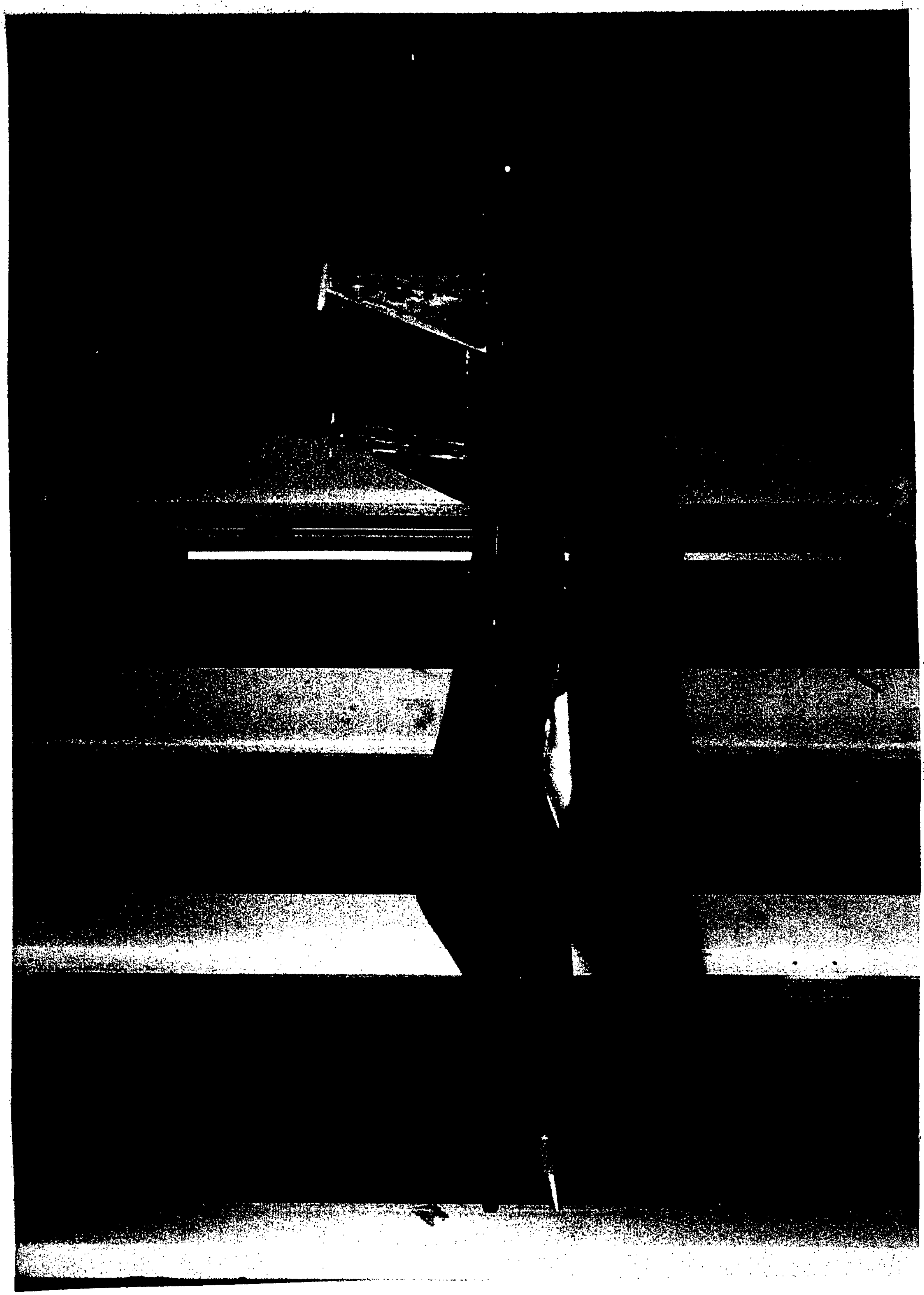

Figure 2.1.3 4.7 % Model - View From Flex. Tail Side

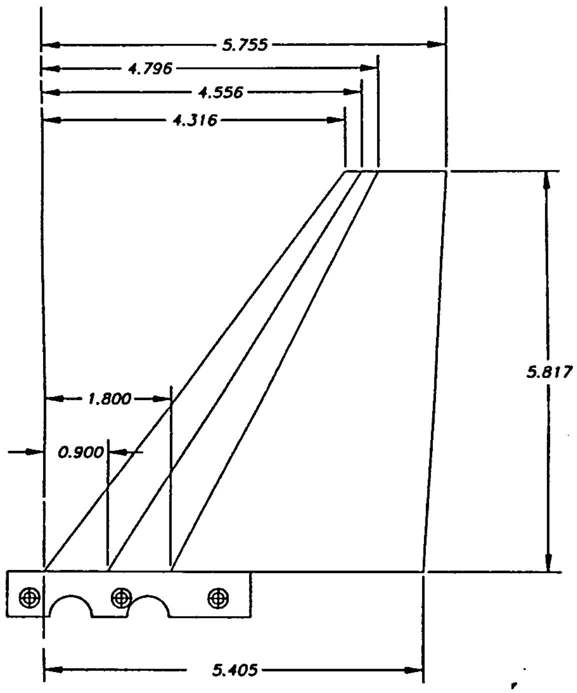

VERT. TAIL GEOMETRY WITHOUT TIP PODS

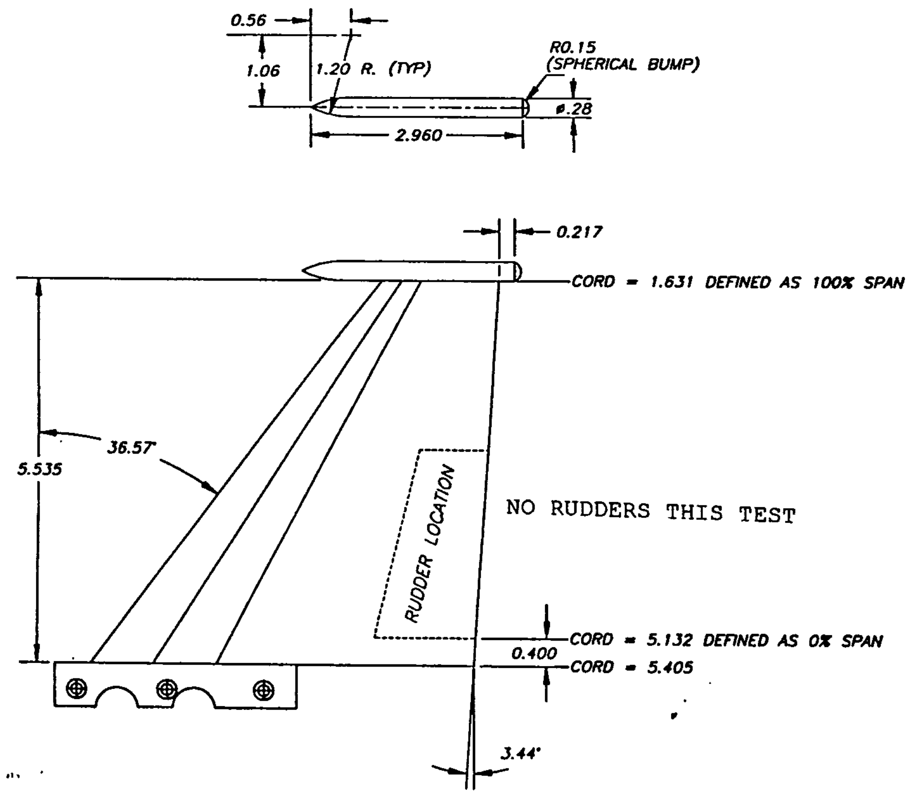

DETAILS OF VERT. TAIL WITH TIP POD

Figure 2.1.4 Geometry of 4.7 % Scale Vertical Tail

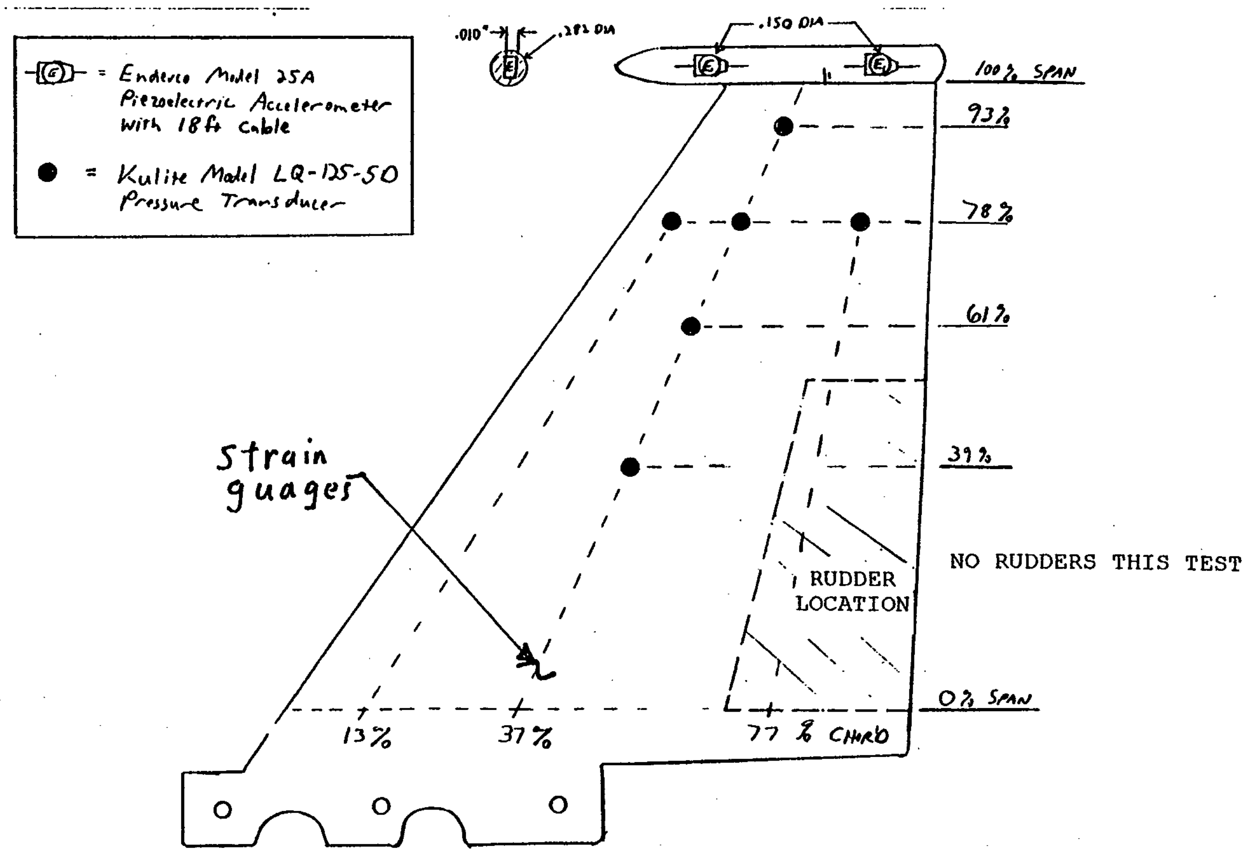

Figure 2.1.5 Instrumentation Layout on Flexible Vertical Tail

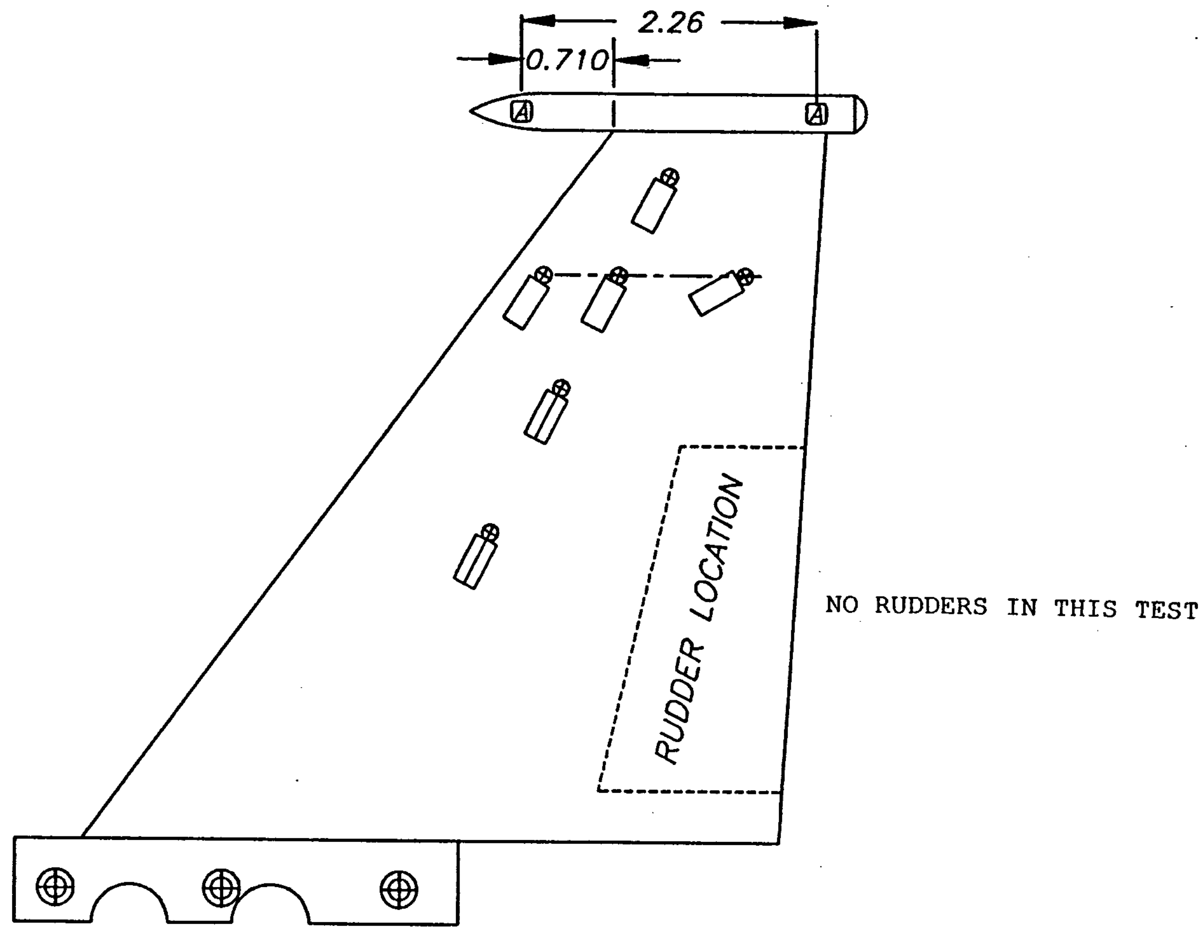

Figure 2.1.6 Pressure Transducer Layout - Both Tails

Table 2.5.1 Test Run Log
Part I

F-15 TWIN FIN BUFFET STUDY
FORCE & MOMENT BASELINE WITH AIR LINES
DYNAMIC PRESSURE DATA ON TAILS
(AND INSTRUMENTED RIGHT STEEL TAIL)
(AND INSTRUMENTED LEFT FLEX TAIL)

TPNS	AOA	BETA	Q (psf)	P(line) psia	Cu
2839	-4	0	56	max	0
2840	0	0	56	max	0
2841	2	0	56	max	0
2842	4	0	56	max	0
2843	6	0	56	max	0
2844	8	0	56	max	0
2845	10	0	56	max	0
2846	12	0	56	max	0
2847	14	0	56	max	0
2848	16	0	56	max	0
2849	18	0	56	max	0
2850	20	0	56	max	0
2851	22	0	56	max	0
2852	24	0	56	max	0
2853	28	0	56	max	0
2854	32	0	56	max	0
2859	-4	-4	56	max	0
2860	0	-4	56	max	0
2861	2	-4	56	max	0
2862	4	-4	56	max	0
2863	6	-4	56	max	0
2864	8	-4	56	max	0
2865	10	-4	56	max	0
2866	12	-4	56	max	0
2867	14	-4	56	max	0
2868	16	-4	56	max	0
2869	18	-4	56	max	0
2870	20	-4	56	max	0
2871	22	-4	56	max	0
2872	24	-4	56	max	0
2873	28	-4	56	max	0
2874	32	-4	56	max	0

TPNS	AOA	BETA	Q (psf)	P(line) psia	Cu
2877	-4	-2	56	max	0
2878	0	-2	56	max	0
2879	2	-2	56	max	0
2880	4	-2	56	max	0
2881	6	-2	56	max	0
2882	8	-2	56	max	0
2883	10	-2	56	max	0
2884	12	-2	56	max	0
2885	14	-2	56	max	0
2886	16	-2	56	max	0
2887	18	-2	56	max	0
2888	20	-2	56	max	0
2889	22	-2	56	max	0
2890	24	-2	56	max	0
2891	28	-2	56	max	0
2892	32	-2	56	max	0
2895	-4	+2	56	max	0
2896	0	+2	56	max	0
2897	2	+2	56	max	0
2898	4	+2	56	max	0
2899	6	+2	56	max	0
2900	8	+2	56	max	0
2901	10	+2	56	max	0
2902	12	+2	56	max	0
2903	14	+2	56	max	0
2904	16	+2	56	max	0
2905	18	+2	56	max	0
2906	20	+2	56	max	0
2907	22	+2	56	max	0
2908	24	+2	56	max	0
2909	28	+2	56	max	0
2910	32	+2	56	max	0

TPNS	AOA	BETA	Q (psf)	P(line) psia	Cu
2913	-4	+4	56	max	0
2914	0	+4	56	max	0
2915	2	+4	56	max	0
2916	4	+4	56	max	0
2917	6	+4	56	max	0
2918	8	+4	56	max	0
2919	10	+4	56	max	0
2920	12	+4	56	max	0
2921	14	+4	56	max	0
2922	16	+4	56	max	0
2923	18	+4	56	max	0
2924	20	+4	56	max	0
2925	22	+4	56	max	0
2926	24	+4	56	max	0
2927	28	+4	56	max	0
2928	32	+4	56	max	0

Table 2.5.1 (Cont.)
Part II

F-15 TWIN FIN BUFFET STUDY
TAIL BUFFET MEASUREMENTS
VARIABLE Cu
DYNAMIC PRESSURE DATA ON TAILS

TPNS	AOA	BETA	Q (psf)	PLENUM PRESSURES (psia)			
				NOSE	GUN BUMP	SM LD EDGE	LG LD EDGE*
2932	28	0	56	35	0	0	0
2933	28	-4	56	35	0	0	0
2934	28	4	56	35	0	0	0
2935	28	0	56	65	0	0	0
2936	28	-4	56	65	0	0	0
2937	28	4	56	65	0	0	0
2938	28	0	56	87	0	0	0
2940	28	-4	56	87	0	0	0
2941	28	4	56	87	0	0	0
2942	28	0	56	0	30	0	0
2943	28	-4	56	0	30	0	0
2944	28	4	56	0	30	0	0
2945	28	0	56	0	45	0	0
2946	28	-4	56	0	45	0	0
2947	28	4	56	0	45	0	0
2948	28	0	56	0	65	0	0
2949	28	-4	56	0	65	0	0
2950	28	4	56	0	65	0	0
2953	28	0	56	0	0	30	0
2954	28	-4	56	0	0	30	0
2955	28	4	56	0	0	30	0
2956	28	0	56	0	0	45	0
2957	28	-4	56	0	0	45	0
2958	28	4	56	0	0	45	0
2959	28	0	56	0	0	65	0
2960	28	-4	56	0	0	65	0
2961	28	4	56	0	0	65	0

TPNS	AOA	BETA	Q (psf)	PLENUM PRESSURES (psia)			
				NOSE	GUN BUMP	SM LD EDGE	LG LD EDGE*
2962	28	0	56	0	0	0	0
2963	28	-4	56	0	0	0	0
2964	28	4	56	0	0	0	0
2965	28	0	56	0	30	30	0
2966	28	-4	56	0	30	30	0
2967	28	4	56	0	30	30	0
2968	28	0	56	0	45	45	0
2969	28	-4	56	0	45	45	0
2970	28	4	56	0	45	45	0
2971	28	0	56	0	65	65	0
2972	28	-4	56	0	65	65	0
2973	28	4	56	0	65	65	0
2974	16	0	56	0	65	65	0
2975	18	0	56	0	65	65	0
2976	20	0	56	0	65	65	0
2977	22	0	56	0	65	65	0
2978	24	0	56	0	65	65	0
2979	16	0	56	0	0	65	0
2980	18	0	56	0	0	65	0
2981	20	0	56	0	0	65	0
2982	22	0	56	0	0	65	0
2983	24	0	56	0	0	65	0
2984	16	0	56	0	0	0	0
2985	18	0	56	0	0	0	0
2986	20	0	56	0	0	0	0
2987	22	0	56	0	0	0	0
2988	24	0	56	0	0	0	0

* - Only used if nothing else proves effective (requires two air lines)

Table 2.5.1 (Cont.)
Part III

F-15 TWIN FIN BUFFET STUDY
TAIL BUFFET MEASUREMENTS
DYNAMIC PRESSURE DATA ON TAILS

TPNS	AOA	BETA	Q (psf)	PLENUM PRESS (psia)		
				NOSE	GUN BUMP	SM LD EDGE
2992	16	-4	56	0	65	0
2993	18	-4	56	0	65	0
2994	20	-4	56	0	65	0
2995	22	-4	56	0	65	0
2996	24	-4	56	0	65	0
2997	26	-4	56	0	65	0
2998	16	0	56	0	65	0
2999	18	0	56	0	65	0
3000	20	0	56	0	65	0
3001	22	0	56	0	65	0
3002	24	0	56	0	65	0
3003	26	0	56	0	65	0
3004	16	4	56	0	65	0
3005	18	4	56	0	65	0
3006	20	4	56	0	65	0
3007	22	4	56	0	65	0
3008	24	4	56	0	65	0
3009	26	4	56	0	65	0
3012	16	-4	56	0	65	65
3013	18	-4	56	0	65	65
3014	20	-4	56	0	65	65
3015	22	-4	56	0	65	65
3016	24	-4	56	0	65	65
3017	26	-4	56	0	65	65
3018	16	0	56	0	65	65
3019	18	0	56	0	65	65
3020	20	0	56	0	65	65
3021	22	0	56	0	65	65
3022	24	0	56	0	65	65
3023	26	0	56	0	65	65
3024	16	4	56	0	65	65
3025	18	4	56	0	65	65
3026	20	4	56	0	65	65
3027	22	4	56	0	65	65
3028	24	4	56	0	65	65
3029	26	4	56	0	65	65

TPNS	AOA	BETA	Q (psf)	PLENUM PRESS. (psia)		
				NOSE	GUN BUMP	SM LD EDGE
3032	16	-4	56	0	0	65
3033	18	-4	56	0	0	65
3034	20	-4	56	0	0	65
3035	22	-4	56	0	0	65
3036	24	-4	56	0	0	65
3037	26	-4	56	0	0	65
3038	16	0	56	0	0	65
3039	18	0	56	0	0	65
3040	20	0	56	0	0	65
3041	22	0	56	0	0	65
3042	24	0	56	0	0	65
3043	26	0	56	0	0	65
3044	16	4	56	0	0	65
3045	18	4	56	0	0	65
3046	20	4	56	0	0	65
3047	22	4	56	0	0	65
3048	24	4	56	0	0	65
3049	26	4	56	0	0	65
3052	16	-4	56	87	0	0
3053	18	-4	56	87	0	0
3054	20	-4	56	87	0	0
3055	22	-4	56	87	0	0
3056	24	-4	56	87	0	0
3057	26	-4	56	87	0	0
3058	16	0	56	87	0	0
3059	18	0	56	87	0	0
3060	20	0	56	87	0	0
3061	22	0	56	87	0	0
3062	24	0	56	87	0	0
3063	26	0	56	87	0	0
3064	16	4	56	87	0	0
3065	18	4	56	87	0	0
3066	20	4	56	87	0	0
3067	22	4	56	87	0	0
3068	24	4	56	87	0	0
3069	26	4	56	87	0	0

Table 2.5.1 (Cont.)
Part IV

F-15 TWIN FIN BUFFET STUDY
TAIL BUFFET MEASUREMENTS
DYNAMIC PRESSURE DATA ON TAILS

TPNS	AOA	BETA	Q (psf)	PLENUM PRESS (psia)		
				NOSE	GUN BUMP	SM LD EDGE
3073	16	-4	56	87	65	0
3074	18	-4	56	87	65	0
3075	20	-4	56	87	65	0
3076	22	-4	56	87	65	0
3077	24	-4	56	87	65	0
3078	26	-4	56	87	65	0
3079	16	0	56	87	65	0
3080	18	0	56	87	65	0
3081	20	0	56	87	65	0
3082	22	0	56	87	65	0
3083	24	0	56	87	65	0
3084	26	0	56	87	65	0
3085	16	4	56	87	65	0
3086	18	4	56	87	65	0
3087	20	4	56	87	65	0
3088	22	4	56	87	65	0
3089	24	4	56	87	65	0
3090	26	4	56	87	65	0
3094	16	-4	56	87	0	65
3095	18	-4	56	87	0	65
3096	20	-4	56	87	0	65
3097	22	-4	56	87	0	65
3098	24	-4	56	87	0	65
3099	26	-4	56	87	0	65
3100	16	0	56	87	0	65
3101	18	0	56	87	0	65
3102	20	0	56	87	0	65
3103	22	0	56	87	0	65
3104	24	0	56	87	0	65
3105	26	0	56	87	0	65
3106	16	4	56	87	0	65
3107	18	4	56	87	0	65
3108	20	4	56	87	0	65
3109	22	4	56	87	0	65
3110	24	4	56	87	0	65
3111	26	4	56	87	0	65

TPNS	AOA	BETA	Q (psf)	PLENUM PRESS. (psia)		
				NOSE	GUN BUMP	SM LD EDGE
3114	16	-4	56	0	45	45
3115	18	-4	56	0	45	45
3116	20	-4	56	0	45	45
3117	22	-4	56	0	45	45
3118	24	-4	56	0	45	45
3119	26	-4	56	0	45	45
3120	16	0	56	0	45	45
3121	18	0	56	0	45	45
31222	20	0	56	0	45	45
3123	22	0	56	0	45	45
3124	24	0	56	0	45	45
3125	26	0	56	0	45	45
3126	16	4	56	0	45	45
3127	18	4	56	0	45	45
3128	20	4	56	0	45	45
3129	22	4	56	0	45	45
3130	24	4	56	0	45	45
3131	26	4	56	0	45	45
3134	16	-4	56	0	30	30
3135	18	-4	56	0	30	30
3136	20	-4	56	0	30	30
3137	22	-4	56	0	30	30
3138	24	-4	56	0	30	30
3139	26	-4	56	0	30	30
3140	16	0	56	0	30	30
3141	18	0	56	0	30	30
3142	20	0	56	0	30	30
3143	22	0	56	0	30	30
3144	24	0	56	0	30	30
3145	26	0	56	0	30	30
3146	16	4	56	0	30	30
3147	18	4	56	0	30	30
3148	20	4	56	0	30	30
3149	22	4	56	0	30	30
3150	24	4	56	0	30	30
3151	26	4	56	0	30	30

Table 2.5.1 (Cont.)
Part V

F-15 TWIN FIN BUFFET STUDY
TAIL BUFFET MEASUREMENTS
DYNAMIC PRESSURE DATA ON TAILS

TPNS	AOA	BETA	Q (psf)	PLENUM PRESS (psia)		
				NOSE	GUN BUMP	SM LD EDGE
3154	16	-4	56	0	0	30
3155	18	-4	56	0	0	30
3156	20	-4	56	0	0	30
3157	22	-4	56	0	0	30
3158	24	-4	56	0	0	30
3159	26	-4	56	0	0	30
3160	16	0	56	0	0	30
3161	18	0	56	0	0	30
3162	20	0	56	0	0	30
3163	22	0	56	0	0	30
3164	24	0	56	0	0	30
3165	26	0	56	0	0	30
3166	16	4	56	0	0	30
3167	18	4	56	0	0	30
3168	20	4	56	0	0	30
3169	22	4	56	0	0	30
3170	24	4	56	0	0	30
3171	26	4	56	0	0	30
3174	16	-4	56	0	0	45
3175	18	-4	56	0	0	45
3176	20	-4	56	0	0	45
3177	22	-4	56	0	0	45
3178	24	-4	56	0	0	45
3179	26	-4	56	0	0	45
3180	16	0	56	0	0	45
3181	18	0	56	0	0	45
3182	20	0	56	0	0	45
3183	22	0	56	0	0	45
3184	24	0	56	0	0	45
3185	26	0	56	0	0	45
3186	16	4	56	0	0	45
3187	18	4	56	0	0	45
3188	20	4	56	0	0	45
3189	22	4	56	0	0	45
3190	24	4	56	0	0	45
3191	26	4	56	0	0	45

TPNS	AOA	BETA	Q (psf)	PLENUM PRESS. (psia)		
				NOSE	GUN BUMP	SM LD EDGE
3194	16	-4	56	0	30	0
3195	18	-4	56	0	30	0
3196	20	-4	56	0	30	0
3197	22	-4	56	0	30	0
3198	24	-4	56	0	30	0
3199	26	-4	56	0	30	0
3200	16	0	56	0	30	0
3201	18	0	56	0	30	0
3202	20	0	56	0	30	0
3203	22	0	56	0	30	0
3204	24	0	56	0	30	0
3205	26	0	56	0	30	0
3206	16	4	56	0	30	0
3207	18	4	56	0	30	0
3208	20	4	56	0	30	0
3209	22	4	56	0	30	0
3210	24	4	56	0	30	0
3211	26	4	56	0	30	0
3216	16	-4	56	87	45	0
3217	18	-4	56	87	45	0
3218	20	-4	56	87	45	0
3219	22	-4	56	87	45	0
3220	24	-4	56	87	45	0
3221	26	-4	56	87	45	0
3222	16	0	56	87	45	0
3223	18	0	56	87	45	0
3224	20	0	56	87	45	0
3225	22	0	56	87	45	0
3226	24	0	56	87	45	0
3227	26	0	56	87	45	0
3228	16	4	56	87	45	0
3229	18	4	56	87	45	0
3230	20	4	56	87	45	0
3231	22	4	56	87	45	0
3232	24	4	56	87	45	0
3233	26	4	56	87	45	0

Table 2.5.1 (Cont.)
Part VI

F-15 TWIN FIN BUFFET STUDY
TAIL BUFFET MEASUREMENTS
DYNAMIC PRESSURE DATA ON TAILS

TPNS	AOA	BETA	Q (psf)	PLENUM PRESS (psia)		
				NOSE	GUN BUMP	SM LD EDGE
3238	-4	0	30	0	0	0
3239	0	0	30	0	0	0
3240	2	0	30	0	0	0
3241	4	0	30	0	0	0
3242	6	0	30	0	0	0
3243	8	0	30	0	0	0
3244	10	0	30	0	0	0
3245	12	0	30	0	0	0
3246	14	0	30	0	0	0
3247	16	0	30	0	0	0
3248	18	0	30	0	0	0
3249	20	0	30	0	0	0
3250	22	0	30	0	0	0
3251	24	0	30	0	0	0
3252	28	0	30	0	0	0
3253	32	0	30	0	0	0
3256	-4	4	30	0	0	0
3257	0	4	30	0	0	0
3258	2	4	30	0	0	0
3259	4	4	30	0	0	0
3260	6	4	30	0	0	0
3261	8	4	30	0	0	0
3262	10	4	30	0	0	0
3263	12	4	30	0	0	0
3264	14	4	30	0	0	0
3265	16	4	30	0	0	0
3266	18	4	30	0	0	0
3267	20	4	30	0	0	0
3268	22	4	30	0	0	0
3269	24	4	30	0	0	0
3270	28	4	30	0	0	0
3271	32	4	30	0	0	0

TPNS	AOA	BETA	Q (psf)	PLENUM PRESS. (psia)		
				NOSE	GUN BUMP	SM LD EDGE
3274	-4	0	30	0	0	45
3275	0	0	30	0	0	45
3276	2	0	30	0	0	45
3277	4	0	30	0	0	45
3278	6	0	30	0	0	45
3279	8	0	30	0	0	45
3280	10	0	30	0	0	45
3281	12	0	30	0	0	45
3282	14	0	30	0	0	45
3283	16	0	30	0	0	45
3284	18	0	30	0	0	45
3285	20	0	30	0	0	45
3286	22	0	30	0	0	45
3287	24	0	30	0	0	45
3288	28	0	30	0	0	45
3289	32	0	30	0	0	45
3292	-4	0	30	0	0	45
3293	0	0	30	0	0	45
3294	2	0	30	0	0	45
3295	4	0	30	0	0	45
3296	6	0	30	0	0	45
3297	8	0	30	0	0	45
3298	10	0	30	0	0	46
3299	12	0	30	0	0	45
3300	14	0	30	0	0	45
3301	16	0	30	0	0	45
3302	18	0	30	0	0	45
3303	20	0	30	0	0	45
3304	22	0	30	0	0	45
3305	24	0	30	0	0	45
3306	28	0	30	0	0	45
3307	32	0	30	0	0	45

Table 2.5.1 (Cont.)
Part VII

F-15 TWIN FIN BUFFET STUDY
TAIL BUFFET MEASUREMENTS
DYNAMIC PRESSURE DATA ON TAILS

TPNS	AOA	BETA	Q (psf)	PLENUM PRESS. (psia)		
				NOSE	GUN BUMP	SM LD EDGE
3310	-4	4	30	0	0	45
3311	0	4	30	0	0	45
3312	2	4	30	0	0	45
3313	4	4	30	0	0	45
3314	6	4	30	0	0	45
3315	8	4	30	0	0	45
3316	10	4	30	0	0	45
3317	12	4	30	0	0	45
3318	14	4	30	0	0	45
3319	16	4	30	0	0	45
3320	18	4	30	0	0	45
3321	20	4	30	0	0	45
3322	22	4	30	0	0	45
3323	24	4	30	0	0	45
3324	28	4	30	0	0	45
3325	32	4	30	0	0	45
3328	-4	0	56	0	0	45
3329	0	0	56	0	0	45
3330	2	0	56	0	0	45
3331	4	0	56	0	0	45
3332	6	0	56	0	0	45
3333	8	0	56	0	0	45
3334	10	0	56	0	0	45
3335	12	0	56	0	0	45
3336	14	0	56	0	0	45
3337	16	0	56	0	0	45
3338	18	0	56	0	0	45
3339	20	0	56	0	0	45
3340	22	0	56	0	0	45
3341	24	0	56	0	0	45
3342	28	0	56	0	0	45
3343	32	0	56	0	0	45

TPNS	AOA	BETA	Q (psf)	PLENUM PRESS. (psia)		
				NOSE	GUN BUMP	SM LD EDGE
3346	-4	4	56	0	0	45
3347	0	4	56	0	0	45
3348	2	4	56	0	0	45
3349	4	4	56	0	0	45
3350	6	4	56	0	0	45
3351	8	4	56	0	0	45
3352	10	4	56	0	0	45
3353	12	4	56	0	0	45
3354	14	4	56	0	0	45
3355	16	4	56	0	0	45
3356	18	4	56	0	0	45
3357	20	4	56	0	0	45
3358	22	4	56	0	0	45
3359	24	4	56	0	0	45
3360	28	4	56	0	0	45
3361	32	4	56	0	0	45
3364	-4	-4	56	0	0	45
3365	0	-4	56	0	0	45
3366	2	-4	56	0	0	45
3367	4	-4	56	0	0	45
3368	6	-4	56	0	0	45
3369	8	-4	56	0	0	45
3370	10	-4	56	0	0	45
3371	12	-4	56	0	0	45
3372	14	-4	56	0	0	45
3373	16	-4	56	0	0	45
3374	18	-4	56	0	0	45
3375	20	-4	56	0	0	45
3376	22	-4	56	0	0	45
3377	24	-4	56	0	0	45
3378	28	-4	56	0	0	45
3379	32	-4	56	0	0	45

Table 2.5.1 (Cont.)
Part VIII

F-15 TWIN FIN BUFFET STUDY
TAIL BUFFET MEASUREMENTS
DYNAMIC PRESSURE DATA ON TAILS

TPNS	AOA	BETA	Q (psf)	PLENUM PRESS (psia)		
				NOSE	GUN BUMP	SM LD EDGE
3382	-4	2	56	0	0	45
3383	0	2	56	0	0	45
3384	2	2	56	0	0	45
3385	4	2	56	0	0	45
3386	6	2	56	0	0	45
3387	8	2	56	0	0	45
3388	10	2	56	0	0	45
3389	12	2	56	0	0	45
3390	14	2	56	0	0	45
3391	16	2	56	0	0	45
3392	18	2	56	0	0	45
3393	20	2	56	0	0	45
3394	22	2	56	0	0	45
3395	24	2	56	0	0	45
3396	28	2	56	0	0	45
3397	32	2	56	0	0	45

TPNS	AOA	BETA	Q (psf)	PLENUM PRESS (psia)		
				NOSE	GUN BUMP	SM LD EDGE
3400	-4	-2	56	0	0	45
3401	0	-2	56	0	0	45
3402	2	-2	56	0	0	45
3403	4	-2	56	0	0	45
3404	6	-2	56	0	0	45
3405	8	-2	56	0	0	45
3406	10	-2	56	0	0	45
3407	12	-2	56	0	0	45
3408	14	-2	56	0	0	45
3409	16	-2	56	0	0	45
3410	18	-2	56	0	0	45
3411	20	-2	56	0	0	45
3412	22	-2	56	0	0	45
3413	24	-2	56	0	0	45
3414	28	-2	56	0	0	45
3415	32	-2	56	0	0	45

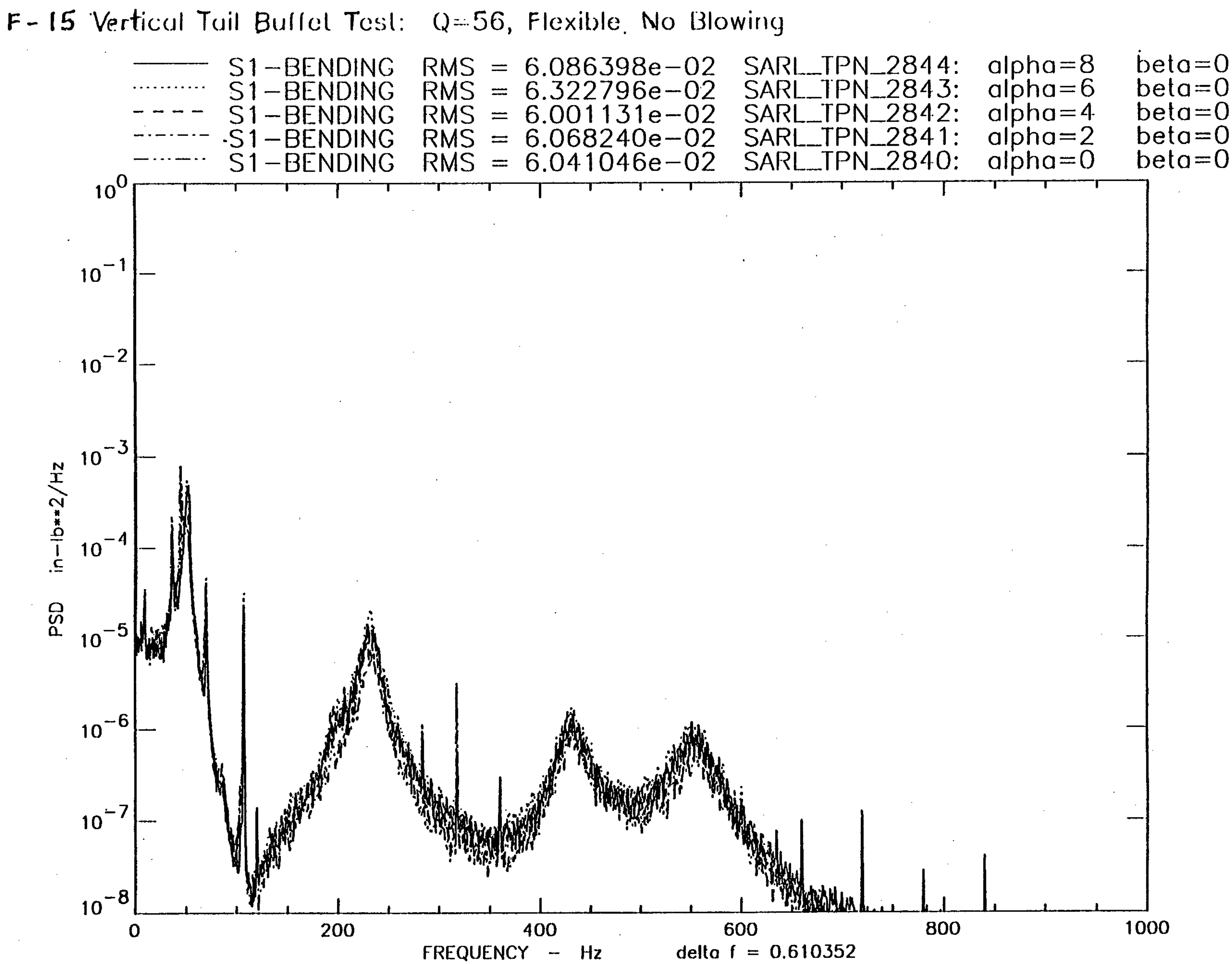

Figure 3.1.1 Flexible Tail, Bending PSD, Q=56 PSF, No Blowing, Beta= 0, Alpha Sweep

Part 1 0 - 8 Deg.

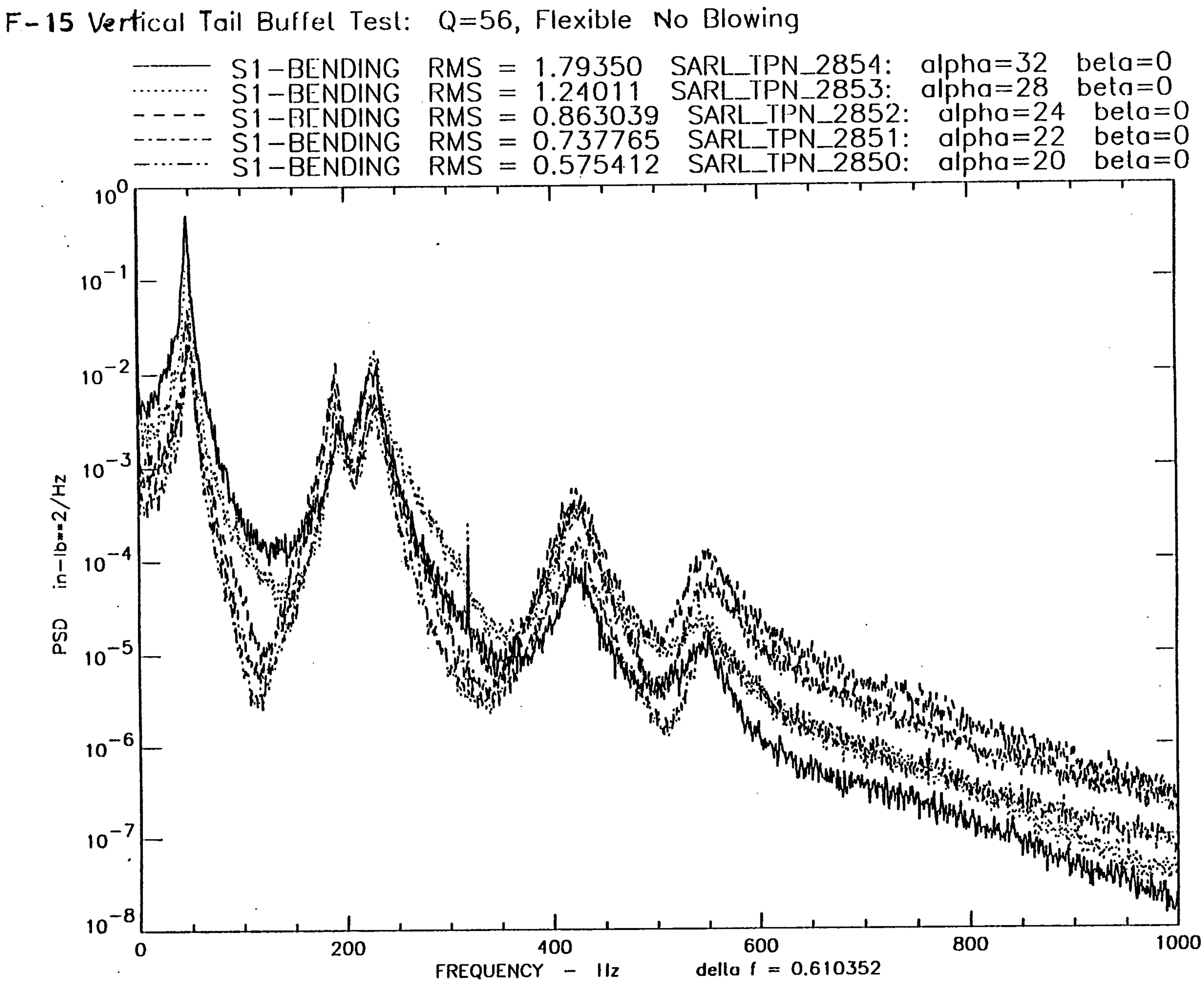

Figure 3.1.1 Flexible Tail, Bending PSD, Q=56 PSF, No Blowing, Beta= 0, Alpha Sweep

Part 2 20- 32 Deg.

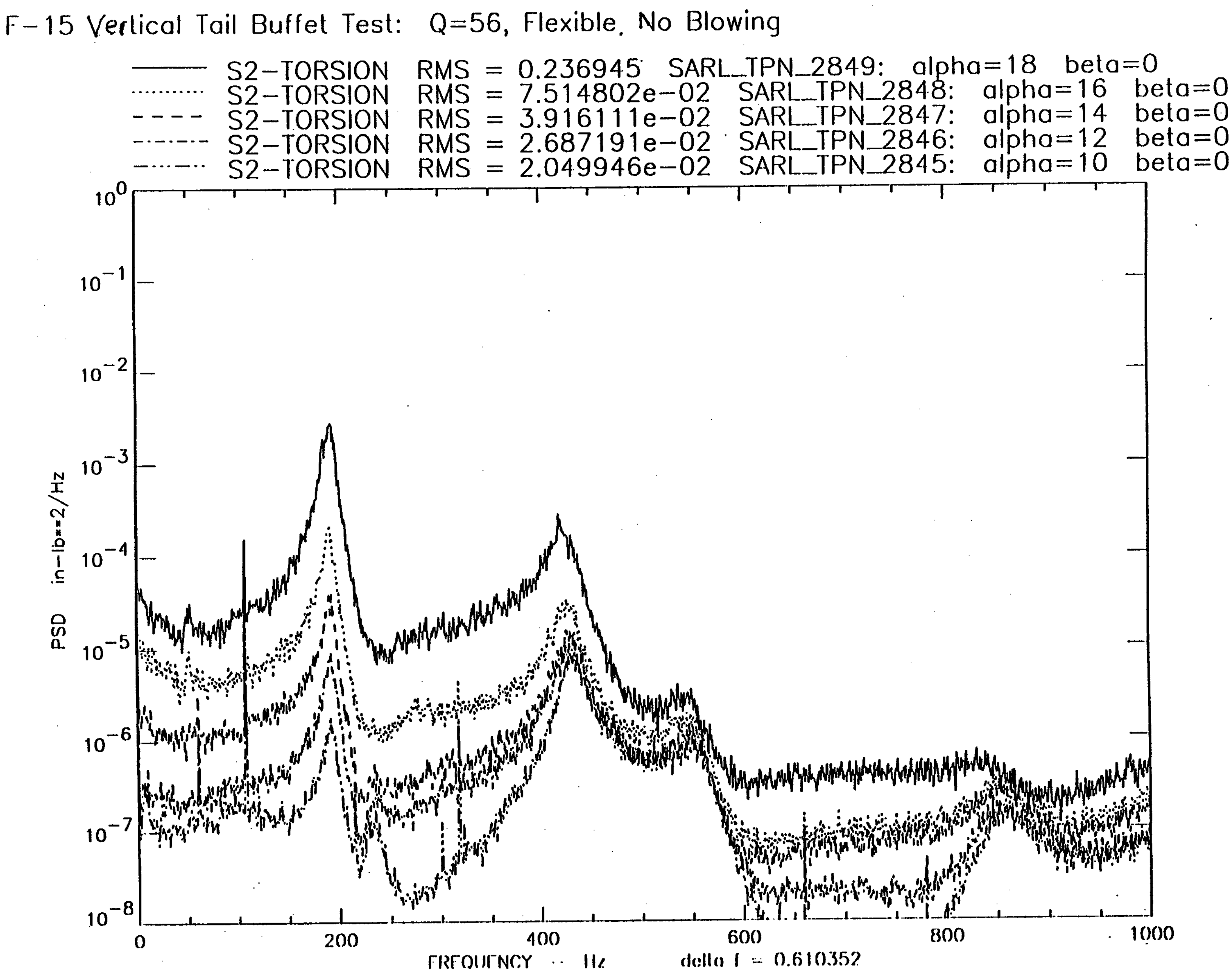

Figure 3.1.2 Flexible Tail, Torsion PSD, Q=56 PSF, No Blowing, Beta= 0, Alpha Sweep

Part 1 10 -18 Deg.

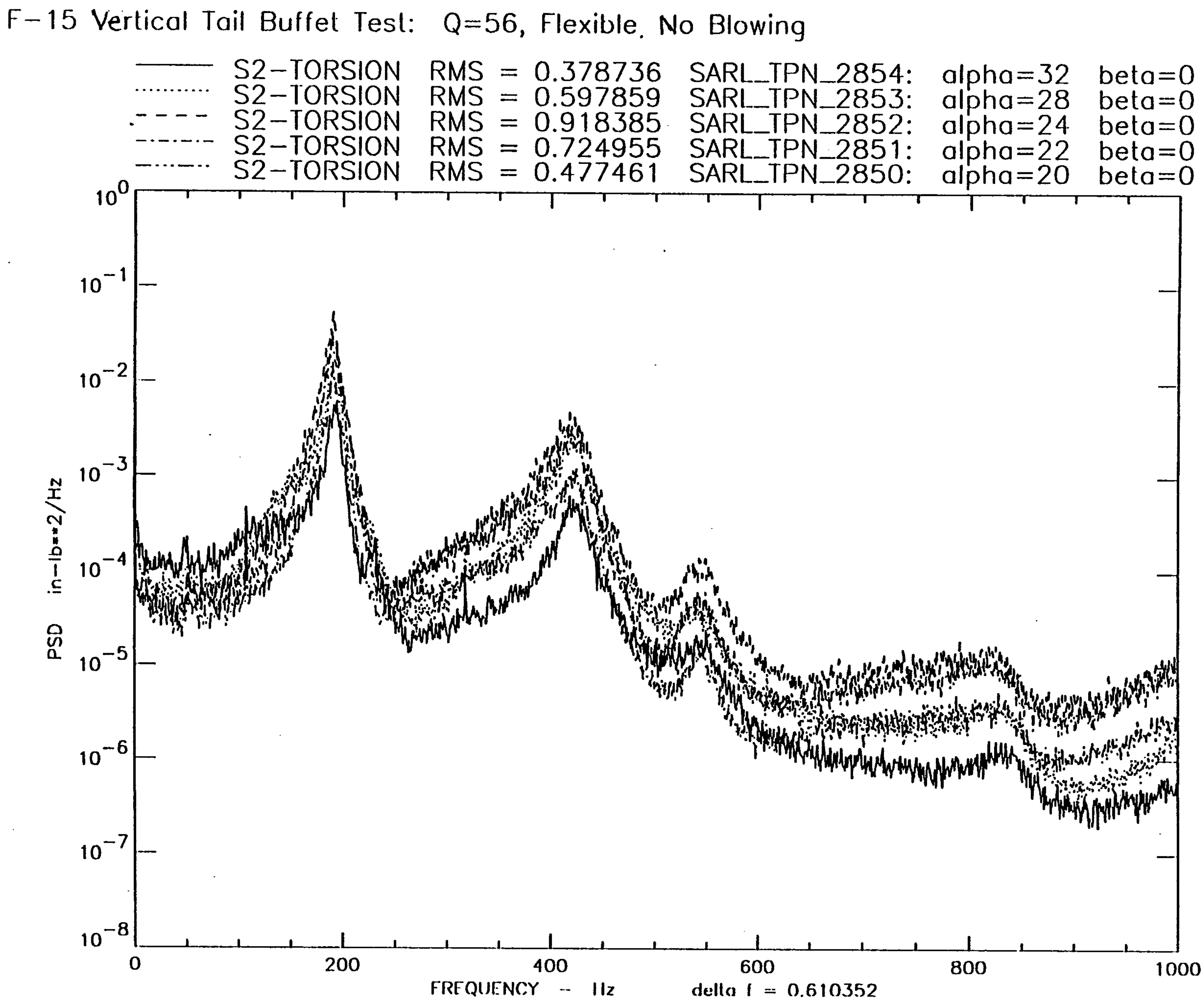

Figure 3.1.2 Flexible Tail, Torsion PSD, Q=56 PSF, No Blowing, Beta= 0, Alpha Sweep Part 2 20- 32 Deg

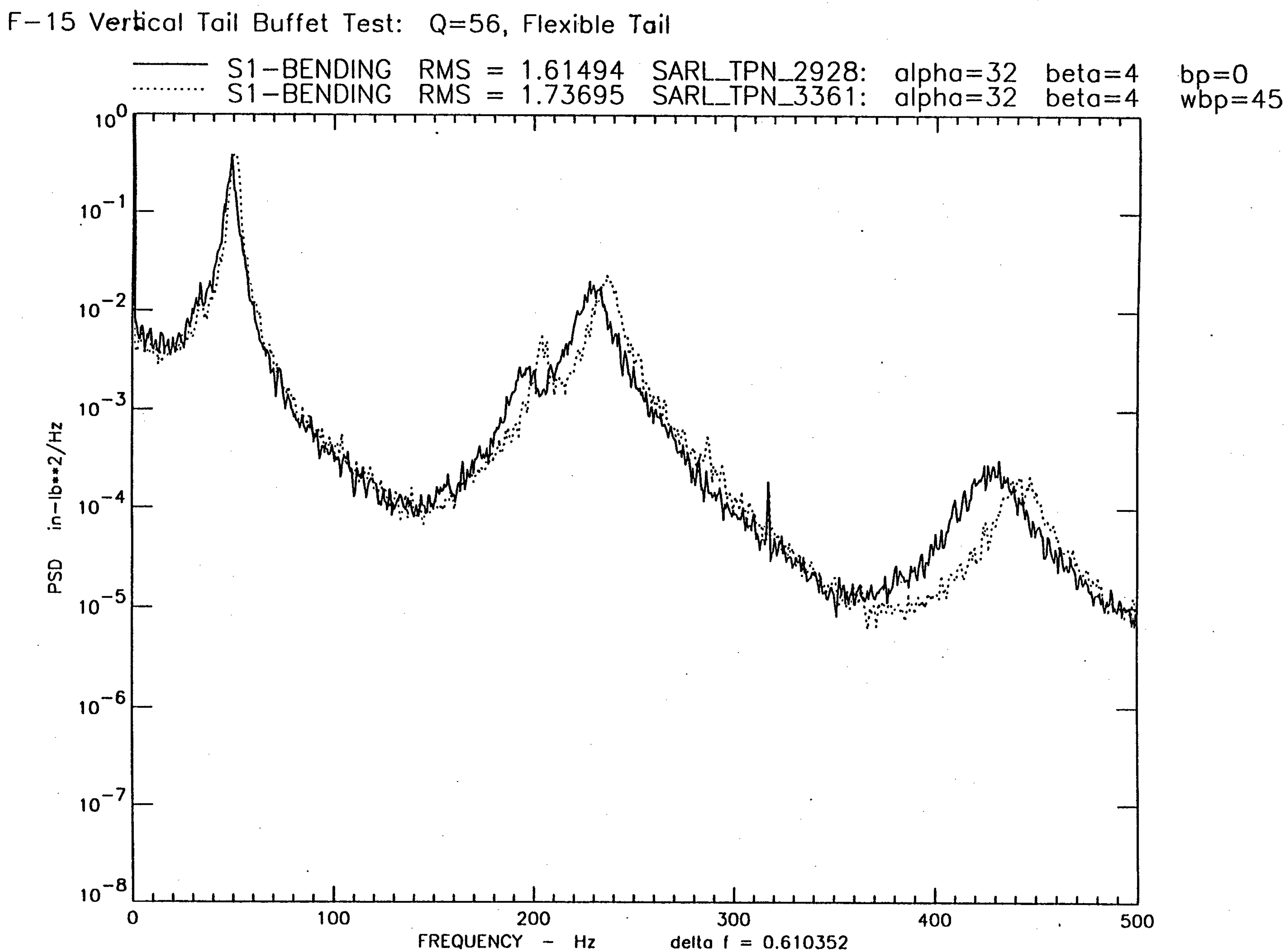

Figure 3.1.3 Flexible Tail, Bending PSD, Q= 56 PSF, Alpha= 32 Deg., Beta = 4 Deg., WBP = 0, 45 Psi

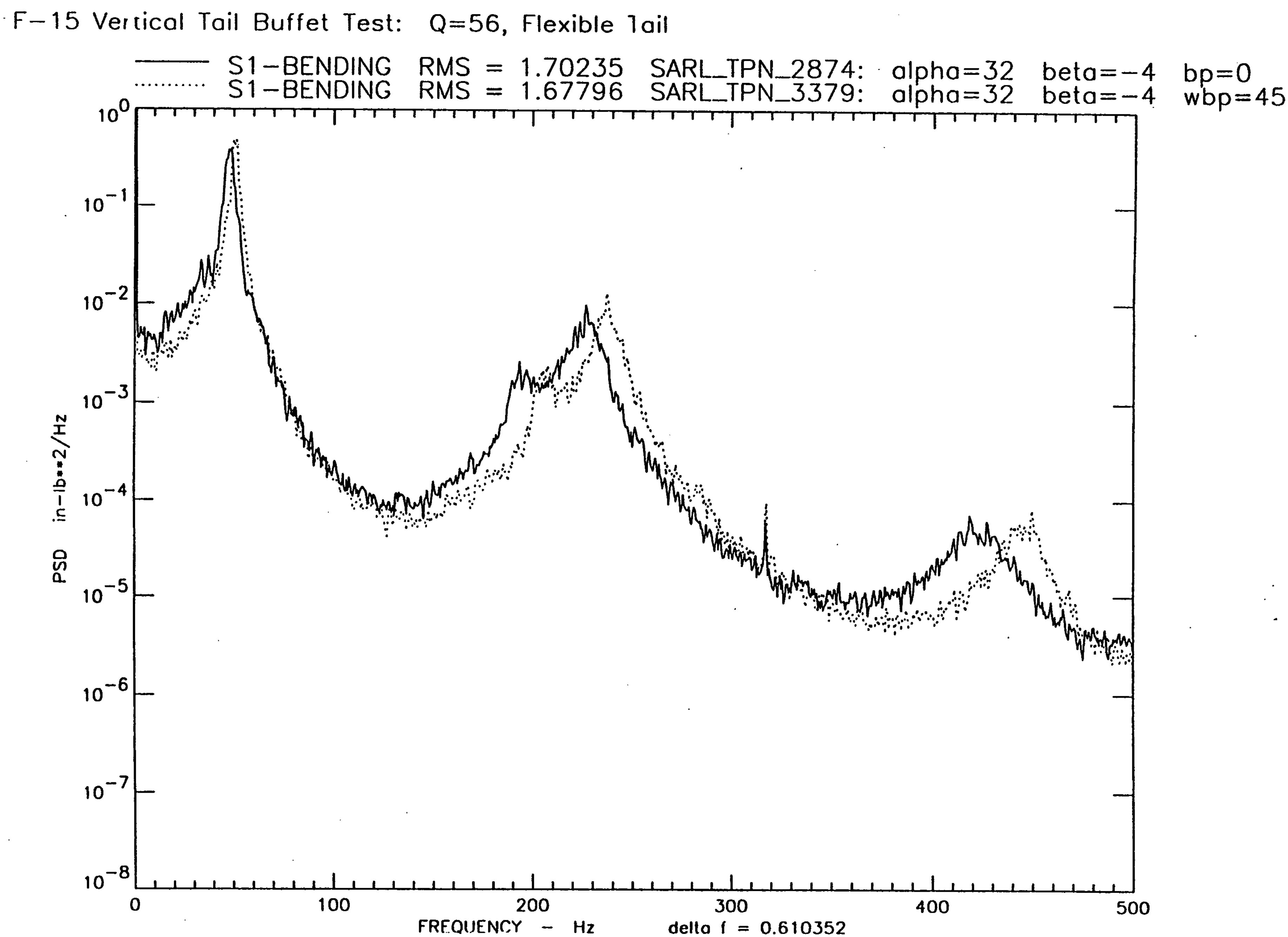

Figure 3.1.4 Flexible Tail, Bending PSD, Q= 56 PSF, Alpha= 32 Deg., Beta = - 4 Deg., WBP = 0, 45 Psi

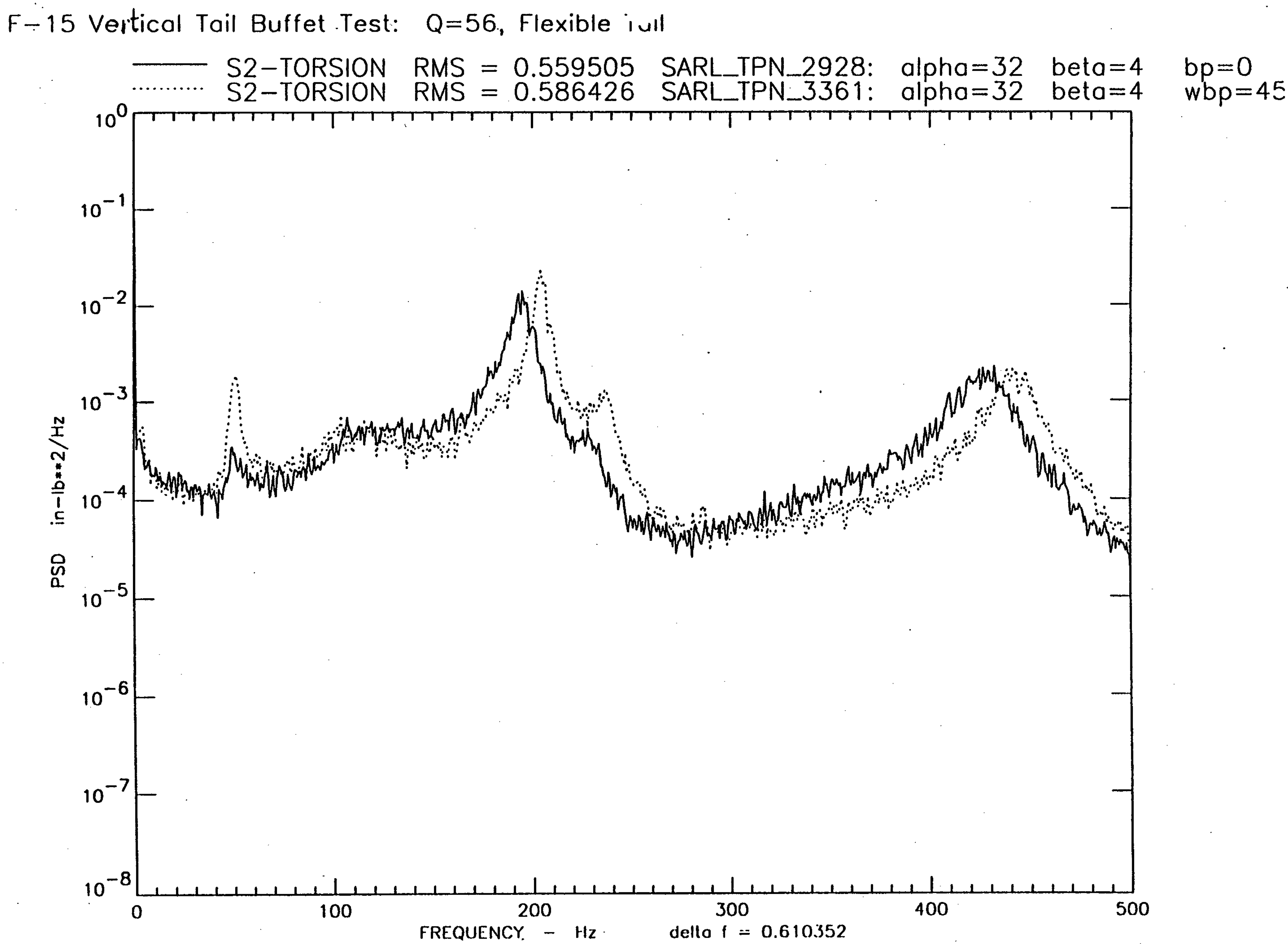

Figure 3.1.5 Flexible Tail, Torsion PSD, Q= 56 PSF, Alpha= 32 Deg., Beta = 4 Deg., WBP = 0, 45 Psi

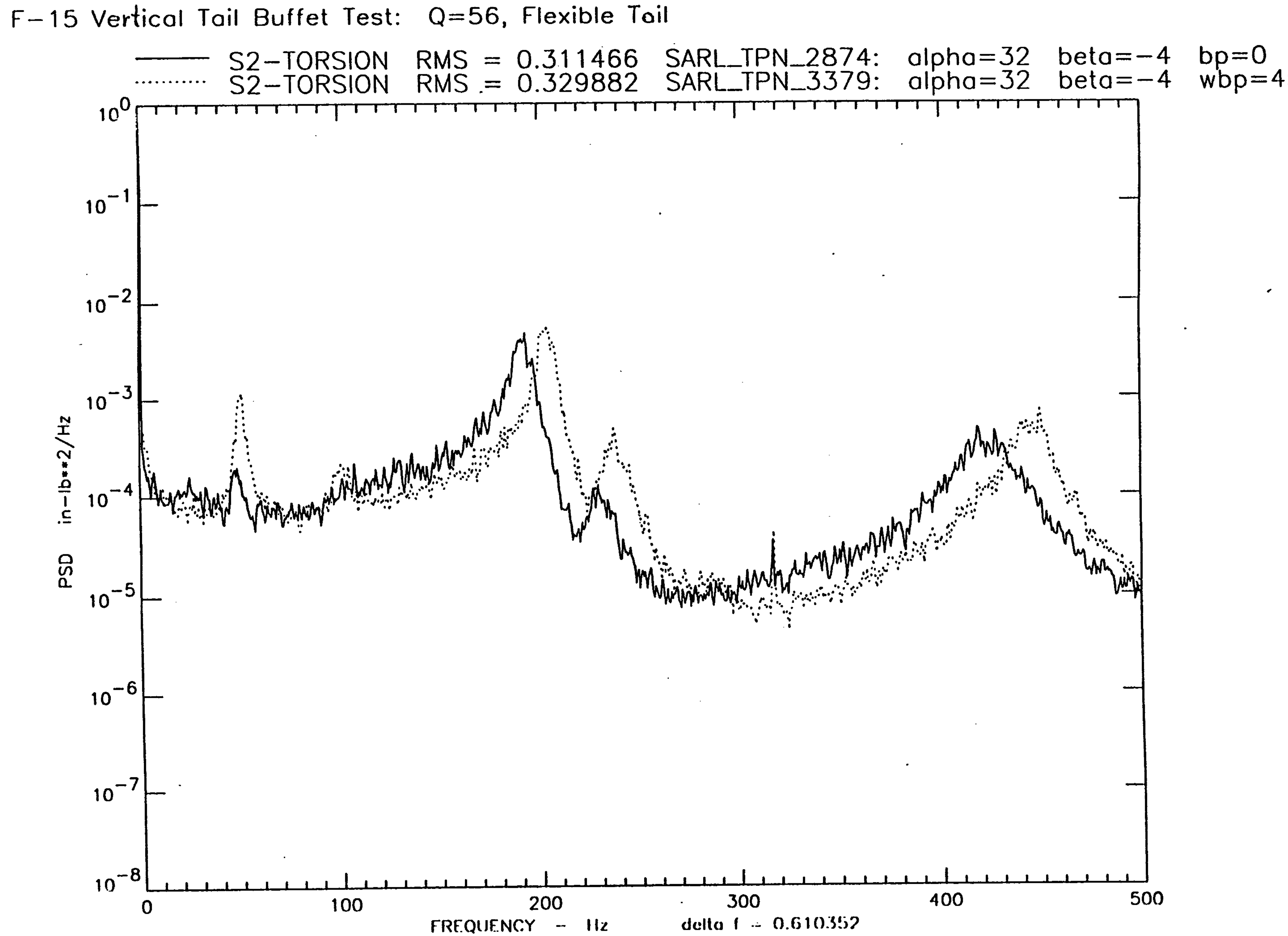

Figure 3.1.6 Flexible Tail, Torsion PSD, Q= 56 PSF, Alpha= 32 Deg., Beta = - 4 Deg., WBP = 0, 45 Psi

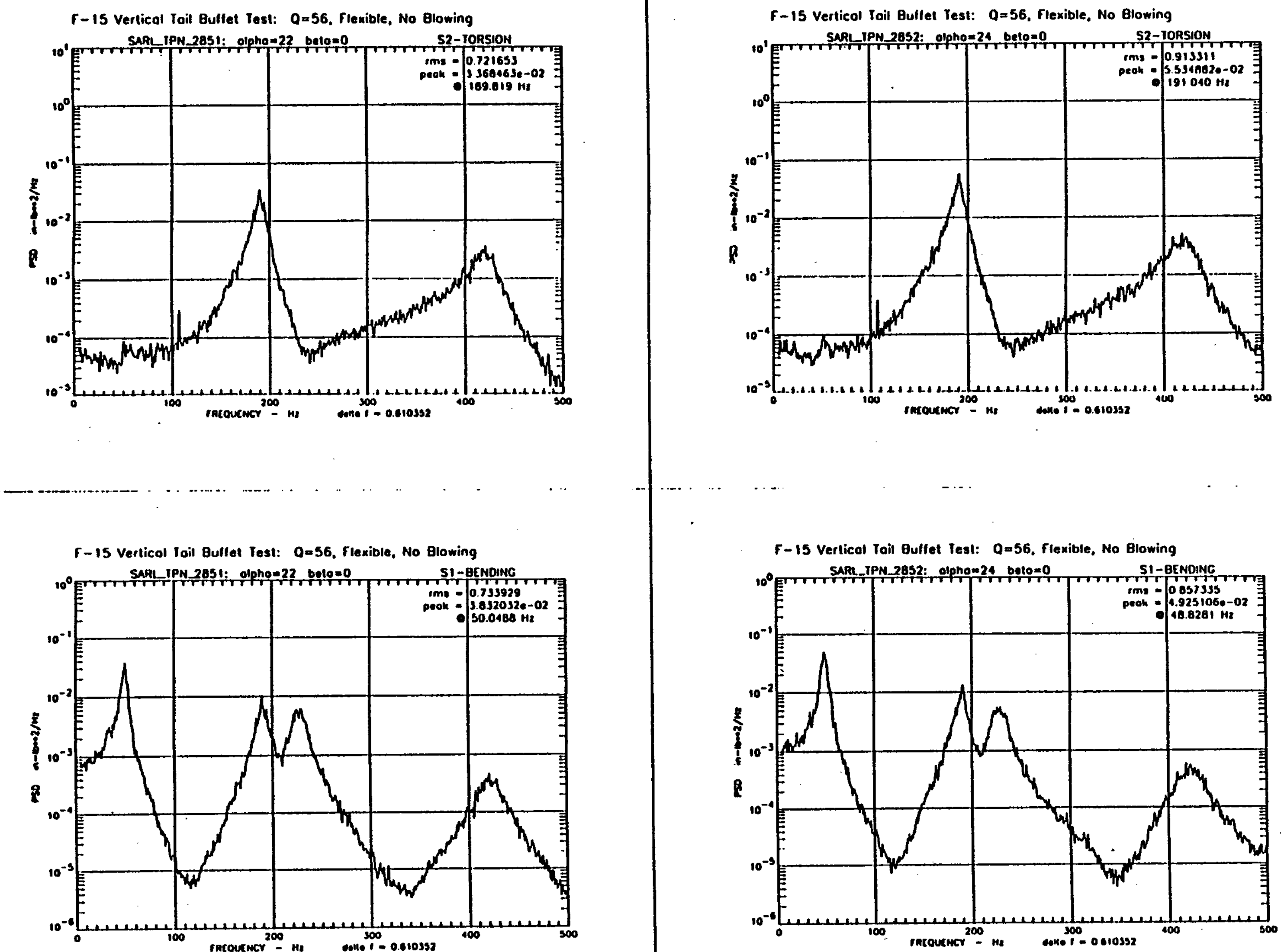

Figure 3.1.7 Flexible Tail PSD's - Bending and Torsion Comparisons, Q = 56 PSF, Beta = 0

Part 1 No Blowing, Alpha = 22 & 24 Deg

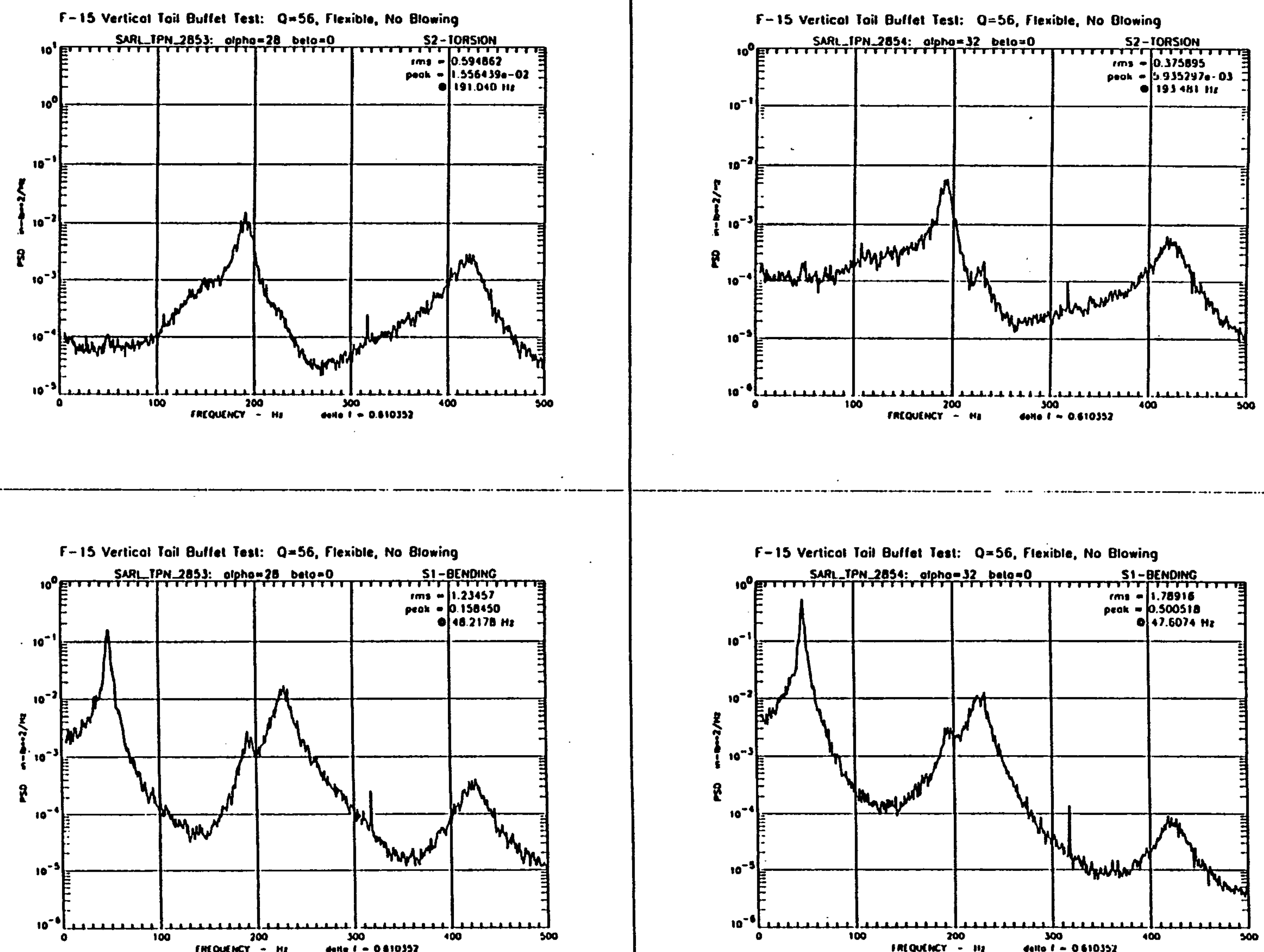

Figure 3.1.7 Flexible Tail PSD's - Bending and Torsion Comparisons, Q = 56 PSF, Beta = 0

Part 2 No Blowing, Alpha = 28 & 32 Deg.

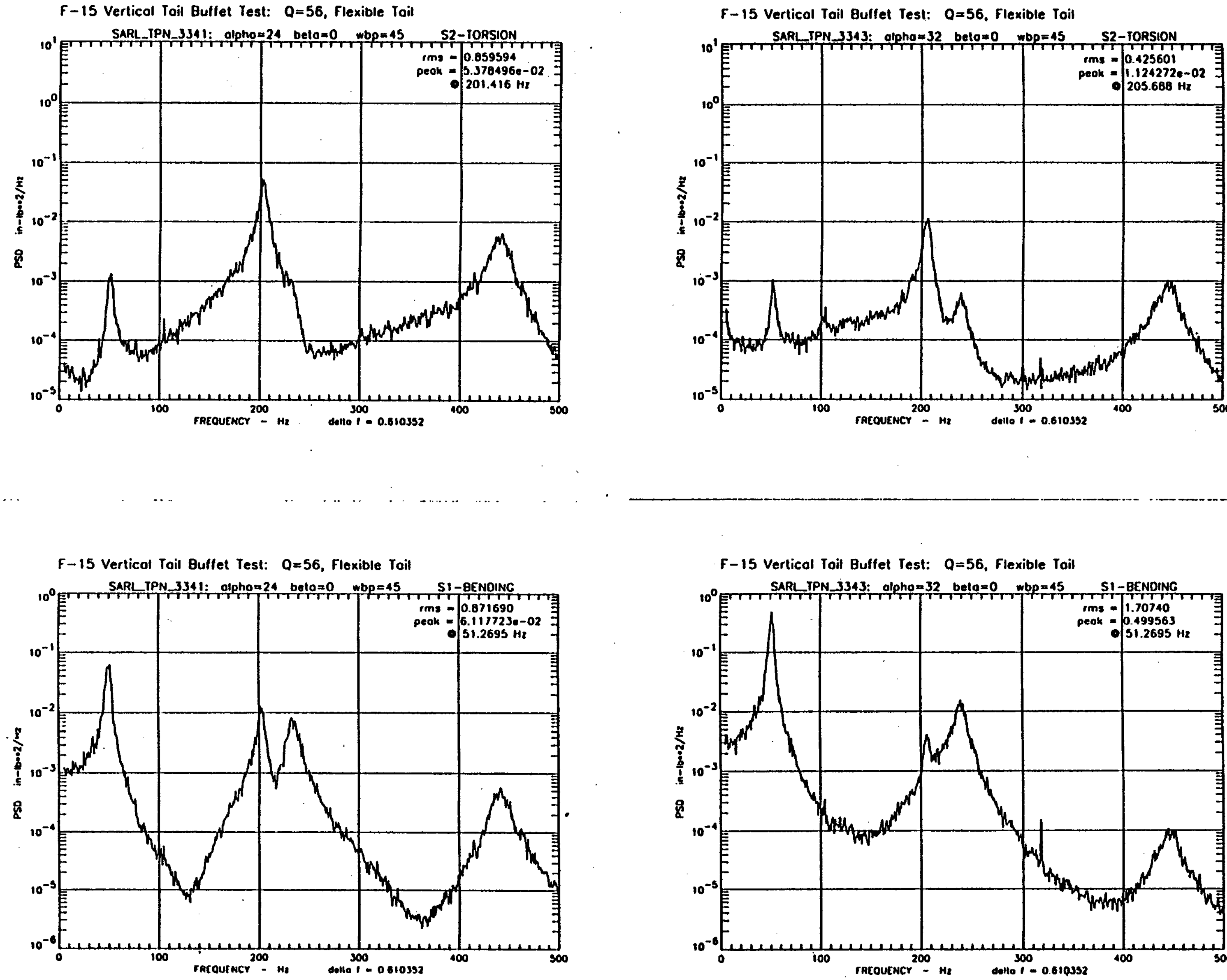

Figure 3.1.7 Flexible Tail PSD's - Bending and Torsion Comparisons, Q = 56 PSF, Beta = 0

Part 3 WBP = 45 Psi, Alpha = 24 & 32 Deg.

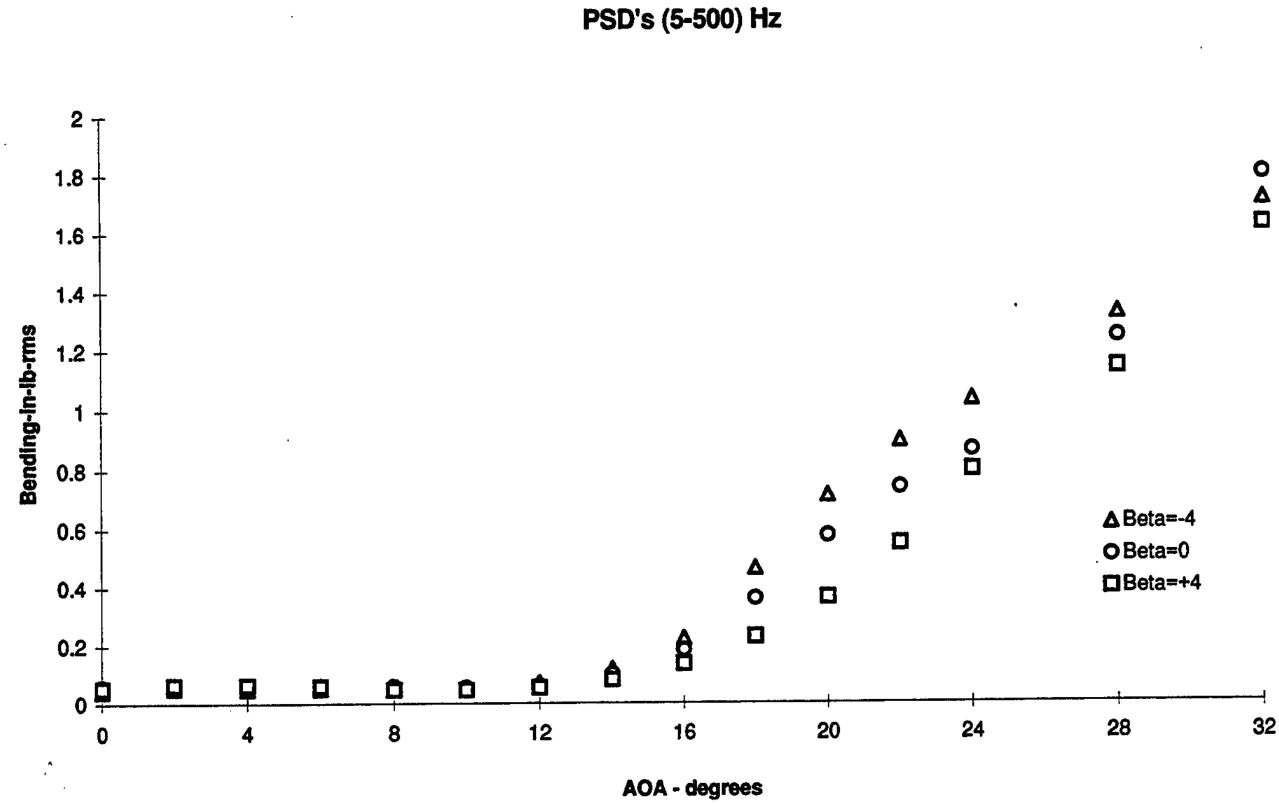

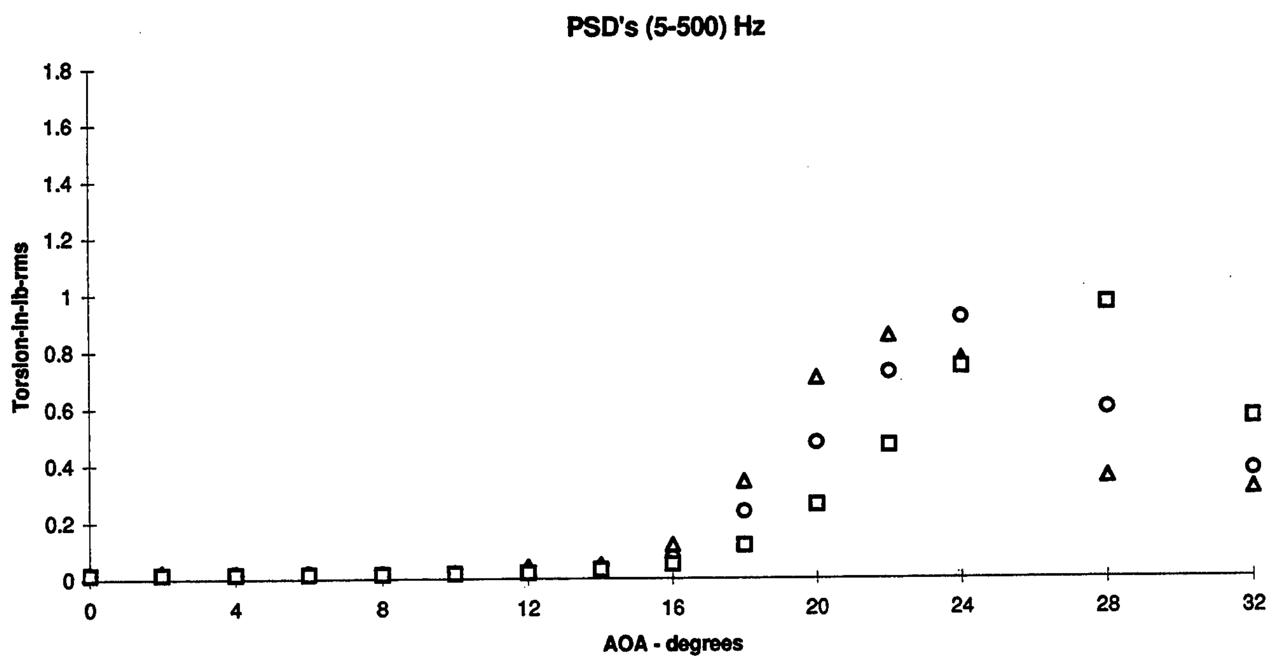

**Figure 3.1.8 - Flex Tail Response vs Angle of Attack
Bending and Torsion, Q = 56 psf, No Blowing**

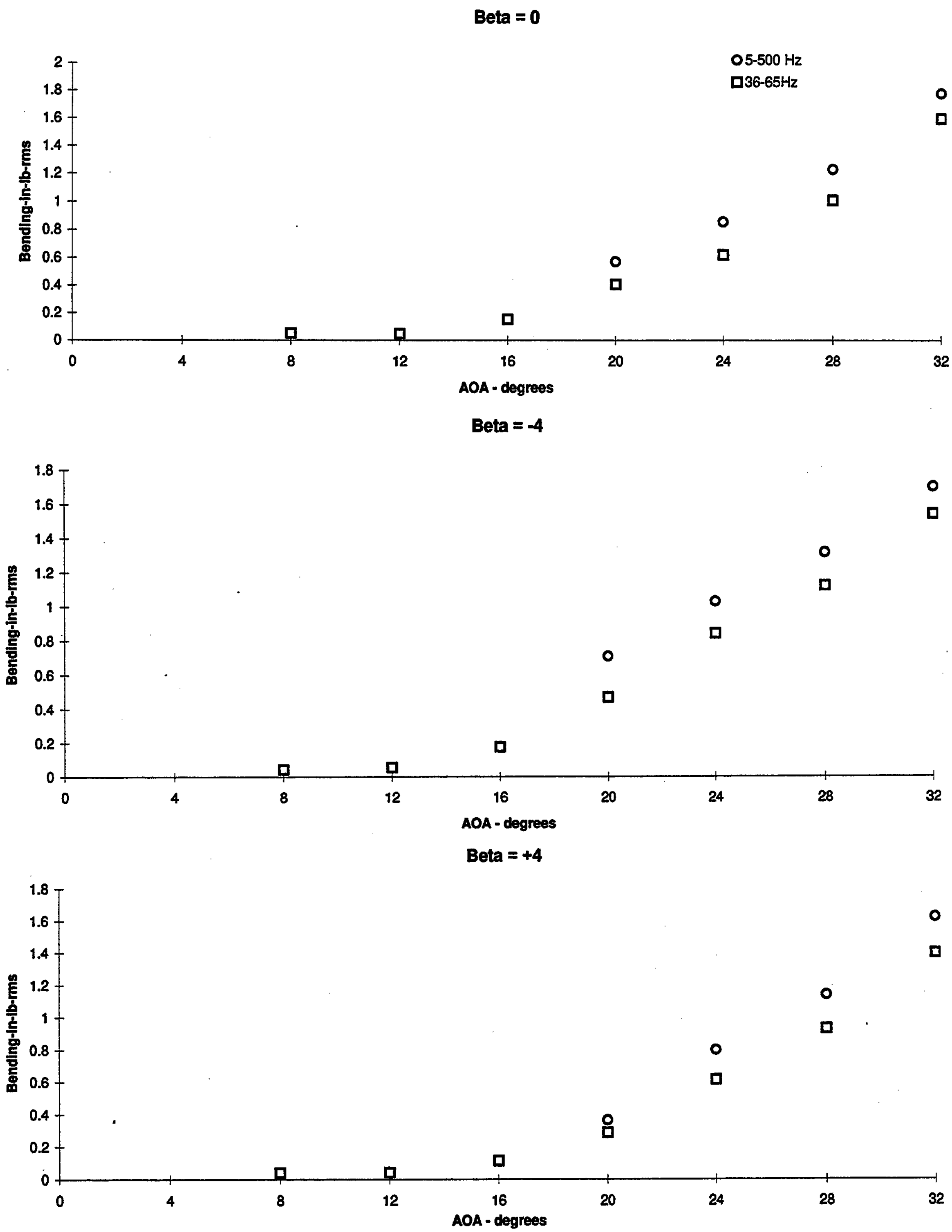

Figure 3.1.9 - Flex Tail Response vs Angle of Attack
Bending, Q = 56 psf, No Blowing

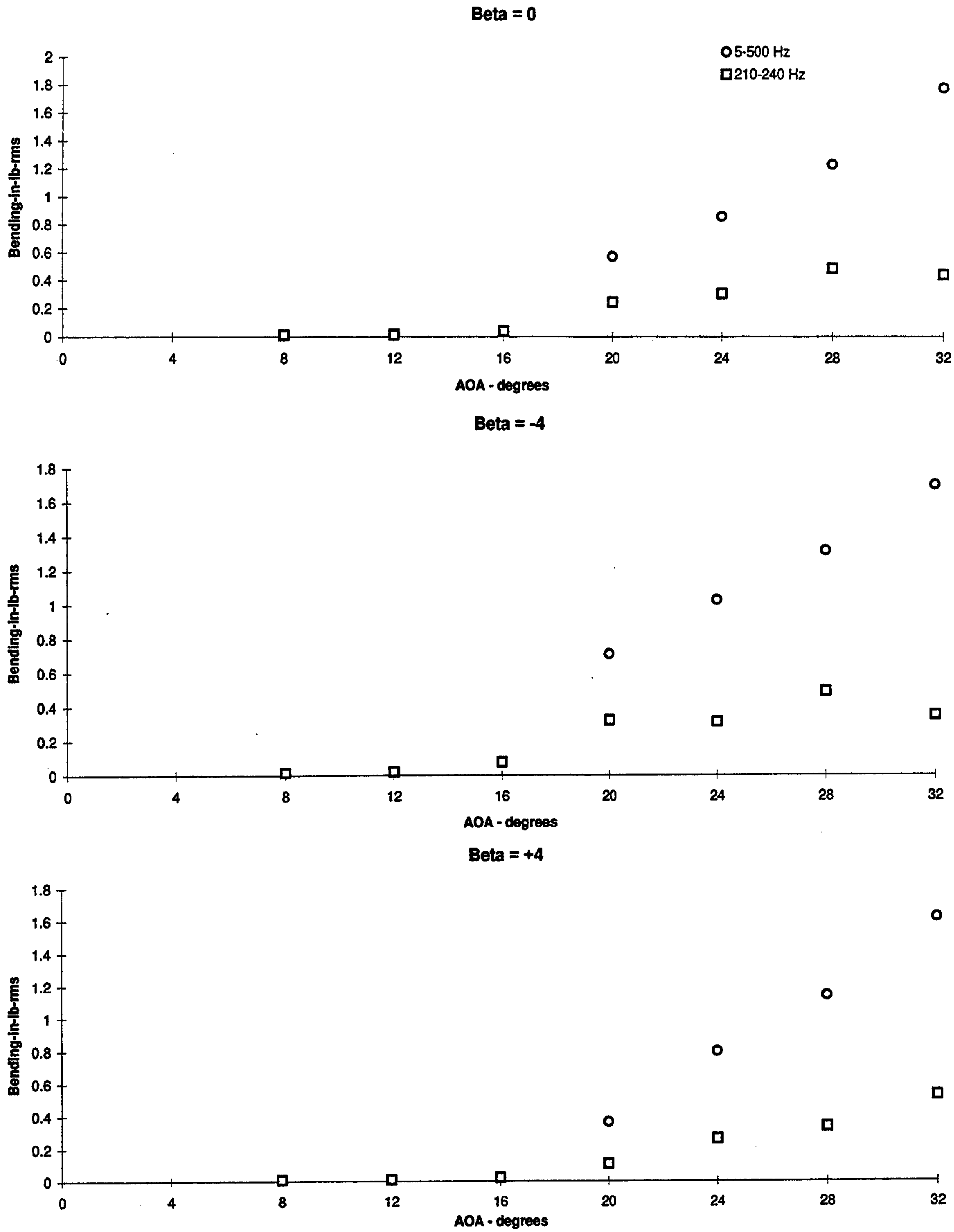

Figure 3.1.10 - Flex Tail Response vs Angle of Attack
Bending, Q = 56 psf, No Blowing

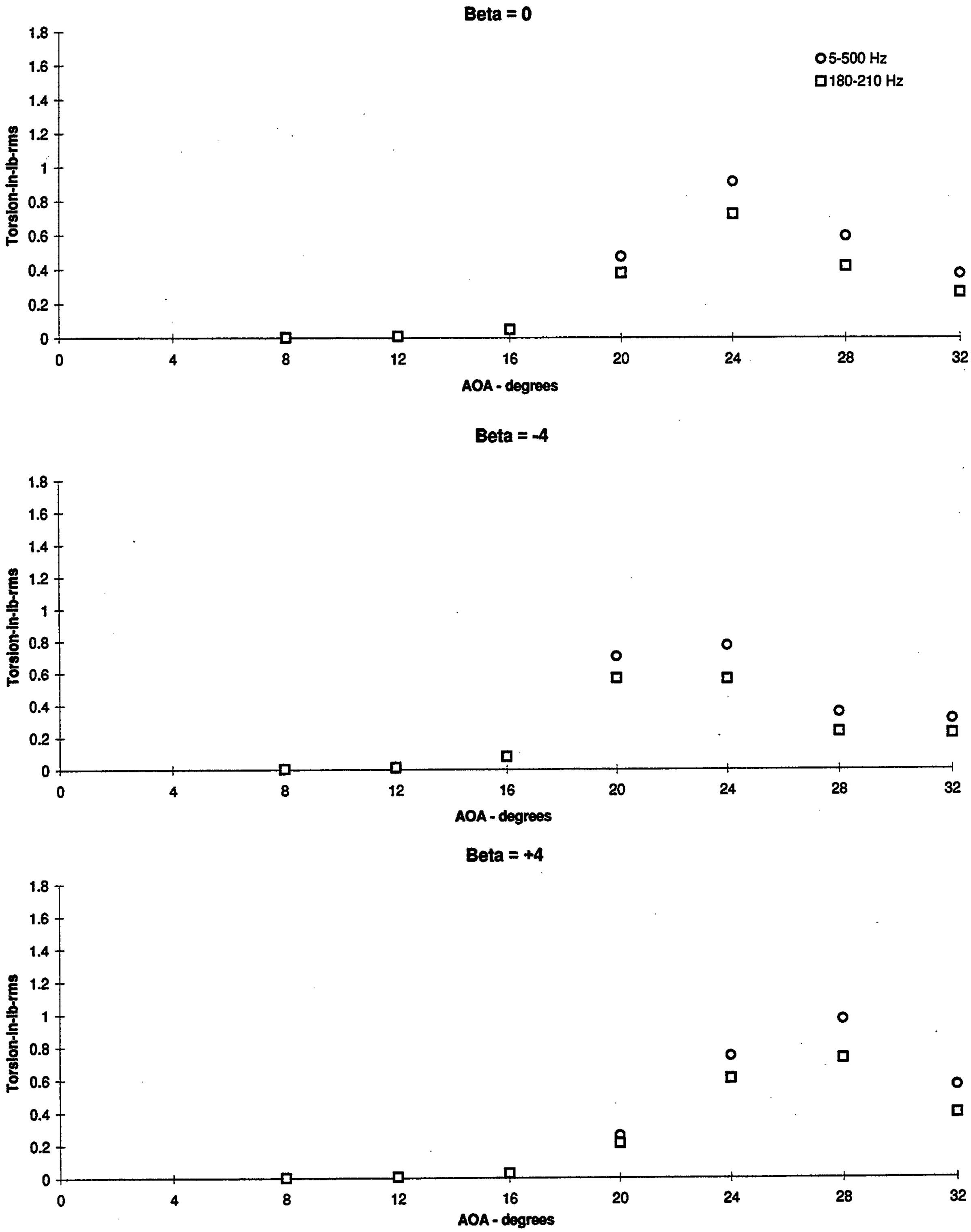

Figure 3.1.11 - Flex Tail Response vs Angle of Attack
Torsion, Q = 56 psf, No Blowing

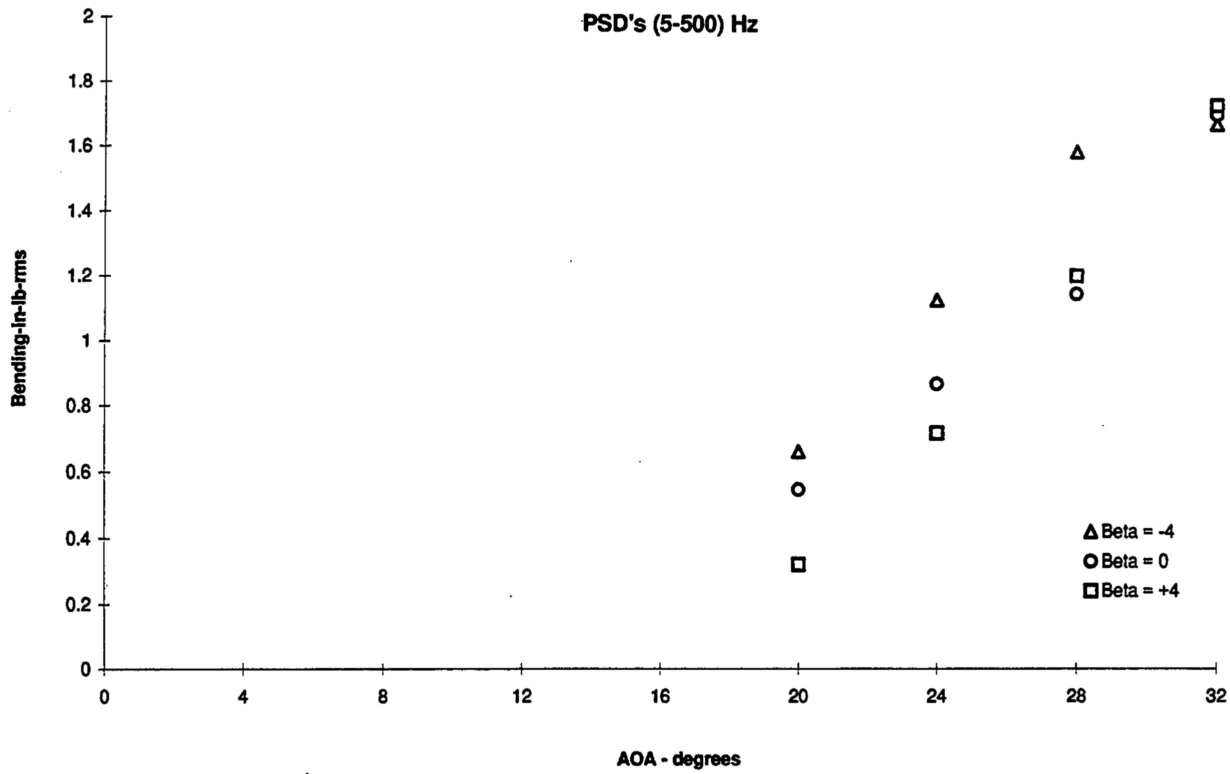

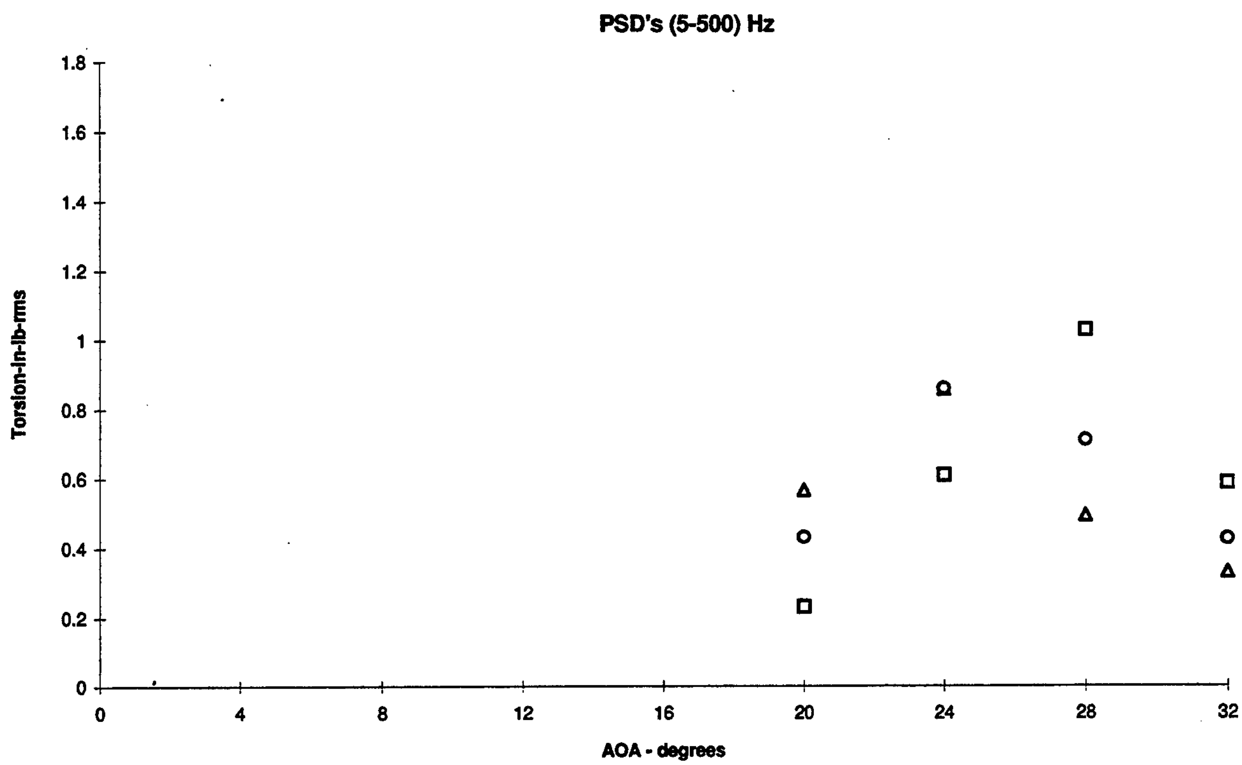

Figure 3.1.12 - Flex Tail Response vs Angle of Attack
Bending and Torsion, Q = 56 psf, Wing Blowing p = 45 psi

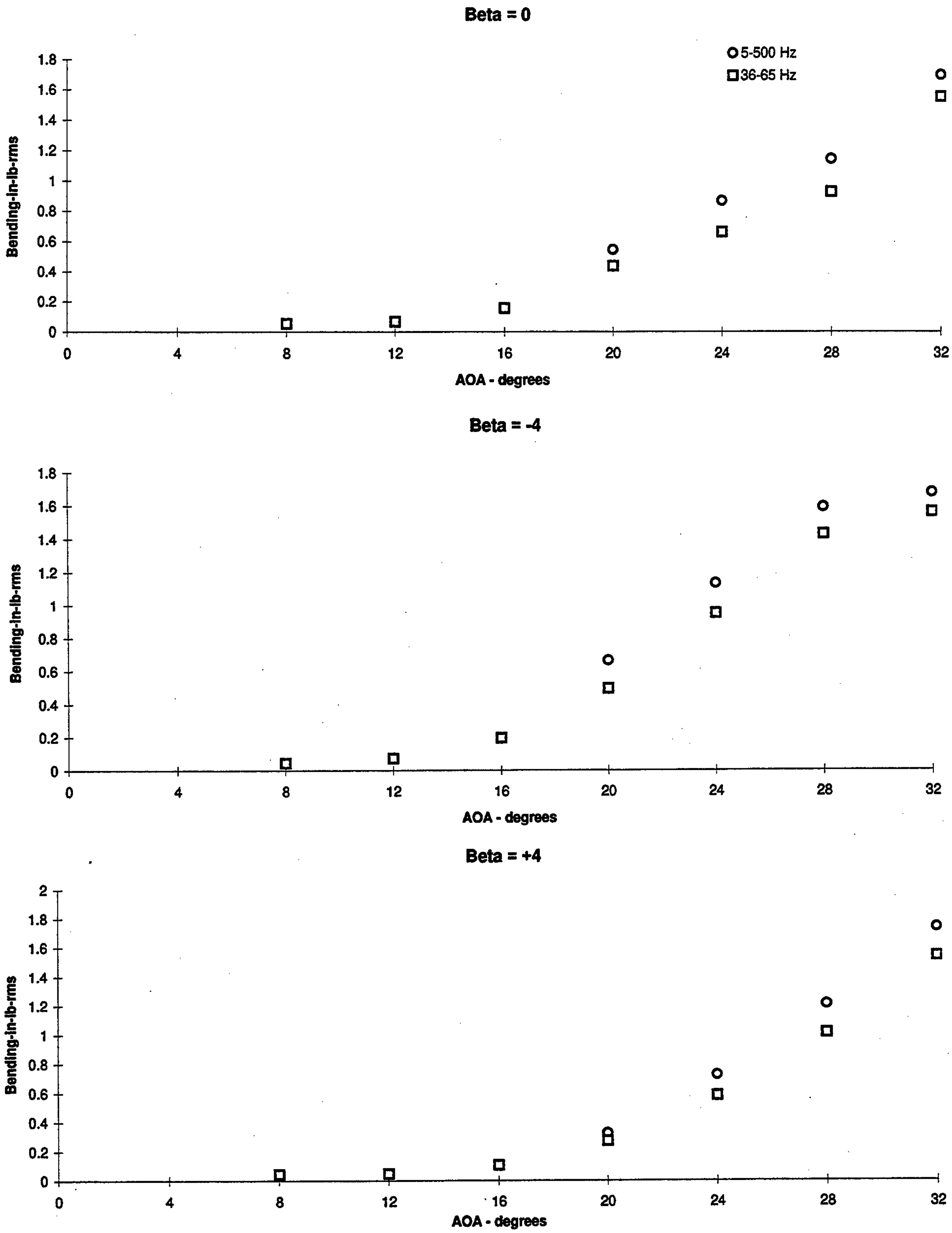

Figure 3.1.13 - Flex Tail Response vs Angle of Attack
Bending, Q = 56 psf, Wing Blowing p = 45 psi

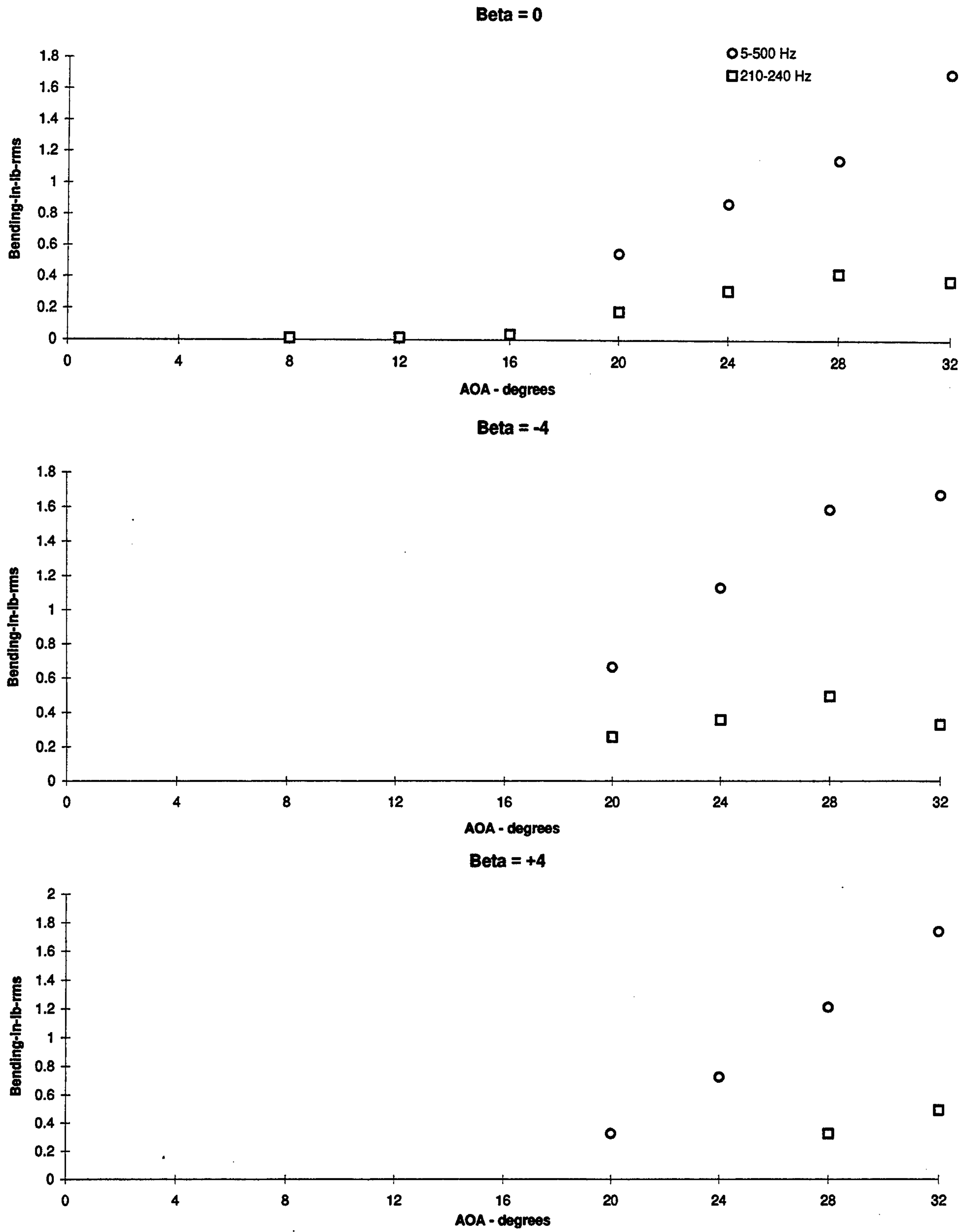

Figure 3.1.14 - Flex Tail Response vs Angle of Attack
Bending, Q = 56 psf, Wing Blowing p = 45 psi

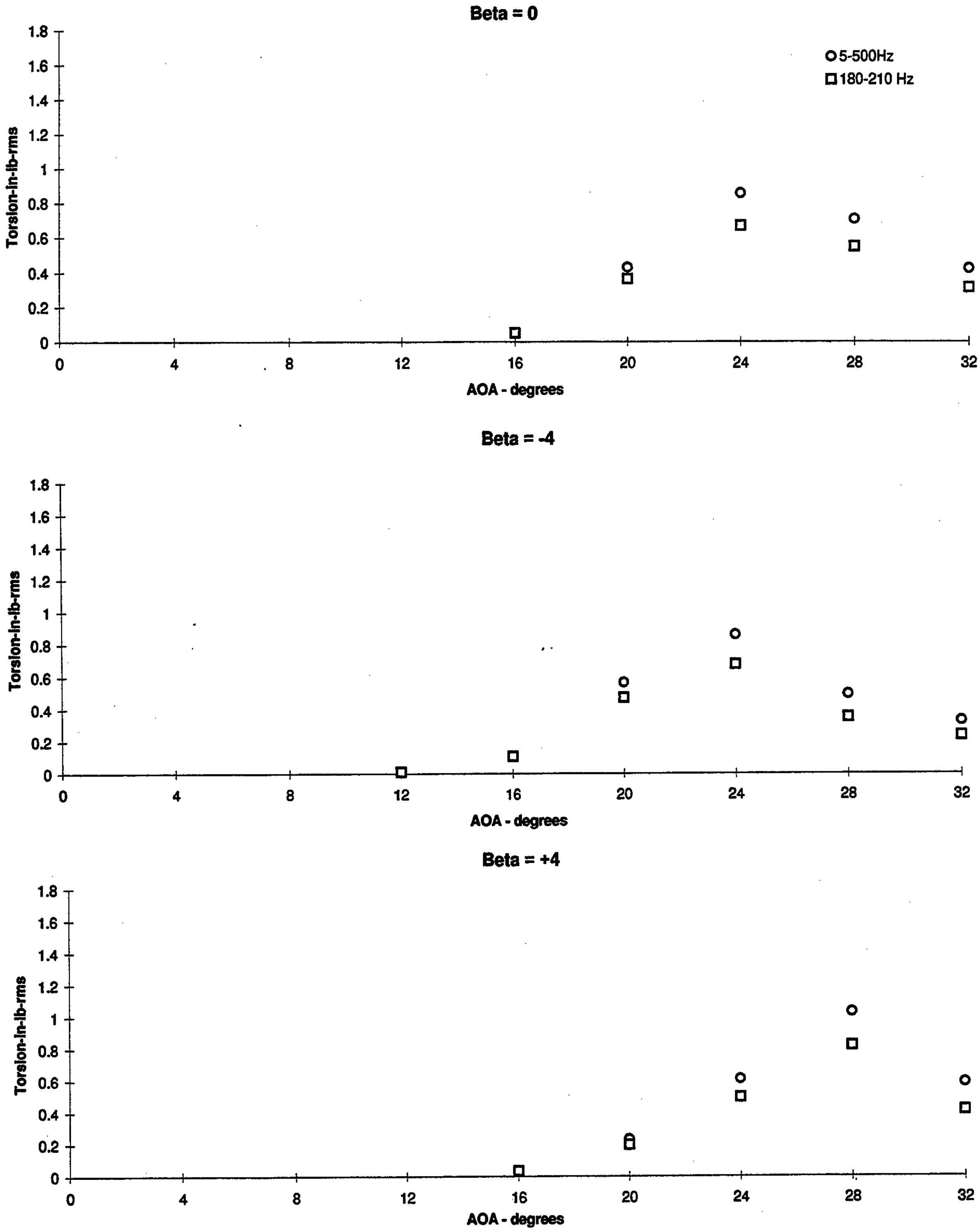

Figure 3.1.15 - Flex Tail Response vs Angle of Attack
Torsion, Q = 56 psf, Wing Blowing p = 45 psi

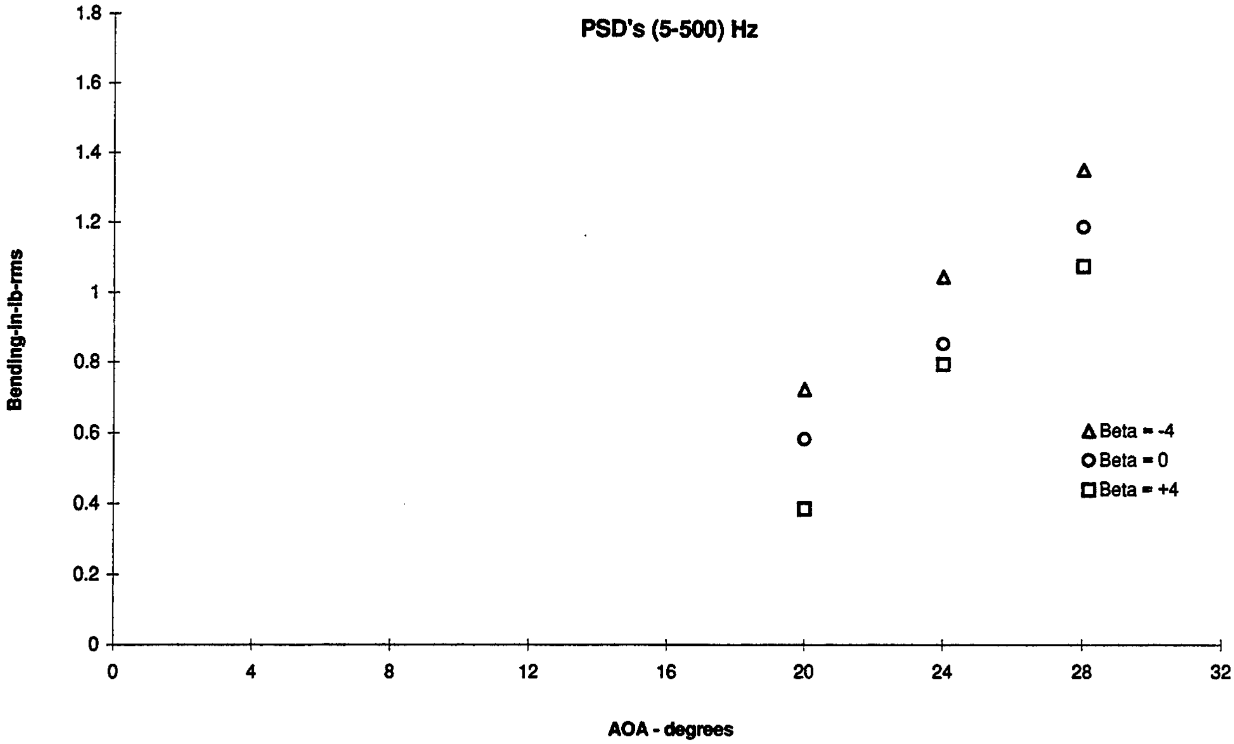

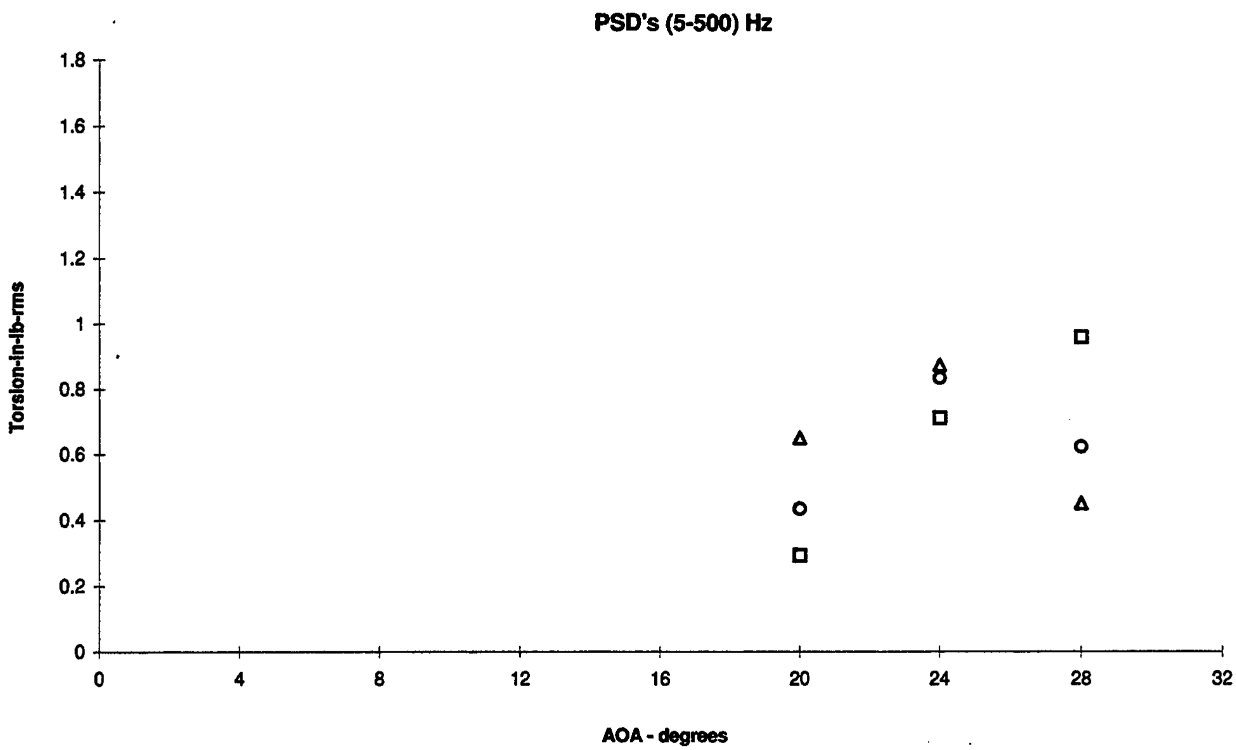

Figure 3.1.16 - Flex Tail Response vs Angle of Attack
Bending and Torsion, Q = 56 psf, Wing Blowing p = 65 psi

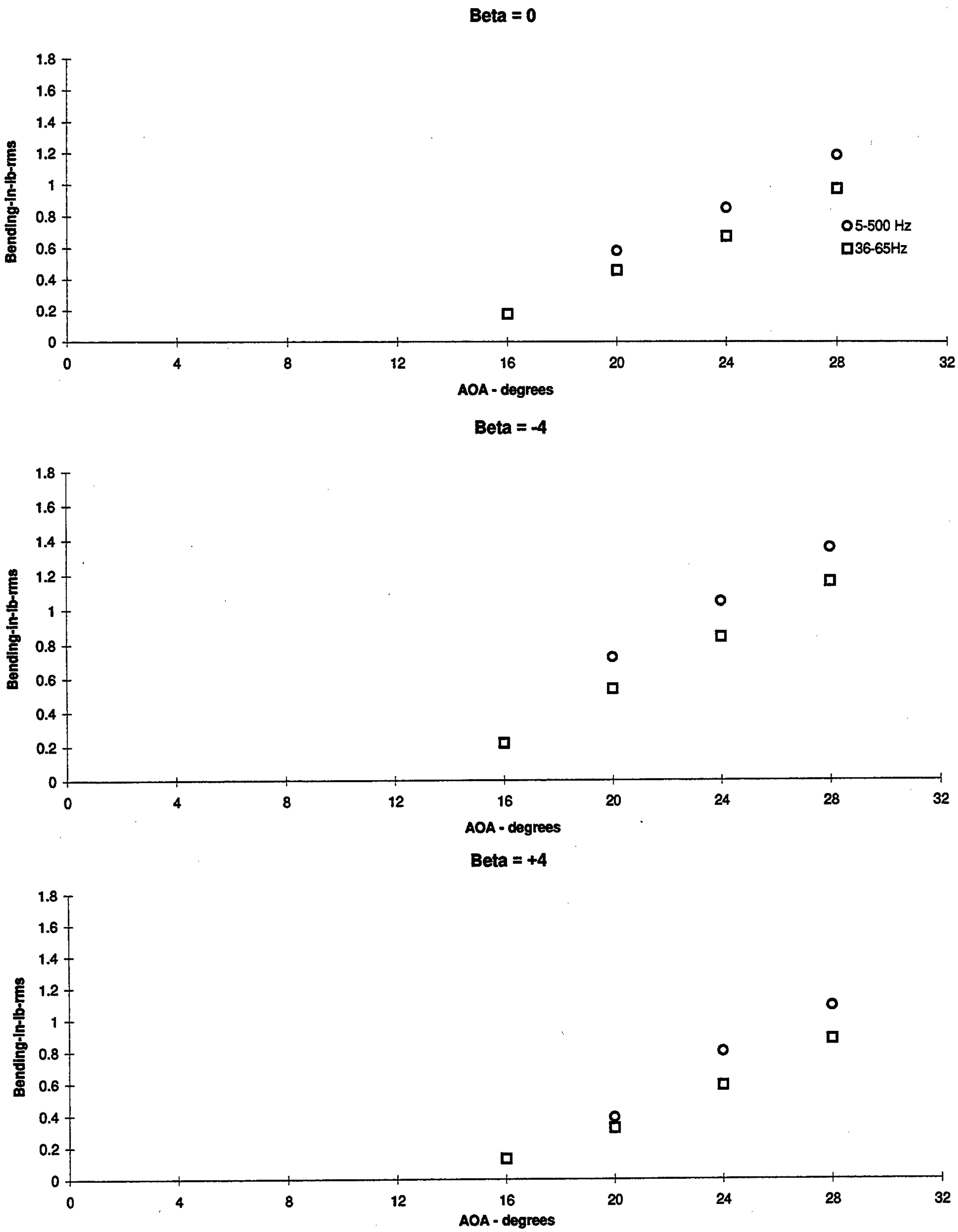

Figure 3.1.17 - Flex Tail Response vs Angle of Attack
Bending, Q = 56 psf, Wing Blowing p = 65 psi

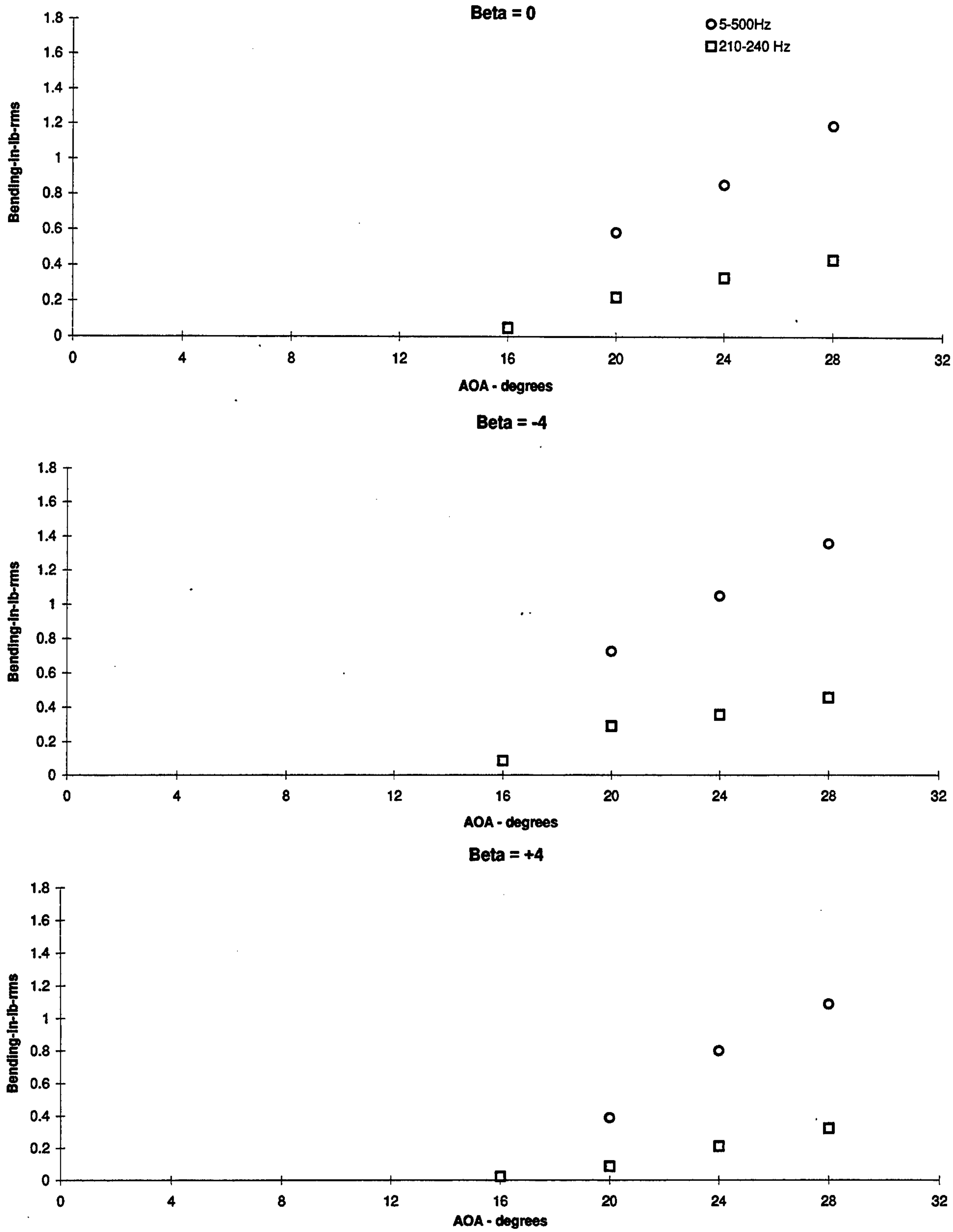

Figure 3.1.18 - Flex Tail Response vs Angle of Attack
Bending, Q = 56 psf, Wing Blowing p = 65 psi

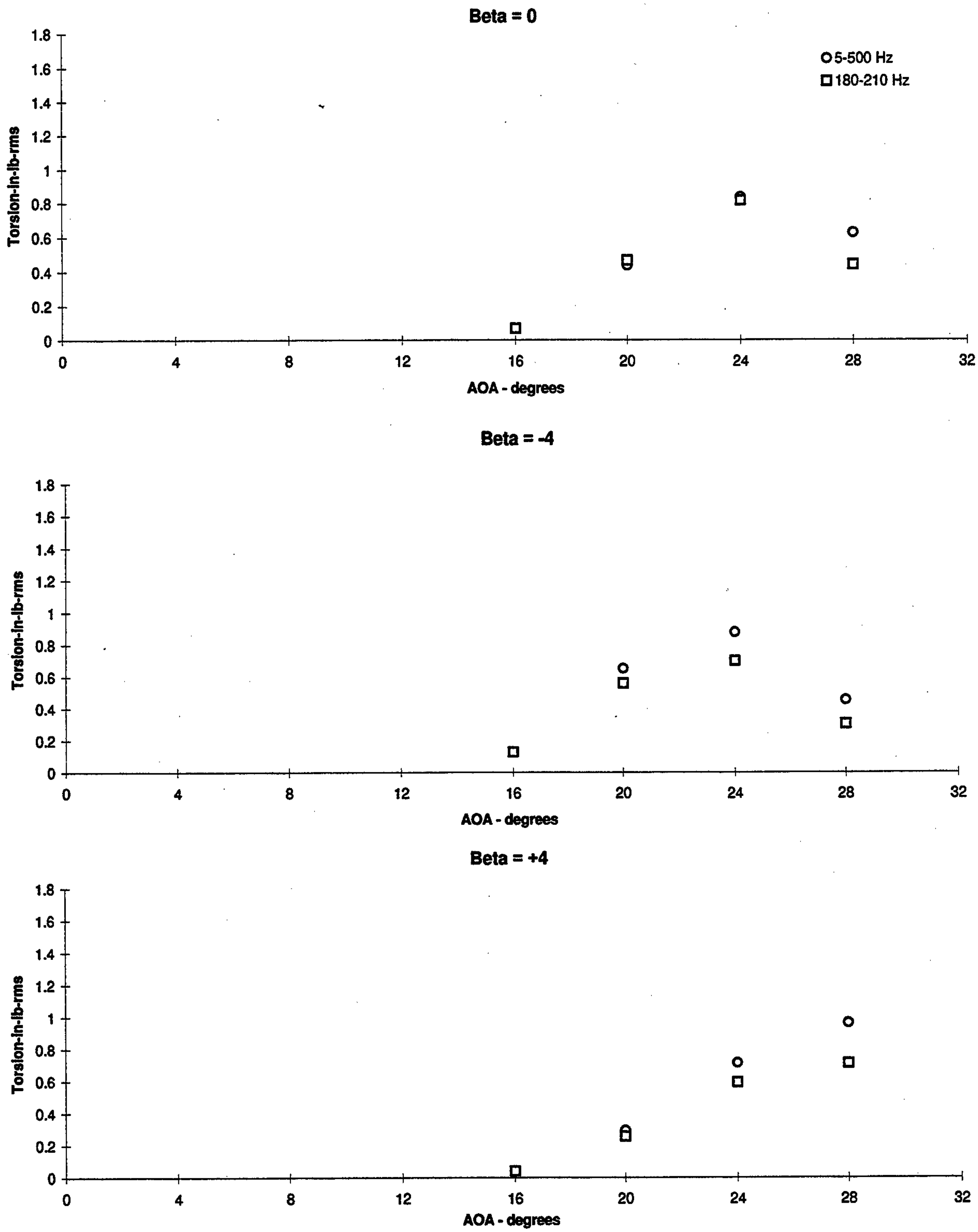

Figure 3.1.19 - Flex Tail Response vs Angle of Attack
Torsion, Q = 56 psf, Wing Blowing p = 65 psi

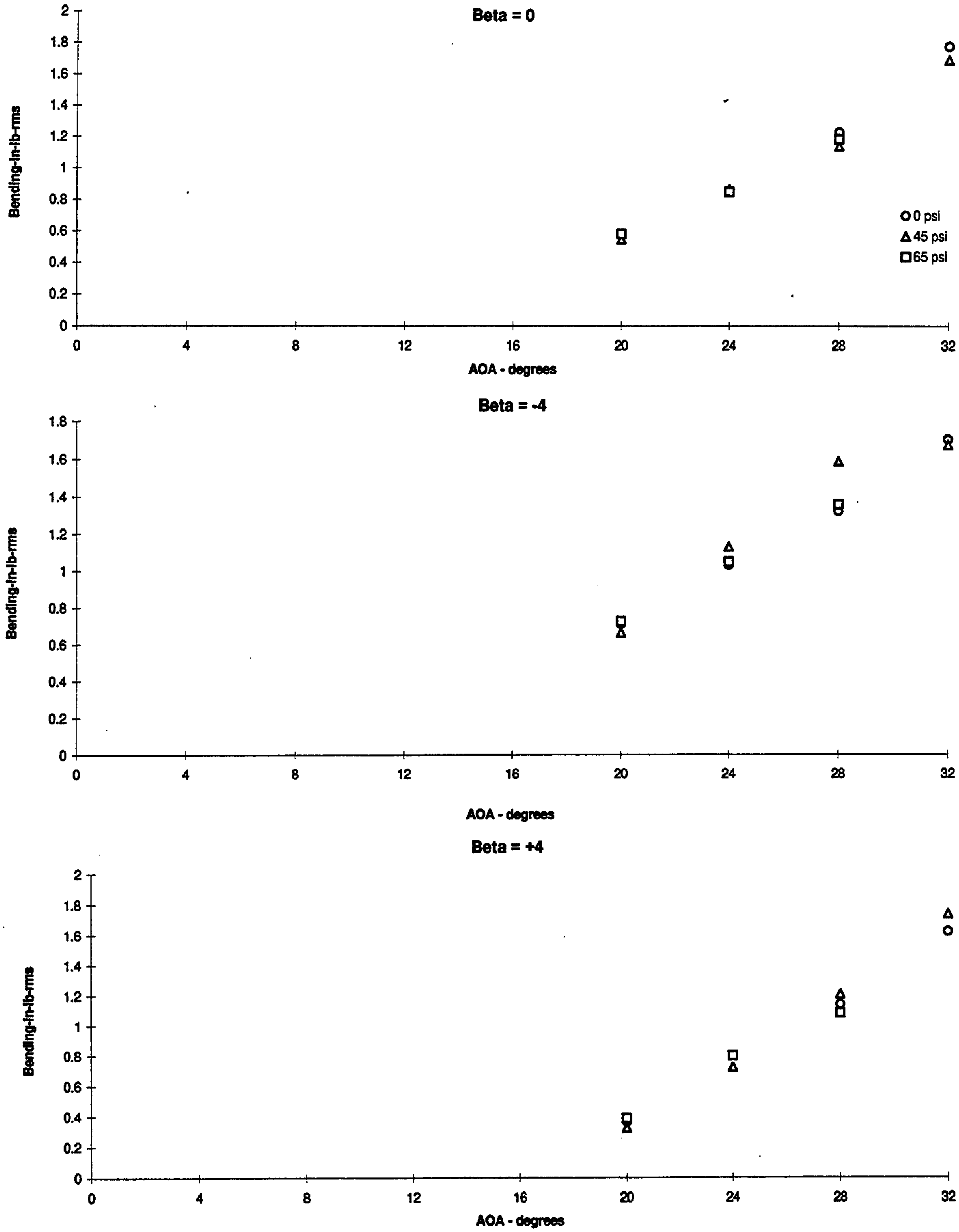

Figure 3.1.20 - Flex Tail Response vs Angle of Attack
Bending, Q = 56 psf, PSD's (5-500) Hz, Wing Blowing Summary

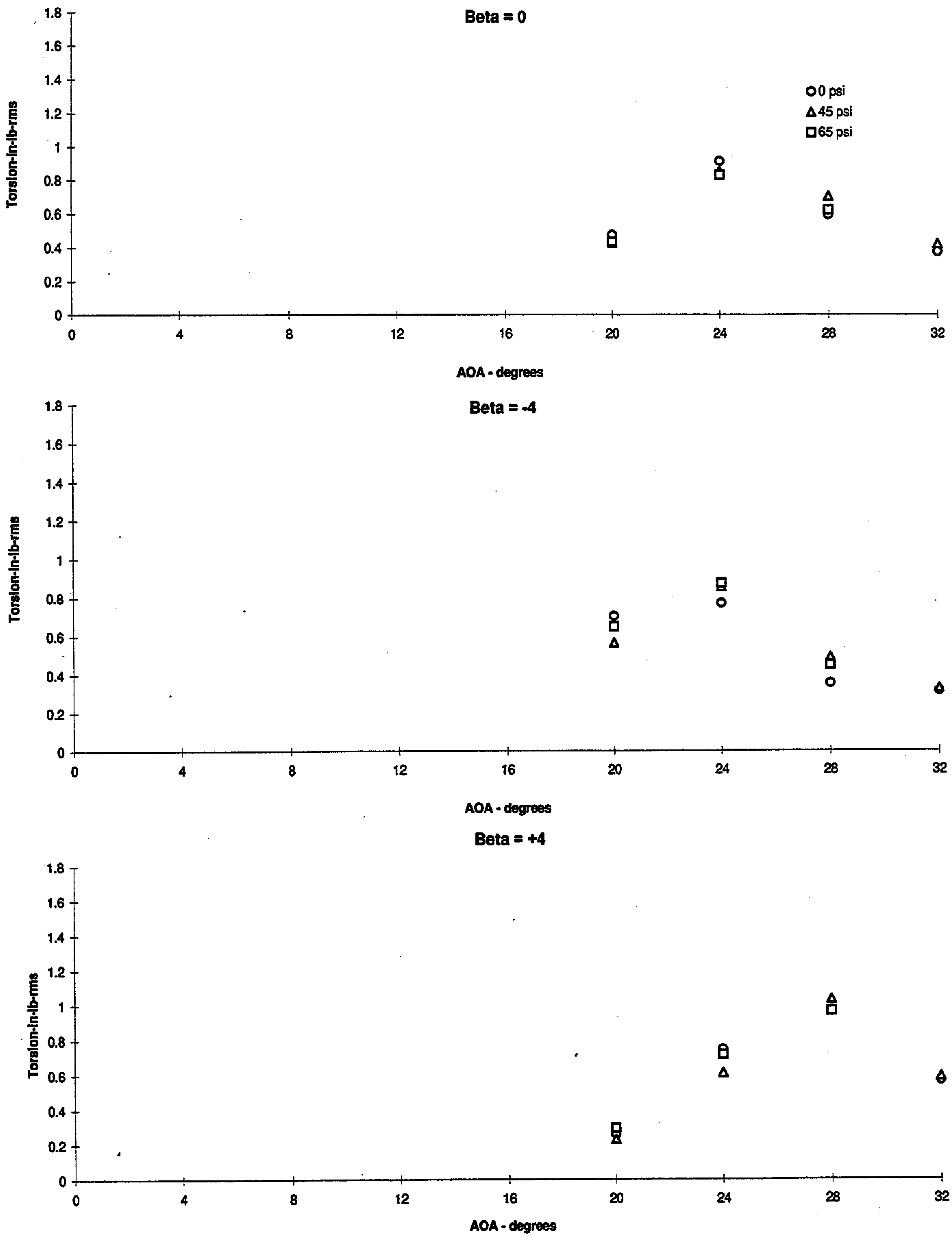

Figure 3.1.21 - Flex Tail Response vs Angle of Attack
Torsion, Q = 56 psf, PSD's 5-500 Hz, Wing Blowing Sumary

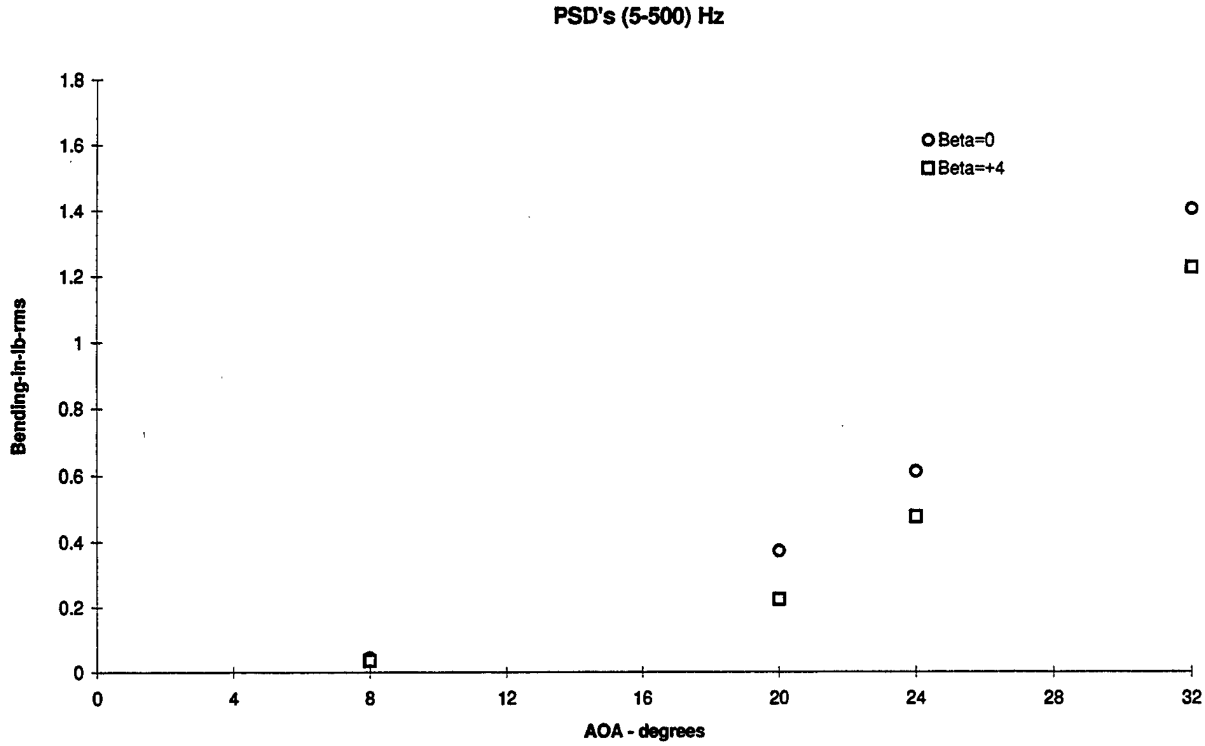

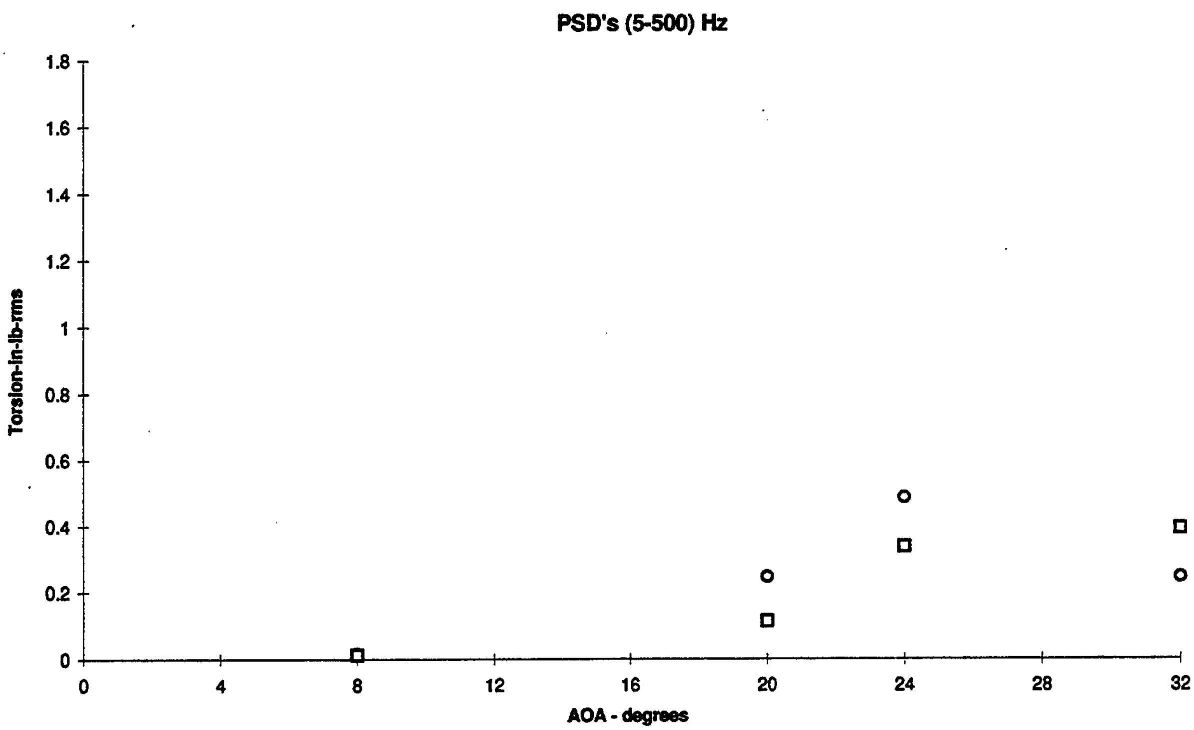

Figure 3.1.22 - Flex Tail Response vs Angle of Attack
Bending and Torsion, Q = 30 psf, No Blowing

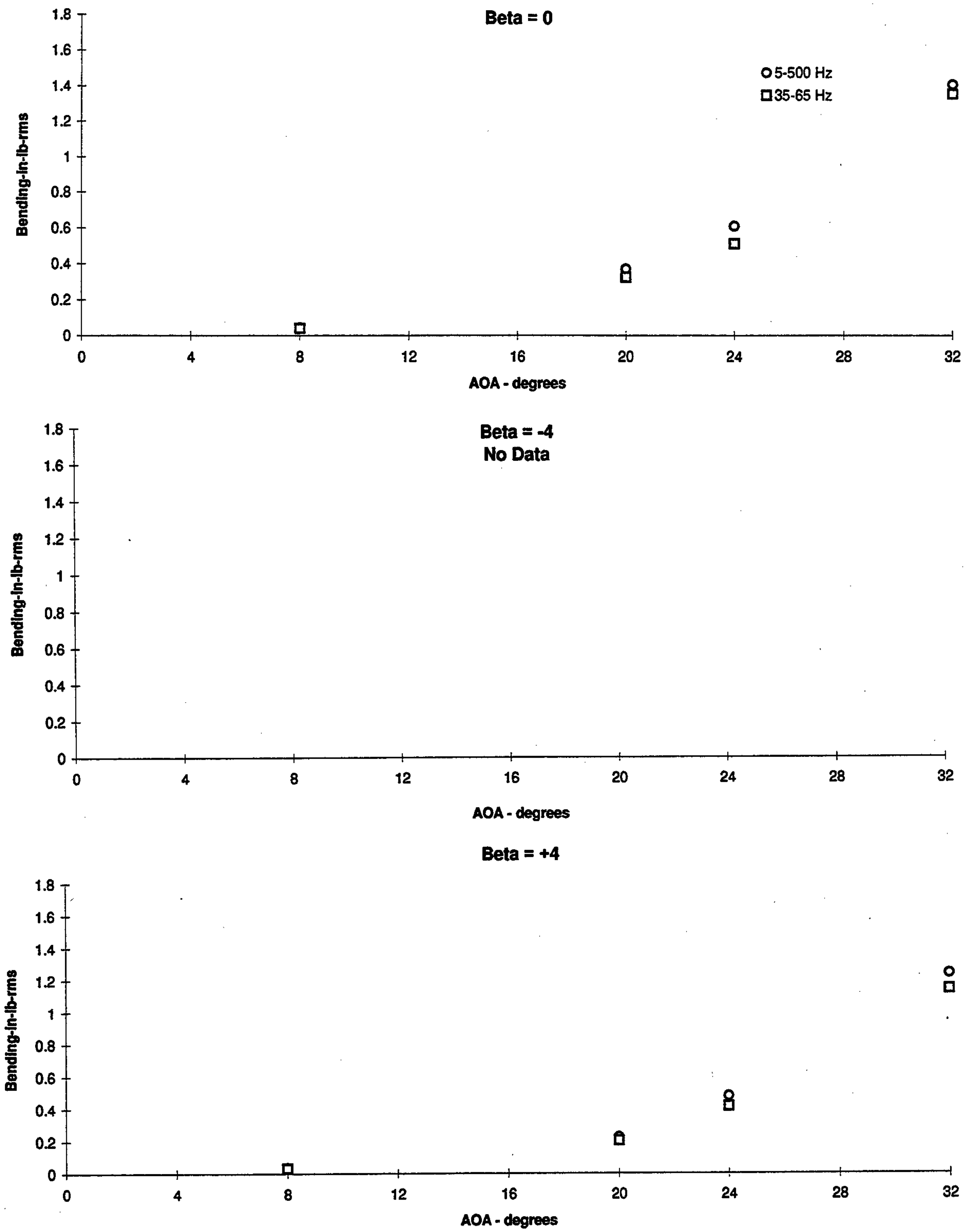

Figure 3.1.23 - Flex Tail Response vs Angle of Attack
Bending, Q = 30 psf, No Blowing

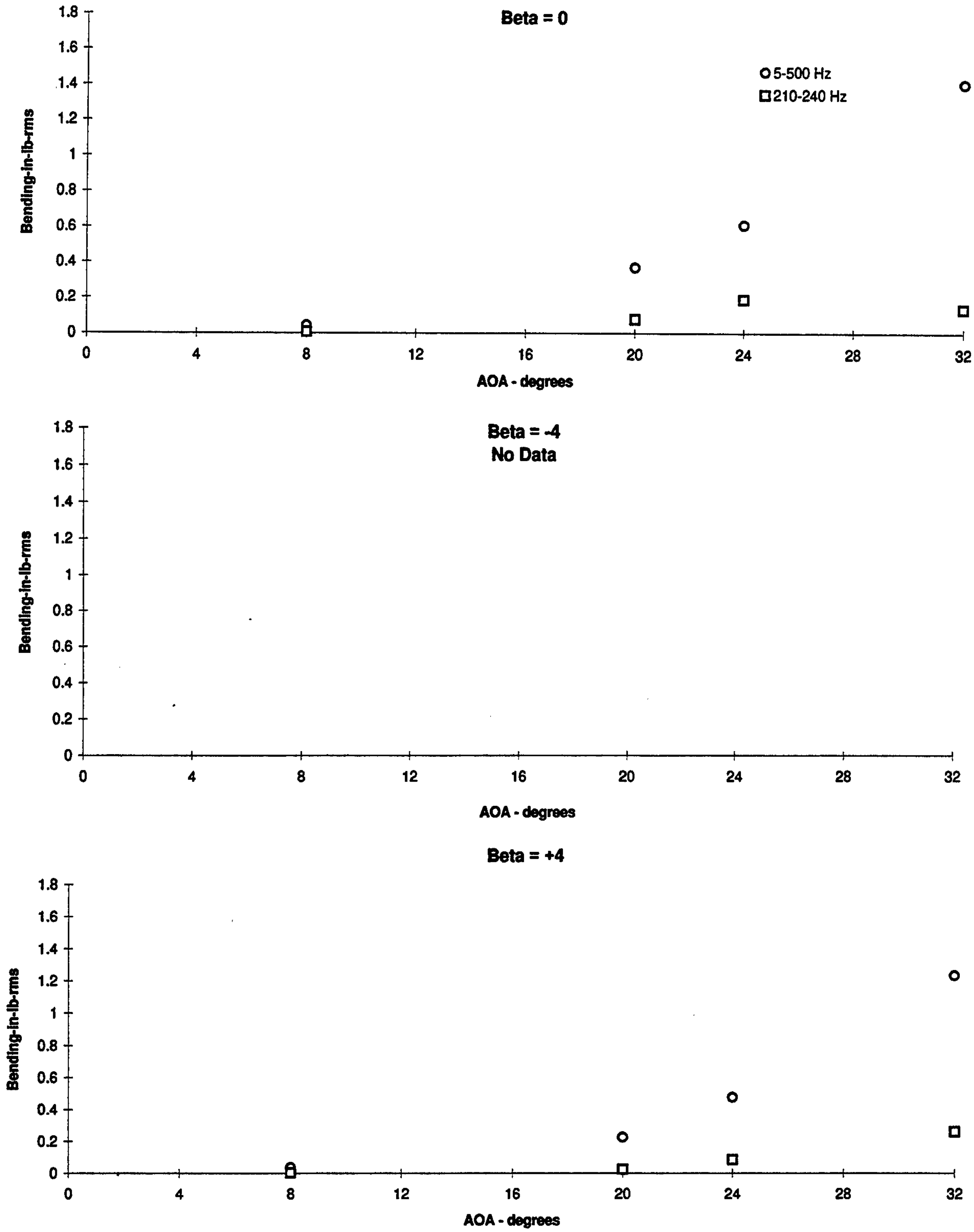

Figure 3.1.24 - Flex Tail Response vs Angle of Attack
Bending, Q = 30 psf, No Blowing

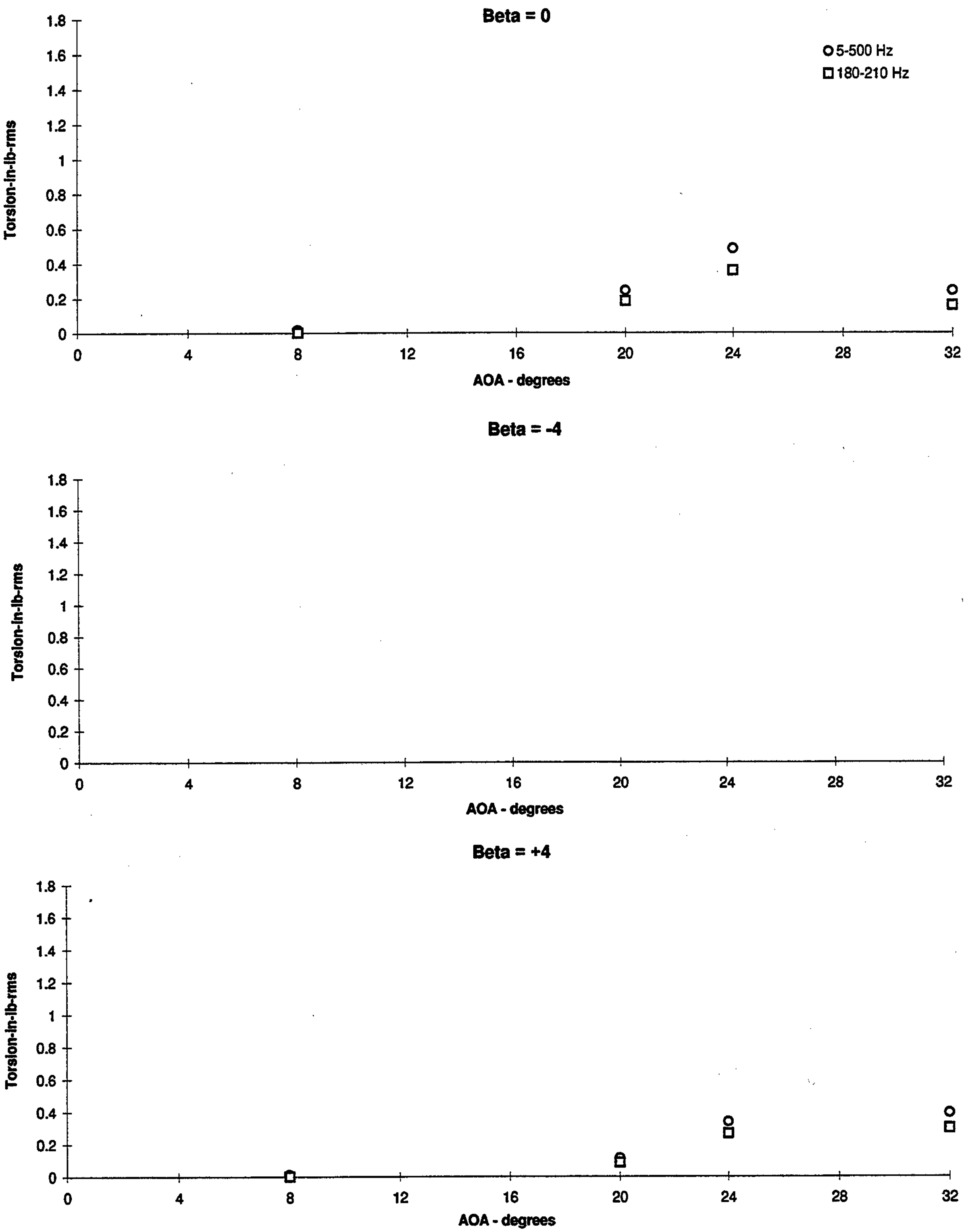

Figure 3.1.25 - Flex Tail Response vs Angle of Attack
Torsion, Q = 30 psf, No Blowing

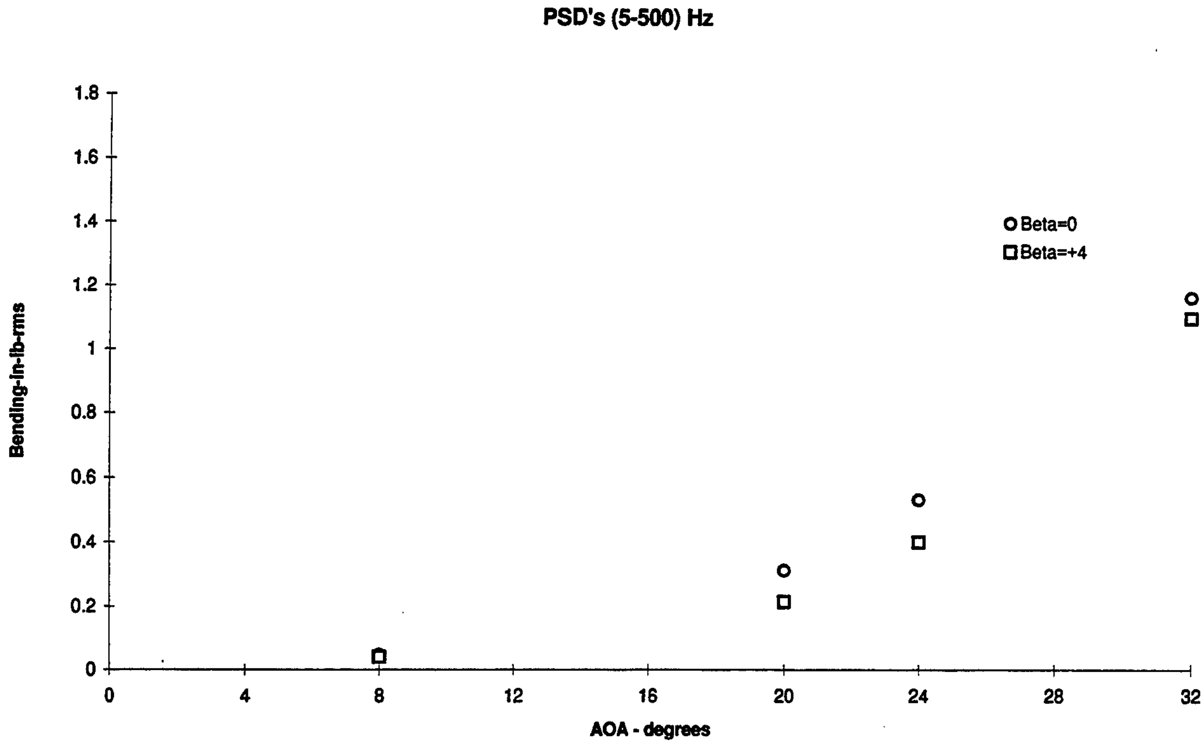

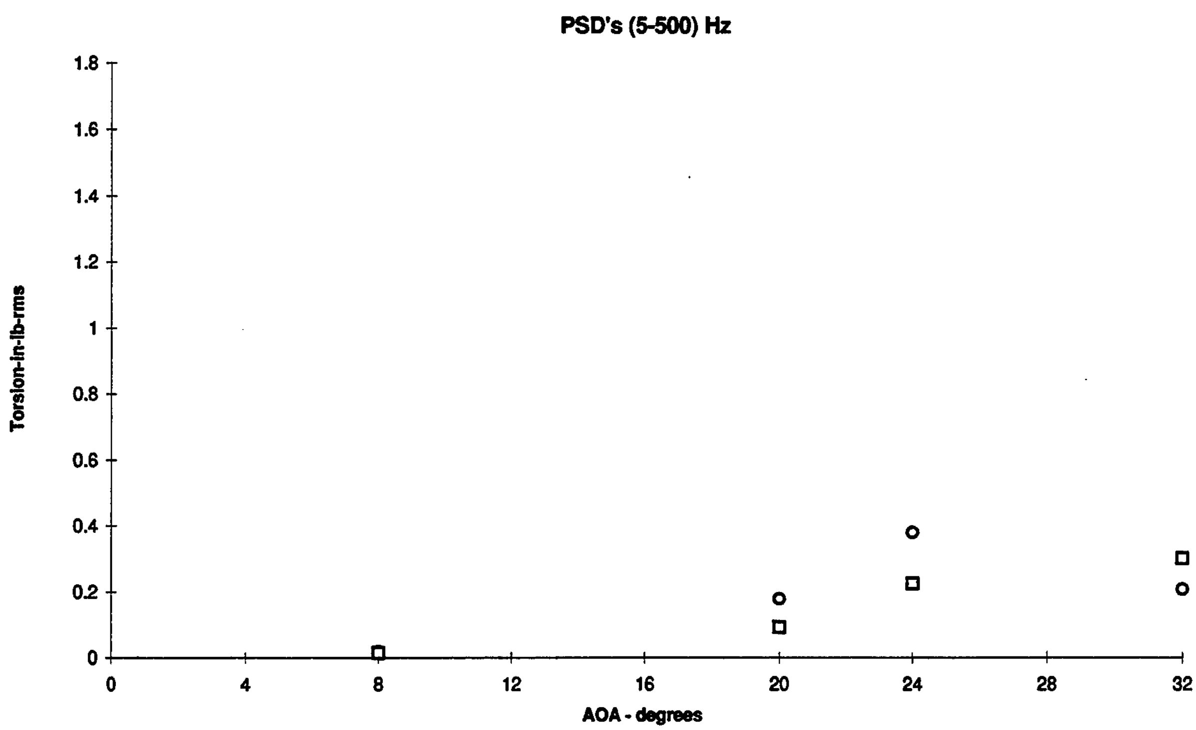

**Figure 3.1.26 - Flex Tail Response vs Angle of Attack
Bending and Torsion, Q = 30 psf, Wing Blowing p = 45 psi**

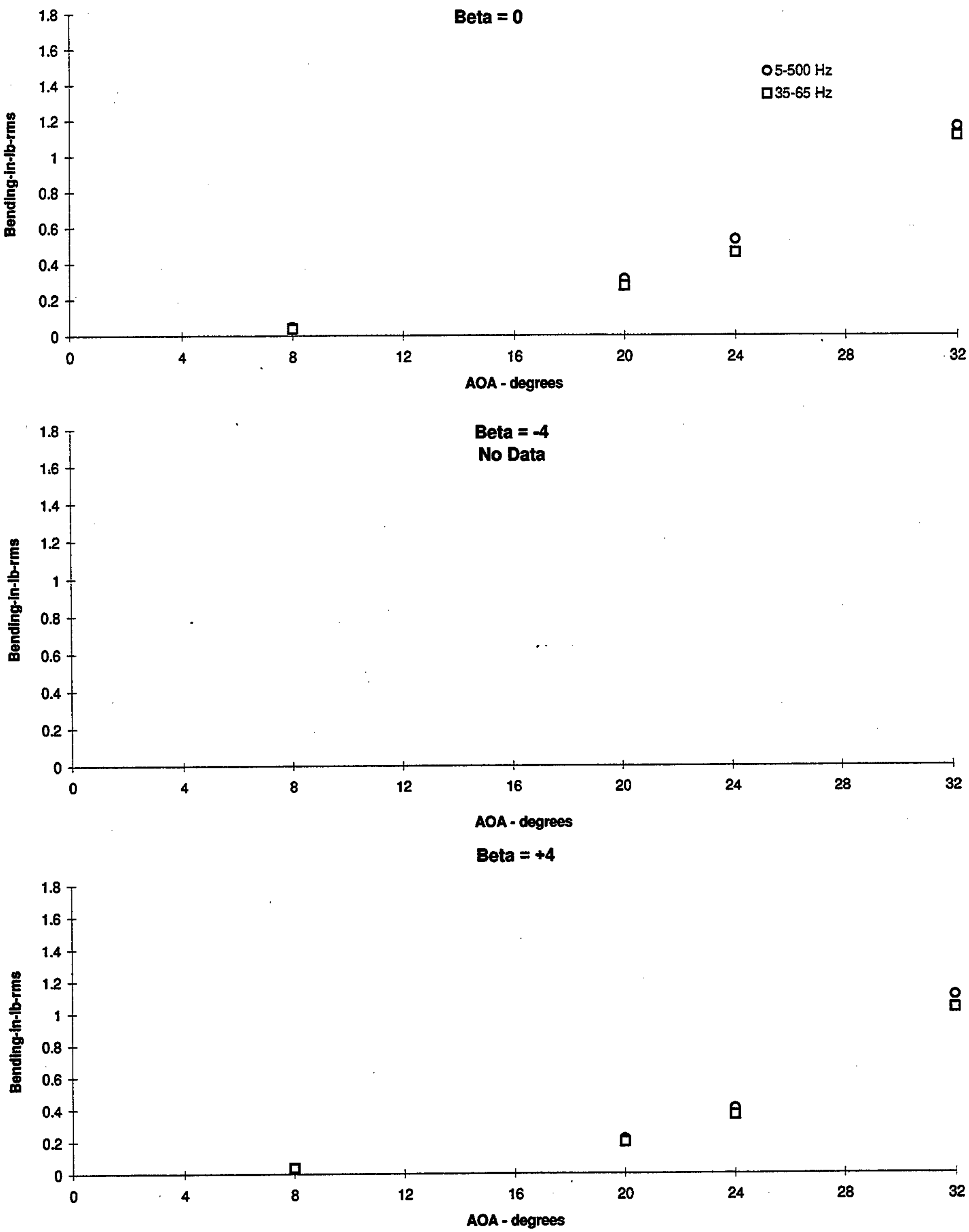

Figure 3.1.27 - Flex Tail Response vs Angle of Attack
Bending, Q = 30 psf, Wing Blowing p = 45 psi

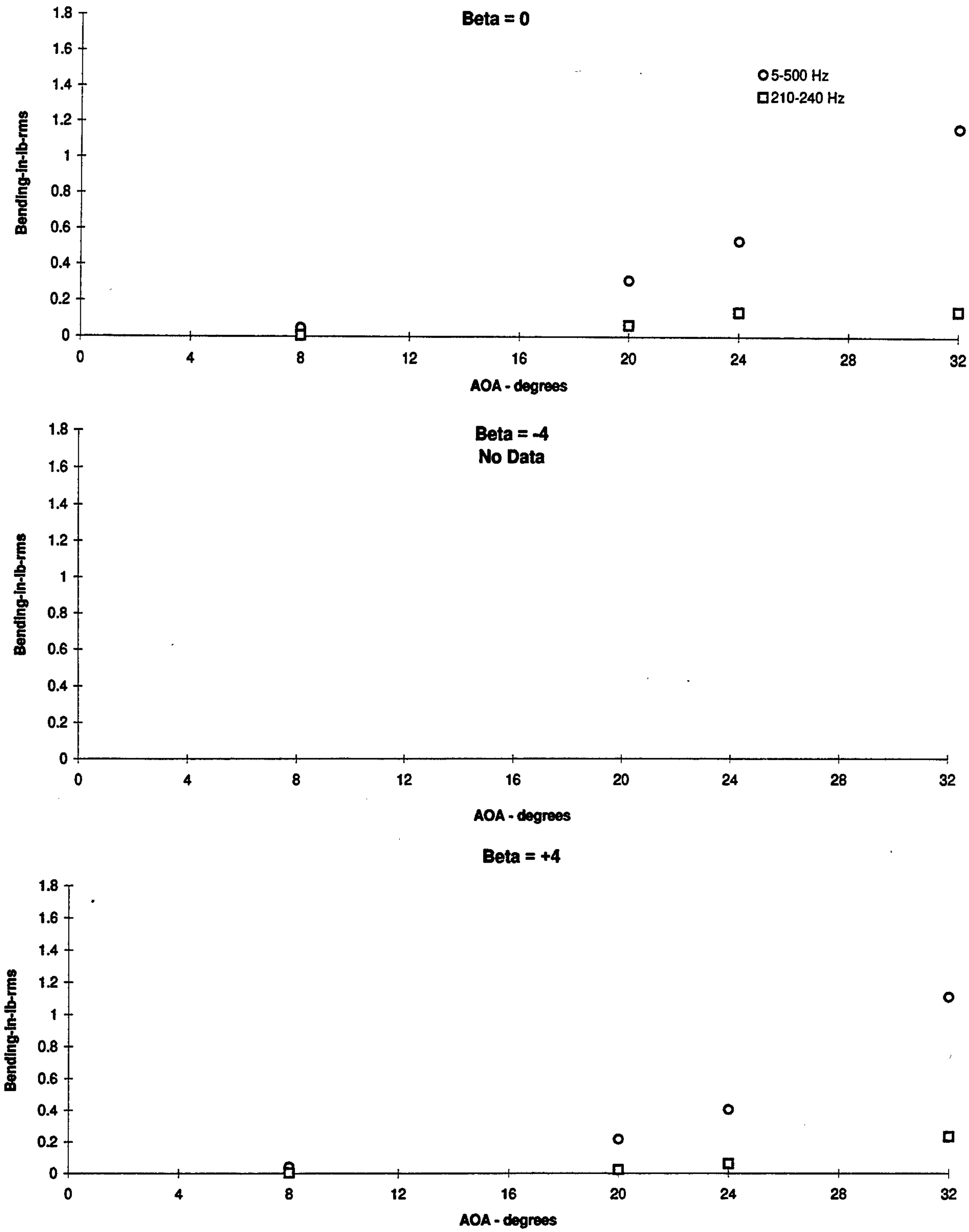

Figure 3.1.28 - Flex Tail Response vs Angle of Attack
Bending, Q = 30 psf, Wing Blowing p = 45 psi

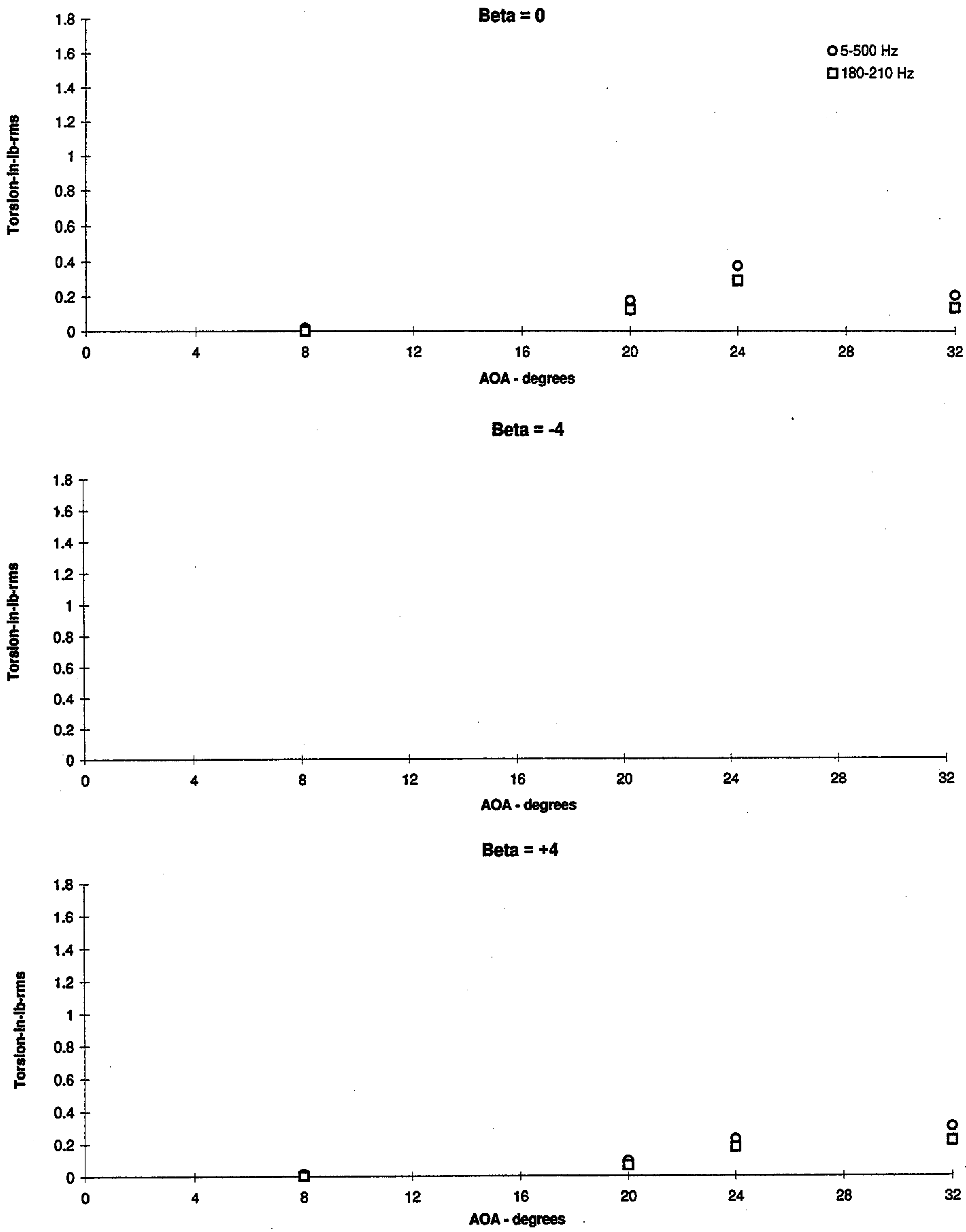

Figure 3.1.29 - Flex Tail Response vs Angle of Attack
Torsion, Q = 30 psf, Wing Blowing p = 45 psi

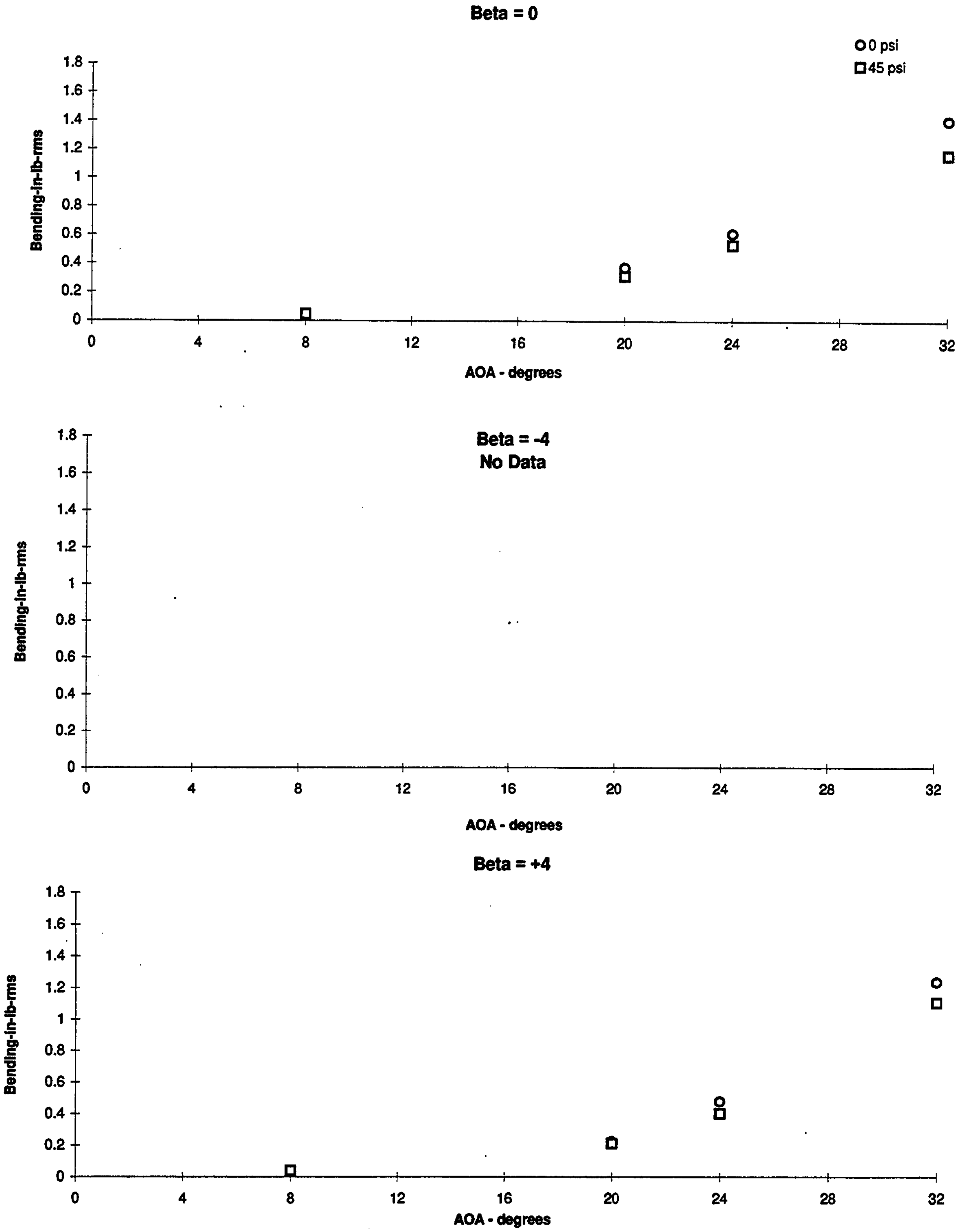

Figure 3.1.30 - Flex Tail Response vs Angle of Attack
Bending, Q = 30 psf, PSD's (5-500) Hz, Wing Blowing

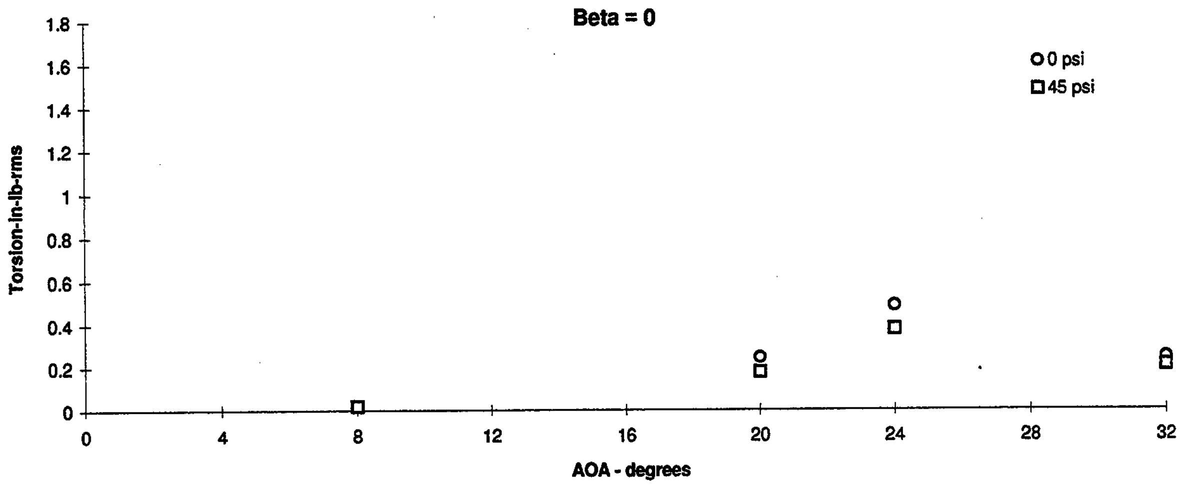

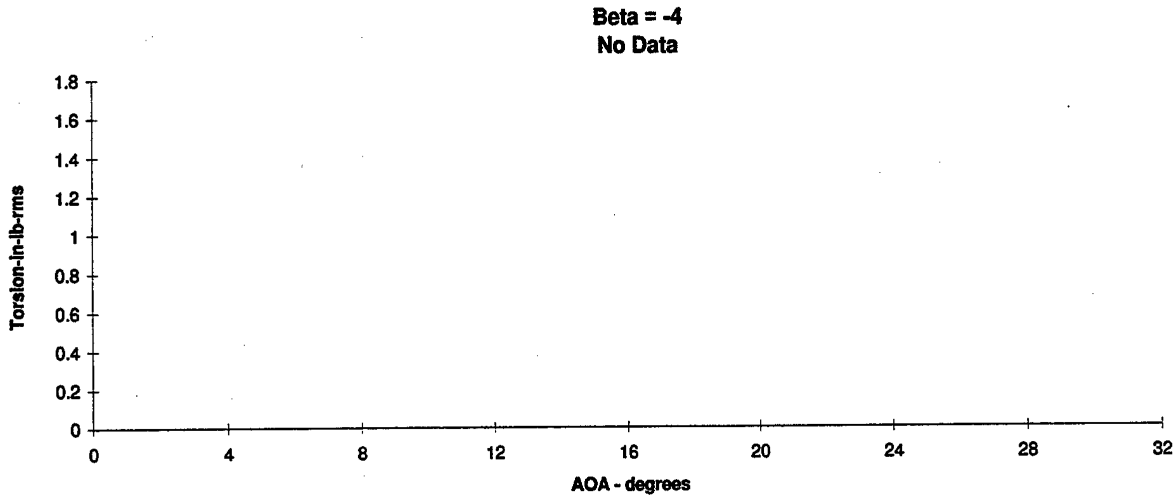

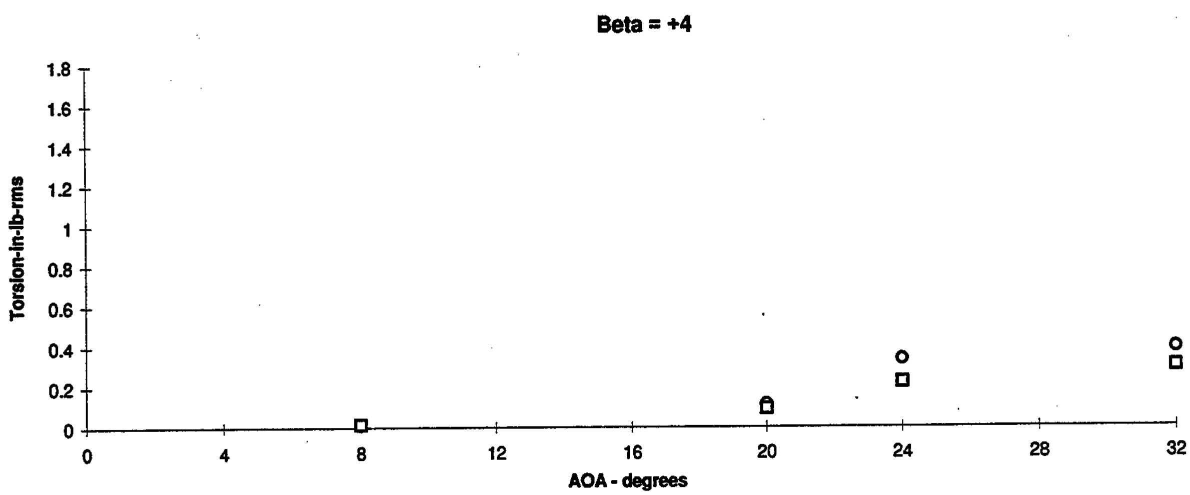

Figure 3.1.31 - Flex Tail Response vs Angle of Attack
Torsion, Q = 30 psf, PSD's (5-500) Hz, Wing Blowing Summary

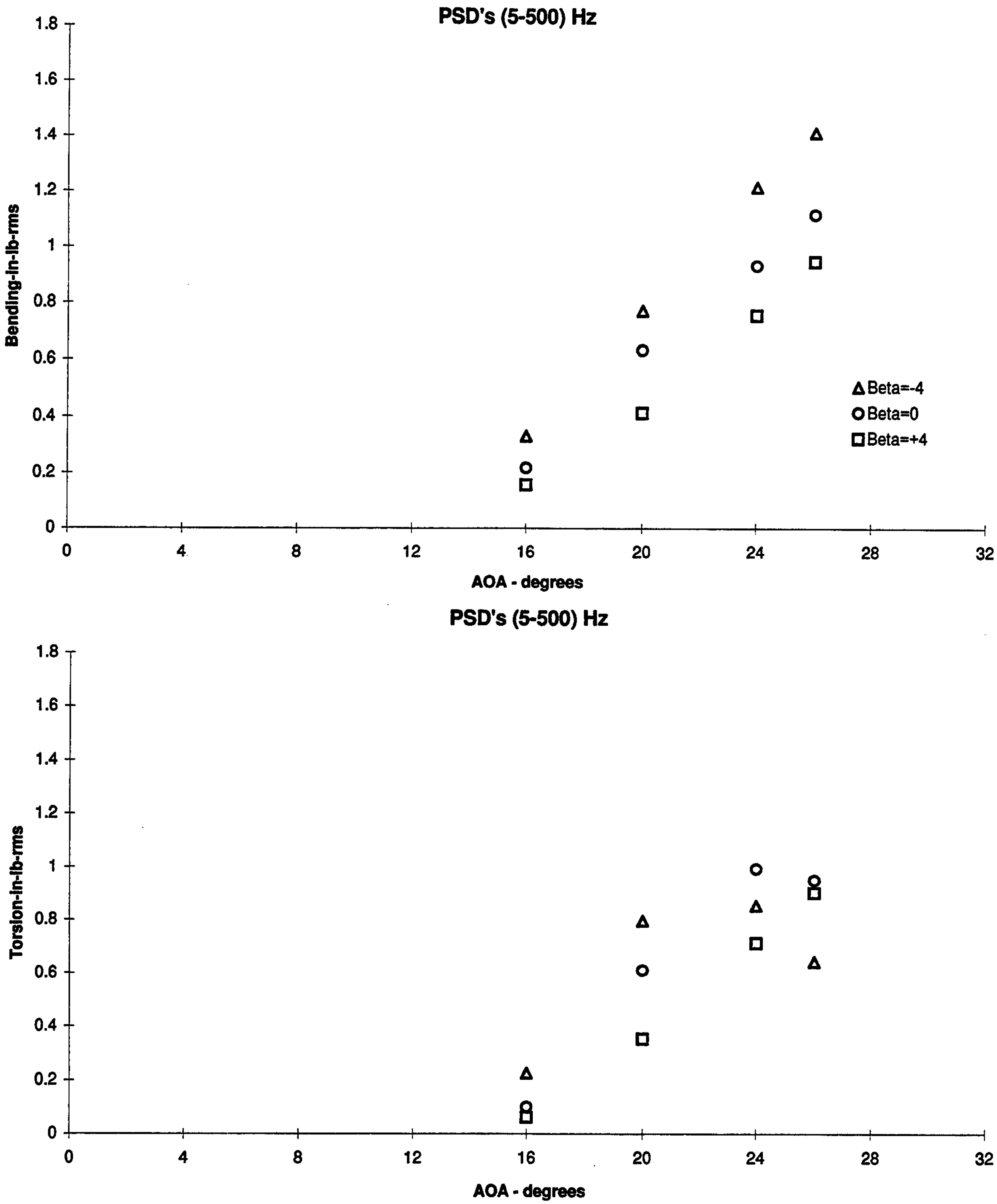

Figure 3.1.32 - Flex Tail Response vs Angle of Attack
Bending and Torsion, Q = 56 psf, Gun Blowing p = 65 psi

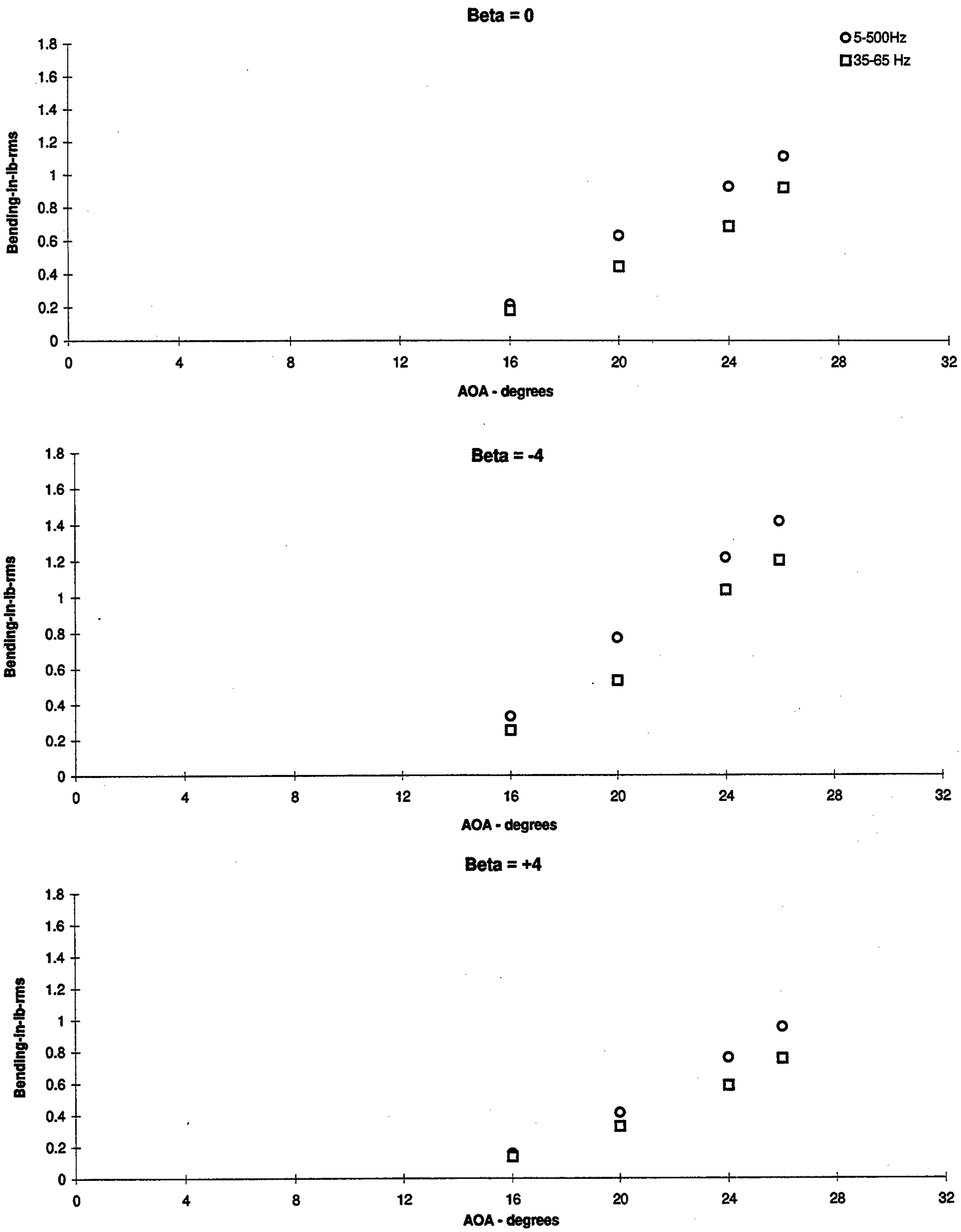

Figure 3.1.33 - Flex Tail Response vs Angle of Attack
Bending, Q = 56 psf, Gun Blowing p = 65 psi

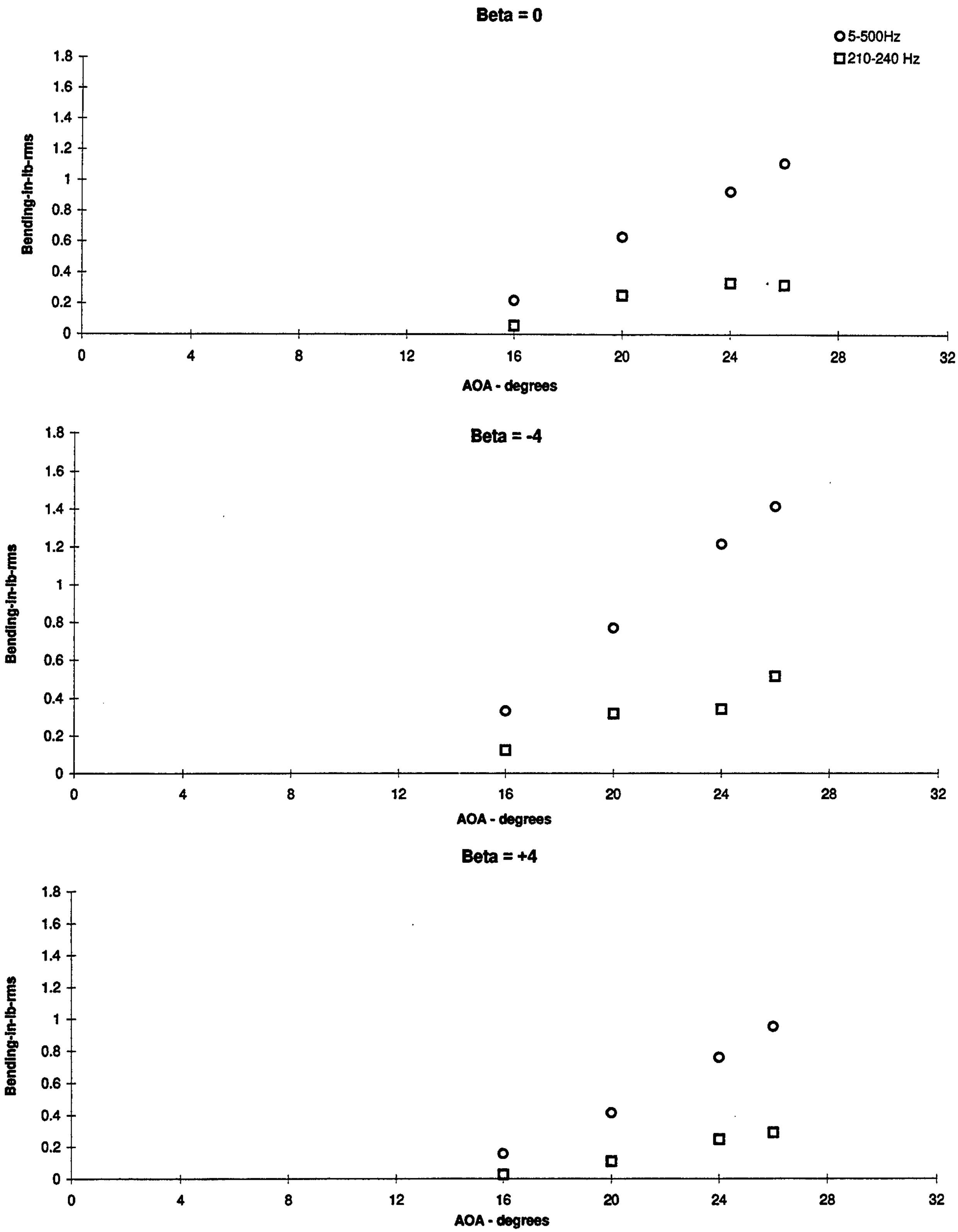

Figure 3.1.34 - Flex Tail Response vs Angle of Attack
Bending, Q = 56 psf, Gun Blowing p = 65 psi

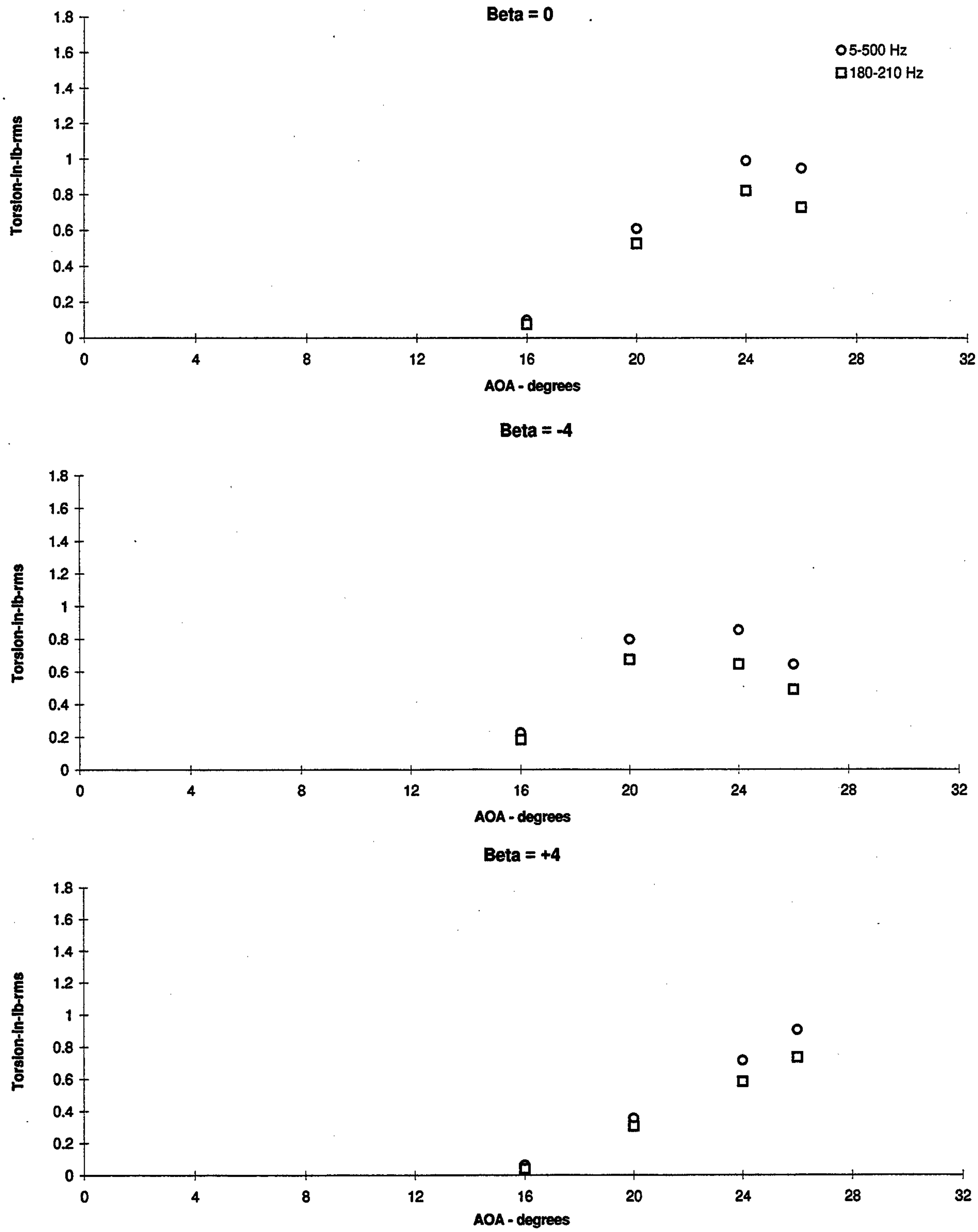

Figure 3.1.35 - Flex Tail Response vs Angle of Attack
Torsion, Q = 56 psf, Gun Blowing p = 65 psi

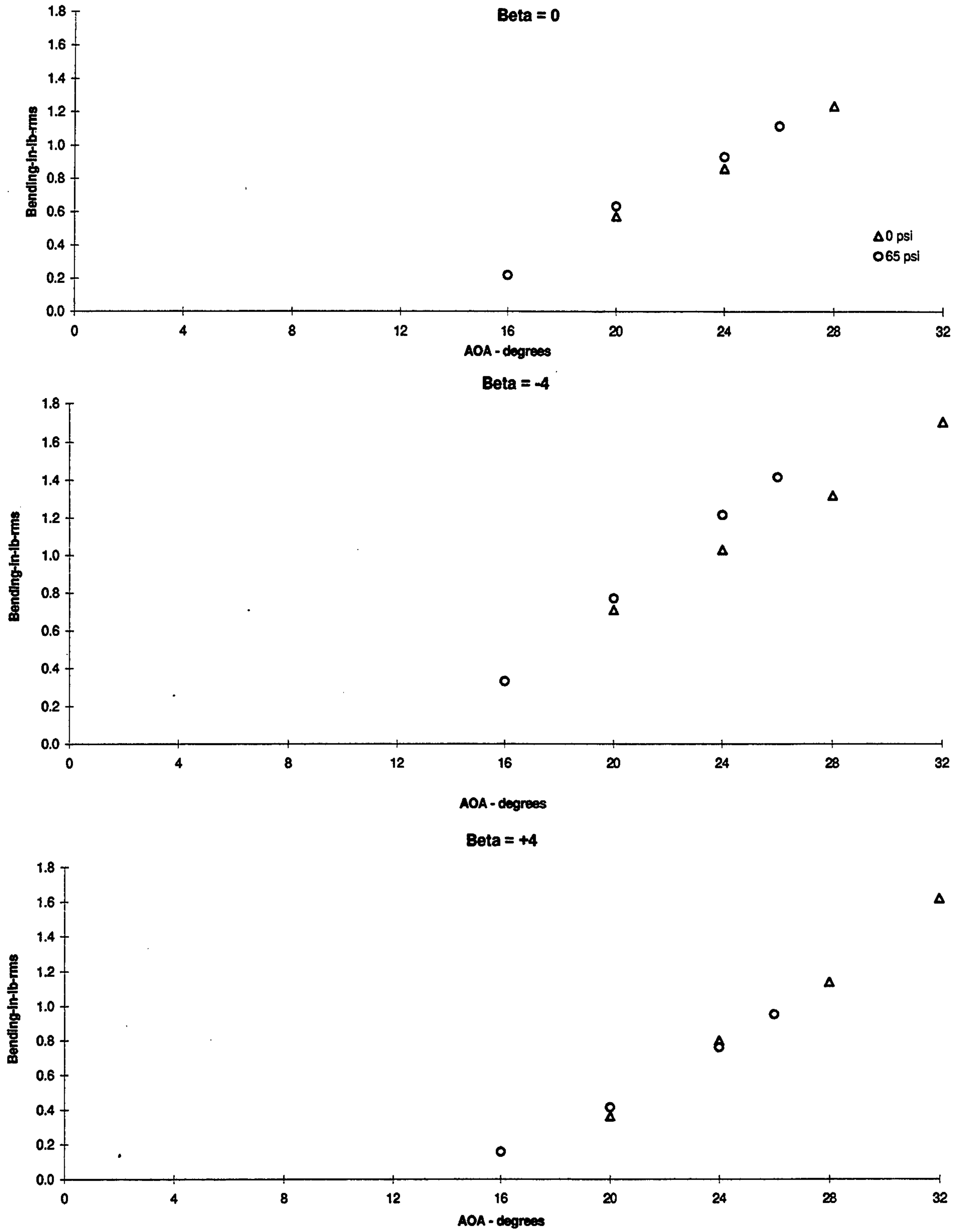

Figure 3.1.36 - Flex Tail Response vs Angle of Attack
Bending, Q = 56 psf, PSD's (5-500) Hz, Gun Blowing Summary

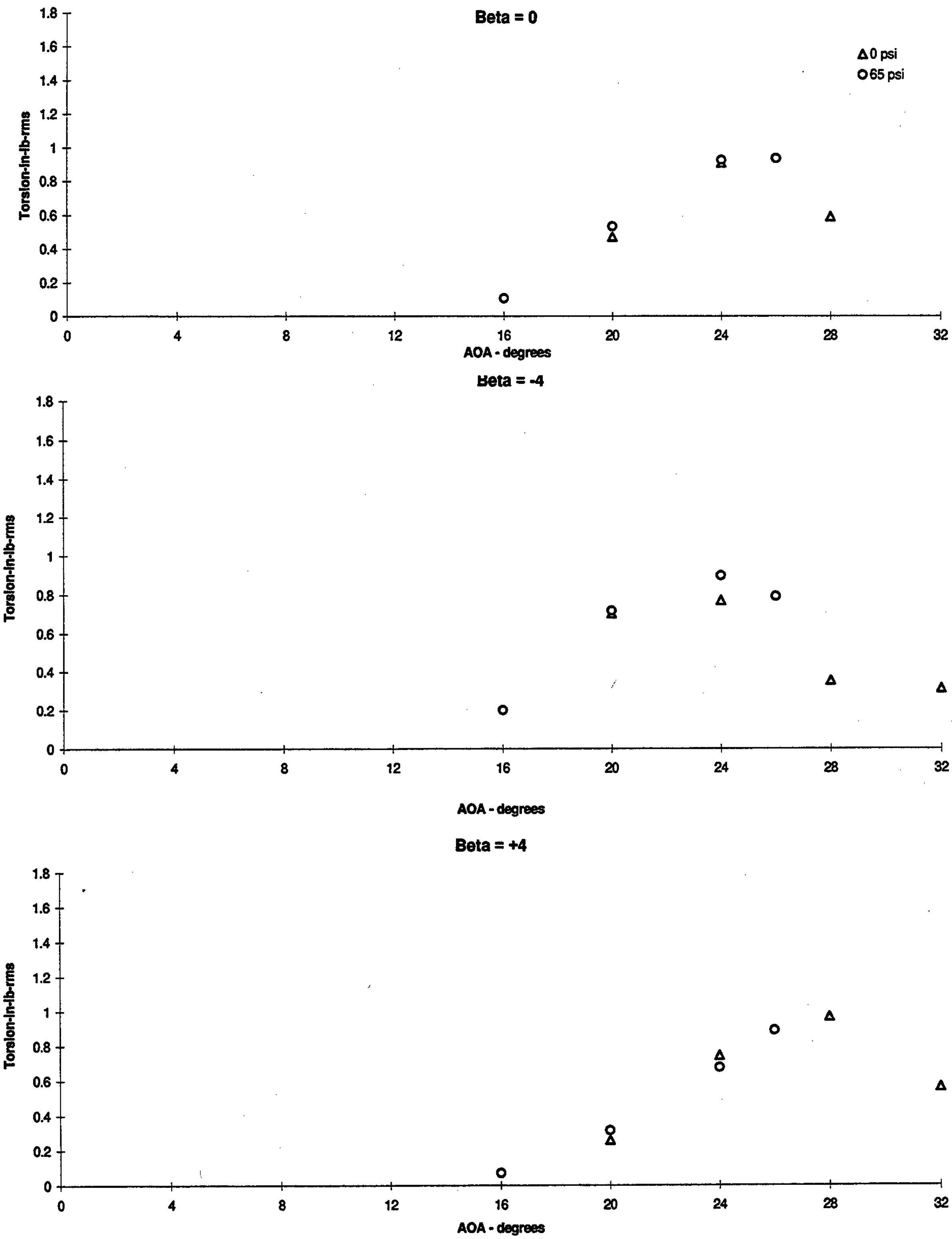

Figure 3.1.37 - Flex Tail Response vs Angle of Attack
Torsion, Q = 56 psf, PSD's (5-500) Hz, Gun Blowing Summary

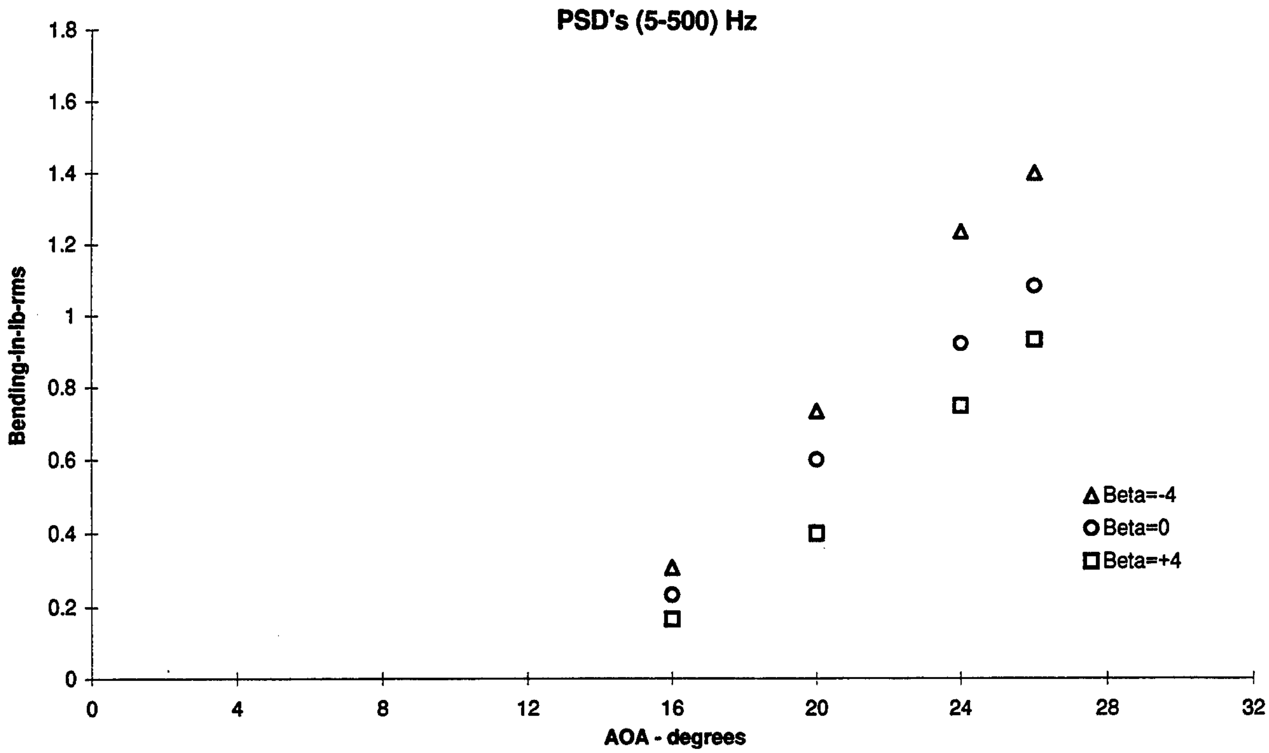

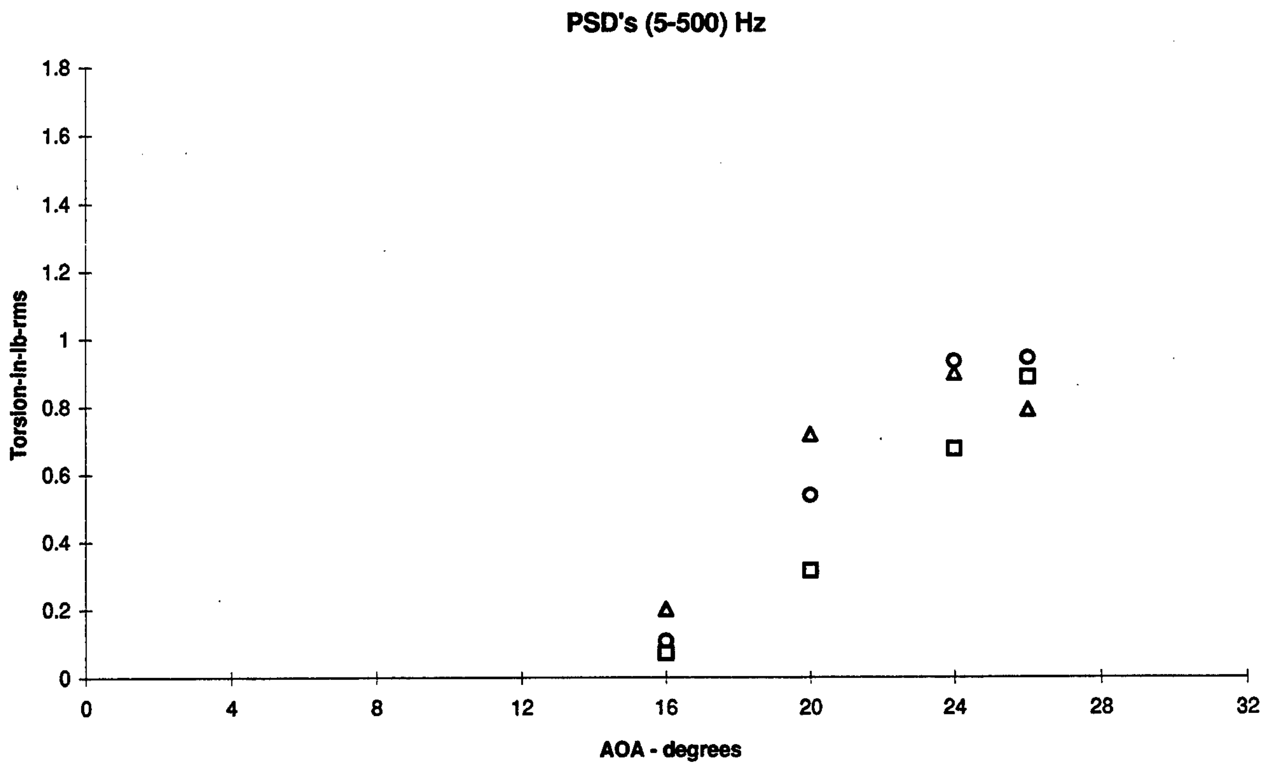

Figure 3.1.38 - Flex Tail Response vs Angle of Attack
Bending and Torsion, Q = 56 psf, Gun and Wing L.E. Blowing p = 65 psi

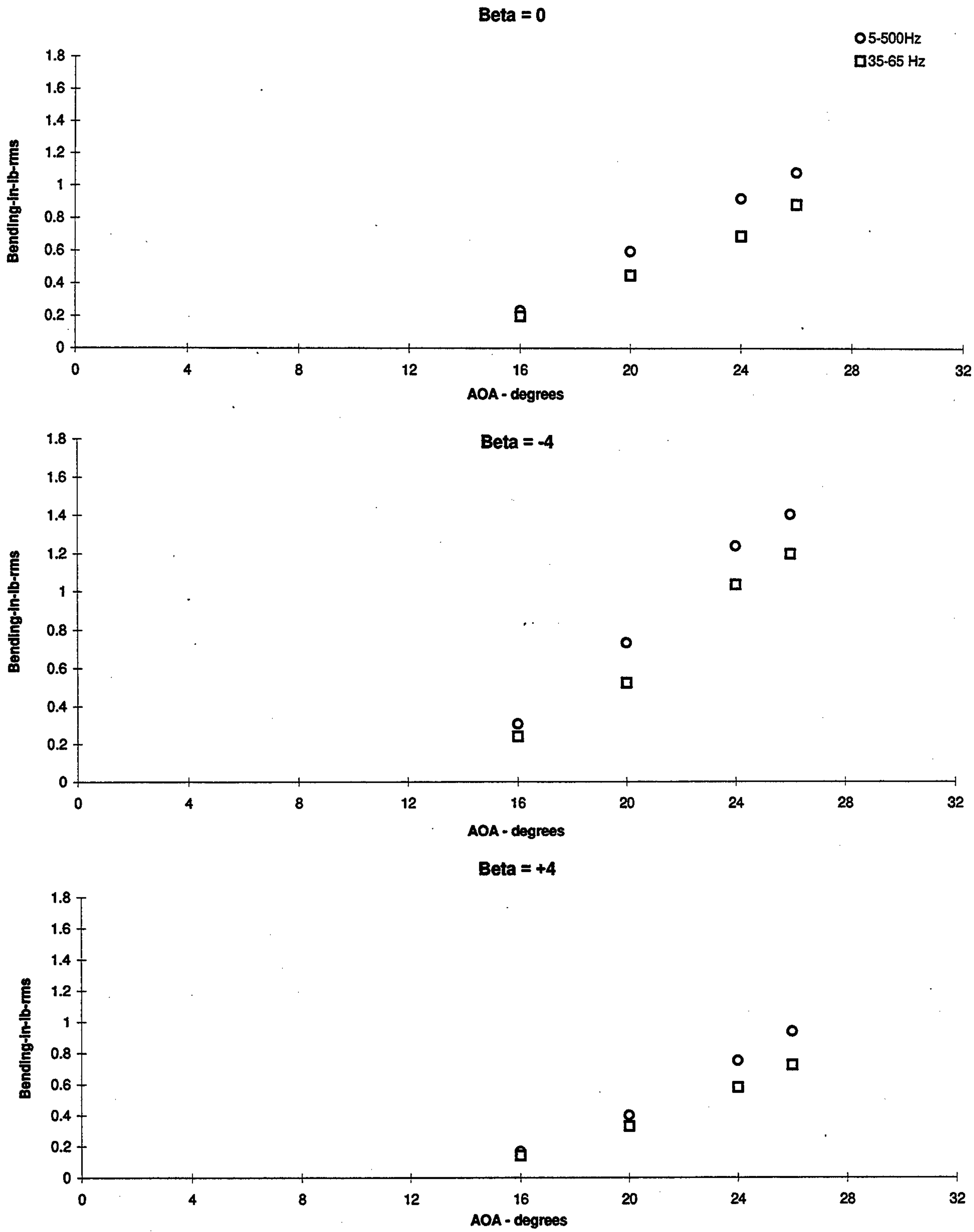

Figure 3.1.39 - Flex Tail Response vs Angle of Attack
Bending, Q = 56 psf, Gun and Wing L.E. Blowing p = 65 psi

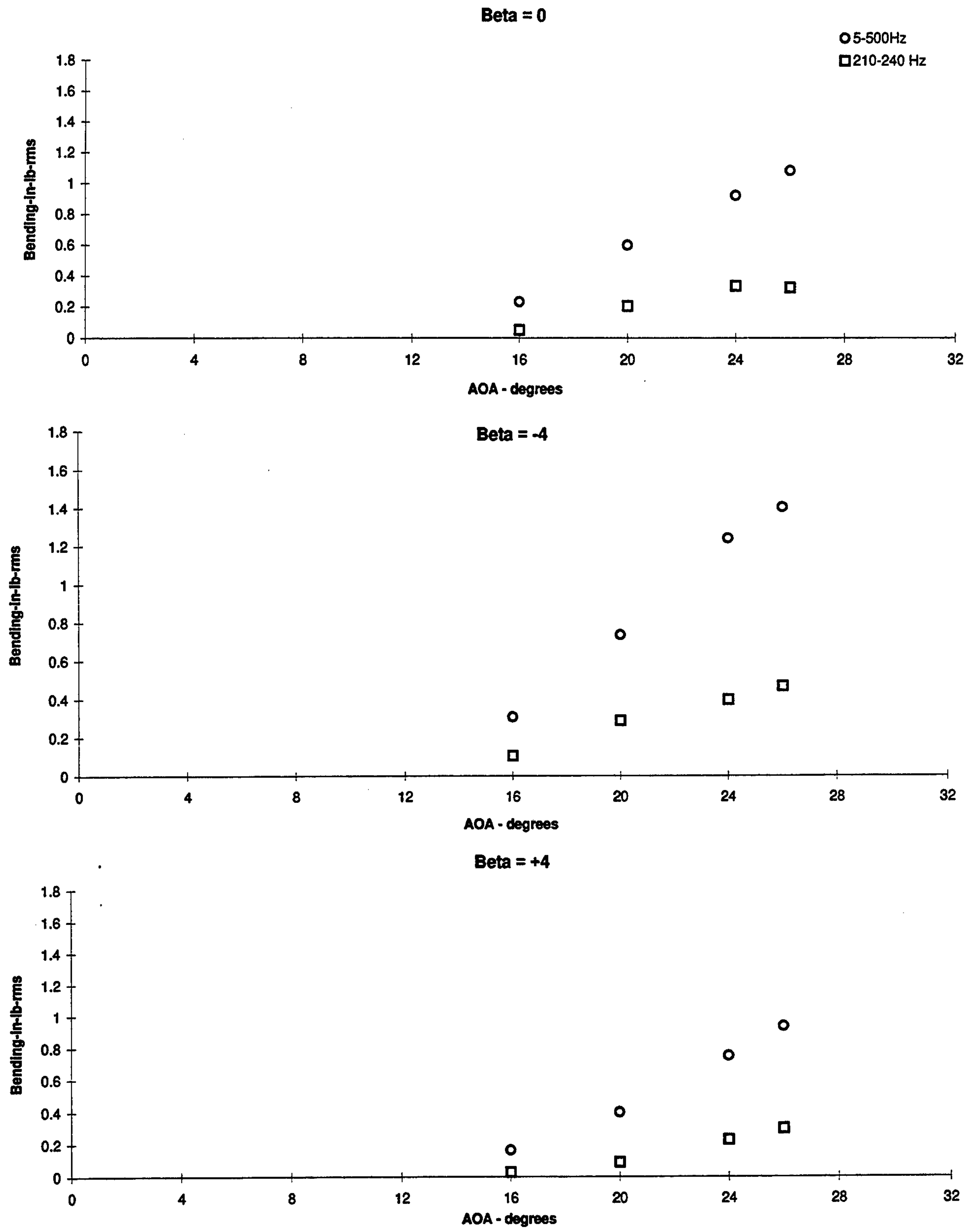

Figure 3.1.40 - Flex Tail Response vs Angle of Attack
Bending, Q = 56 psf, Gun and Wing L.E. Blowing p = 65 psi

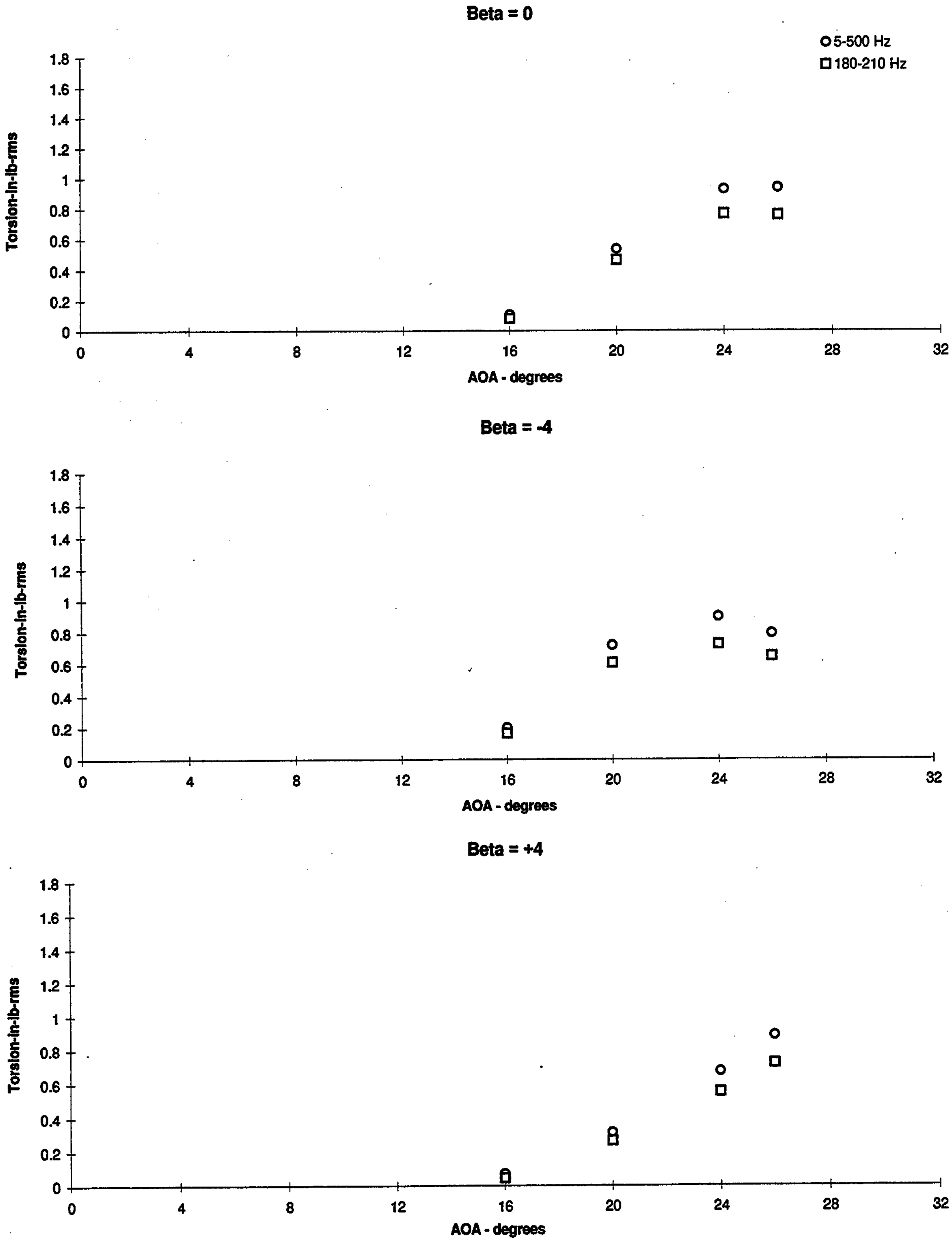

Figure 3.1.41 - Flex Tail Response vs Angle of Attack
Torsion, Q = 56 psf, Gun and Wing L.E. Blowing p = 65 psi

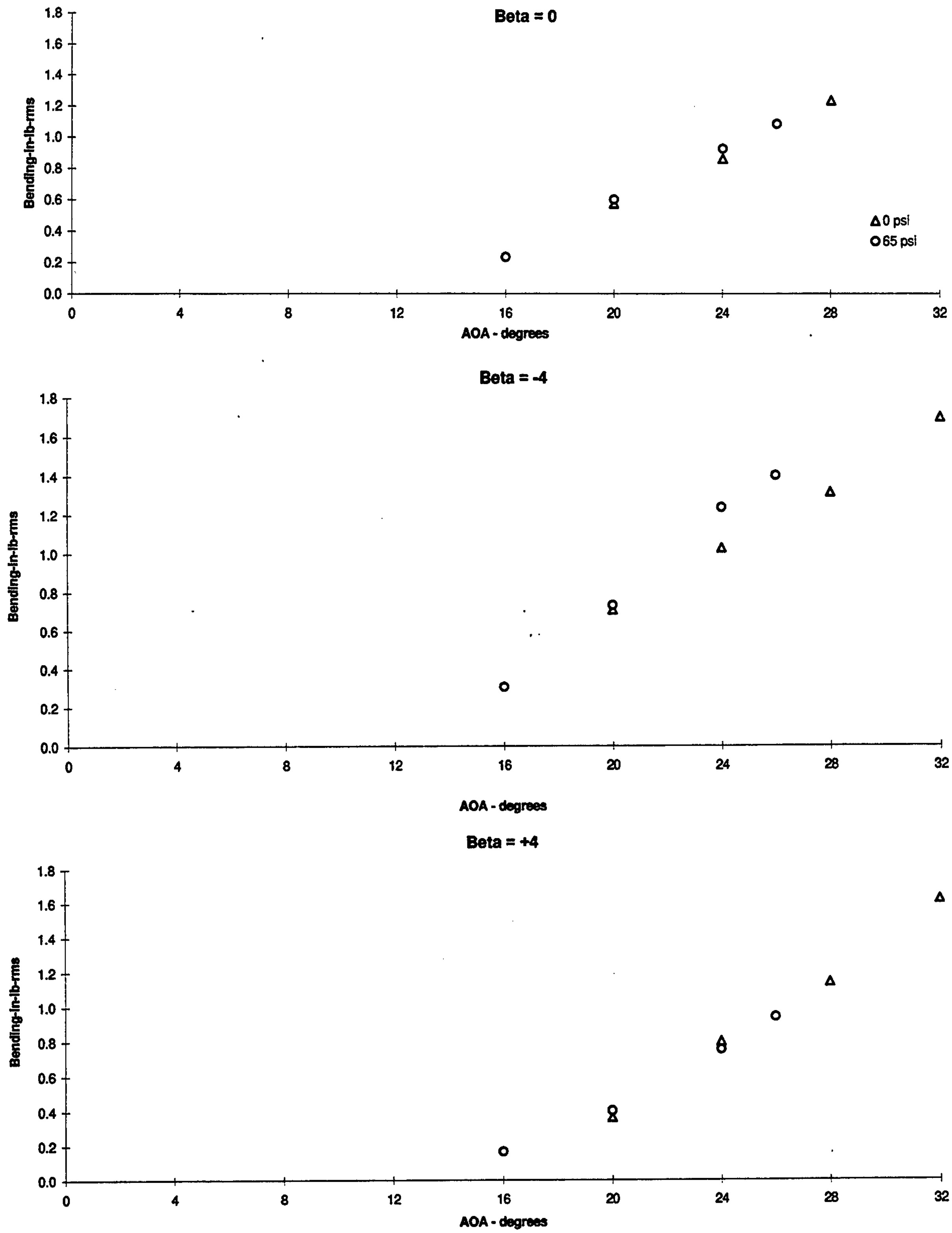

Figure 3.1.42 - Flex Tail Response vs Angle of Attack
Bending, Q = 56 psf, PSD's (5-500) Hz, Gun and Wing LE Blowing Summary

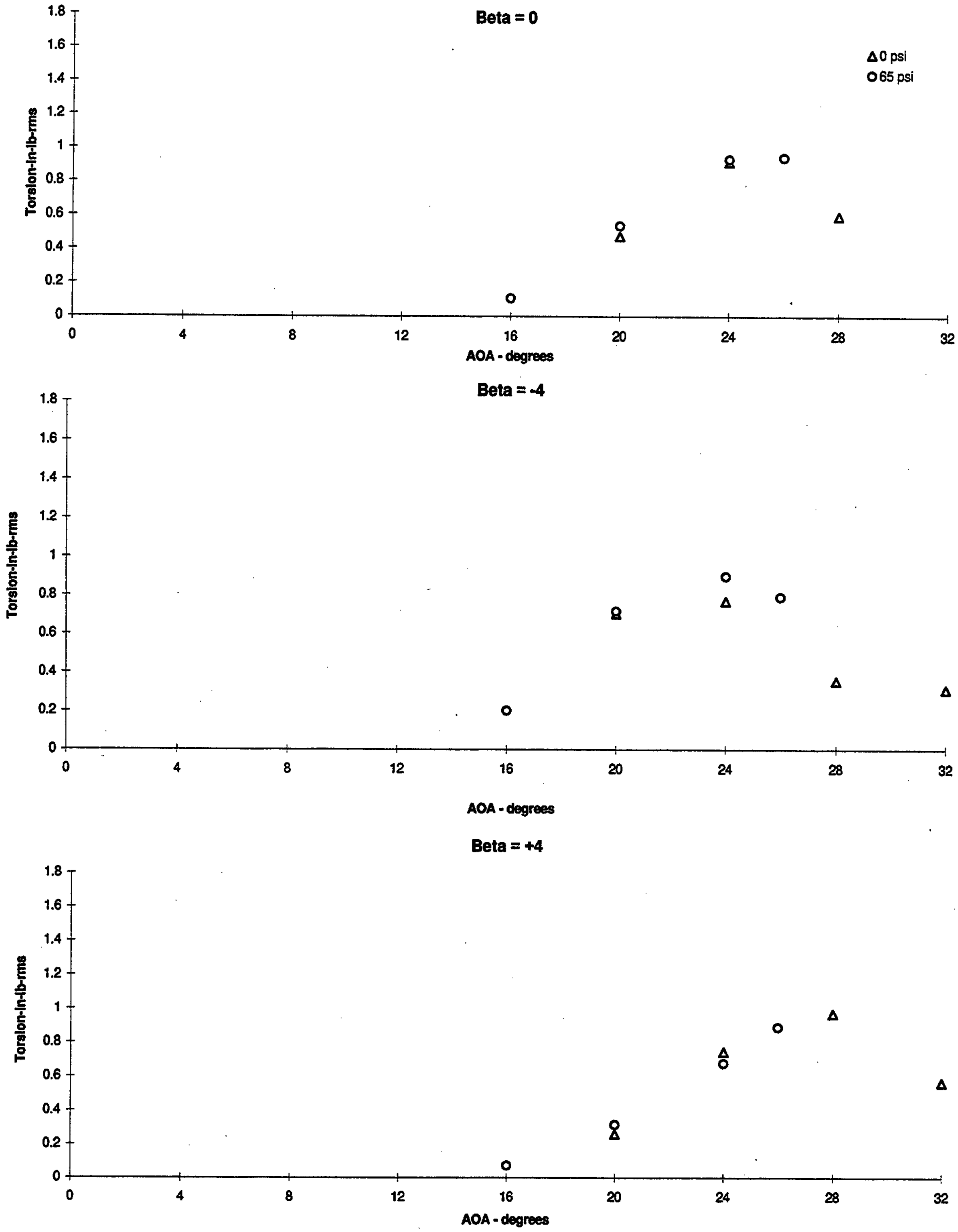

Figure 3.1.43 - Flex Tail Response vs Angle of Attack
Torsion, Q = 56 psf, PSD's (5-500) Hz, Gun and Wing LE Blowing Summary

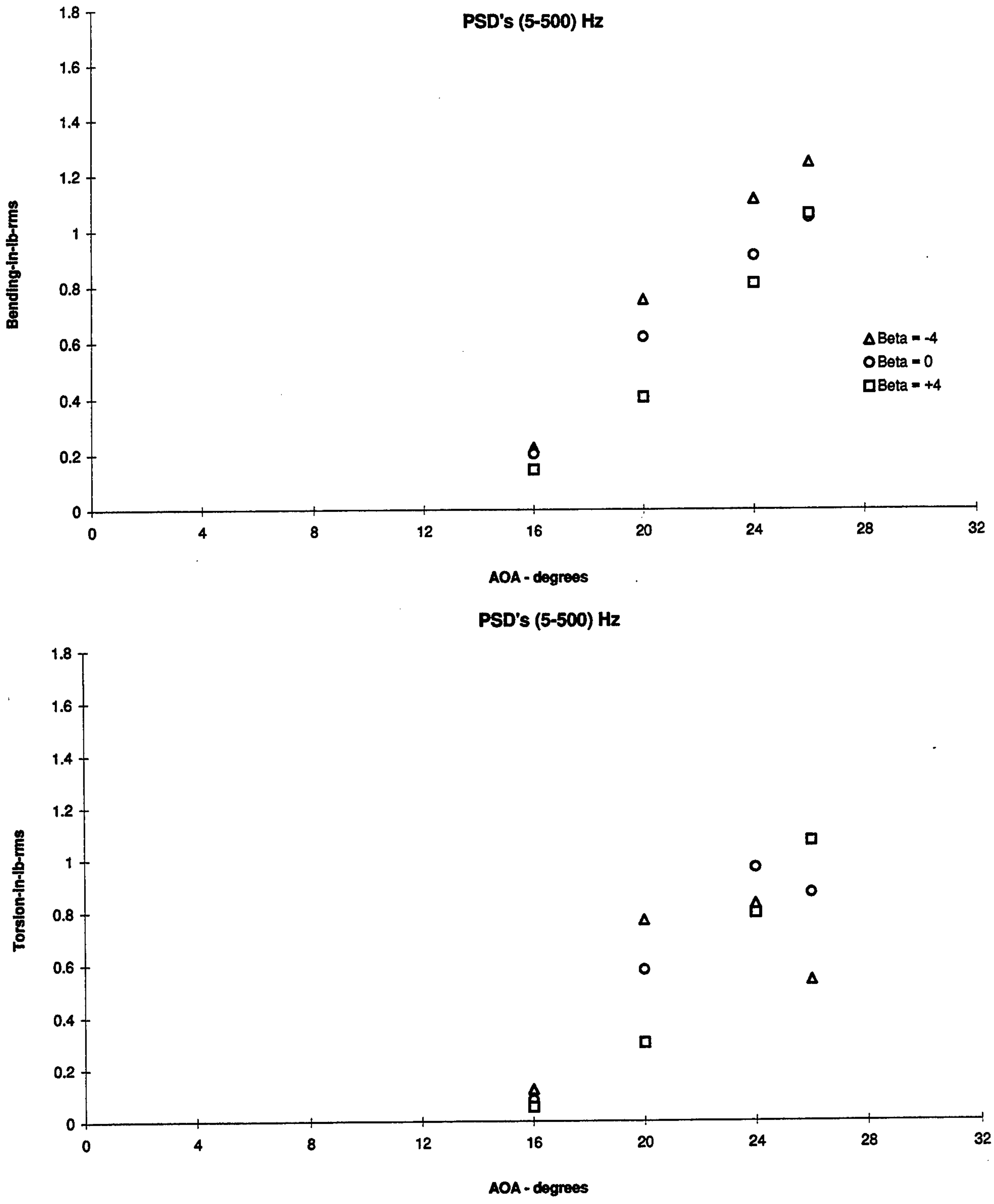

Figure 3.1.44 - Flex Tail Response vs Angle of Attack Bending and Torsion, Q = 56 psf, Nose Blowing p = 87 psi

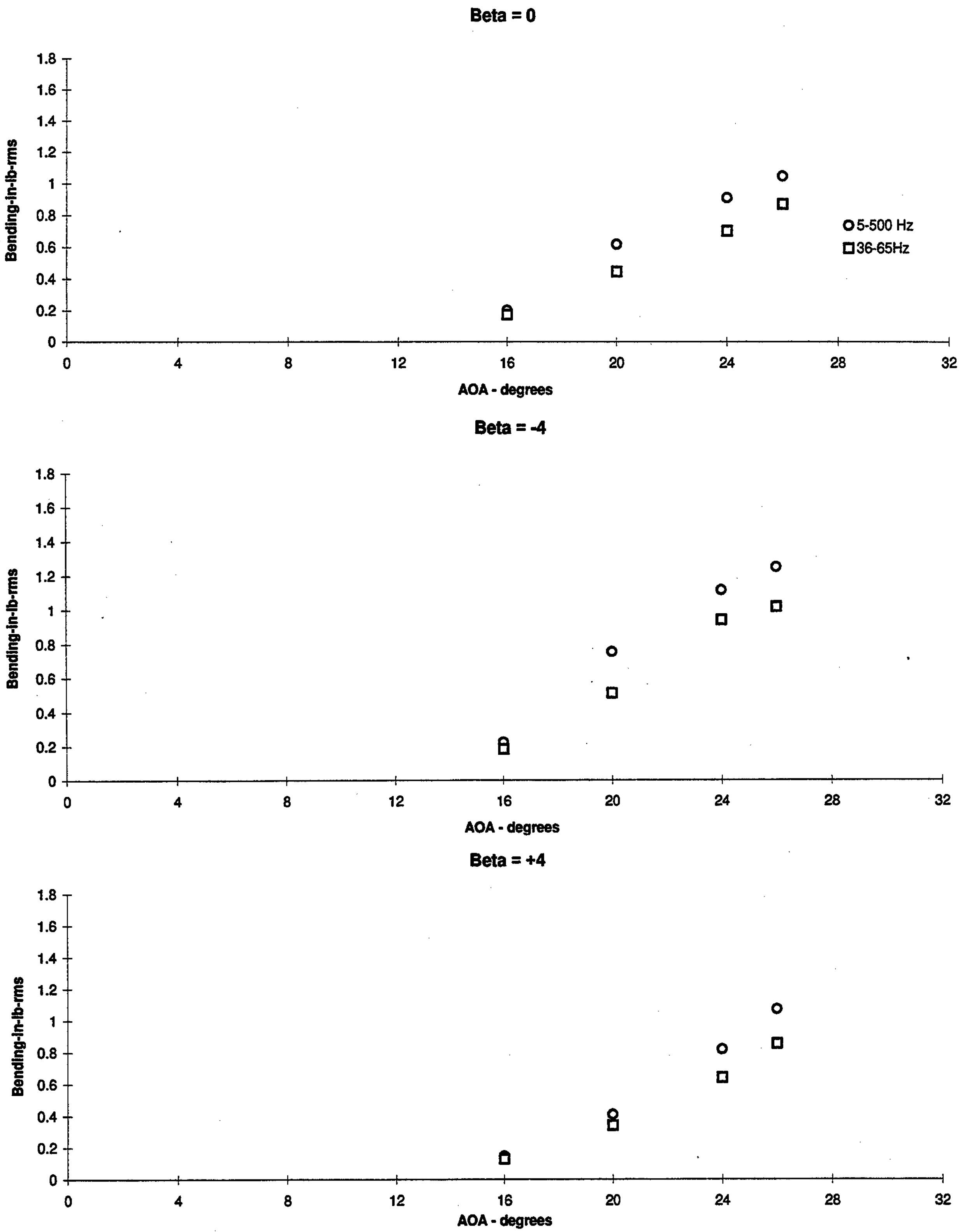

Figure 3.1.45 - Flex Tail Response vs Angle of Attack
Bending, Q = 56 psf, Nose Blowing p = 87 psi

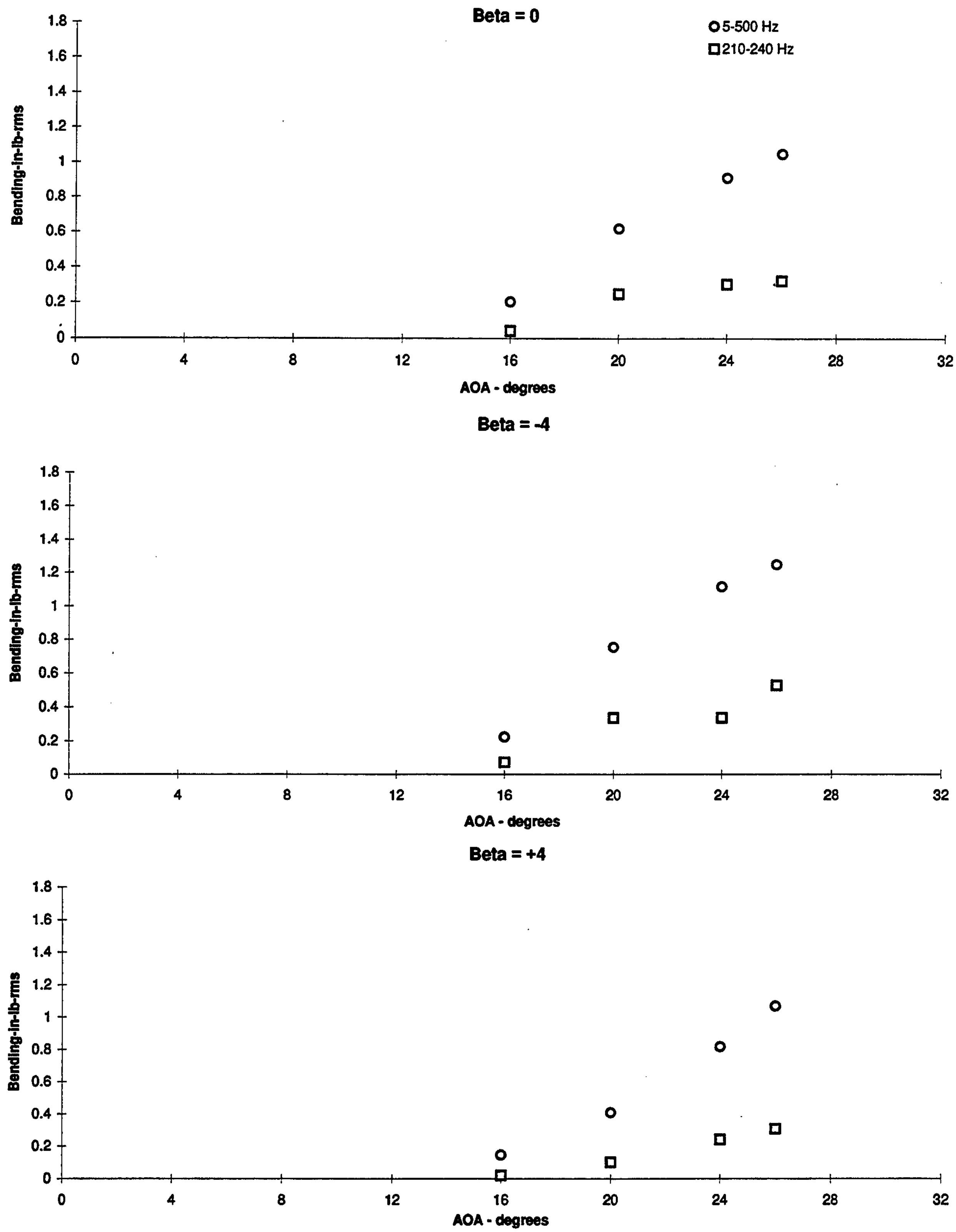

Figure 3.1.46 - Flex Tail Response vs Angle of Attack
Bending, Q = 56 psf, Nose Blowing p = 87 psi

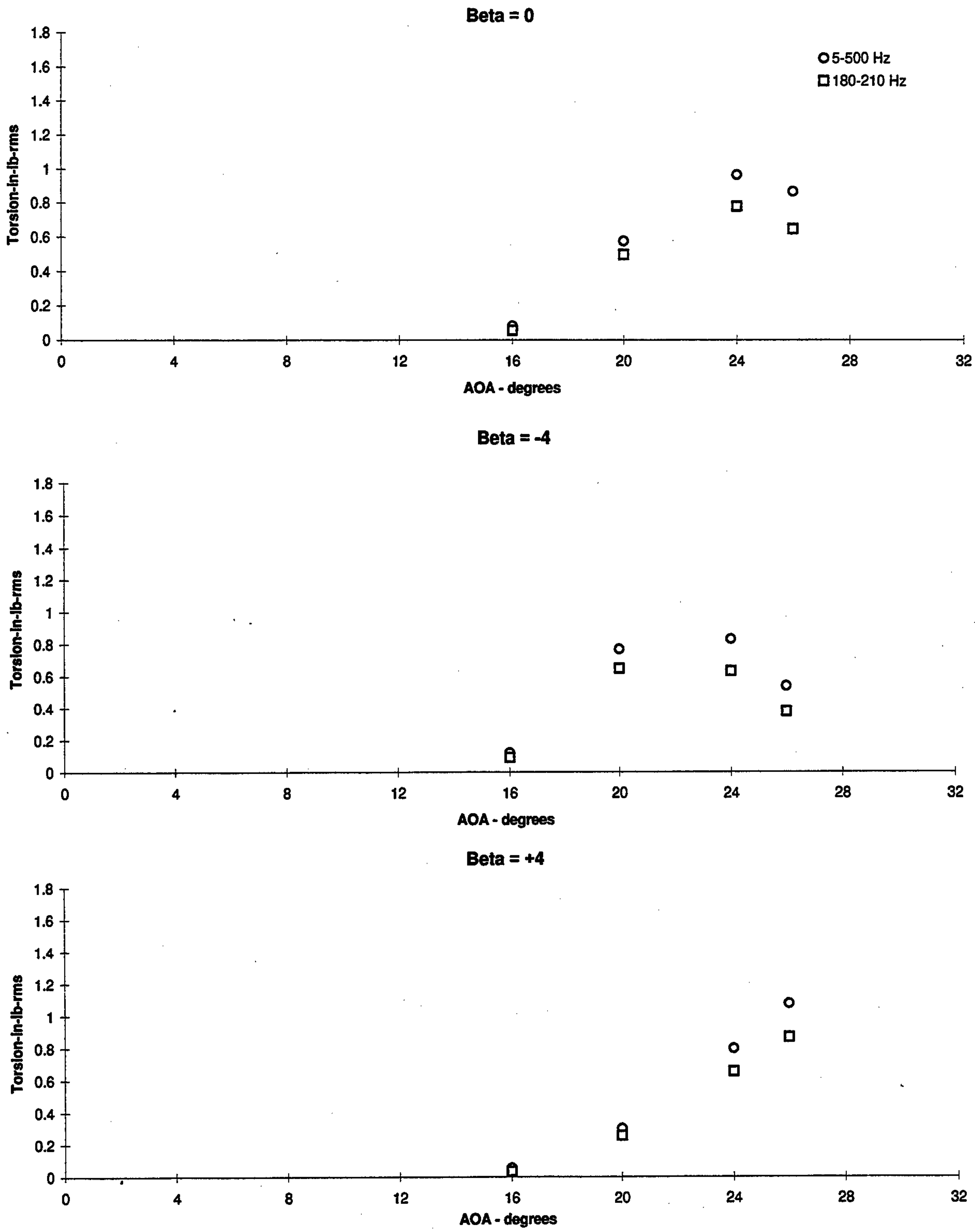

Figure 3.1.47 - Flex Tail Response vs Angle of Attack
Torsion, Q = 56 psf, Nose Blowing p = 87 psi

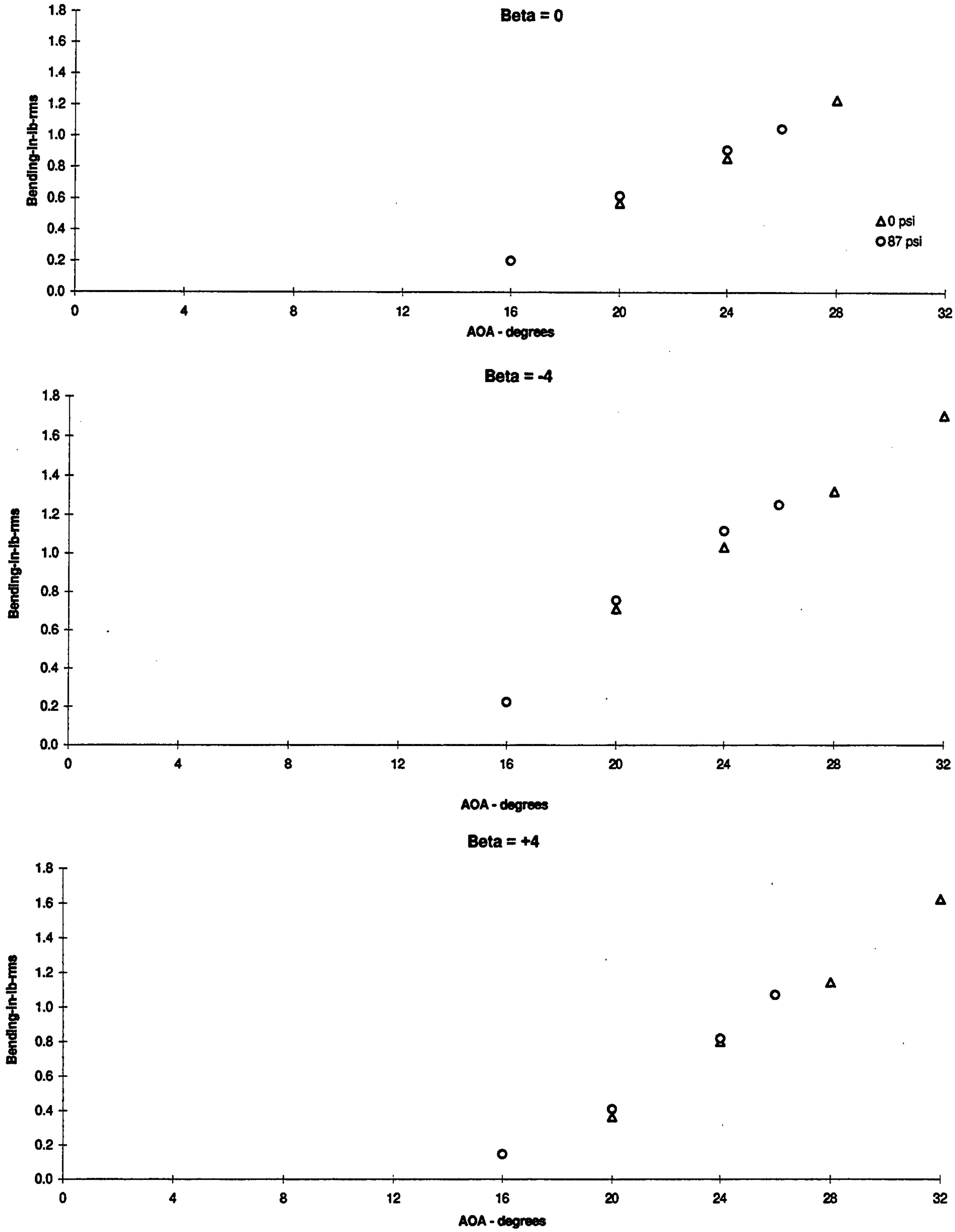

Figure 3.1.48 - Flex Tail Response vs Angle of Attack
Bending, Q = 56 psf, PSD's (5-500) Hz, Nose Blowing Summary

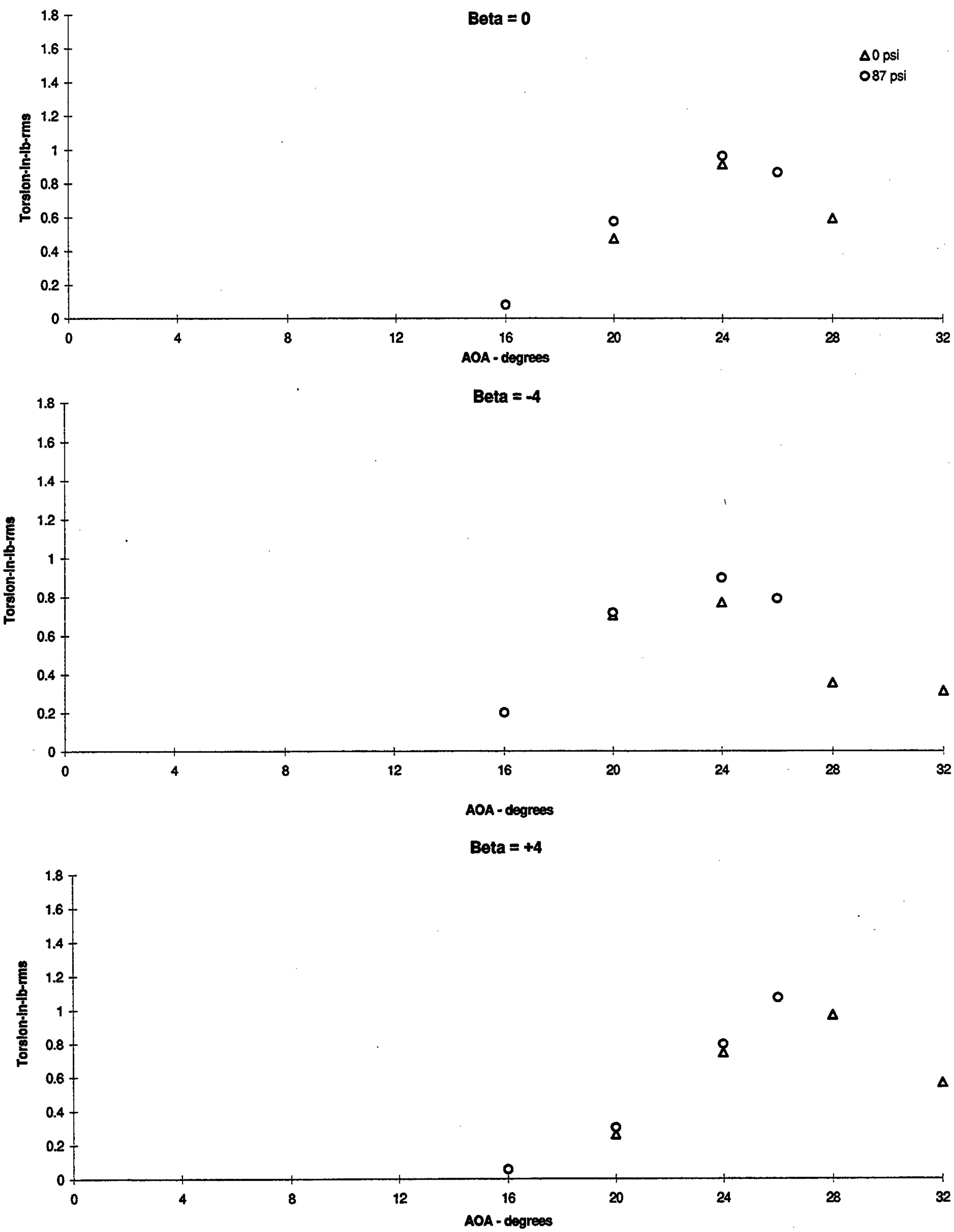

Figure 3.1.49 - Flex Tail Response vs Angle of Attack
Torsion, Q = 56 psf, PSD's (5-500) Hz, Nose Blowing Summary

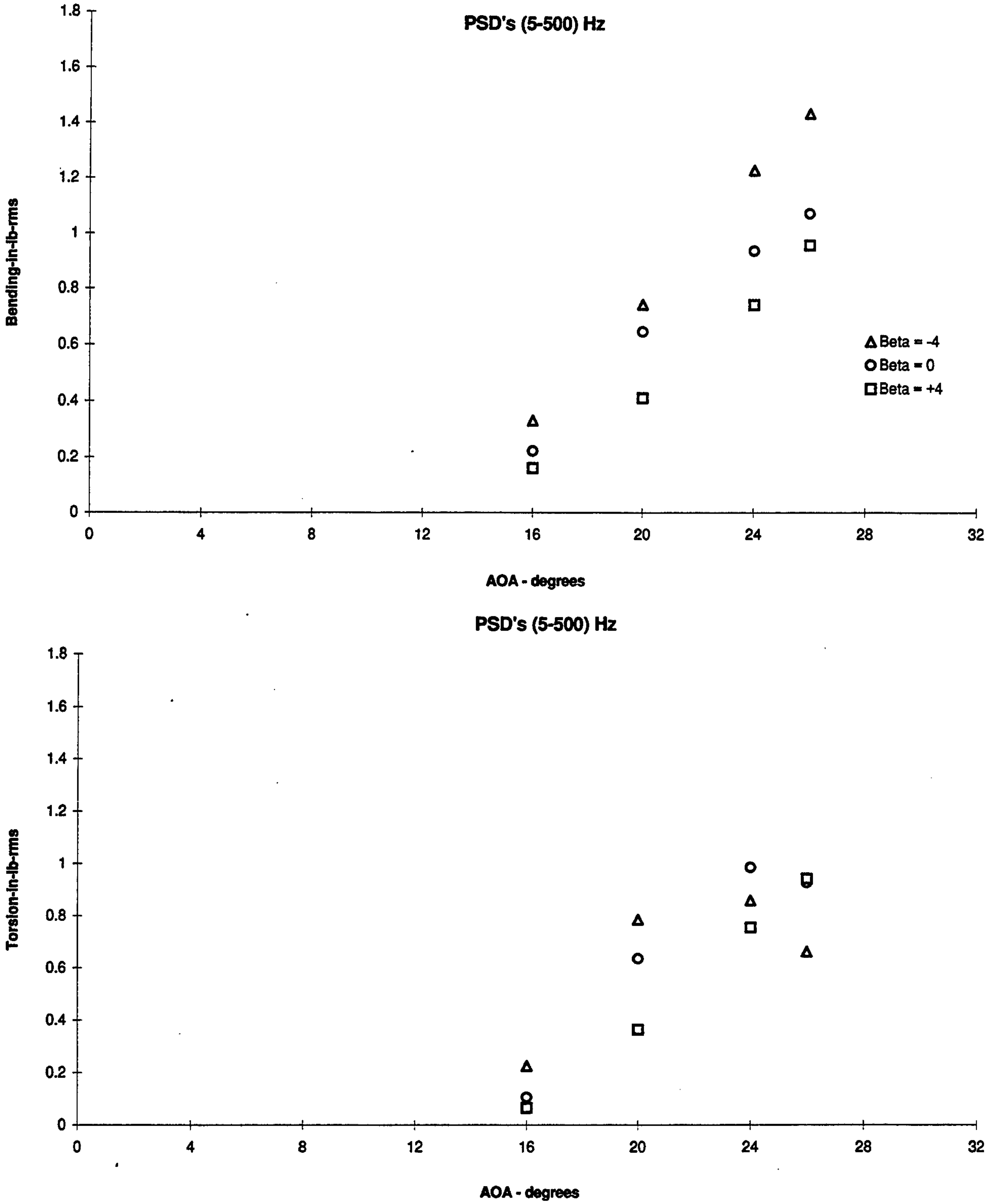

Figure 3.1.50 - Flex Tail Response vs Angle of Attack
Bending and Torsion, Q = 56 psf, Nose Blowing p = 87 psi, Gun p = 65 psi

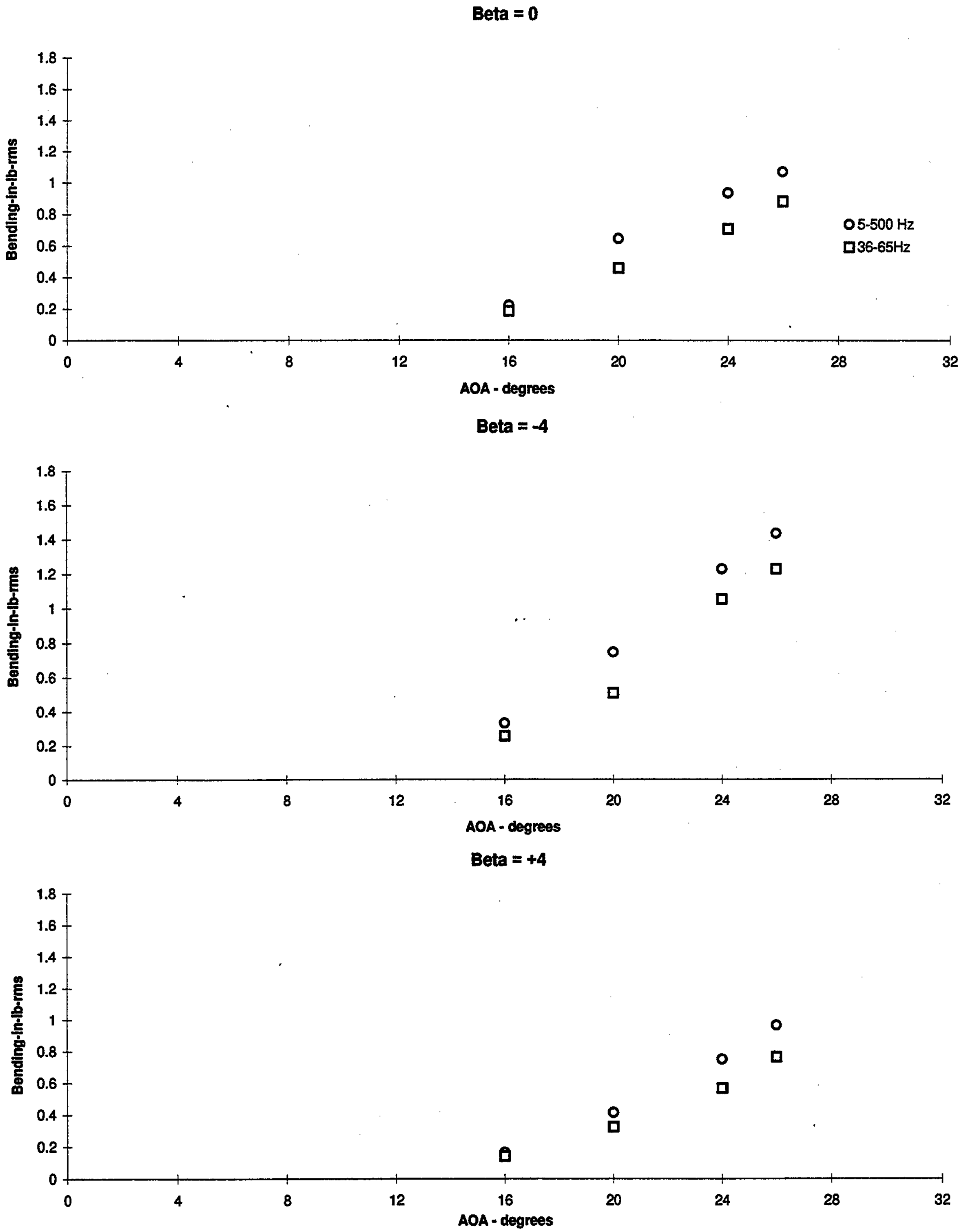

Figure 3.1.51 - Flex Tail Response vs Angle of Attack
Bending, Q = 56 psf, Nose Blowing p = 87 psi, Gun p = 65 psi

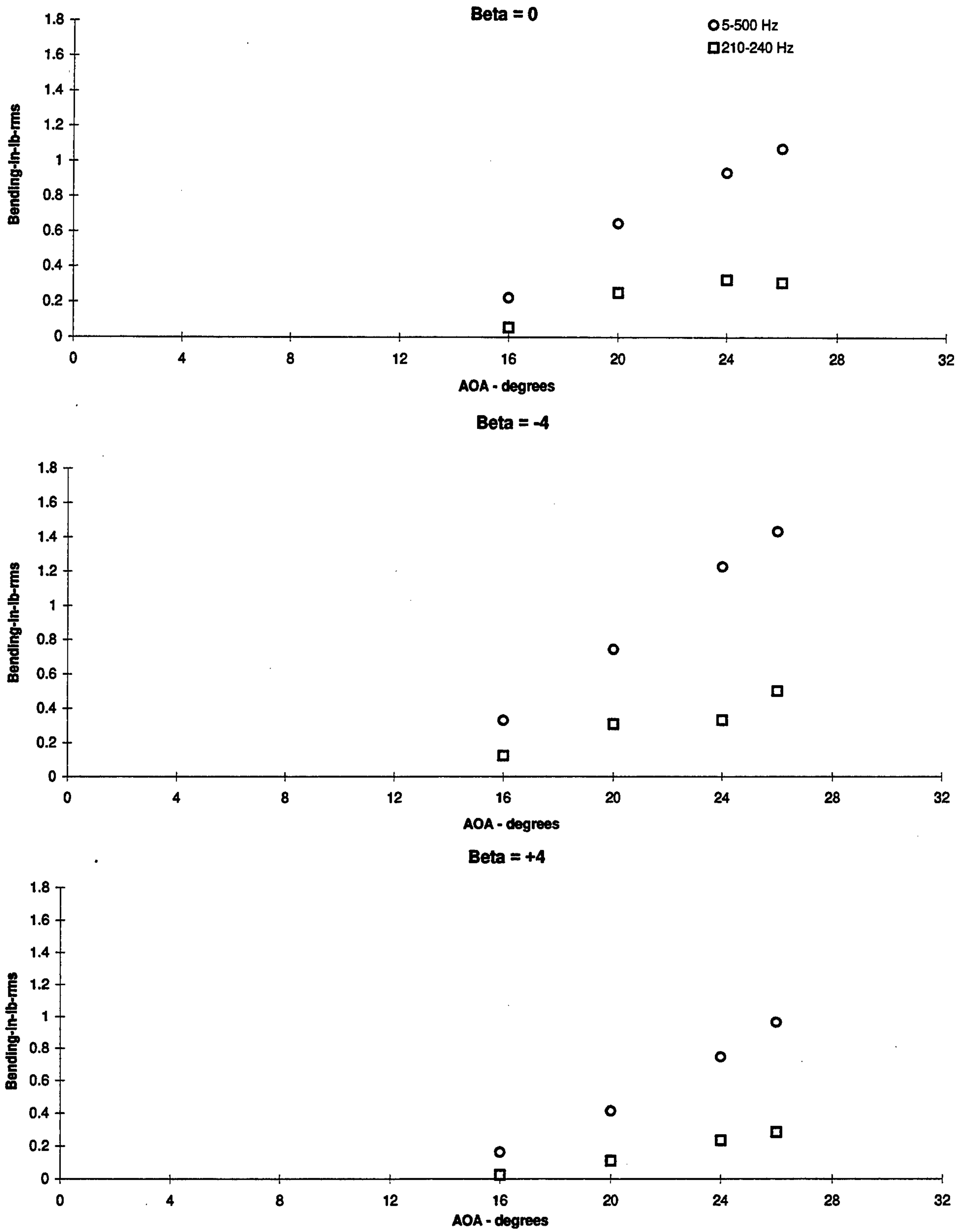

Figure 3.1.52 - Flex Tail Response vs Angle of Attack
Bending, Q = 56 psf, Nose Blowing p = 87 psi, Gun p = 65 psi

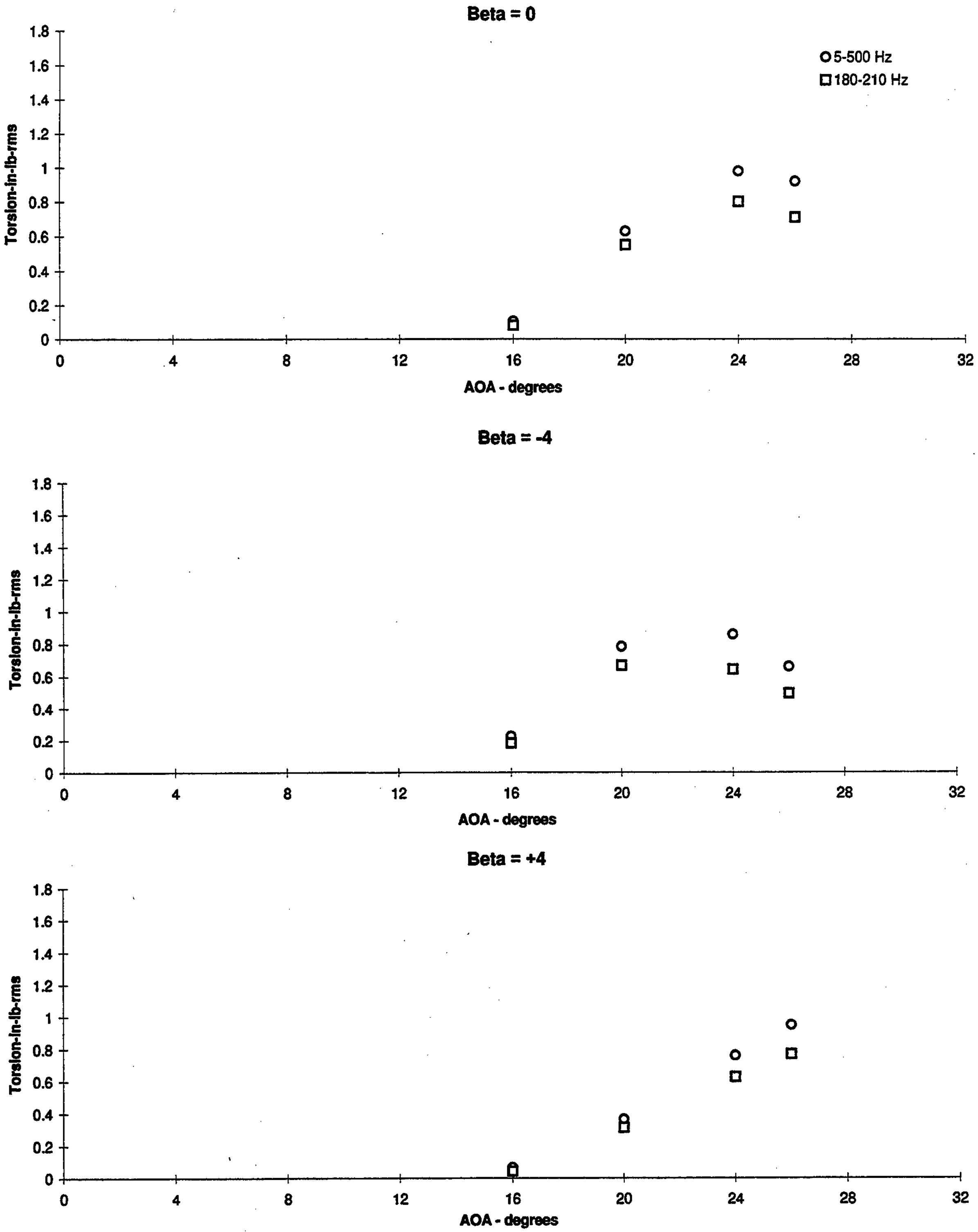

Figure 3.1.53 - Flex Tail Response vs Angle of Attack
Torsion, Q = 56 psf, Nose Blowing p = 87 psi, Gun p = 65 psi

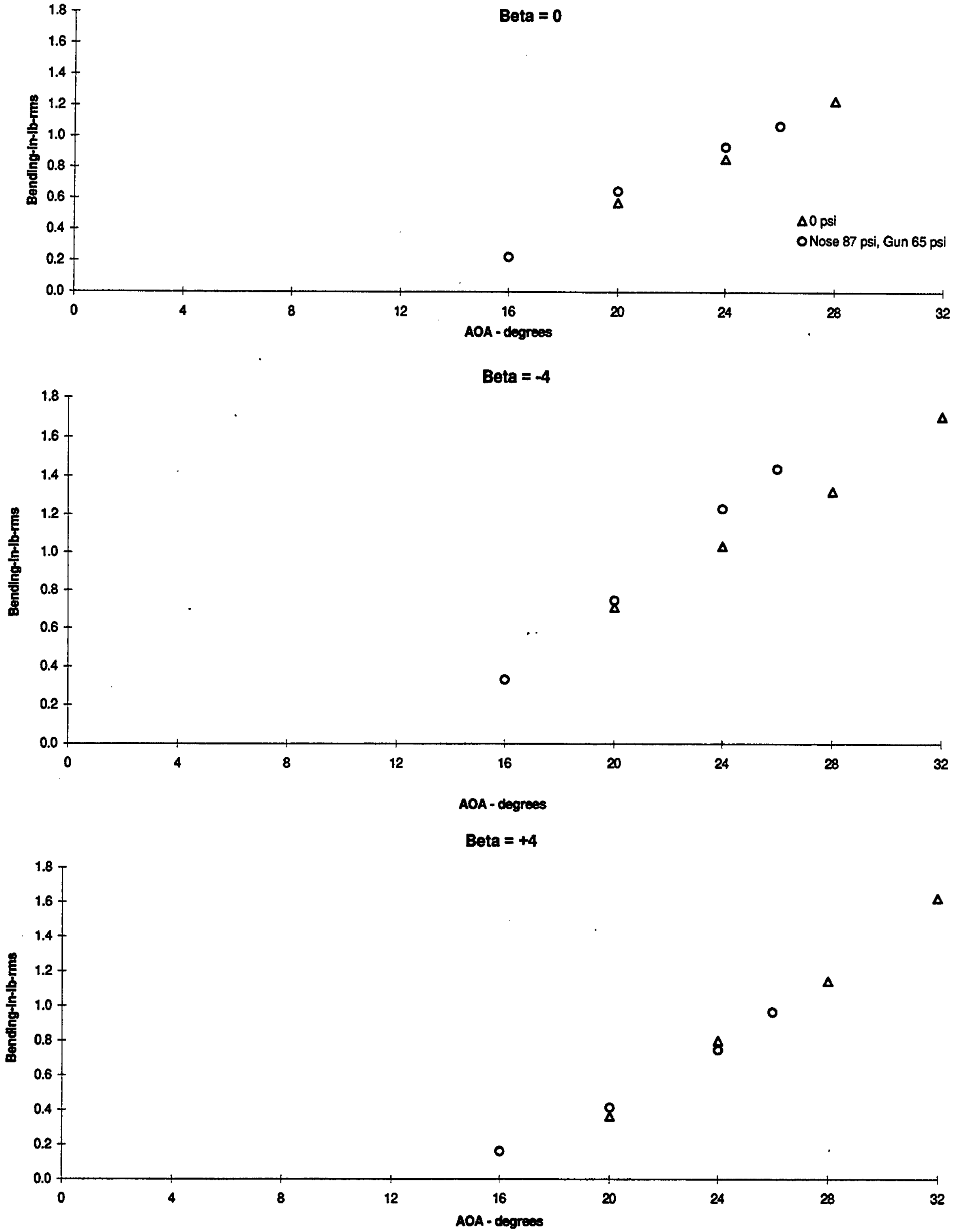

Figure 3.1.54 - Flex Tail Response vs Angle of Attack
Bending, Q = 56 psf, PSD's (5-500) Hz, Nose and Gun Blowing Summary

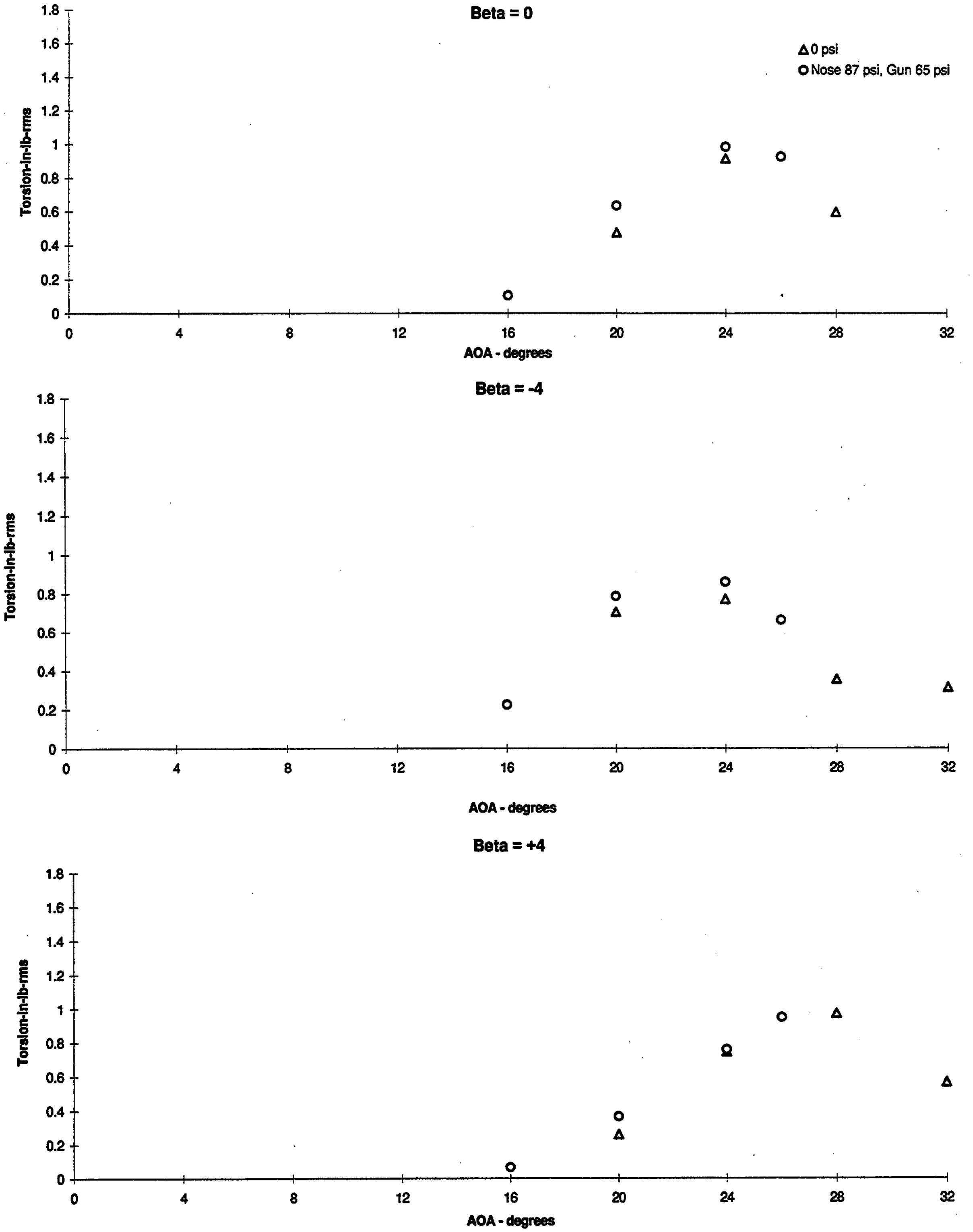

Figure 3.1.55 - Flex Tail Response vs Angle of Attack
Torsion, Q = 56 psf, PSD's (5-500) Hz, Nose and Gun Blowing Summary

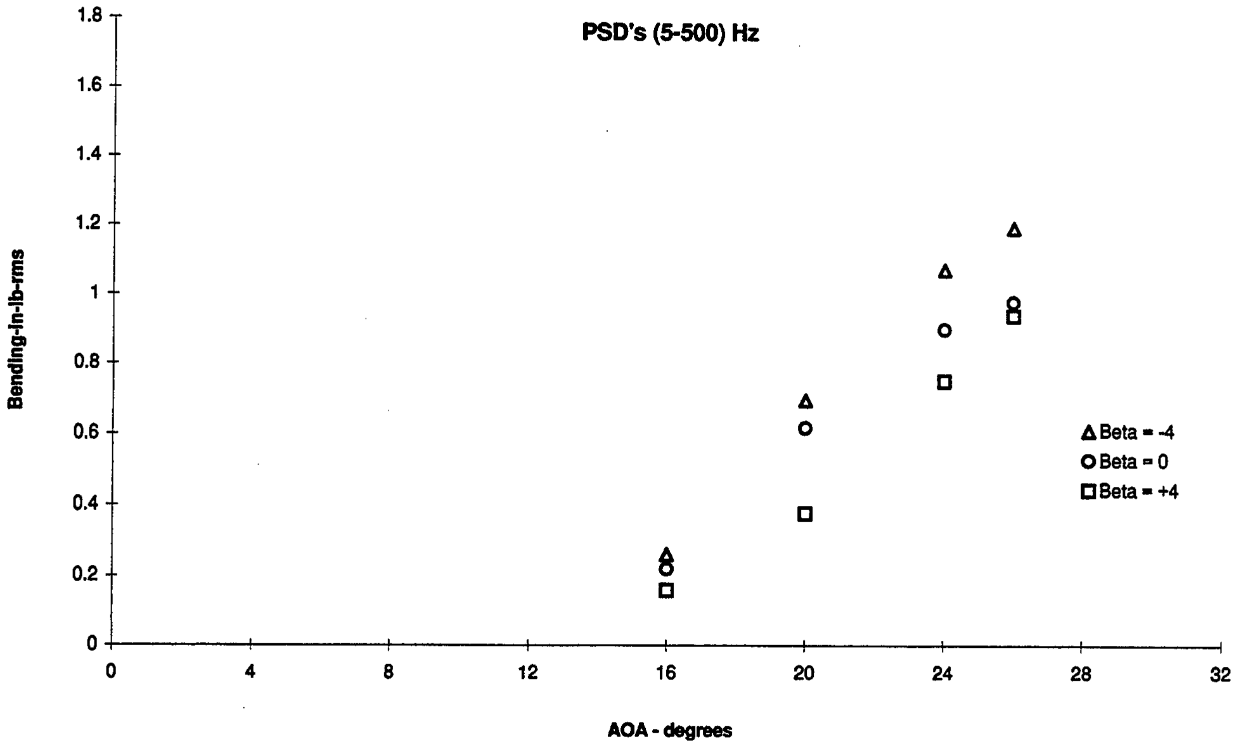

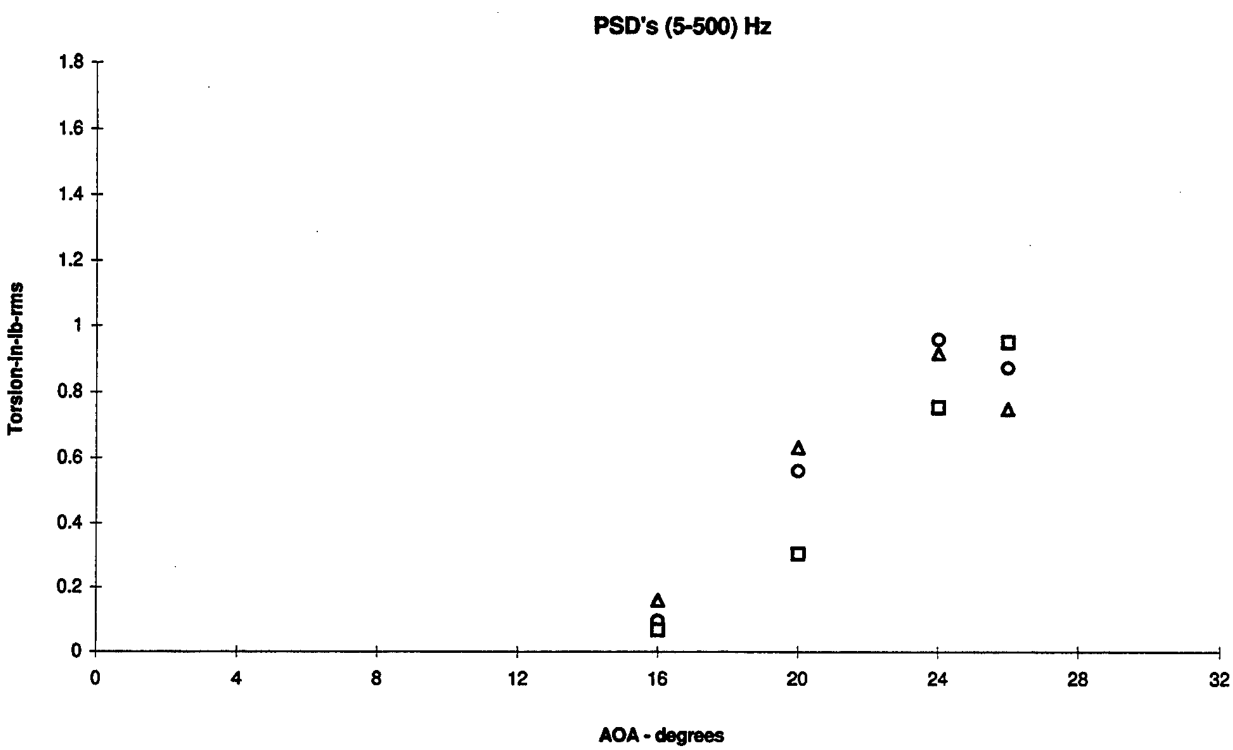

Figure 3.1.56 - Flex Tail Response vs Angle of Attack
Bending and Torsion, Q = 56 psf, Nose Blowing p = 87 psi, Wing L.E. p = 65 psi

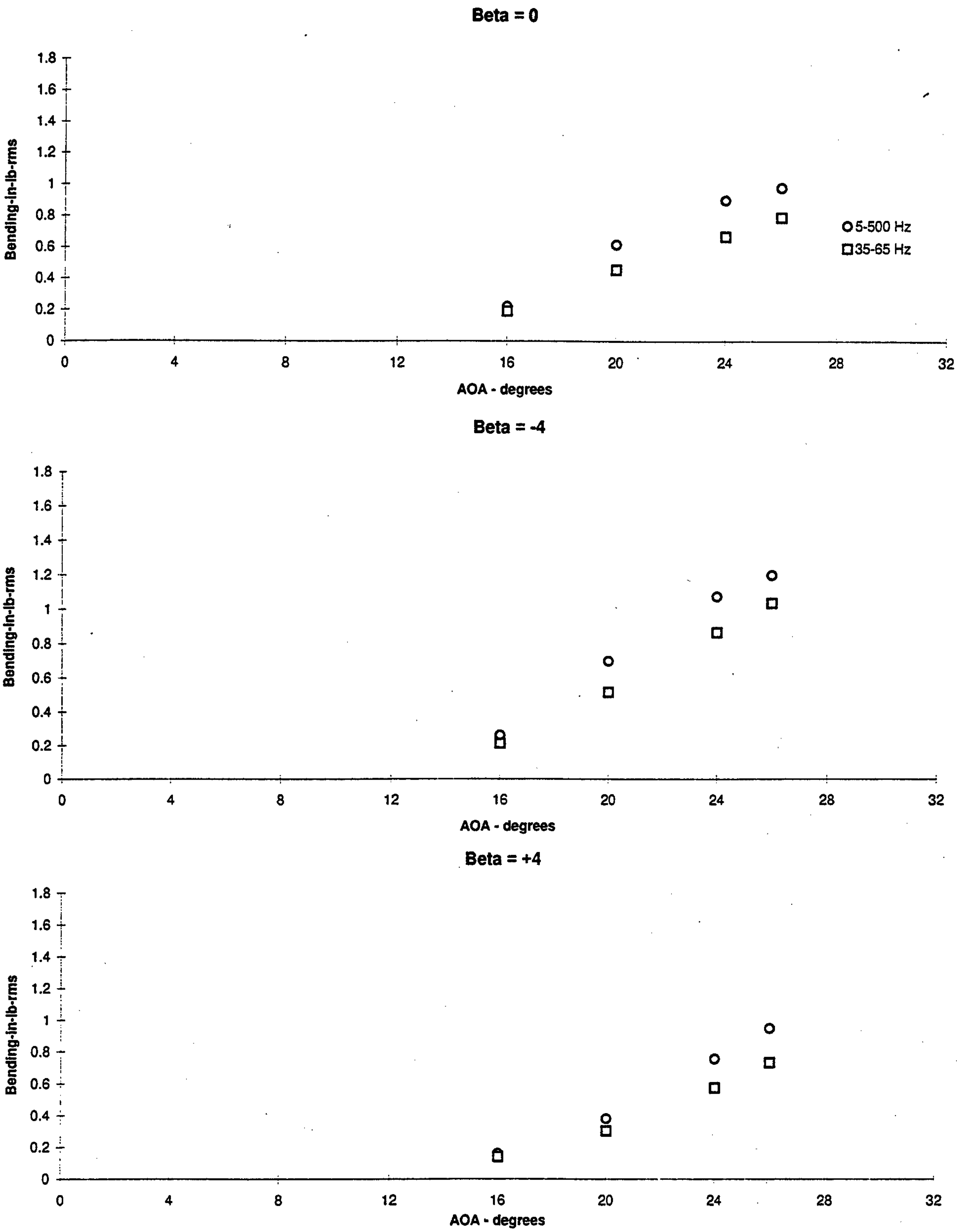

Figure 3.1.57 - Flex Tail Response vs Angle of Attack
Bending, Q = 56 psf, Nose Blowing p = 87 psi, Wing L.E. p = 65 psi

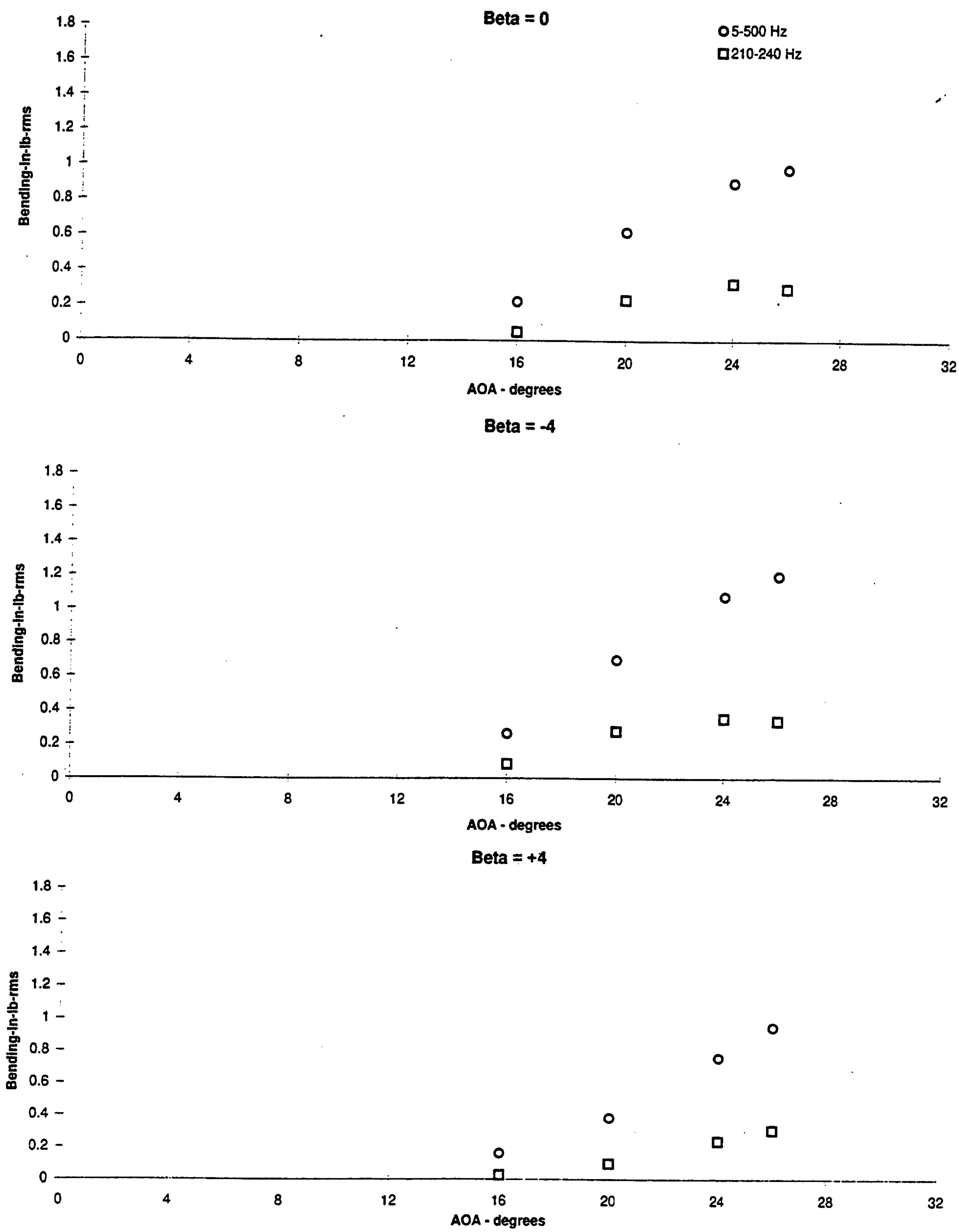

Figure 3.1.58 - Flex Tail Response vs Angle of Attack
Bending, Q = 56 psf, Nose Blowing p = 87 psi, Wing L.E. p = 65 psi

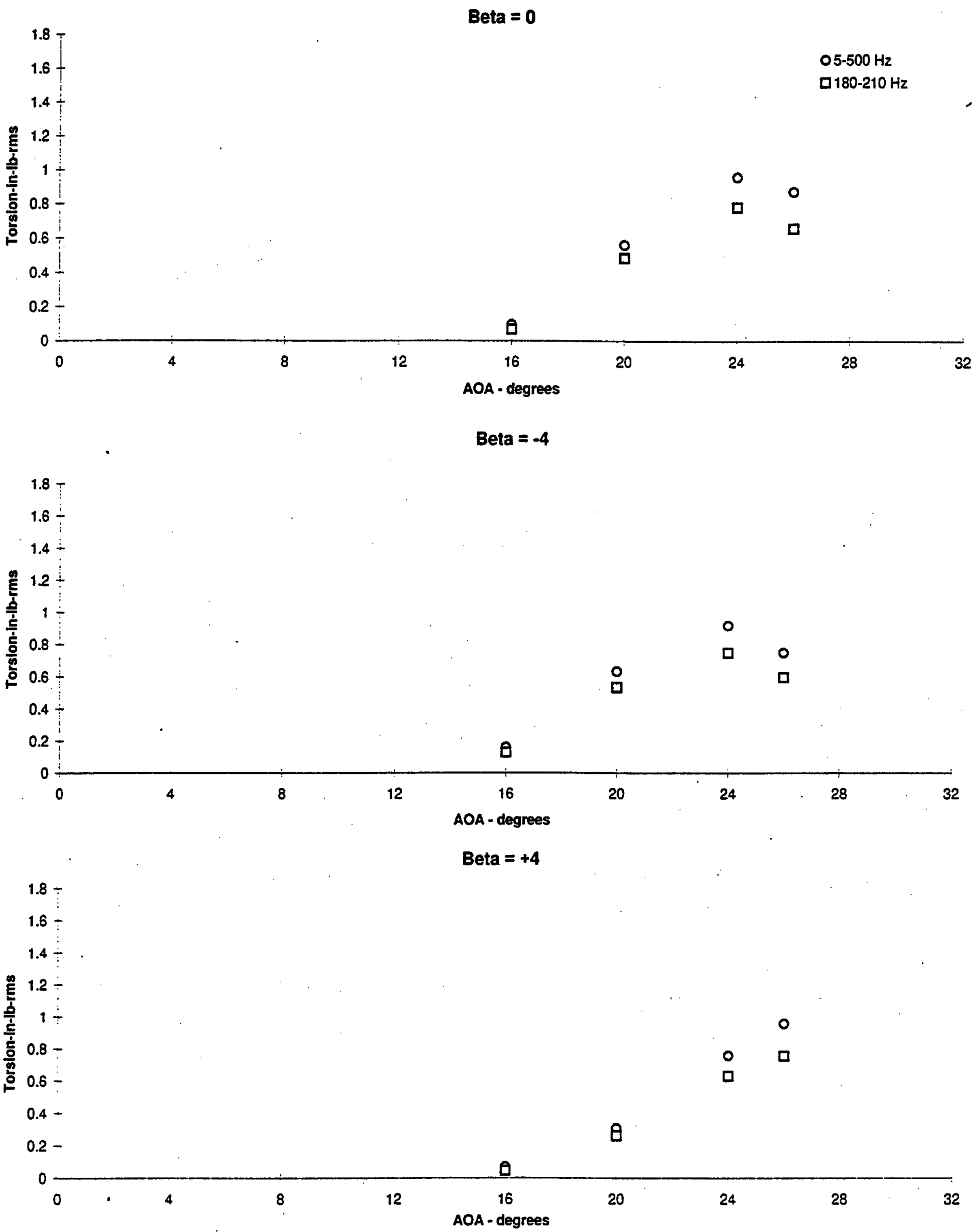

Figure 3.1.59 - Flex Tail Response vs Angle of Attack
Torsion, Q = 56 psf, Nose Blowing p = 87 psi, Wing L.E. p = 65 psi

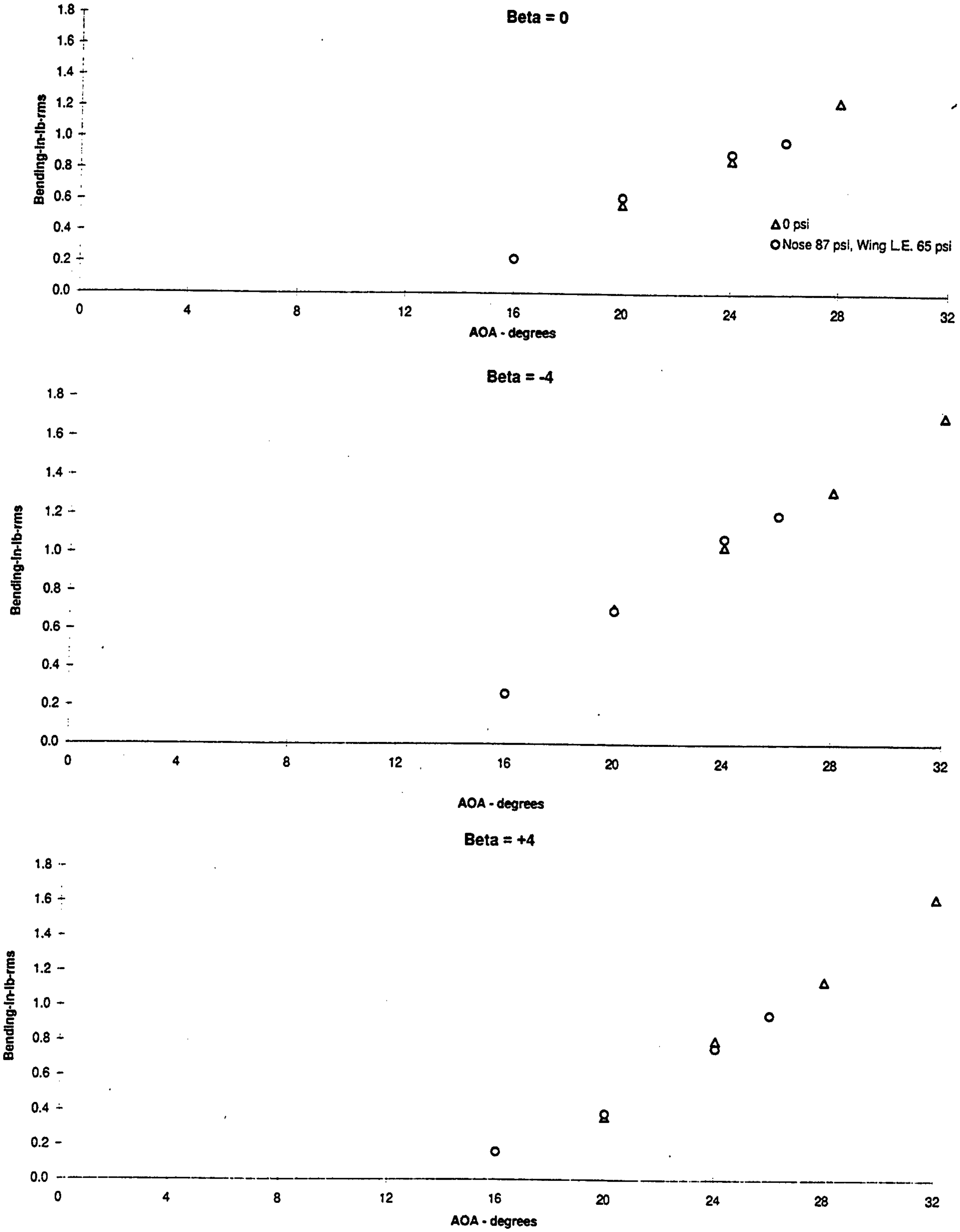

Figure 3.1.60 - Flex Tail Response vs Angle of Attack
Bending, Q = 56 psf, PSD's (5-500) Hz, Nose and Wing L.E. Blowing Summary

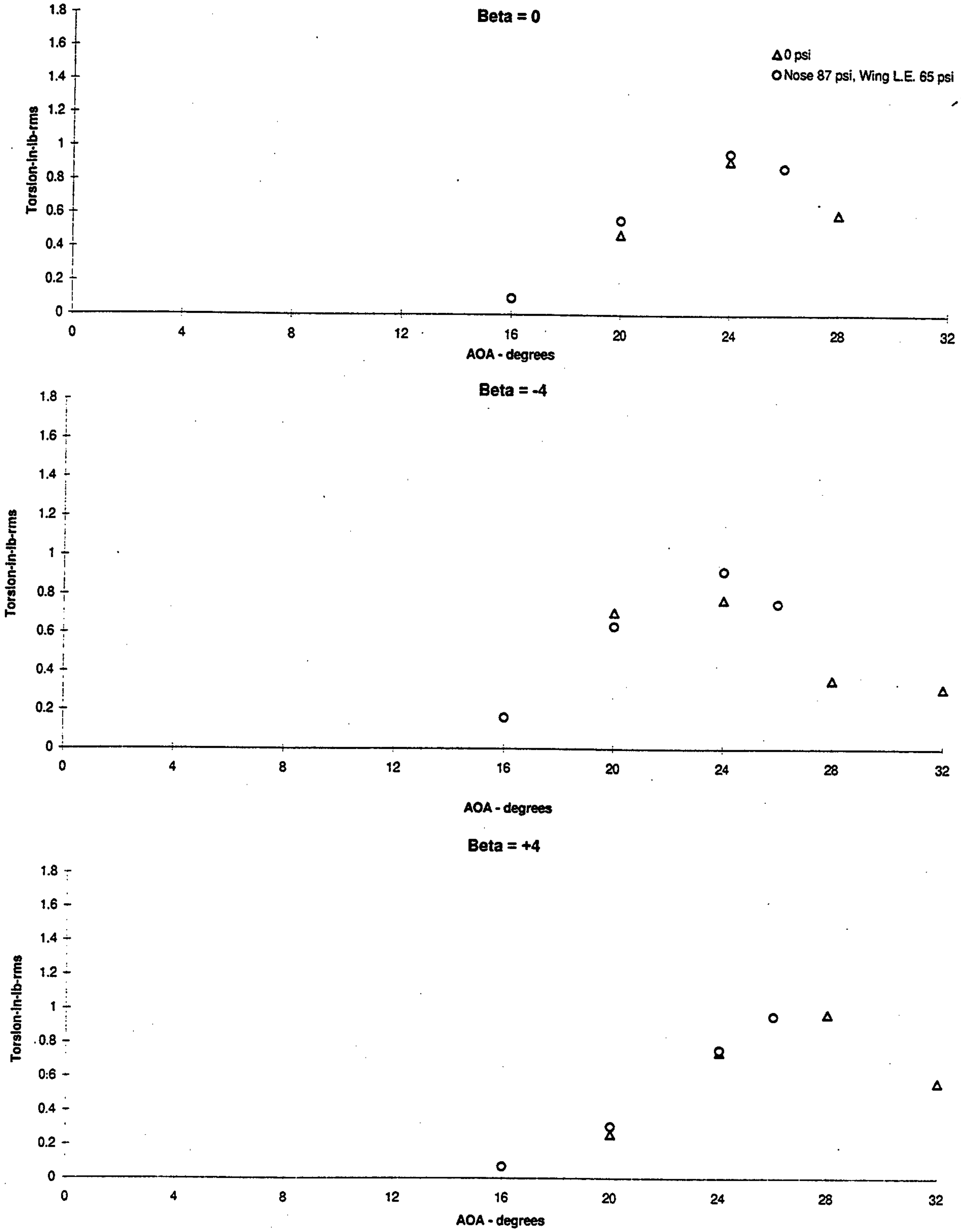

Figure 3.1.61 - Flex Tail Response vs Angle of Attack
Torsion, Q = 56 psf, PSD's (5-500) Hz, Nose and Wing L.E. Blowing Summary

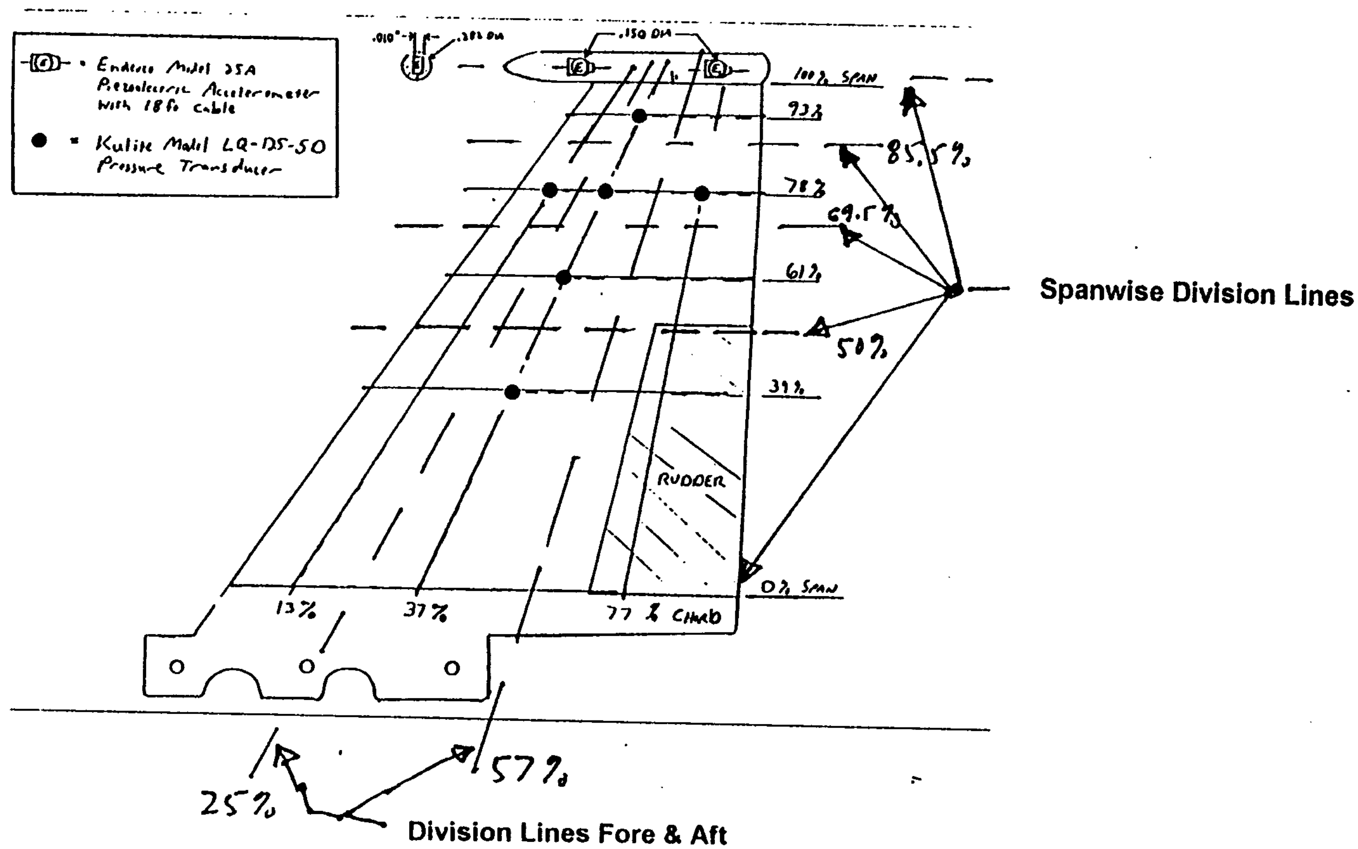

Figure 3.1.62 Sections Used in Pressure Integration

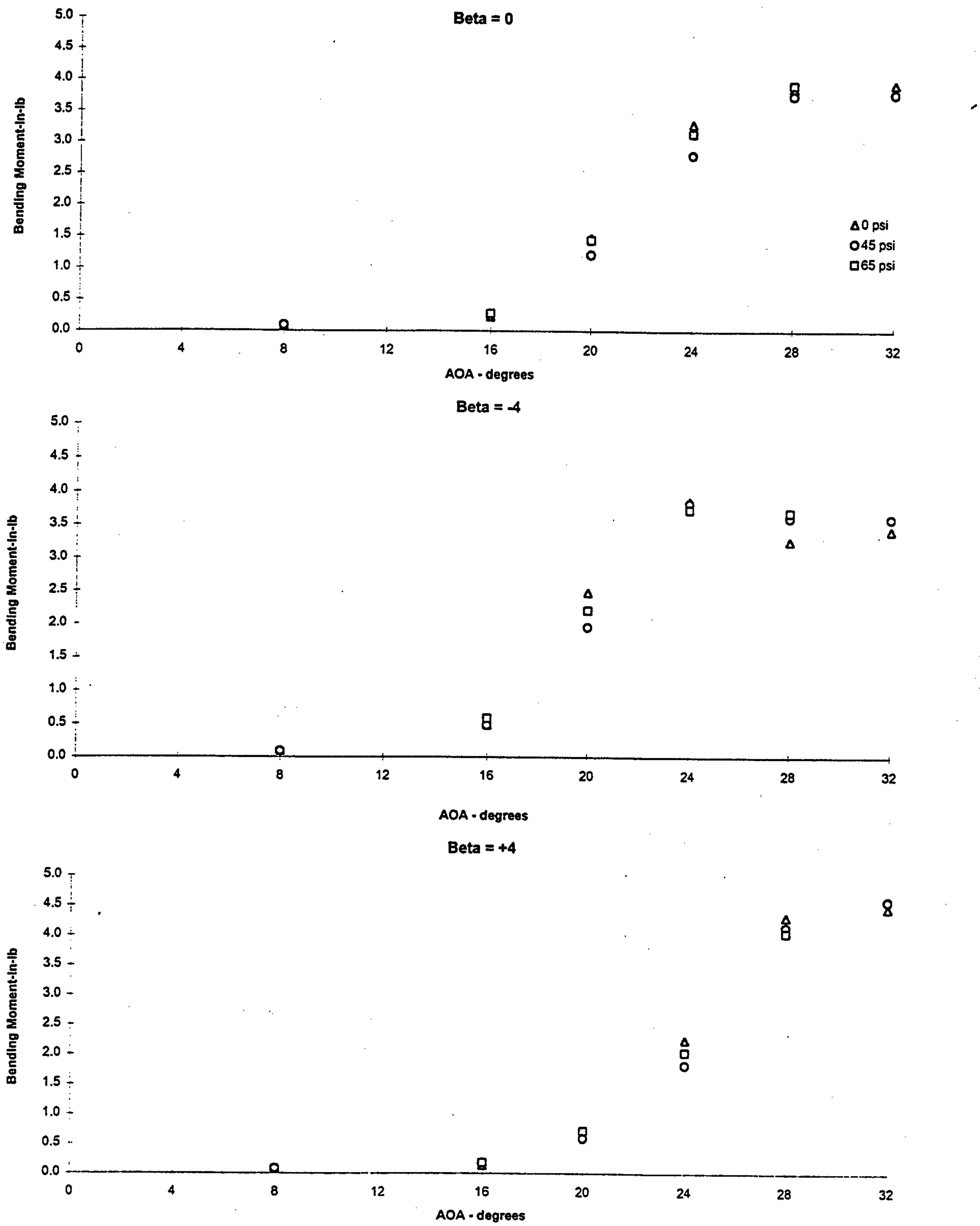

Figure 3.1.63 Flex Tail Bending Moment From Pressure Integration Vs Angle of Attack, Q = 56 PSF, Wing Blowing

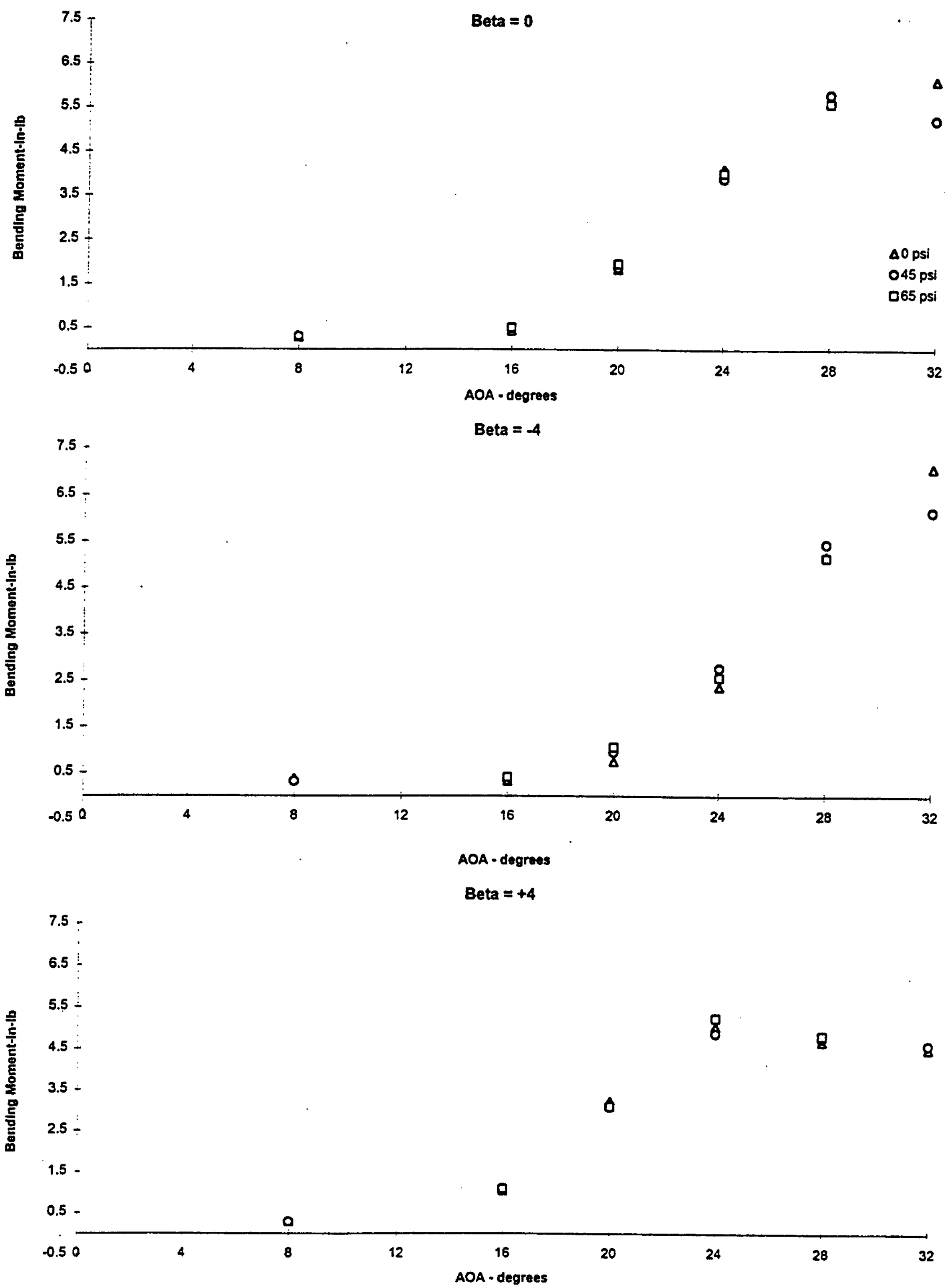

Figure 3.1.64 Rigid Tail Bending Moment From Pressure Integration Vs Angle of Attack, Q = 56 PSF, Wing Blowing

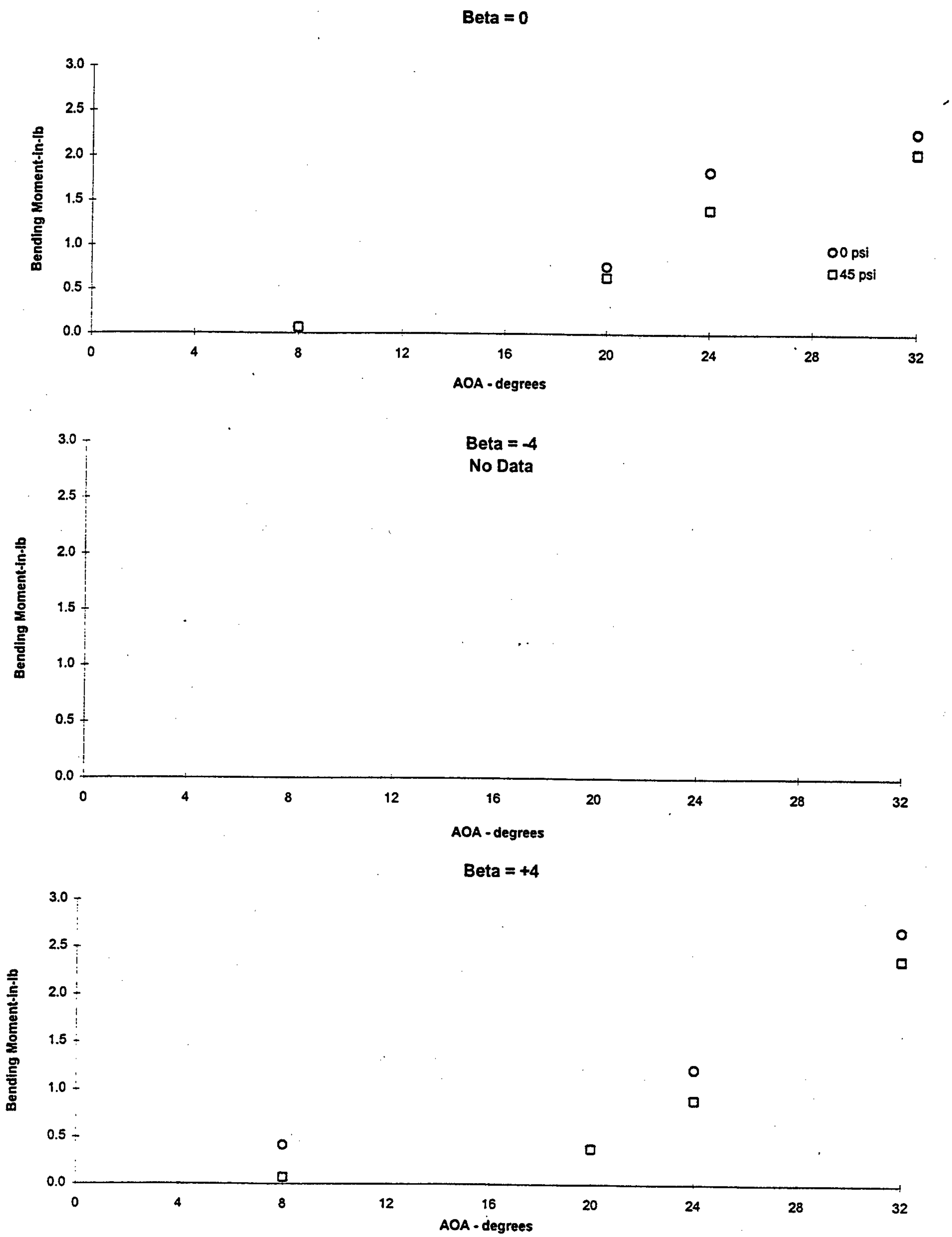

Figure 3.1.65 Flex Tail Bending Moment From Pressure Integration Vs Angle of Attack, Q = 30 PSF, Wing Blowing

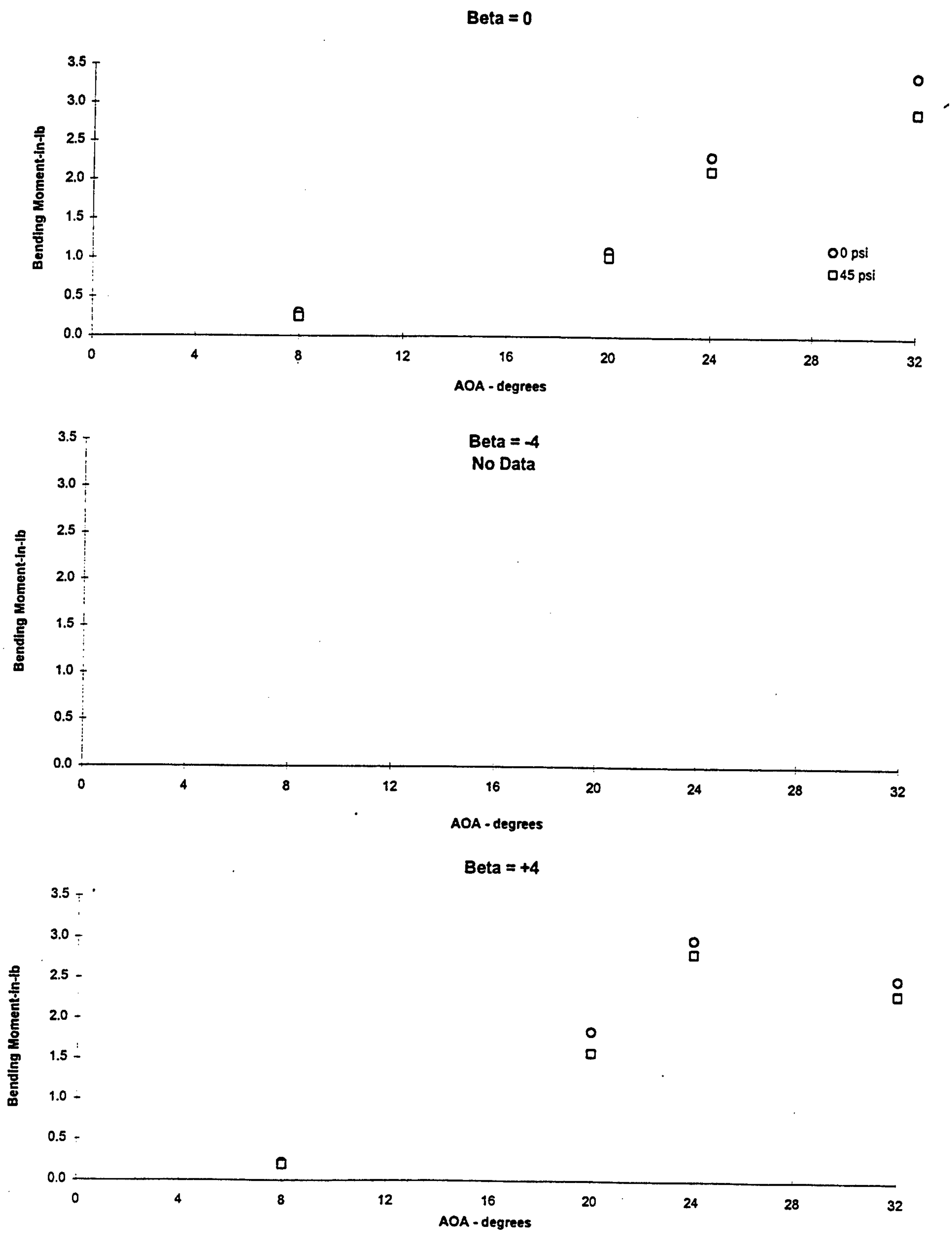

Figure 3.1.66 Rigid Tail Bending Moment From Pressure Integration Vs Angle of Attack, Q = 30 PSF, Wing Blowing

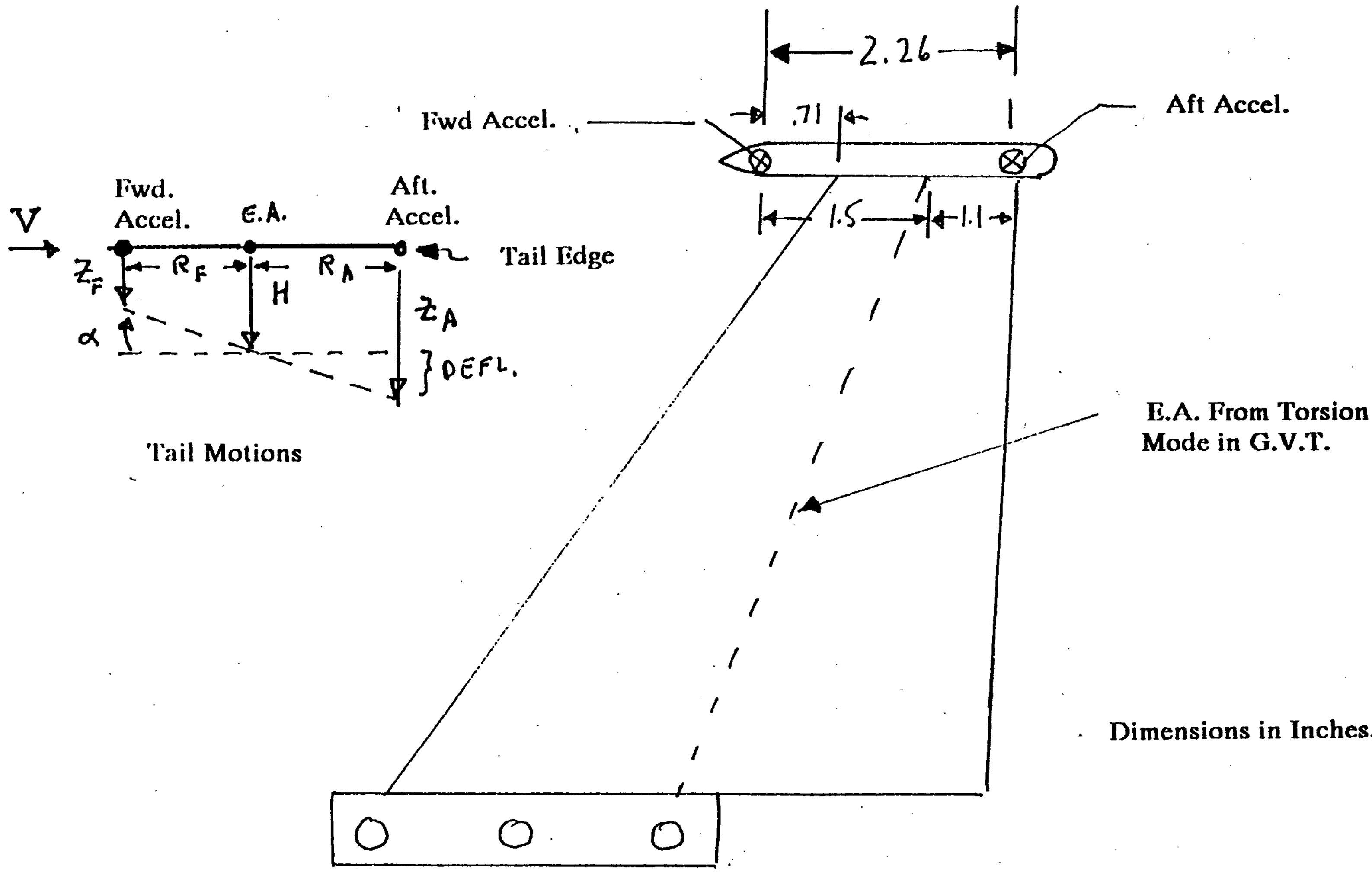

Figure 3.2.1 Geometry for Acceleration Data

F-15 TPN_2854: alpha=32 beta=0 bp=0

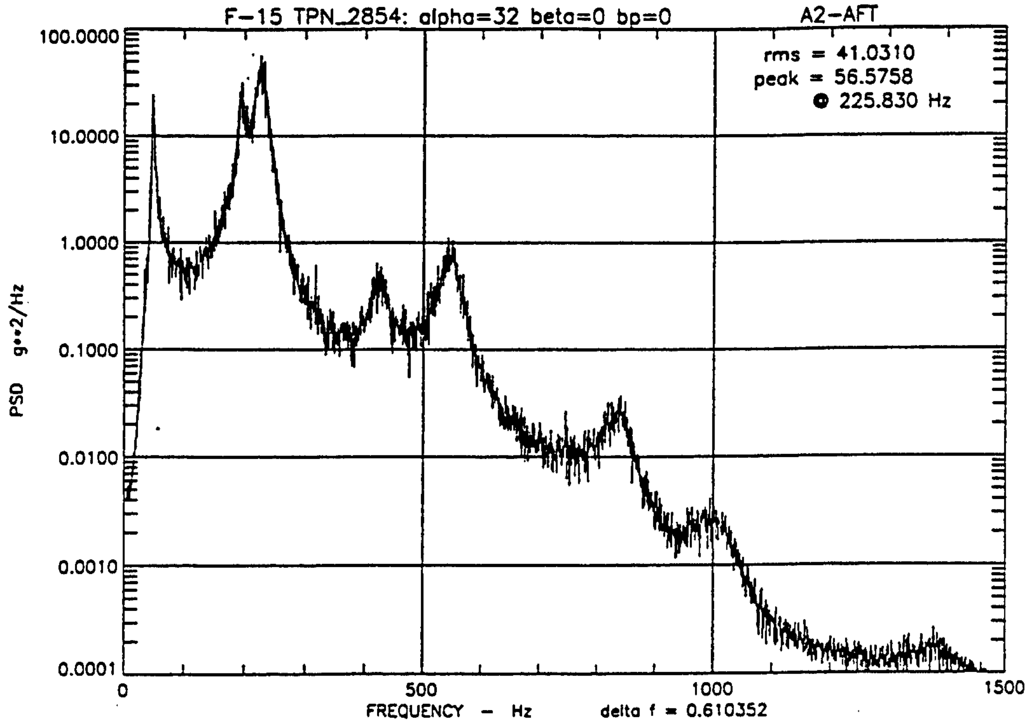

F-15 TPN_2854: alpha=32 beta=0 bp=0

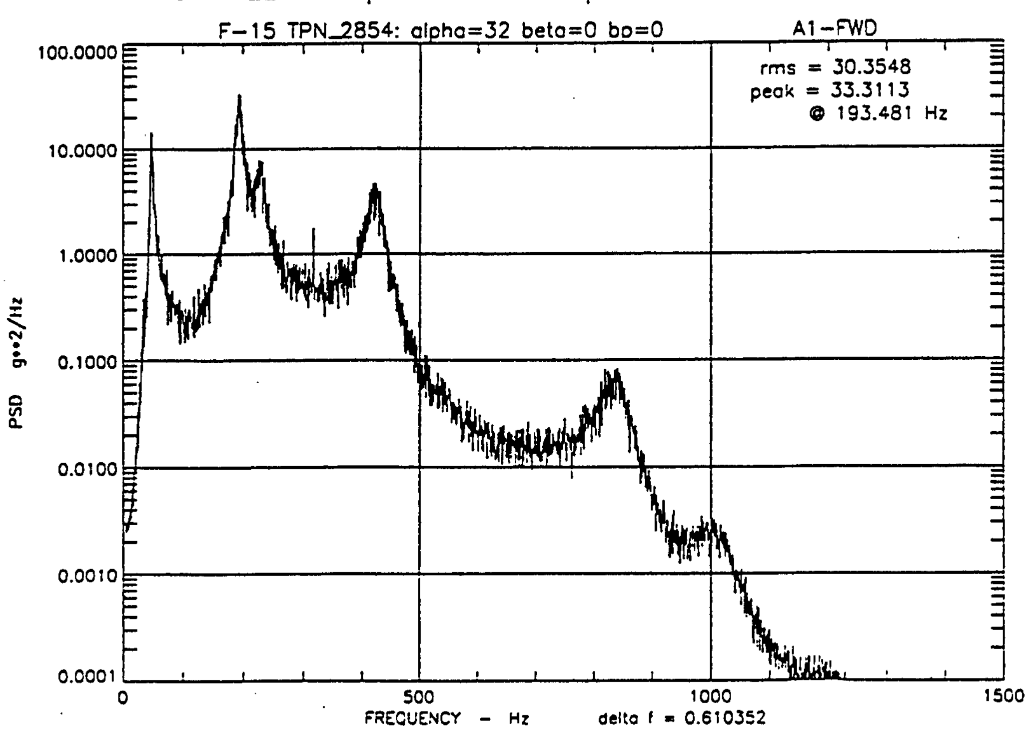

Figure 3.2.2 Accelertion PSD's , Q=56 PSF, Beta = 0, Alpha = 32 Deg, No Blowing

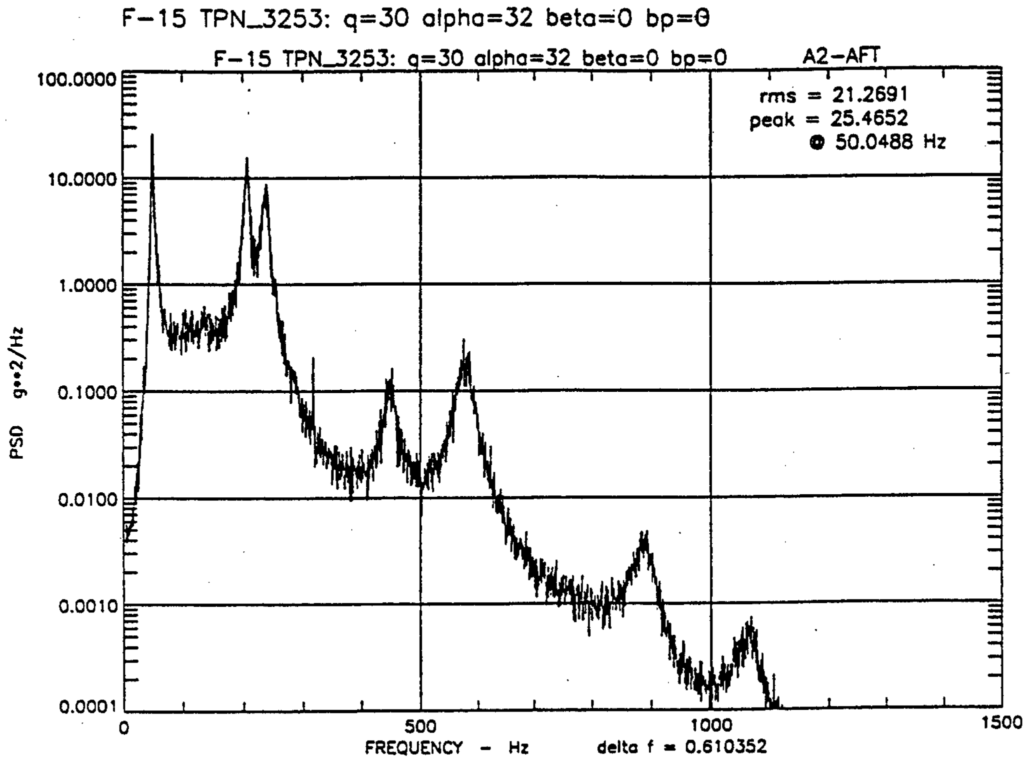

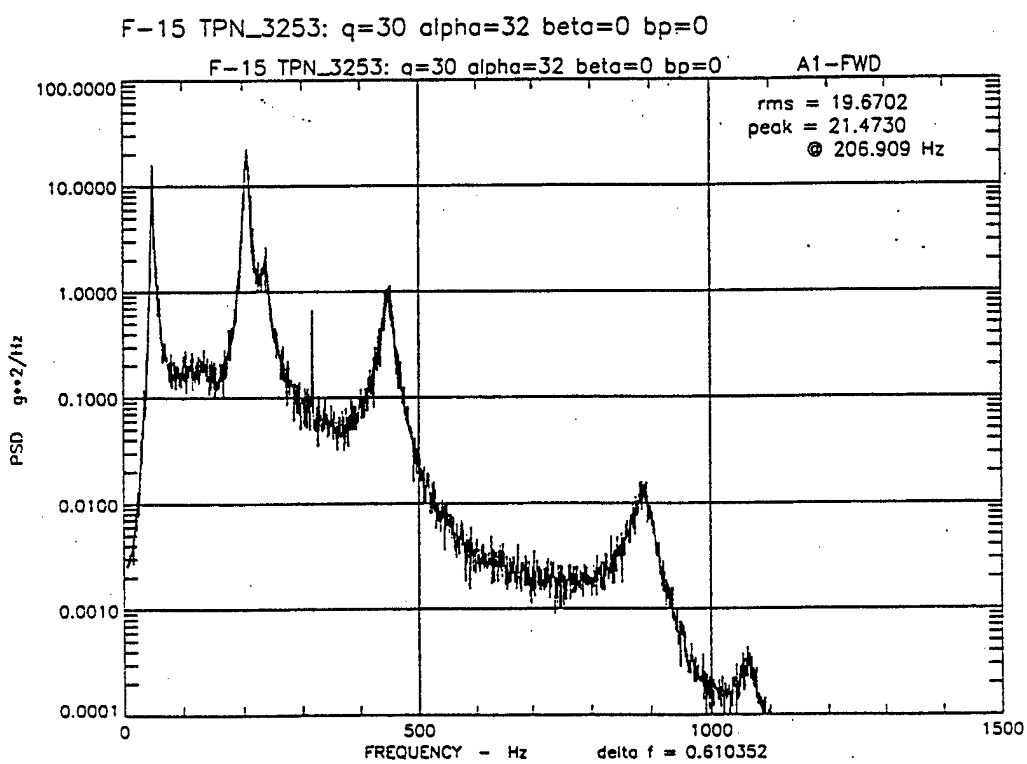

Figure 3.2.3 Acceleration PSD's , Q= 30 PSF, Beta = 0, Alpha= 32 Deg, No Blowing

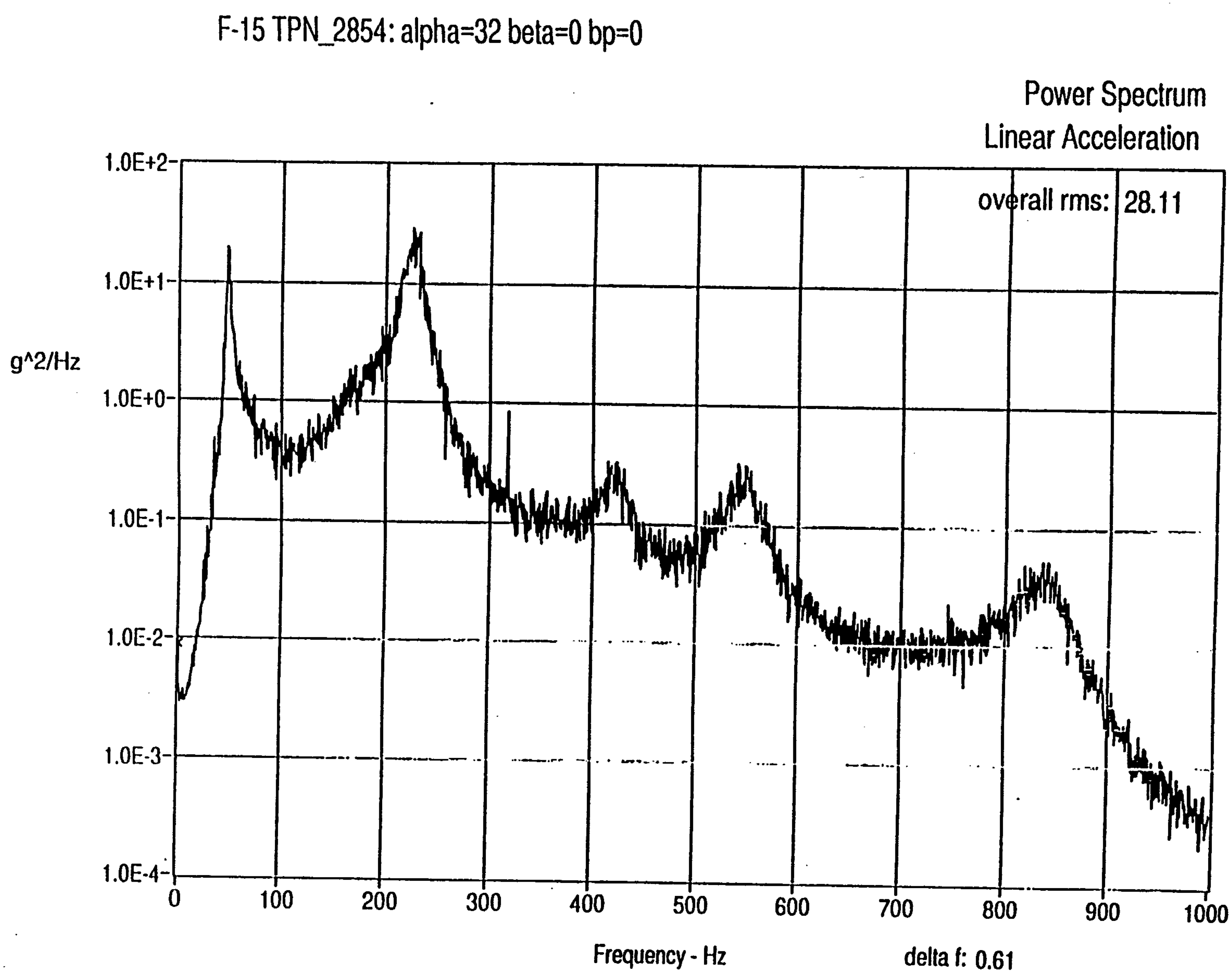

Figure 3.2.4 Bending Accelertion PSD's , Q =56 PSF, Beta = 0, Alpha = 32 Deg, No Blowing

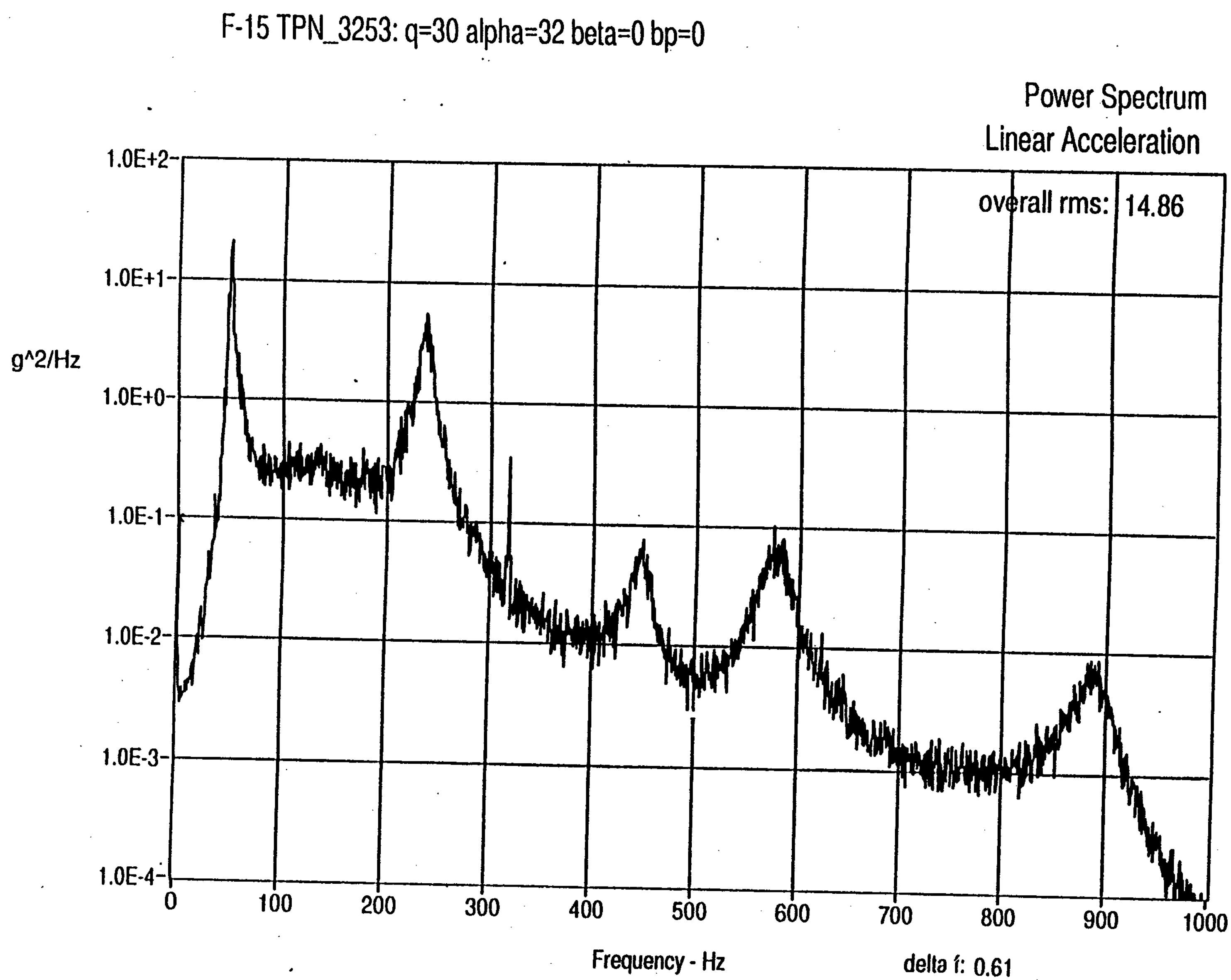

Figure 3.2.5 Bending Acceleration PSD's , Q = 30 PSF, Beta = 0, Alpha= 32 Deg, No Blowing

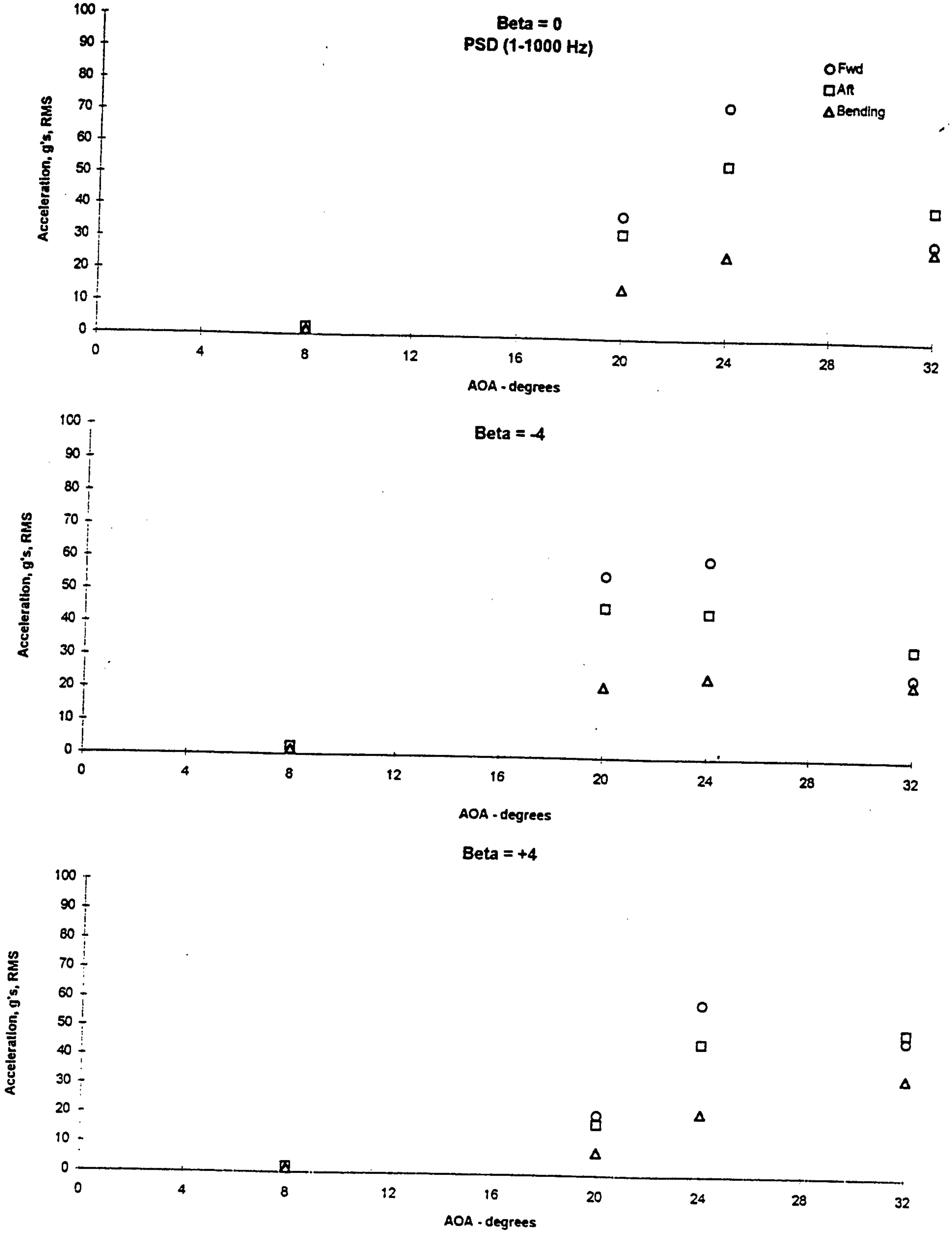

Figure 3.2.6 Flex. Tail Acceleration vs Angle of Attack, Q = 56 PSF, Beta = 0, -4, 4 , No Blowing

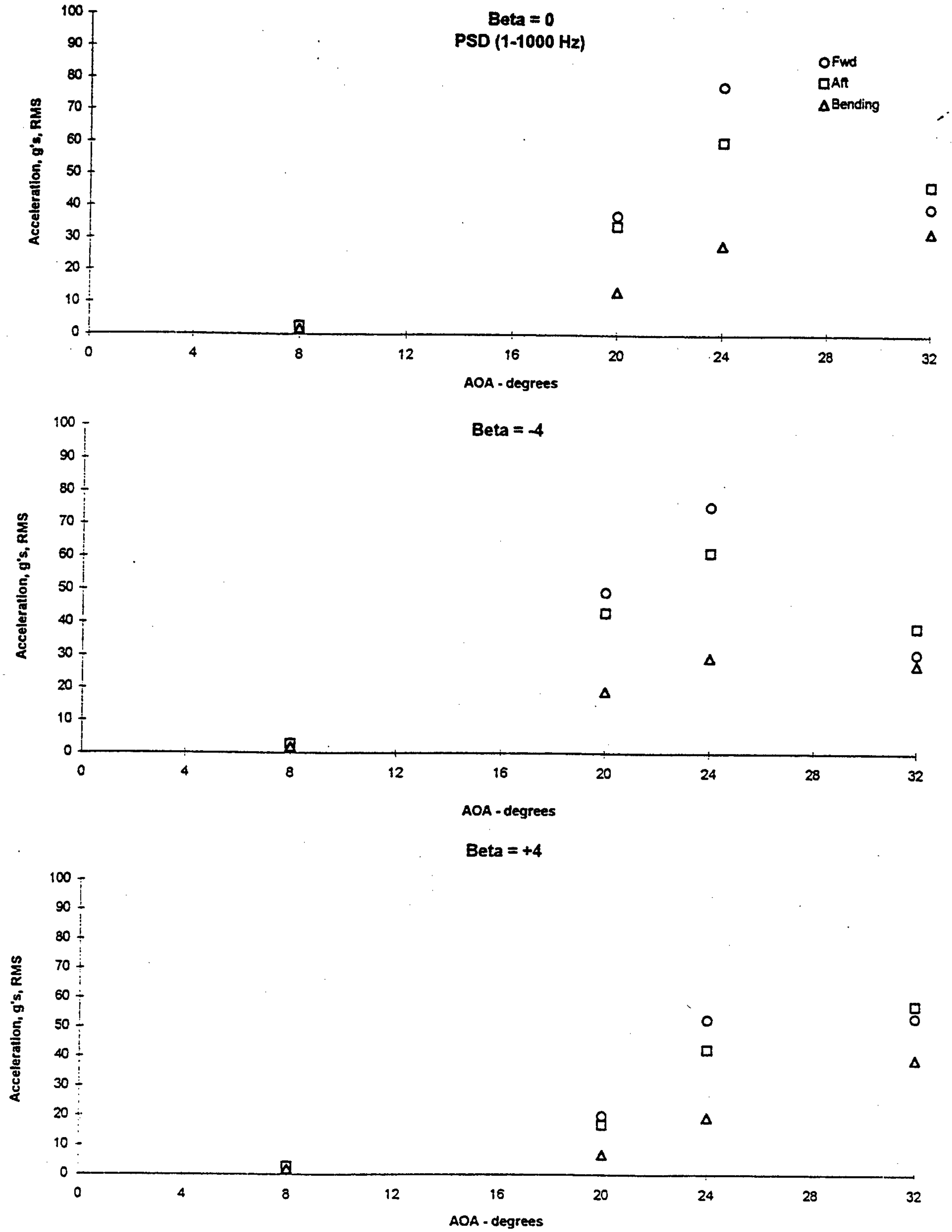

Figure 3.2.7 Flex. Tail Acceleration vs Angle of Attack, Q= 56 PSF, Beta =0, -4, 4 , WBP = 45 psi

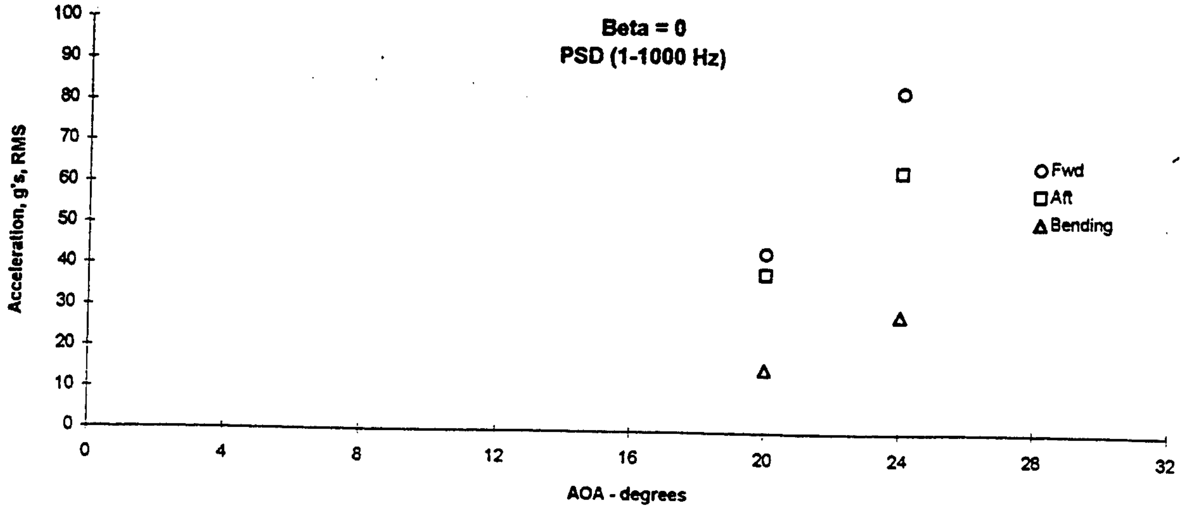

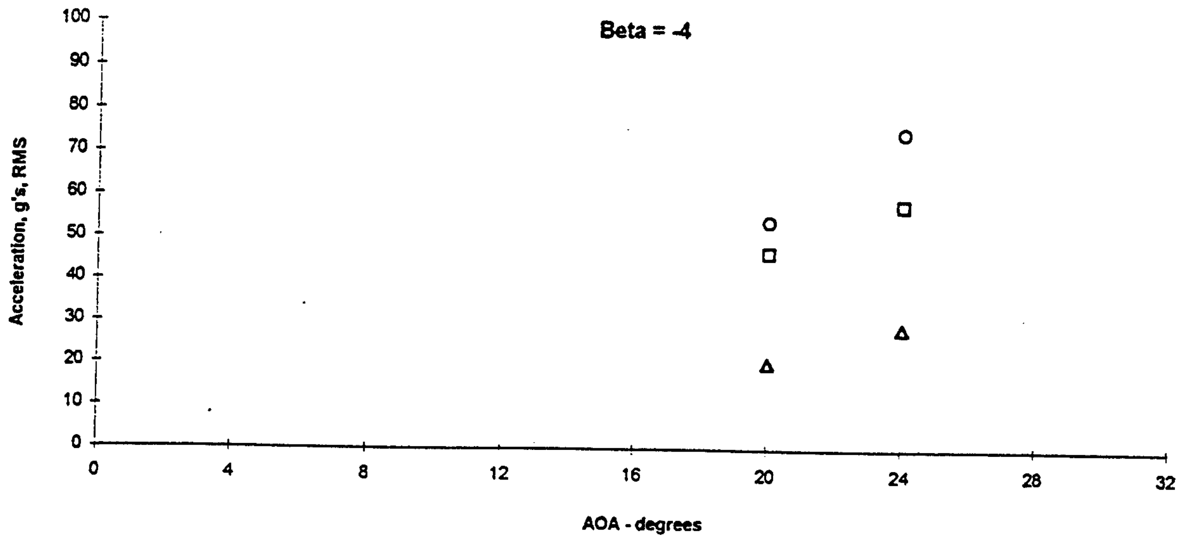

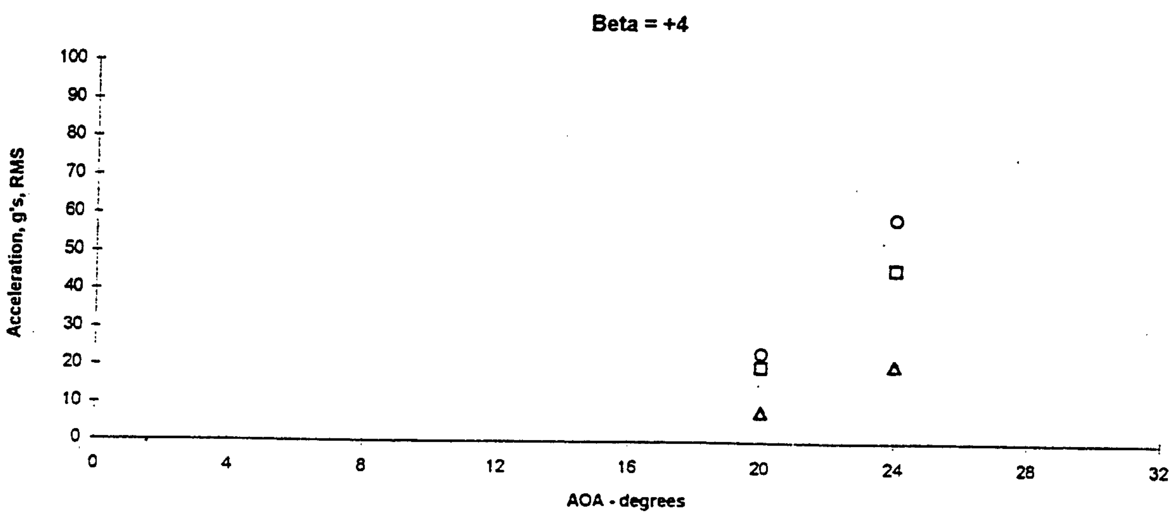

Figure 3.2.8 Flex. Tail Acceleration vs Angle of Attack, Q= 56 PSF, Beta =0, -4, 4 , WBP = 65 Psi

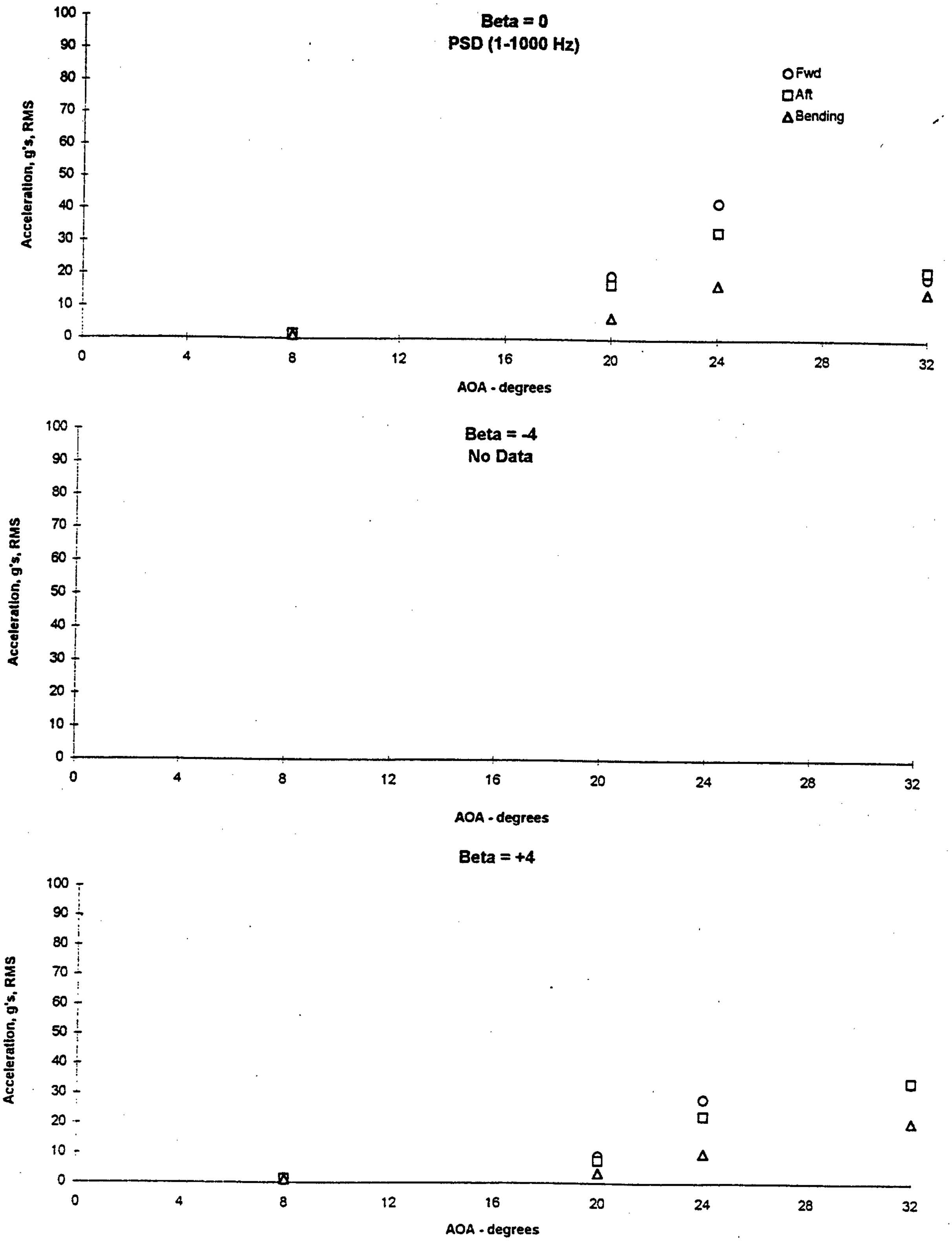

Figure 3.2.9 Flex. Tail Acceleration vs Angle of Attack, Q= 30 PSF, Beta =0, -4, 4 , No Blowing

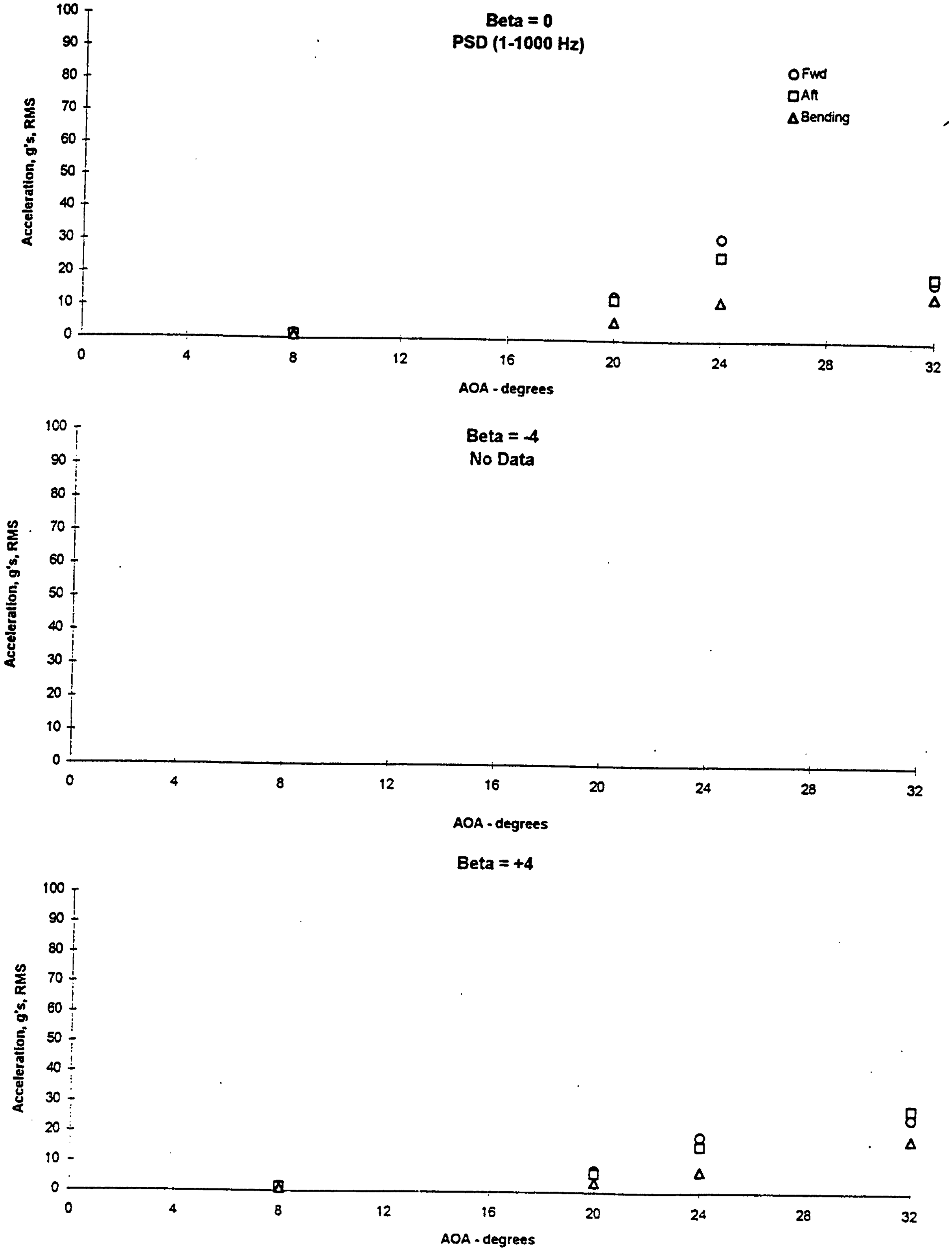

Figure 3.2.10 Flex. Tail Acceleration vs Angle of Attack, Q = 30 PSF, Beta =0, -4, 4, WBP = 45 psi

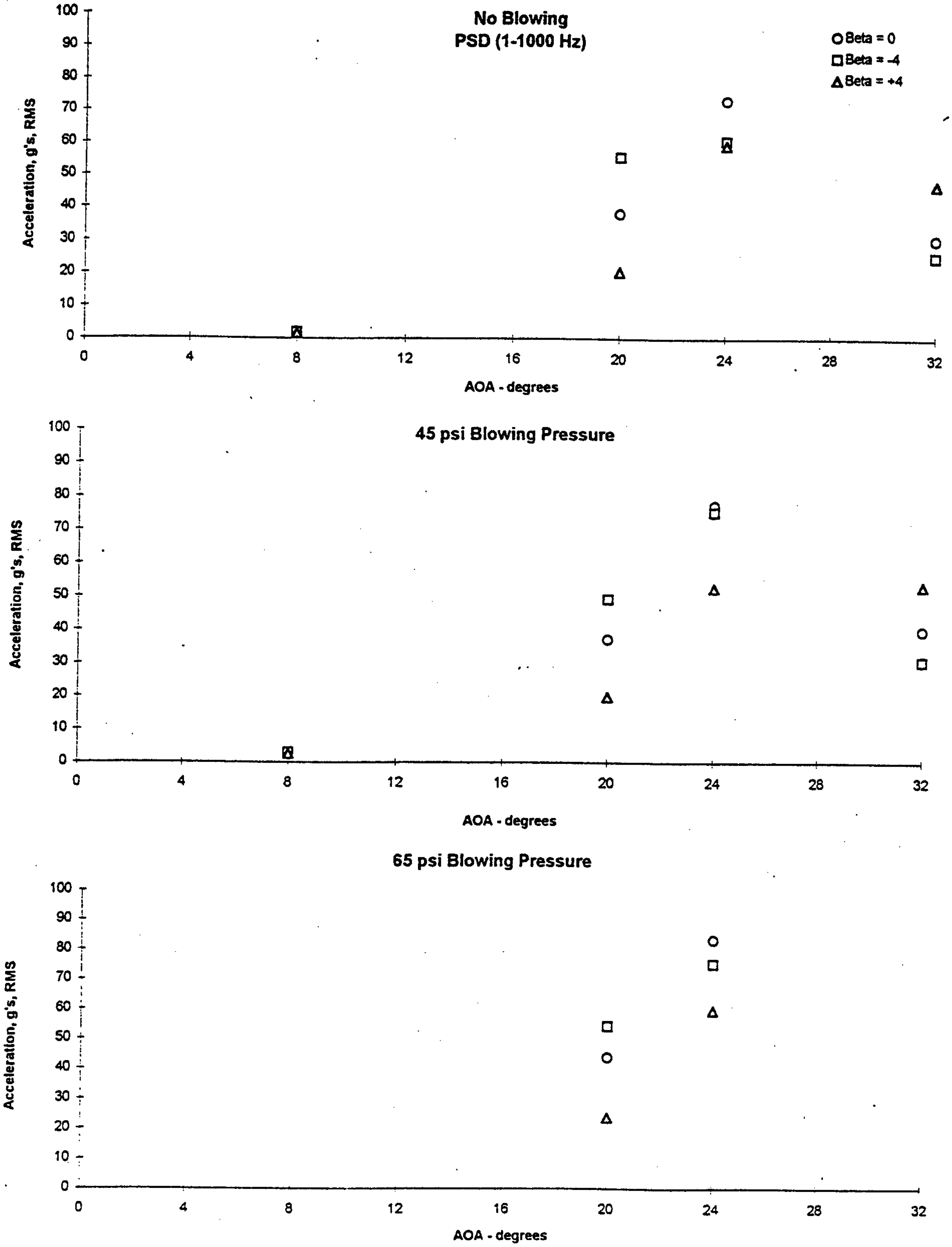

Figure 3.2.11 Flex. Tail Acceleration vs Angle of Attack, Q = 30 PSF, Beta =0, -4, 4, WBP = 65 psi

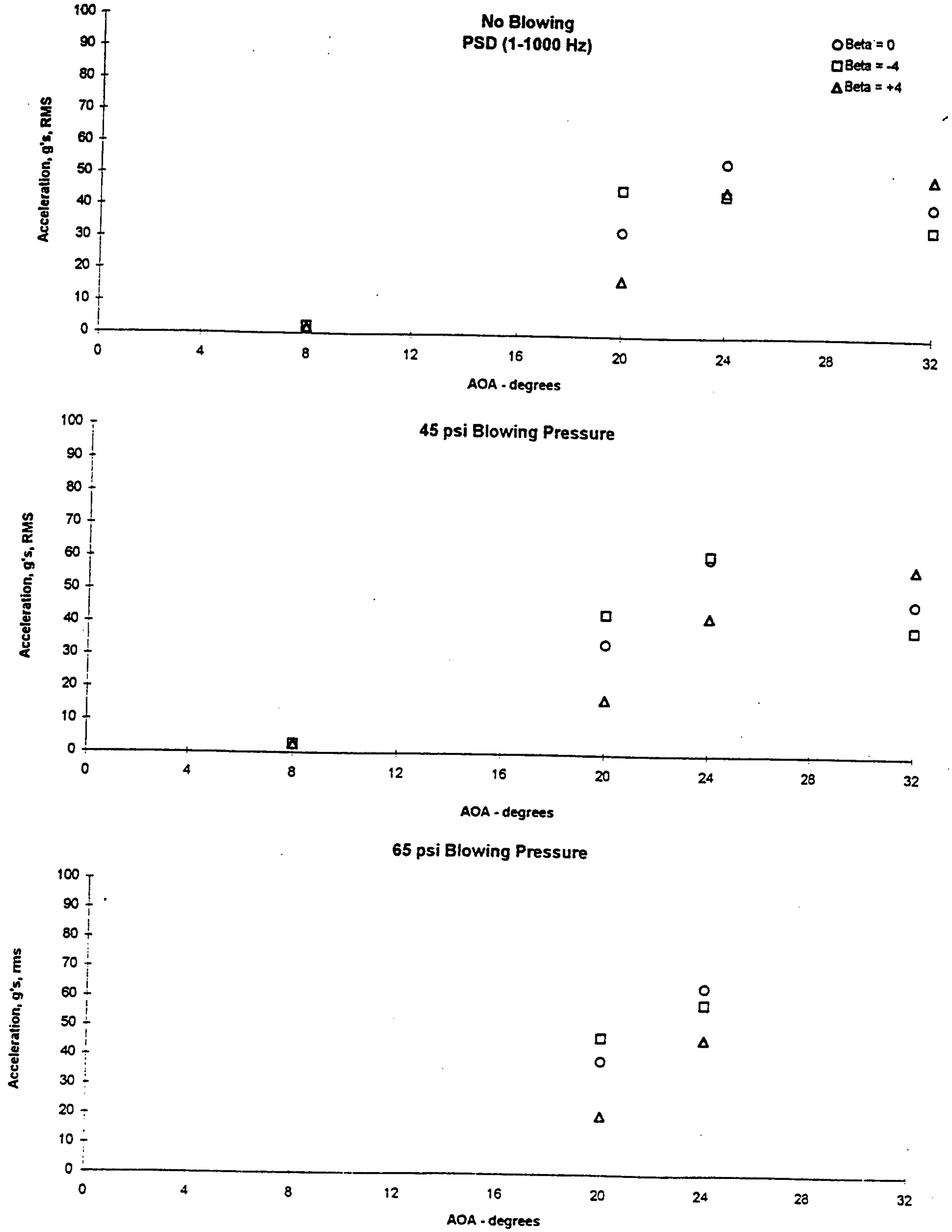

Figure 3.2.12 Flex Tail Acceleration Vs Angle of Attack, Fwd Accel., Q= 56 PSF, Beta = 0, -4, 4, WBP = 0, 45, 65 psi

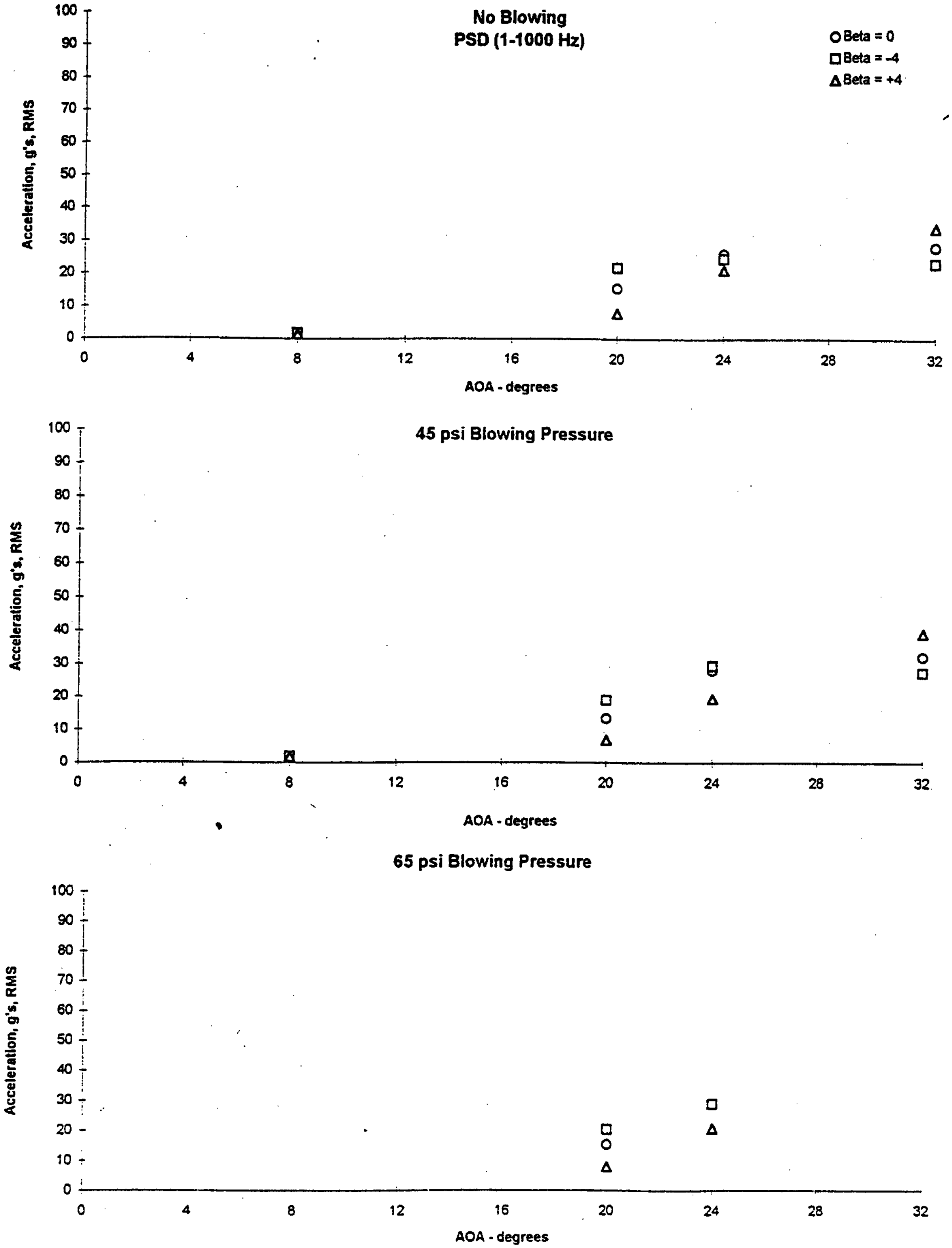

Figure 3.2.13 Flex Tail Acceleration Vs Angle of Attack, Aft Accel., Q= 56 PSF, Beta = 0, -4, 4, WBP = 0, 45, 65 psi

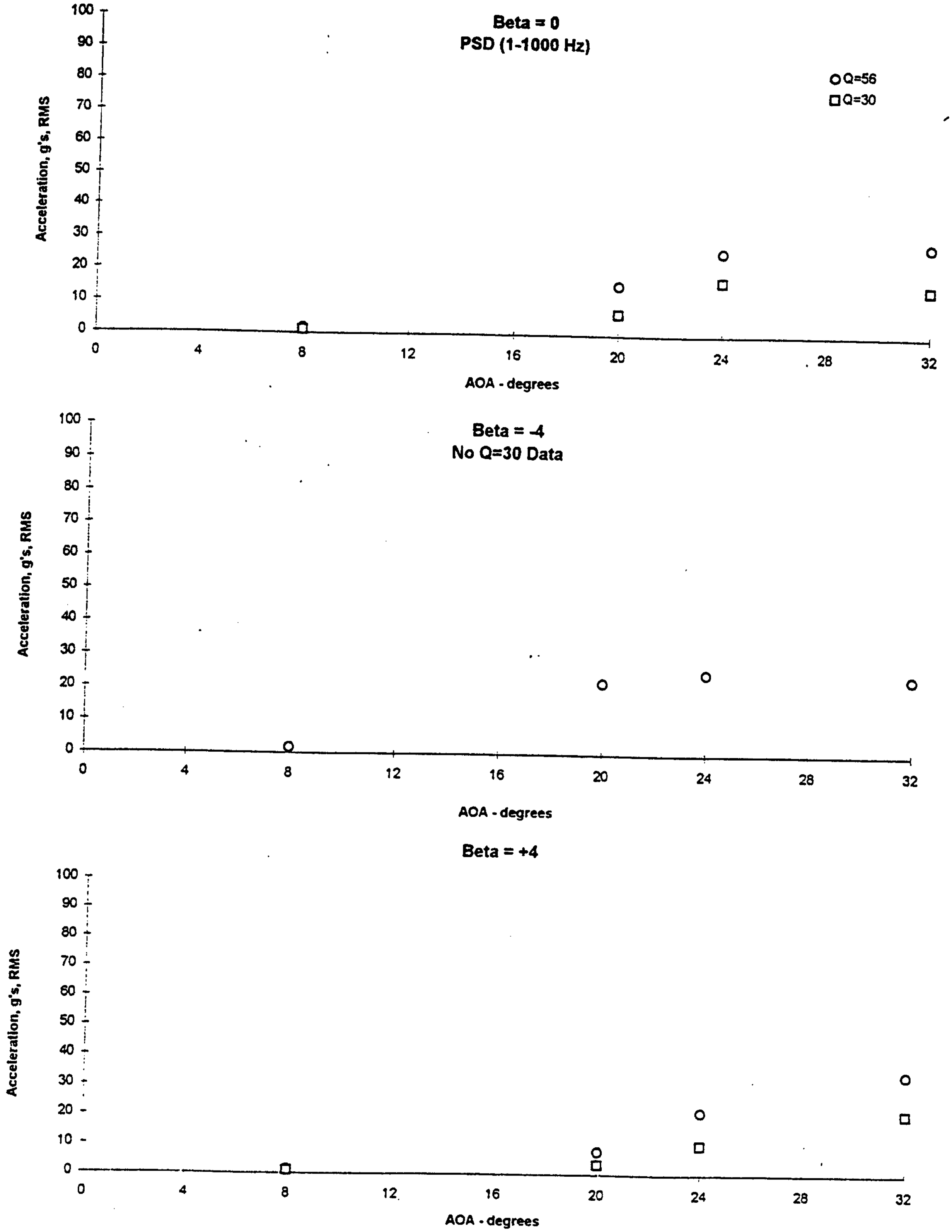

Figure 3.2.14 Flex Tail Acceleration vs Angle of Attack, Bending, Q= 30, 56 PSF, Beta = 0, -4, 4, WBP = 0

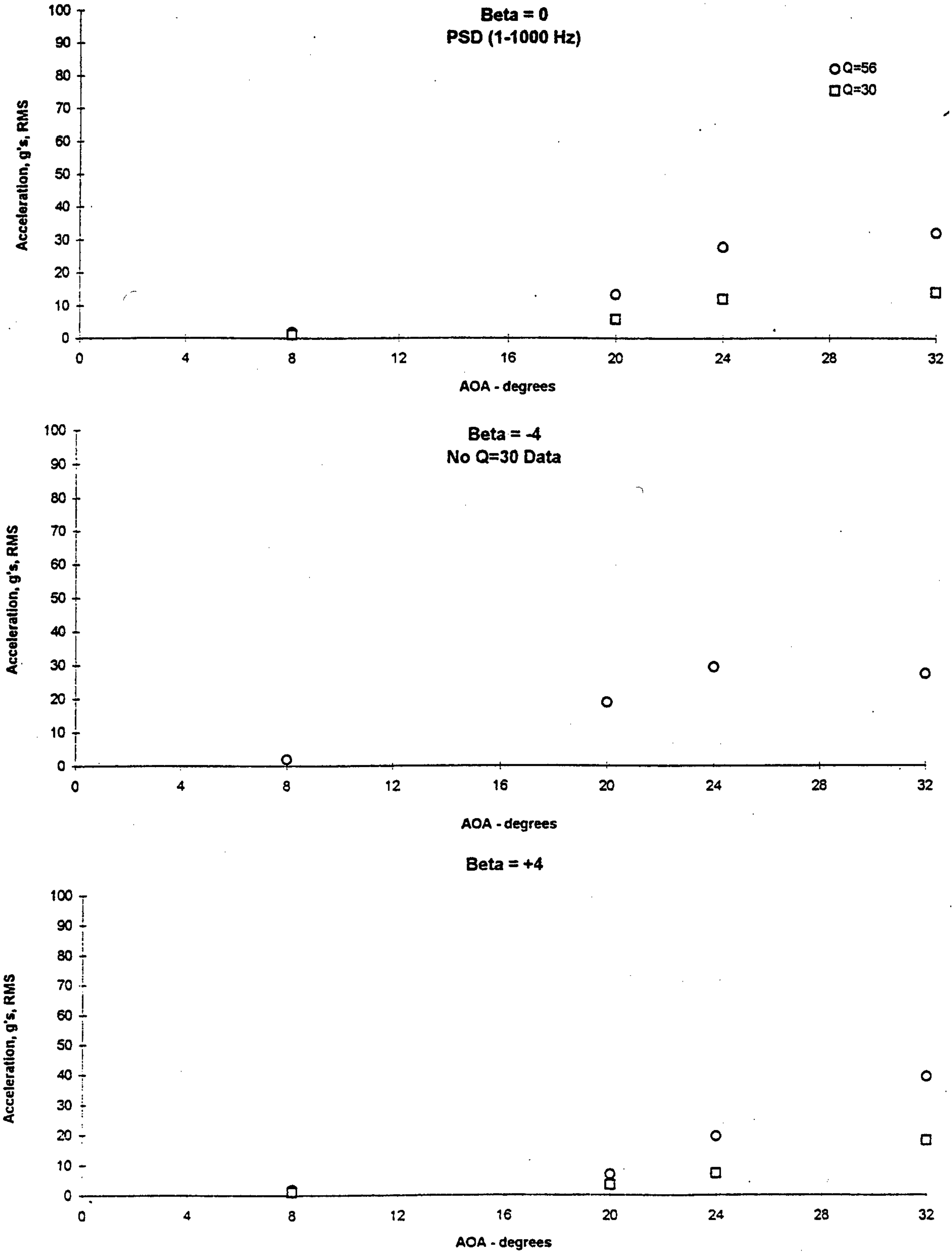

Figure 3.2.15 Flex Tail Acceleration vs Angle of Attack, Bending, Q= 30, 56 PSF, Beta = 0, -4, 4, WBP = 45 psi

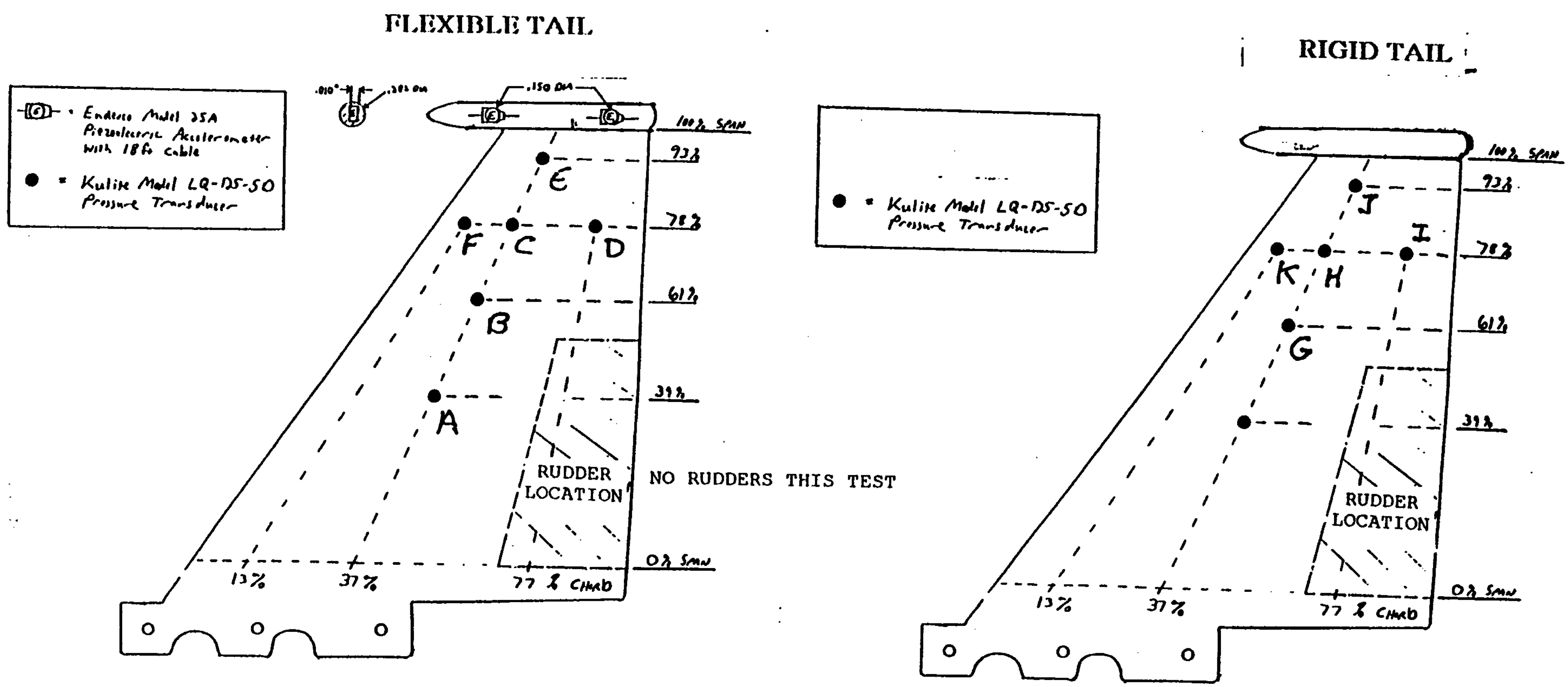

Figure 3.3.1 Pressure Pick-Ups -- Letter Indentification

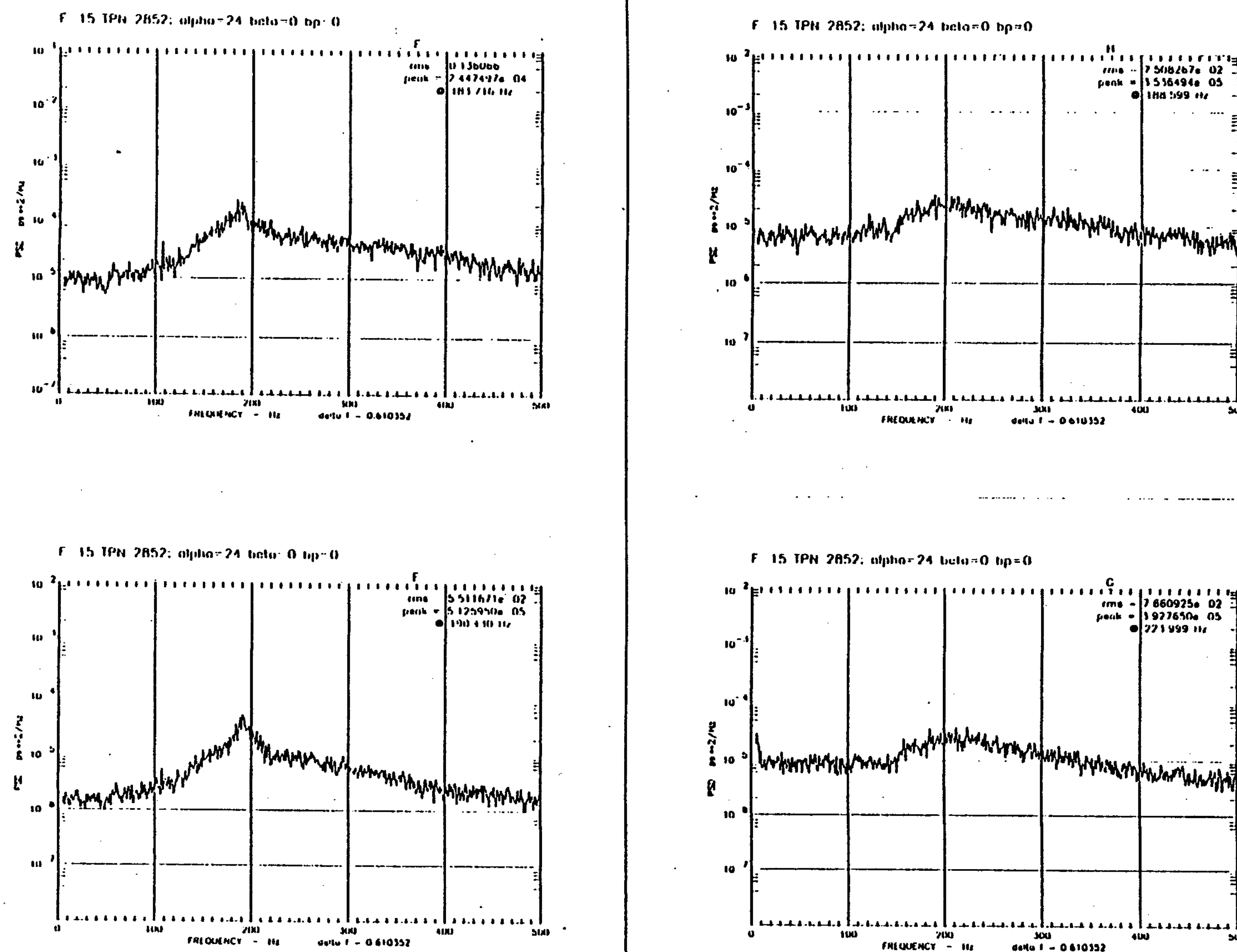

Figure 3.3.2 Pressure PSD's - Flex. and Rigid Tails, Q=56 PSF, Beta = 0, Alpha= 24 deg, WBP= 0

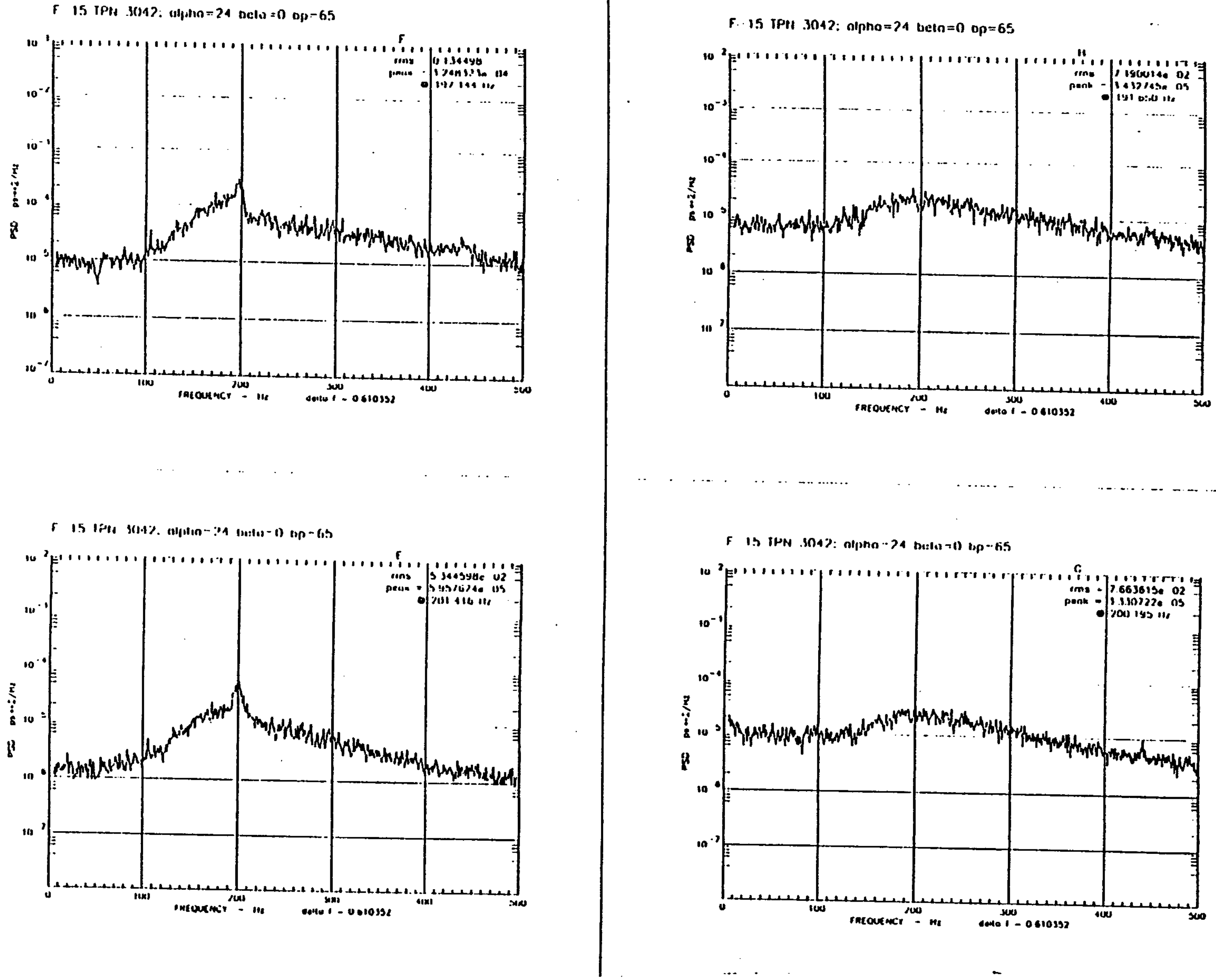

Figure 3.3.3 Pressure PSD's - Flex. and Rigid Tails, Q=56 PSF, Beta = 0, Alpha= 24 deg, WBP = 65 psi

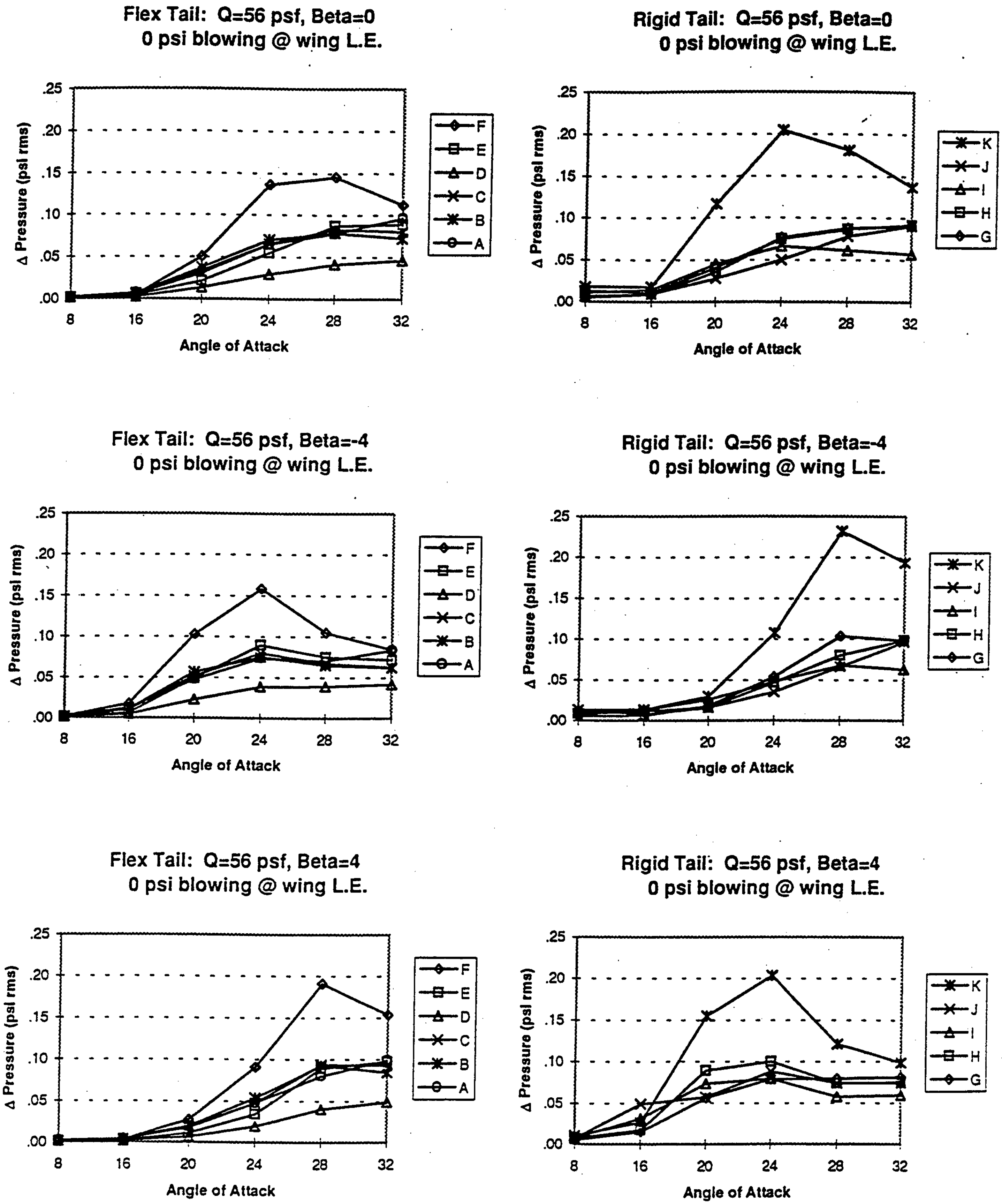

Figure 3.3.4 Flex. And Rigid Tails - RMS Pressures Vs Alpha, Q= 56 PSF, Beta=0, -4, 4

WBP =0

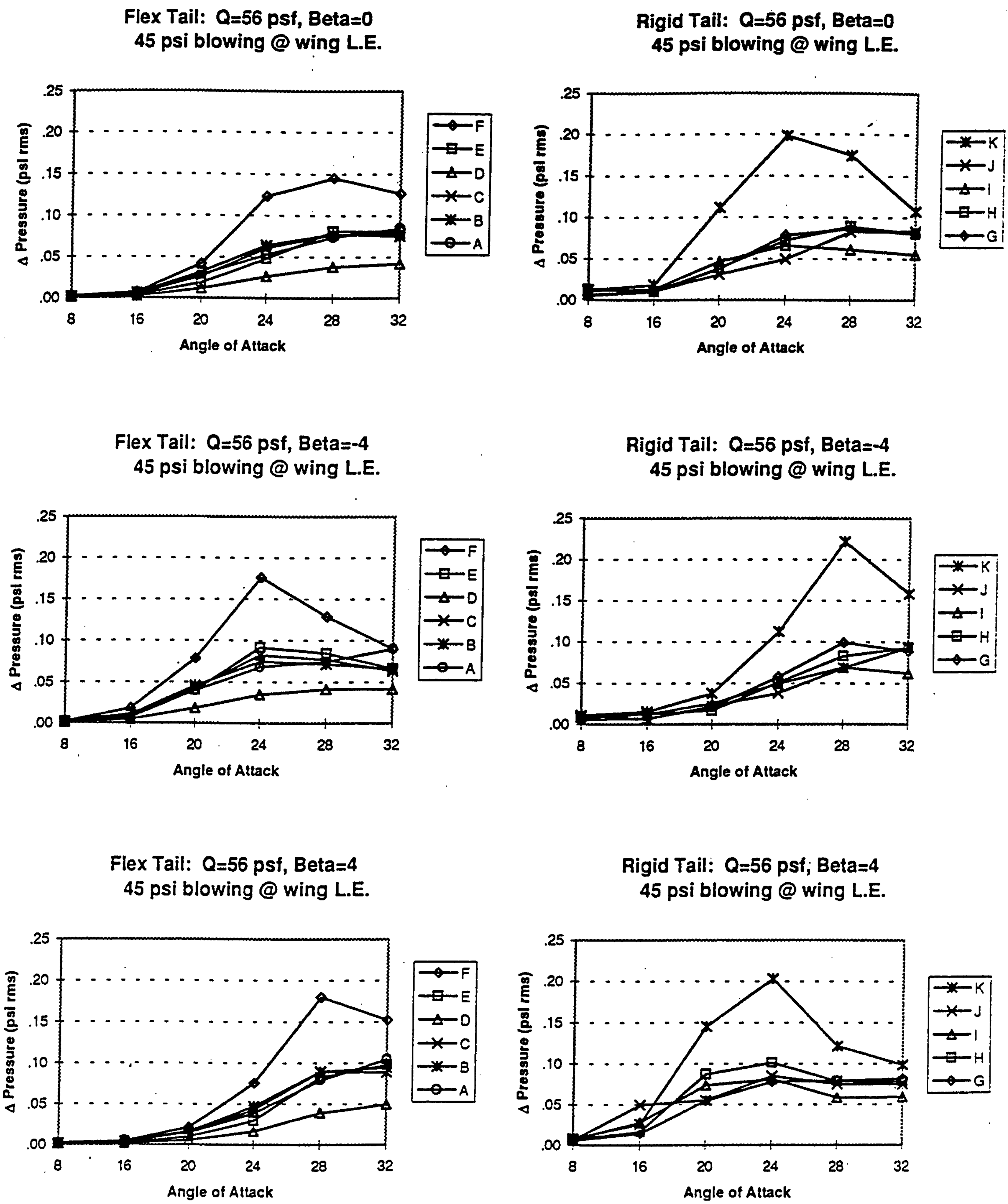

Figure 3.3.5 Flex. And Rigid Tails - RMS Pressures Vs Alpha, Q= 56 PSF, Beta=0, -4, 4

WBP =45 psi

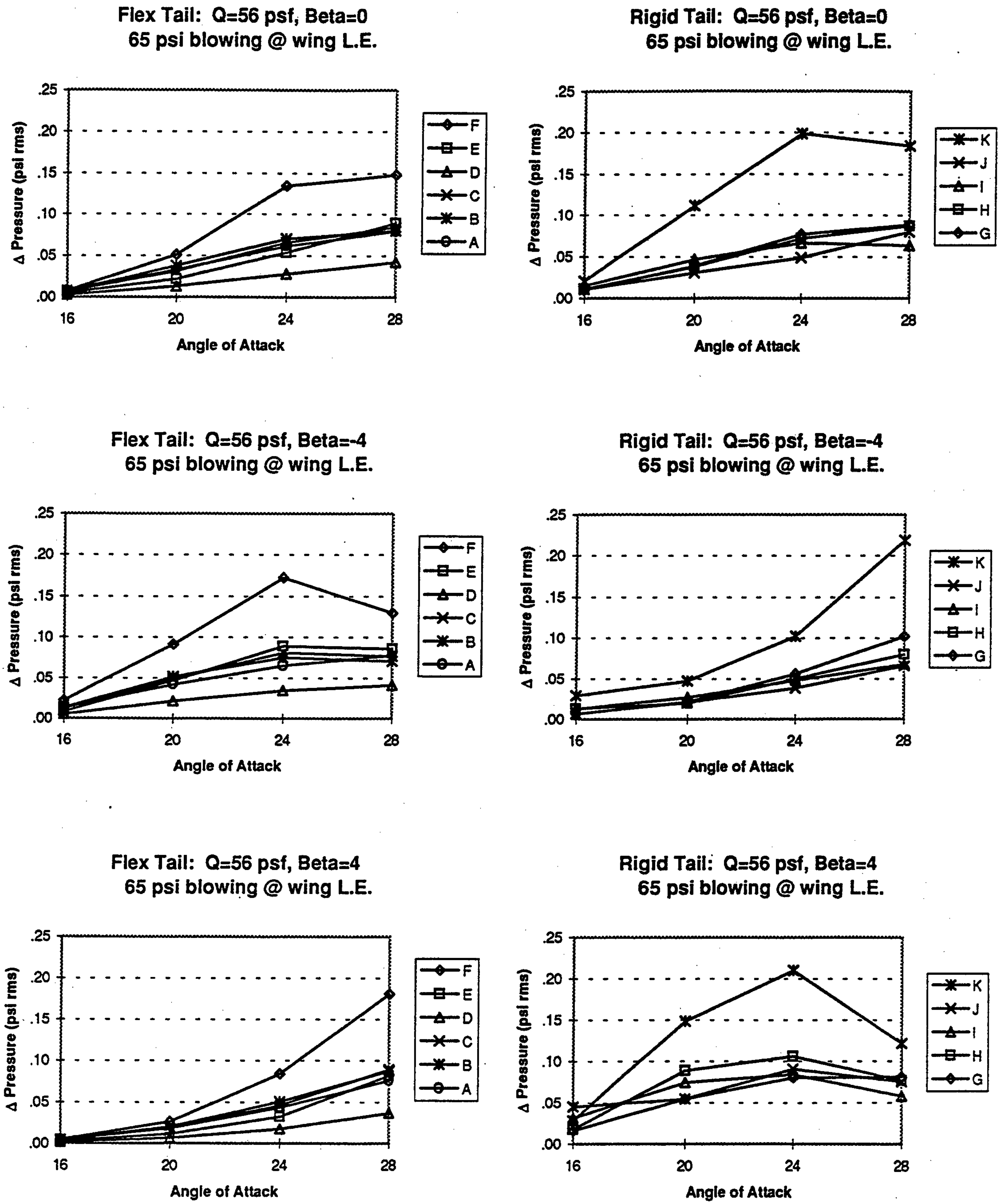

Figure 3.3.6 Flex. And Rigid Tails - RMS Pressures Vs Alpha, Q= 56 PSF, Beta=0, -4, 4

WBP =65 psi

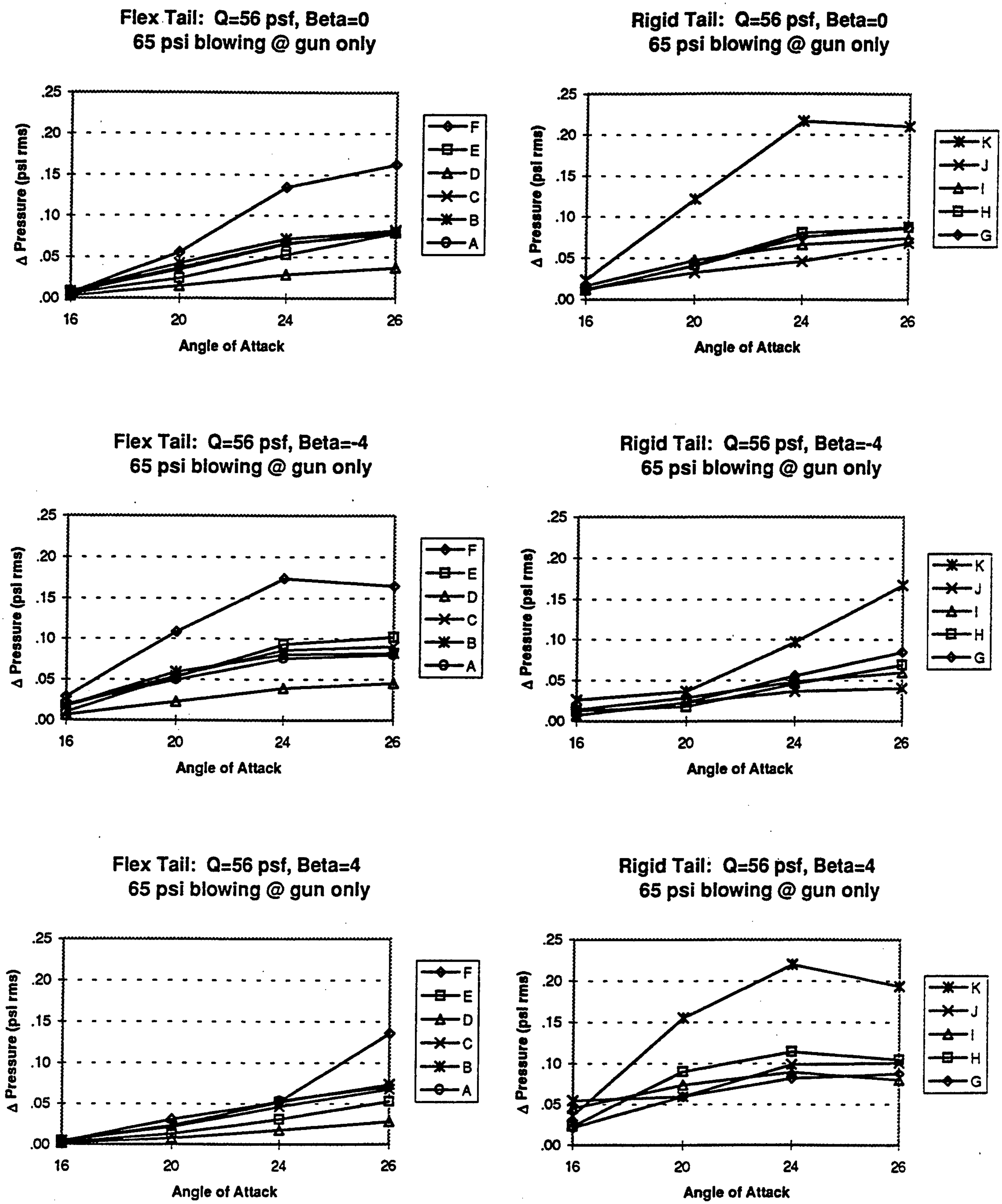

Figure 3.3.7 Flex. And Rigid Tails - RMS Pressures Vs Alpha, Q= 56 PSF, Beta=0, -4, 4
GBP = 65 psi

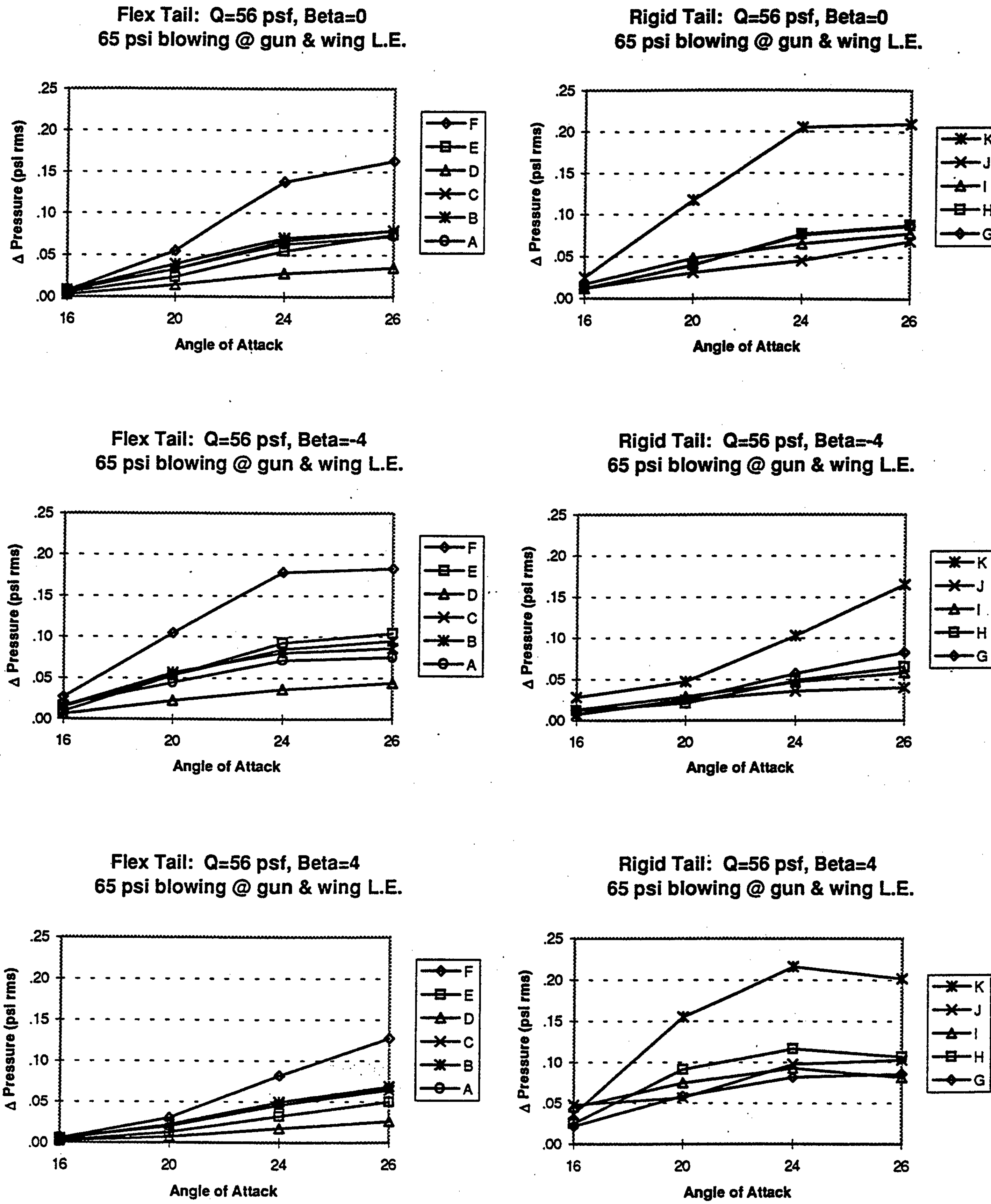

Figure 3.3.8 Flex. And Rigid Tails - RMS Pressures Vs Alpha, Q= 56 PSF, Beta=0, -4, 4

WBP = 65 psi, GBP = 65 psi

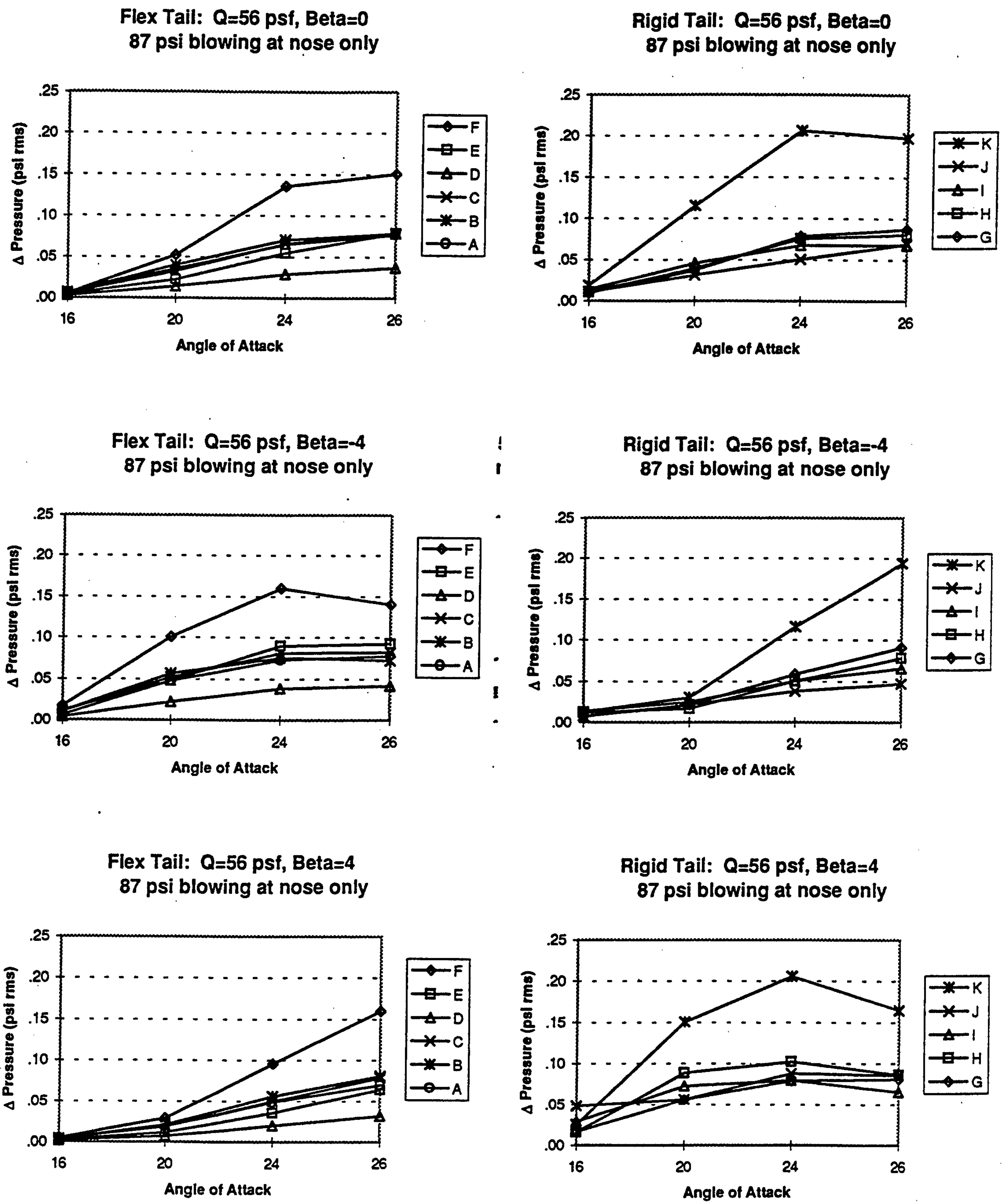

Figure 3.3.9 Flex. And Rigid Tails - RMS Pressures Vs Alpha, Q= 56 PSF, Beta=0, -4, 4

NBP = 87 psi

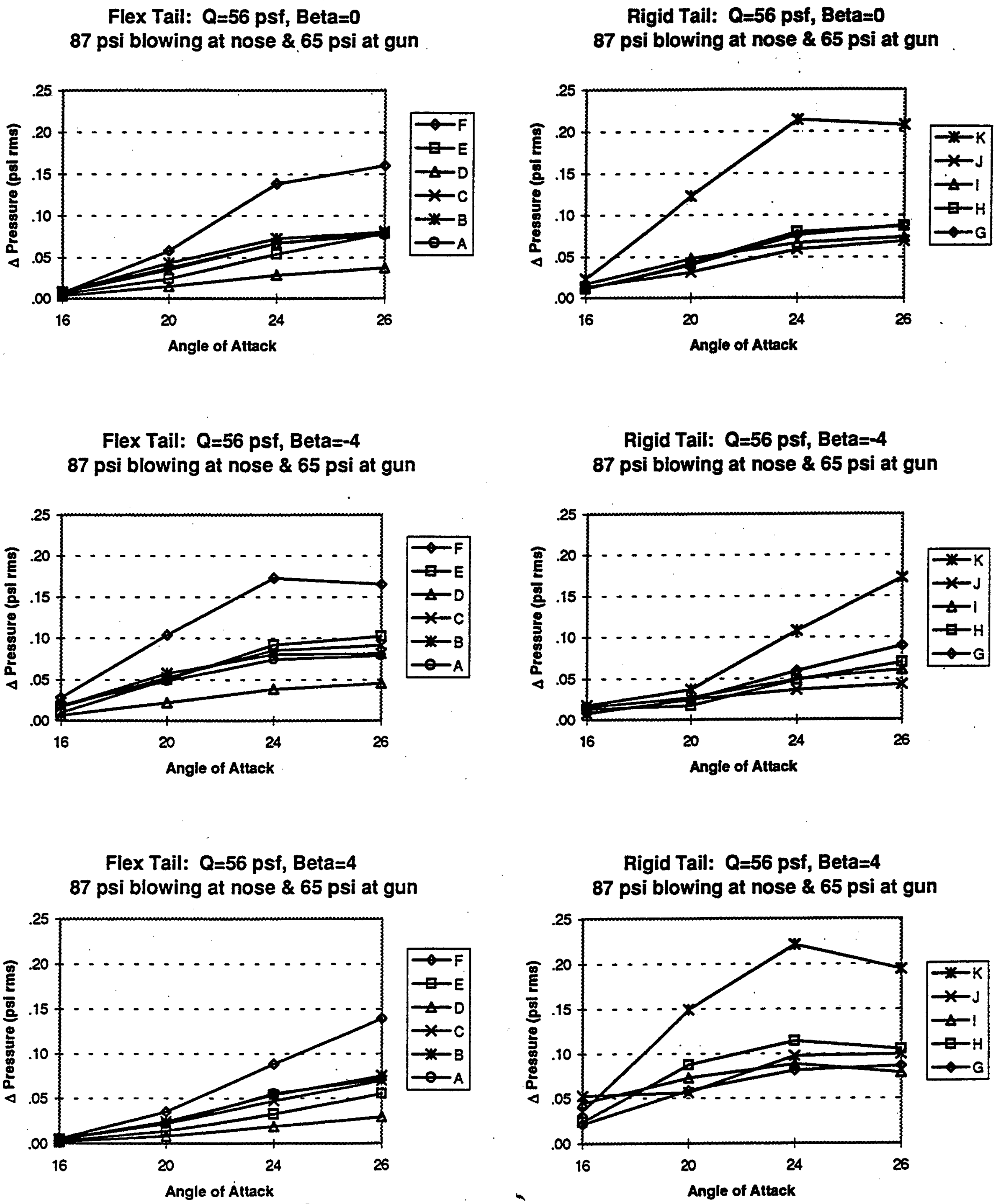

Figure 3.3.10 Flex. And Rigid Tails - RMS Pressures Vs Alpha, Q= 56 PSF, Beta=0, -4, 4

NBP = 87 psi, GBP = 65 psi

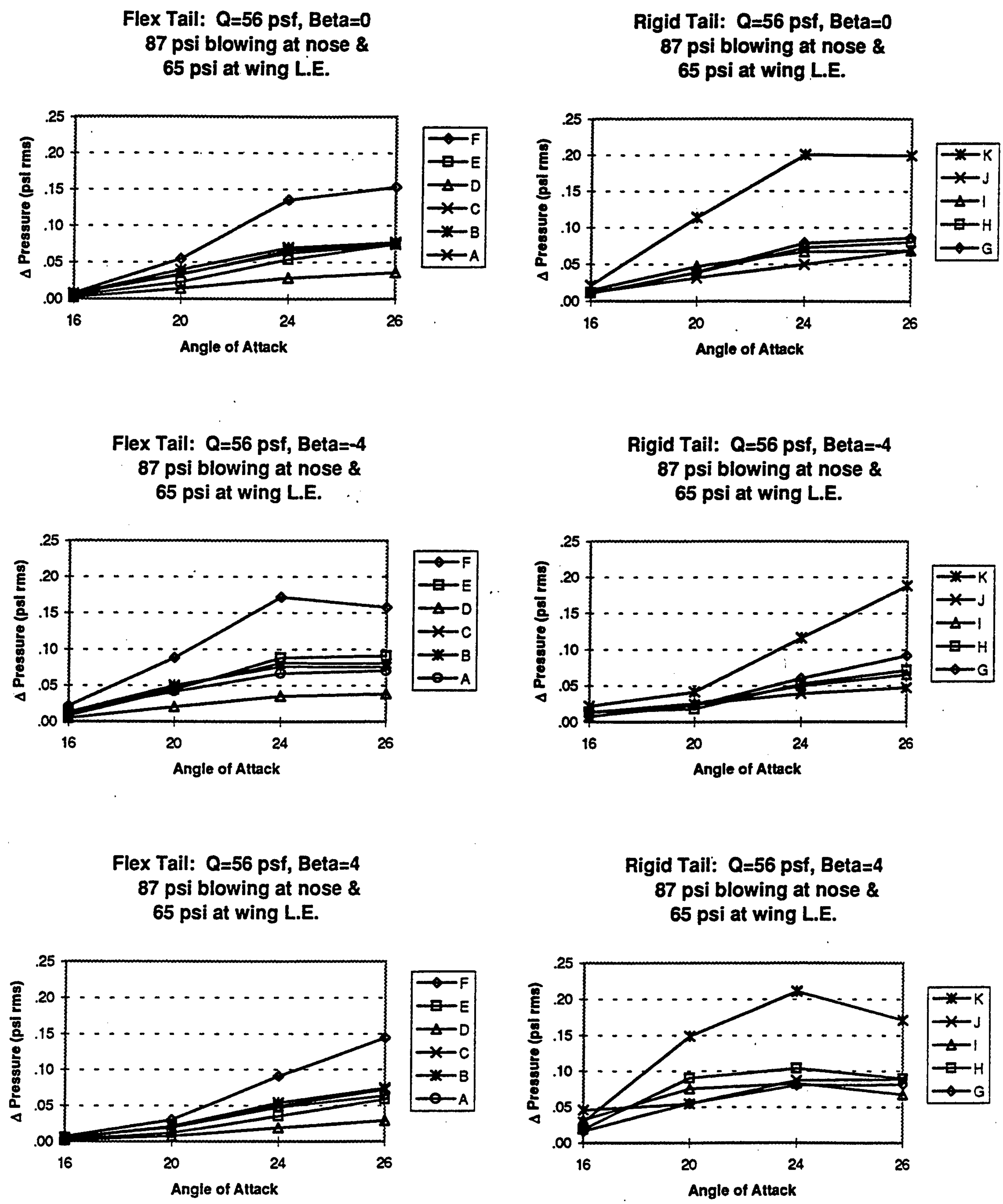

Figure 3.3.11 Flex. And Rigid Tails - RMS Pressures Vs Alpha, Q= 56 PSF, Beta=0, -4, 4

NBP = 87 psi, WBP = 65 psi

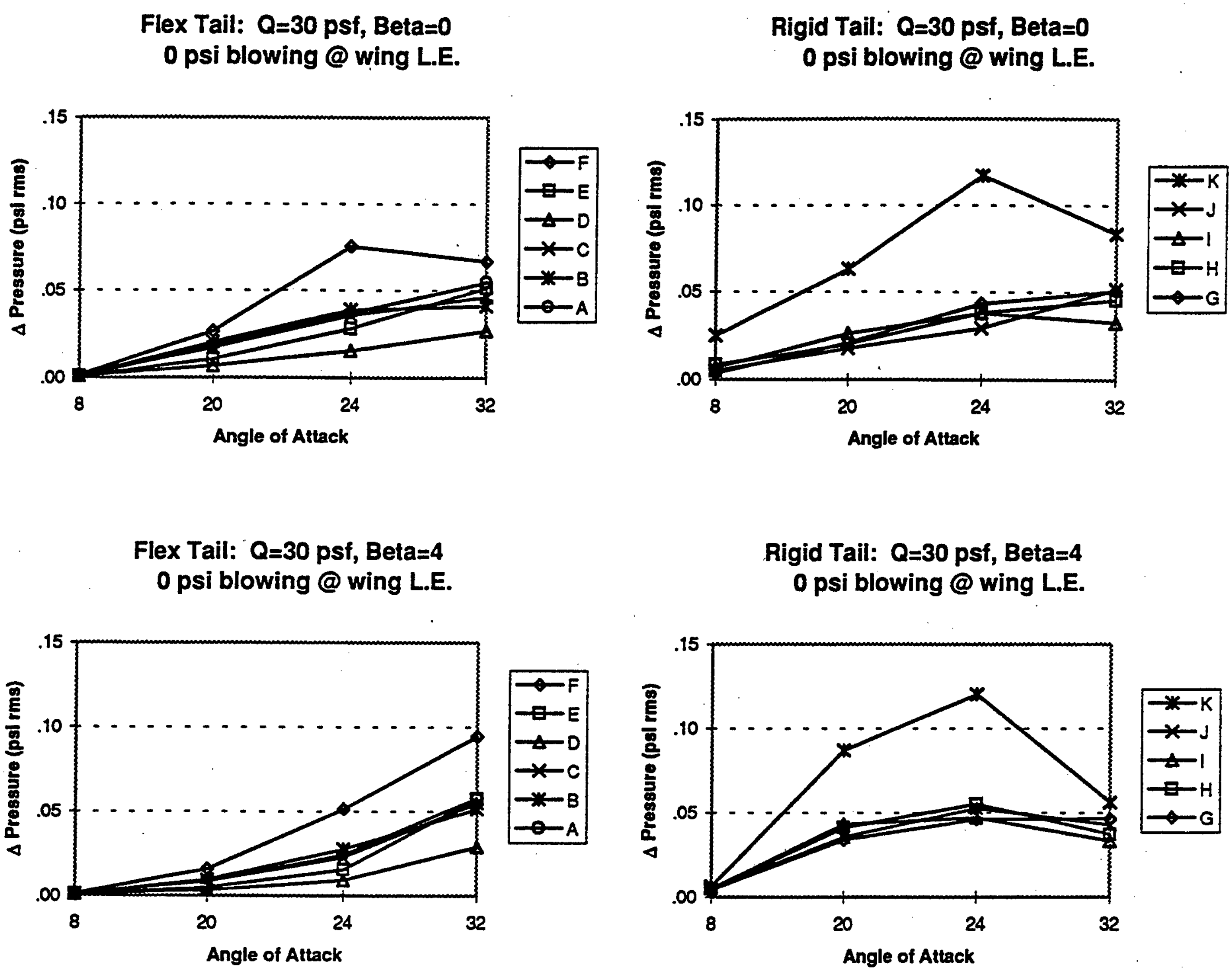

Figure 3.3.12 Flex. And Rigid Tails - RMS Pressures Vs Alpha, Q= 30 PSF, Beta=0, -4, 4

WBP =0

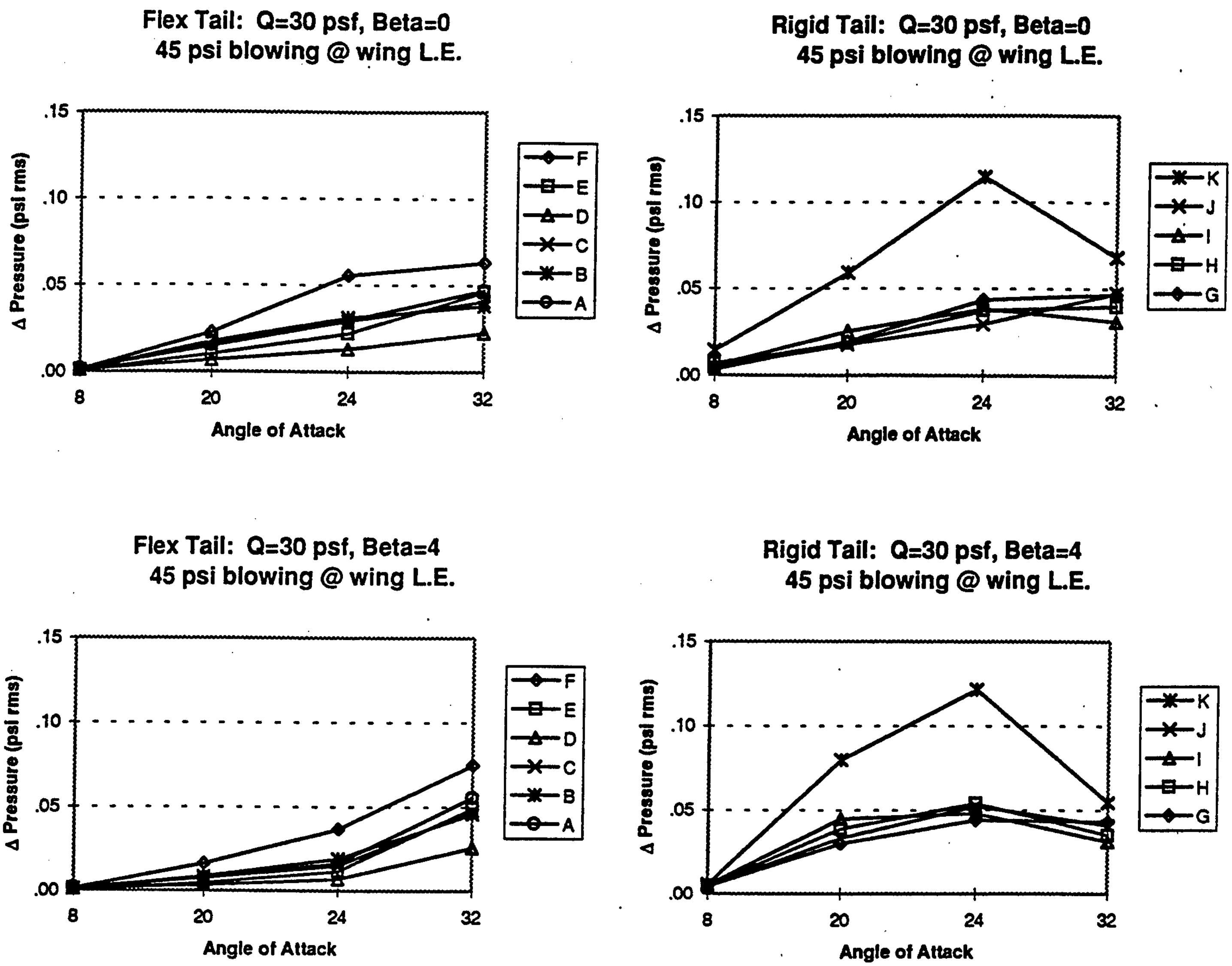

Figure 3.3.13 Flex. And Rigid Tails - RMS Pressures Vs Alpha, Q= 30 PSF, Beta=0, -4, 4 WBP =45 psi

F-15 TPN_2850: alpha=20 beta=0 bp=0

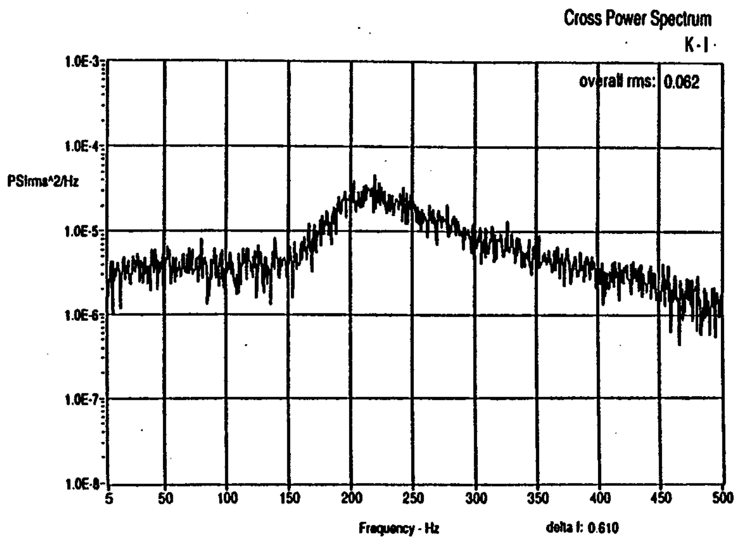

F-15 TPN_2854: alpha=32 beta=0 bp=0

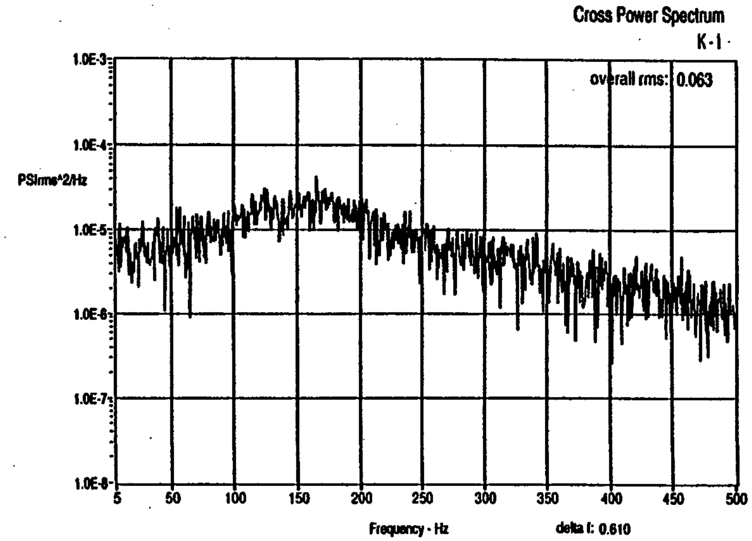

F-15 TPN_2844: alpha=8 beta=0 bp=0

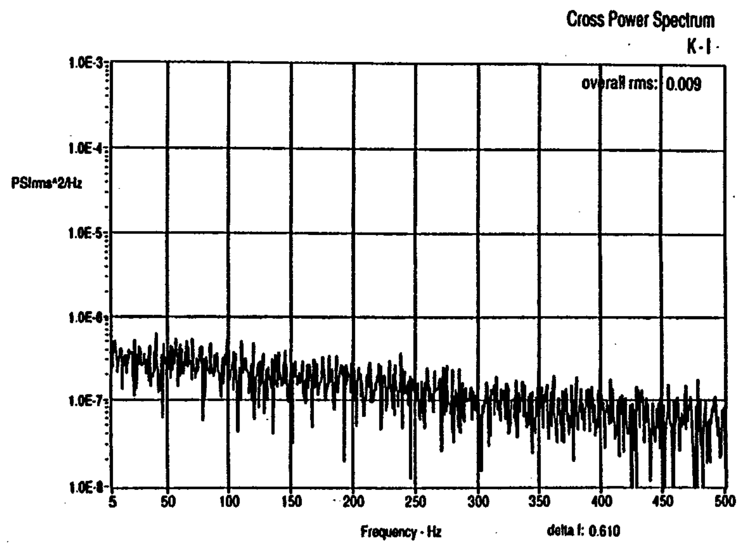

F-15 TPN_2852: alpha=24 beta=0 bp=0

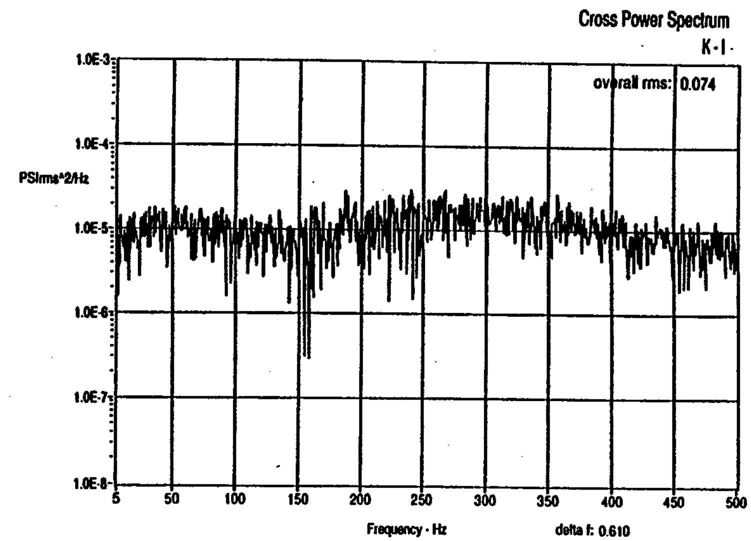

Figure 3.3.14 CSD (Modulus) of Pressure- Rigid Tail, Q = 56 PSF, Beta = 0, WBP = 0, Alpha Sweep

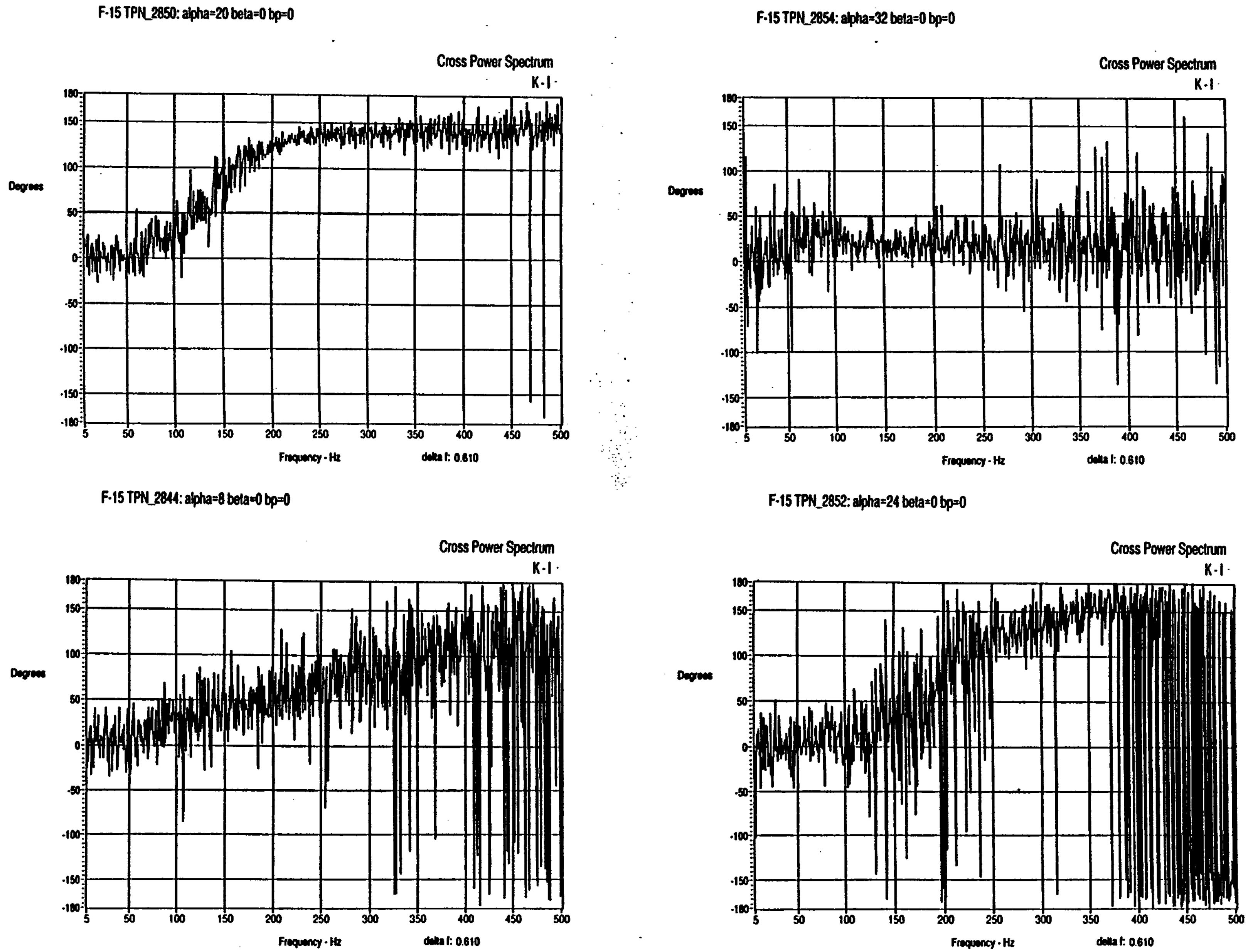

Figure 3.3.15 CSD (Phase) of Pressure- Rigid Tail, Q = 56 PSF, Beta = 0, WBP = 0, Alpha Sweep

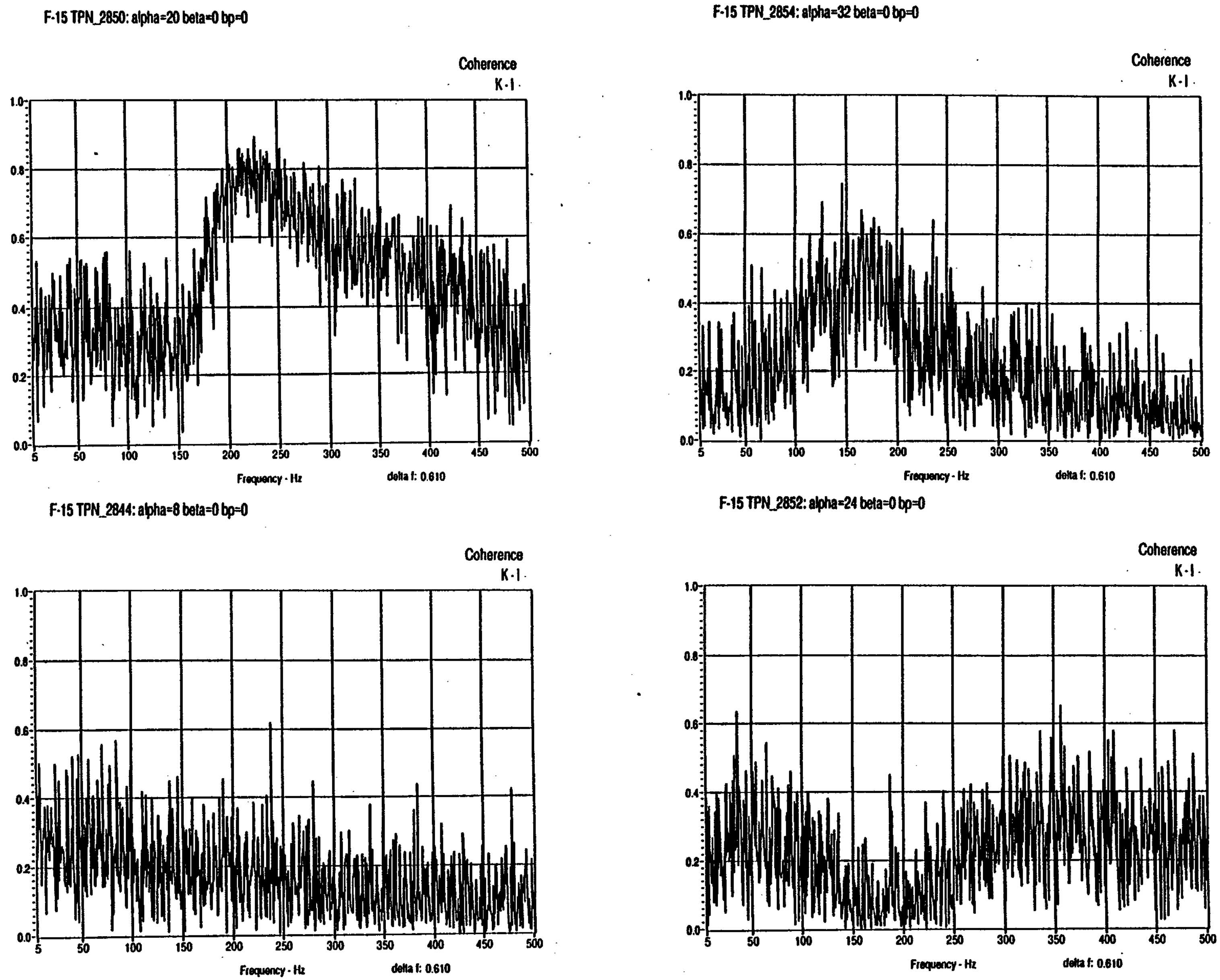

Figure 3.3.16 Coherence- Pressure- Rigid Tail, Q = 56 PSF, Beta = 0, WBP =0, Alpha Sweep

Table 3.3.1 RMS Values of CSD Modulus Vs Alpha

Q= 56 psf, Beta = -4, 0, 4 deg, WBP + 0, 45, 65 psi

0 psi blowing pressure:

Beta = 4:

Alpha	K-H	K-I	K-J	K-G	G-H	G-I
8	.004	.004	.004	.003	.003	.003
20	.108	.090	.067	.078	.061	.051
24	.127	.074	.103	.107	.074	.047
32	.071	.050	.054	.065	.056	.040

Beta = 0:

Alpha	K-H	K-I	K-J	K-G	G-H	G-I
8	.013	.009	.005	.004	.004	.003
20	.068	.062	.050	.059	.035	.034
24	.118	.074	.070	.103	.061	.044
32	.096	.063	.080	.089	.071	.045

Beta = -4:

Alpha	K-H	K-I	K-J	K-G	G-H	G-I
8	.006	.008	.007	.004	.003	.004
20	.012	.020	.012	.013	.014	.011
24	.066	.050	.041	.064	.044	.032
32	.118	.071	.102	.116	.080	.047

45 psi blowing pressure:

Beta = 4:

Alpha	K-H	K-I	K-J	K-G	G-H	G-I
8	.004	.004	.003	.003	.003	.003
20	.102	.088	.065	.074	.059	.050
24	.130	.078	.100	.108	.074	.048
32	.073	.050	.055	.064	.058	.040

Beta = 0:

Alpha	K-H	K-I	K-J	K-G	G-H	G-I
8	.010	.007	.004	.004	.004	.003
20	.063	.060	.052	.060	.035	.035
24	.113	.072	.067	.101	.059	.044
32	.080	.055	.069	.072	.062	.041

Beta = -4:

Alpha	K-H	K-I	K-J	K-G	G-H	G-I
8	.004	.007	.006	.004	.003	.004
20	.015	.021	.018	.017	.015	.012
24	.070	.052	.044	.067	.047	.034
32	.104	.067	.088	.098	.072	.047

Table 3.3.1 (Concluded)

65 psi blowing pressure

Beta = 4:

Alpha:	K-H	K-I	K-J	K-G	G-H	G-I
8						
20	.105	.090	.064	.075	.059	.051
24	.135	.081	.106	.111	.077	.049
32						

Beta = 0:

Alpha:	K-H	K-I	K-J	K-G	G-H	G-I
8						
20	.062	.060	.052	.061	.035	.036
24	.113	.073	.067	.101	.059	.043
32						

Beta = -4:

Alpha:	K-H	K-I	K-J	K-G	G-H	G-I
8						
20	.020	.025	.021	.021	.017	.013
24	.066	.048	.043	.065	.047	.033
32						

Table 3.3.2 Sample Correlation Coefficients

Q= 56 psf, (5-500 Hz)

0 psi blowing pressure:

Beta = 4:

Alpha	K-H	G-H	F-C
8	.248		.630
20	.862	.764	.964
24	.805		.974
32	.701	.531	.877

Beta = 0:

Alpha	K-H	G-H	F-C
8	.705		.529
20	.951		.974
24	.900		.964
32	.718		.824

Beta = -4:

Alpha	K-H	G-H	F-C
8	.387		.554
20	.313	.665	.955
24	.865		.926
32	.727		.787

45 psi blowing pressure:

Beta = 4:

Alpha	K-H	G-H
8		
20	.839	.733
24		
32		

65 psi blowing pressure:

Beta = 4:

Alpha	K-H	G-H
8		
20	.854	.738
24		
32		

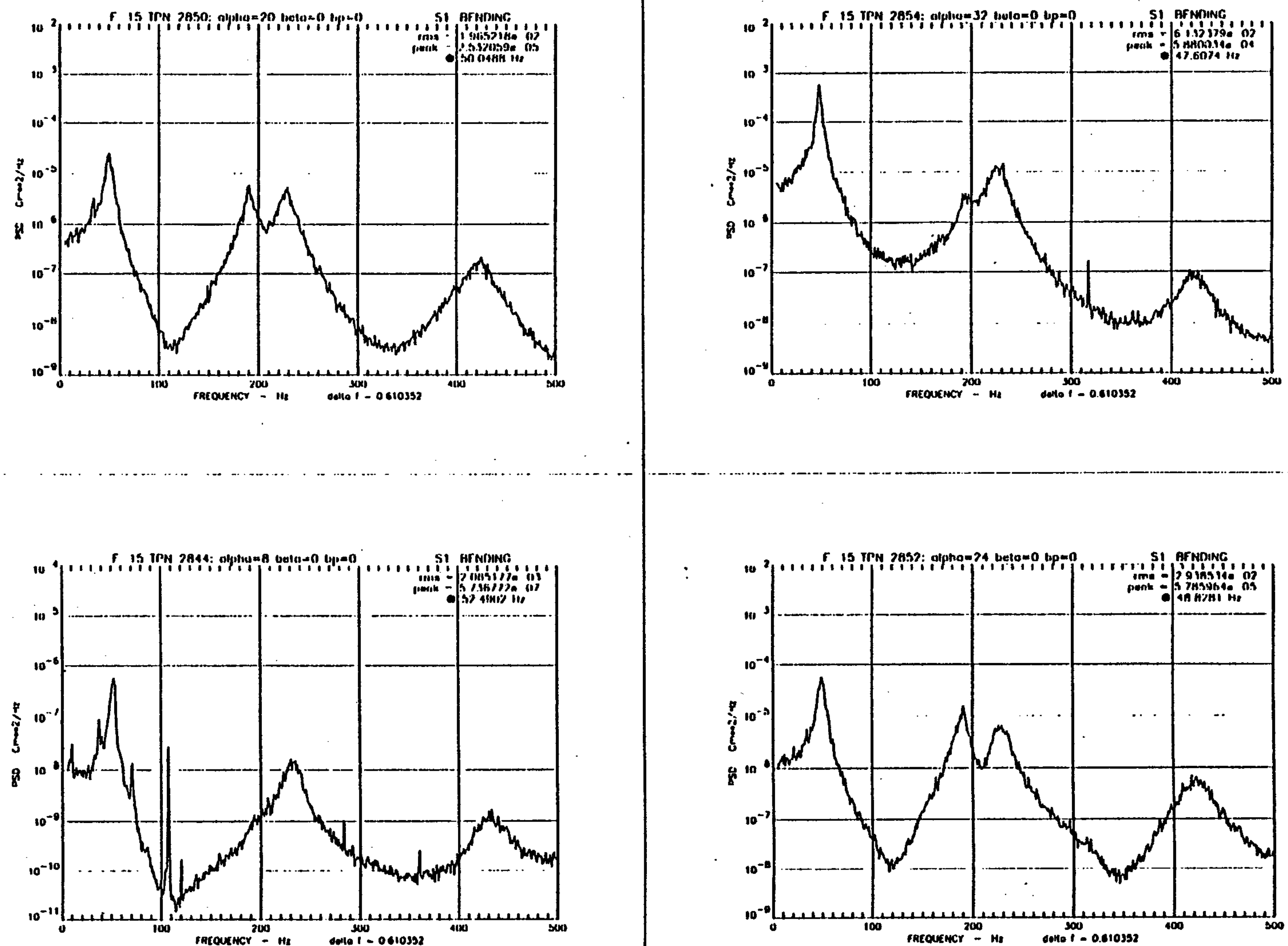

Figure 3.4.1 Flex. Tail PSD- Bending Coeff. vs Alpha, Q=56 PSF, Beta = 0, No Blowing

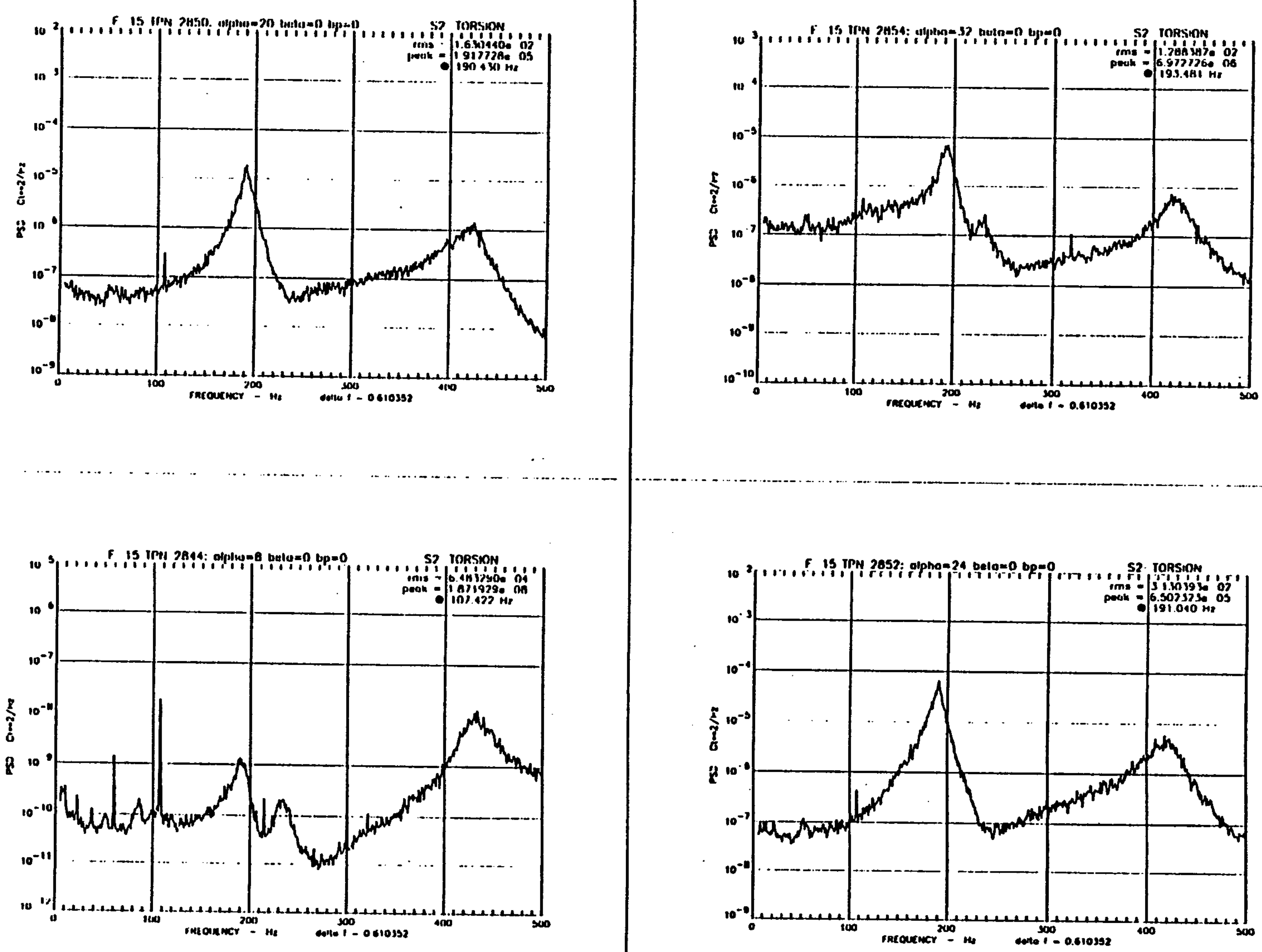

Figure 3.4.2 Flex. Tail PSD - Torsion Coeff. vs Alpha, Q=56 PSF, Beta = 0, No Blowing

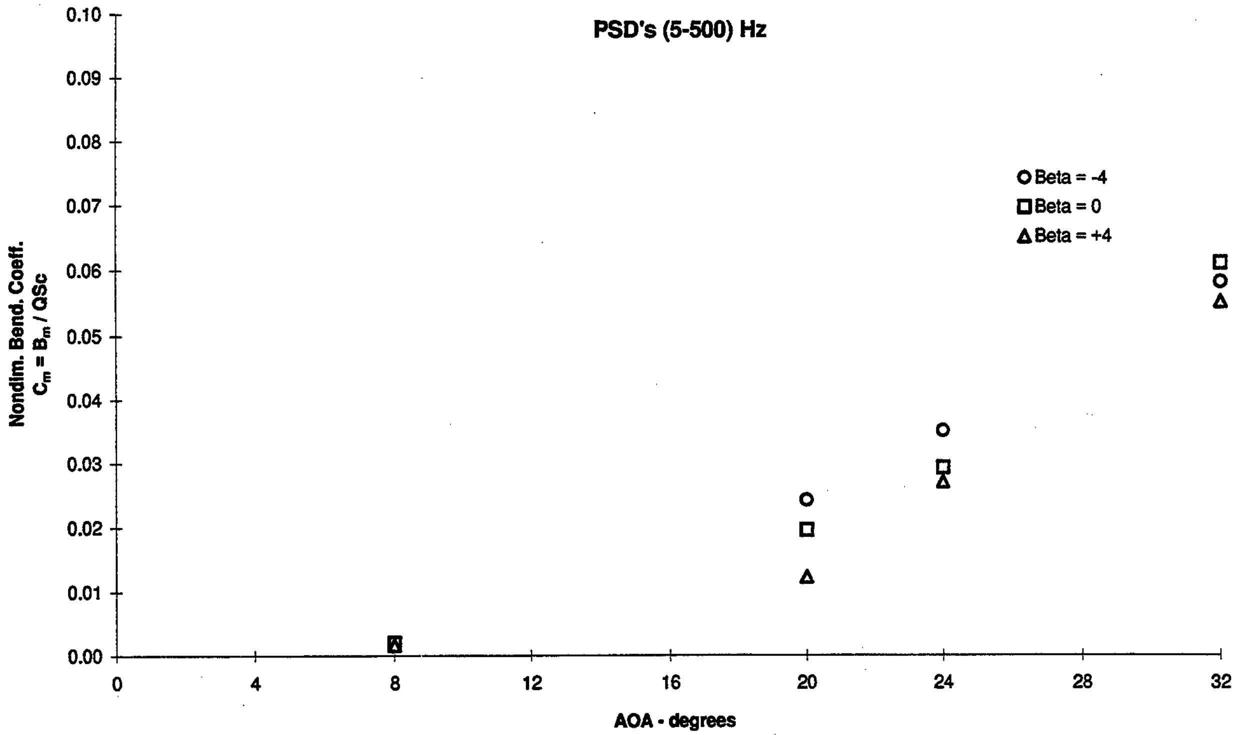

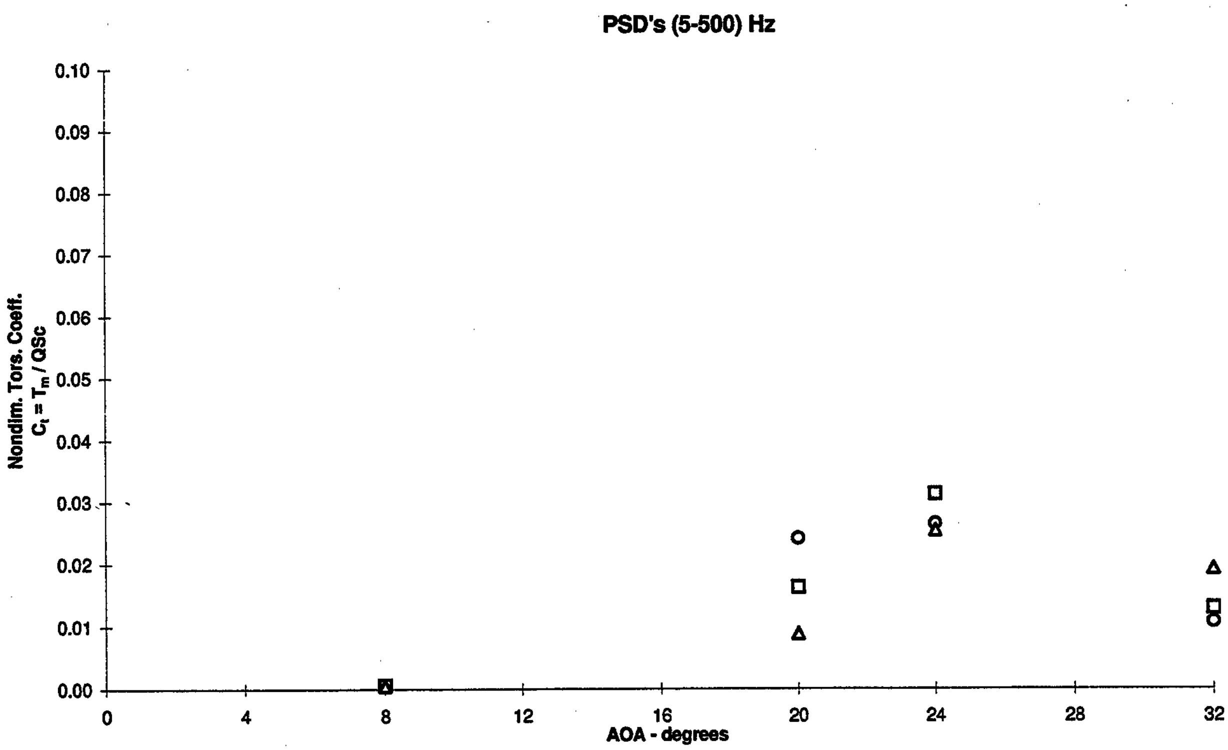

Figure 3.4.3 - Flex Tail Response vs Angle of Attack
Nondimensional Bending and Torsion, Q = 56 psf, No Blowing

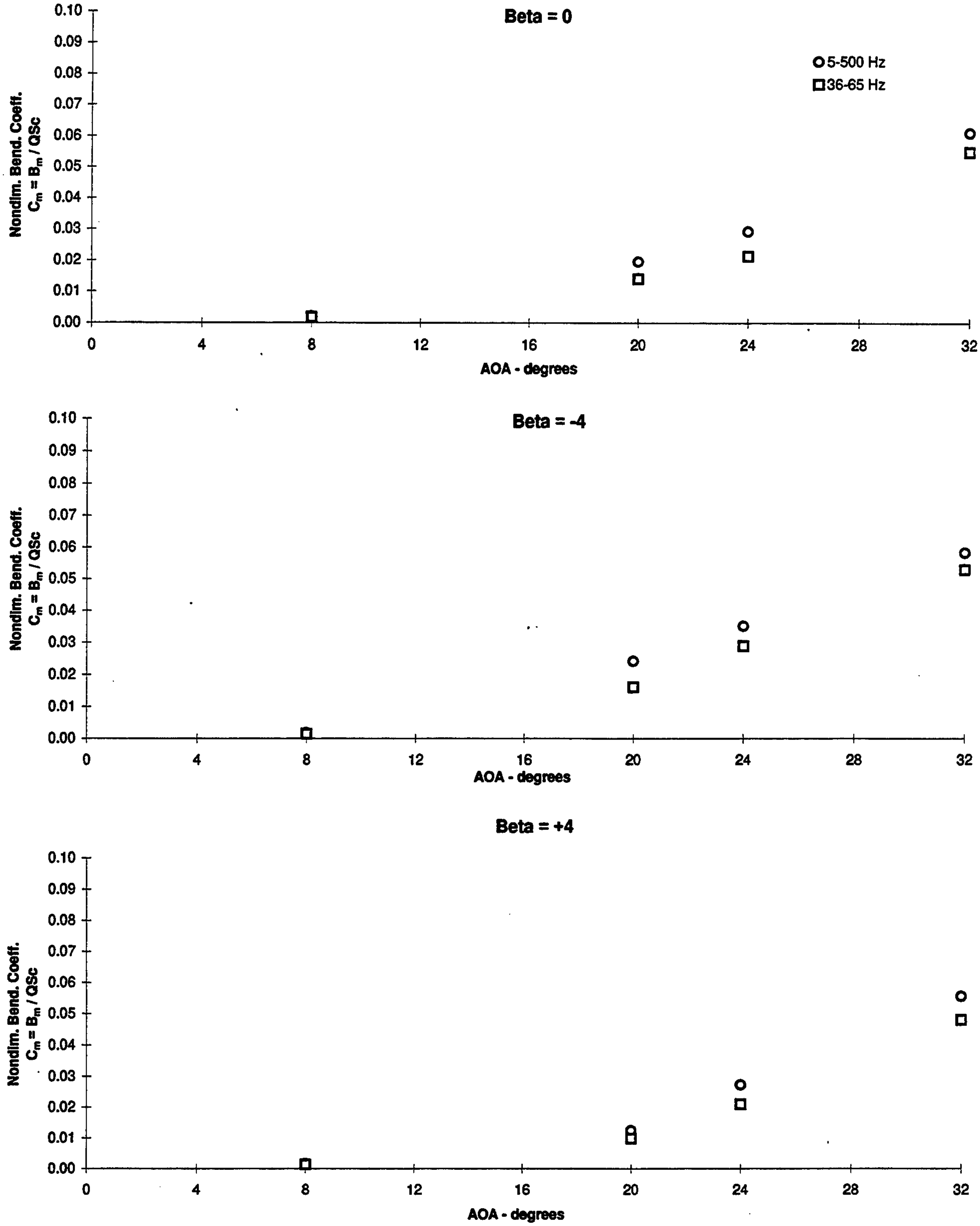

Figure 3.4.4 - Flex Tail Response vs Angle of Attack
Nondimensional Bending, Q = 56 psf, No Blowing

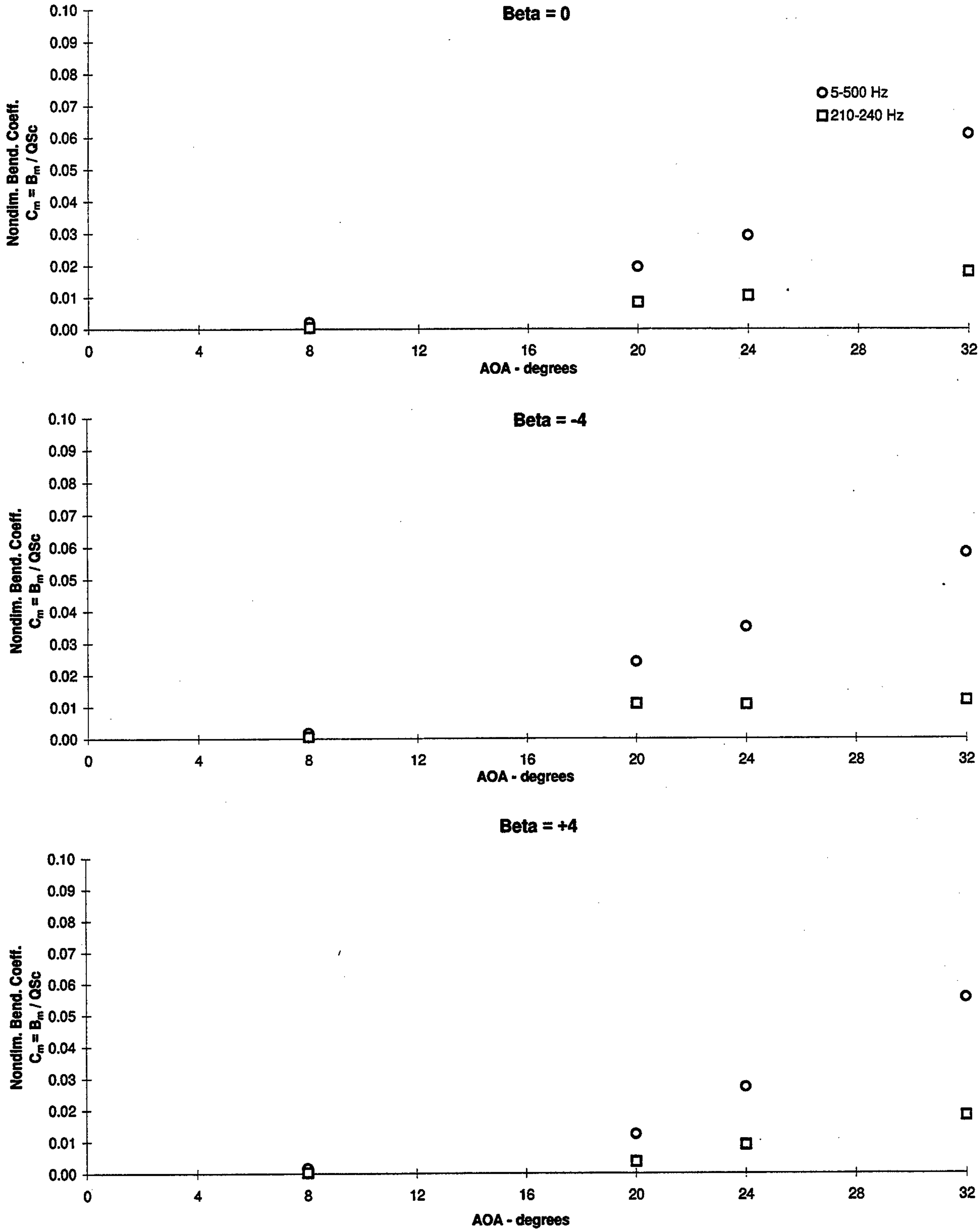

Figure 3.4.5 - Flex Tail Response vs Angle of Attack
Nondimensional Bending, Q = 56 psf, No Blowing

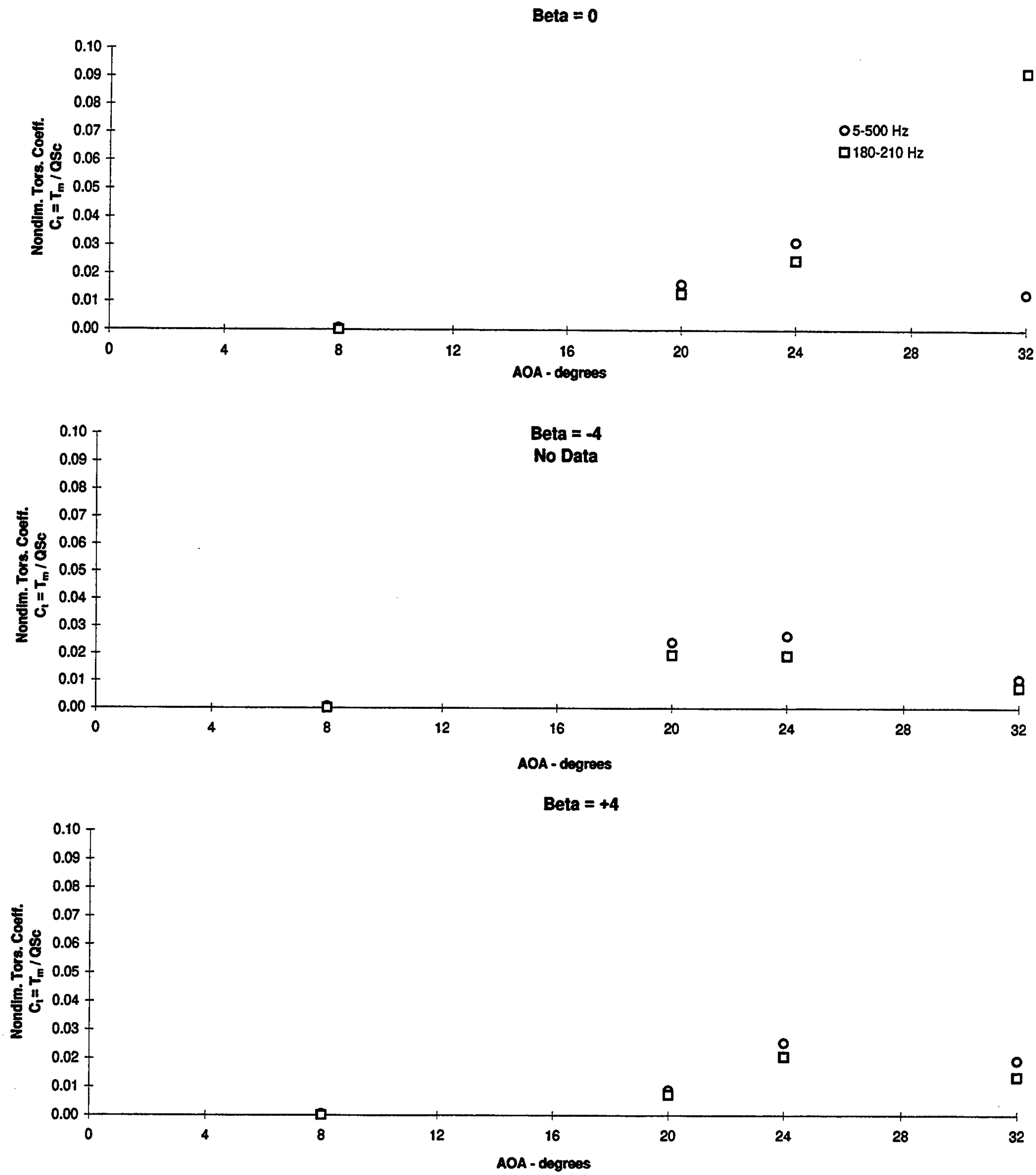

Figure 3.4.6 - Flex Tail Response vs Angle of Attack
Nondimensional Torsion, Q = 56 psf, No Blowing

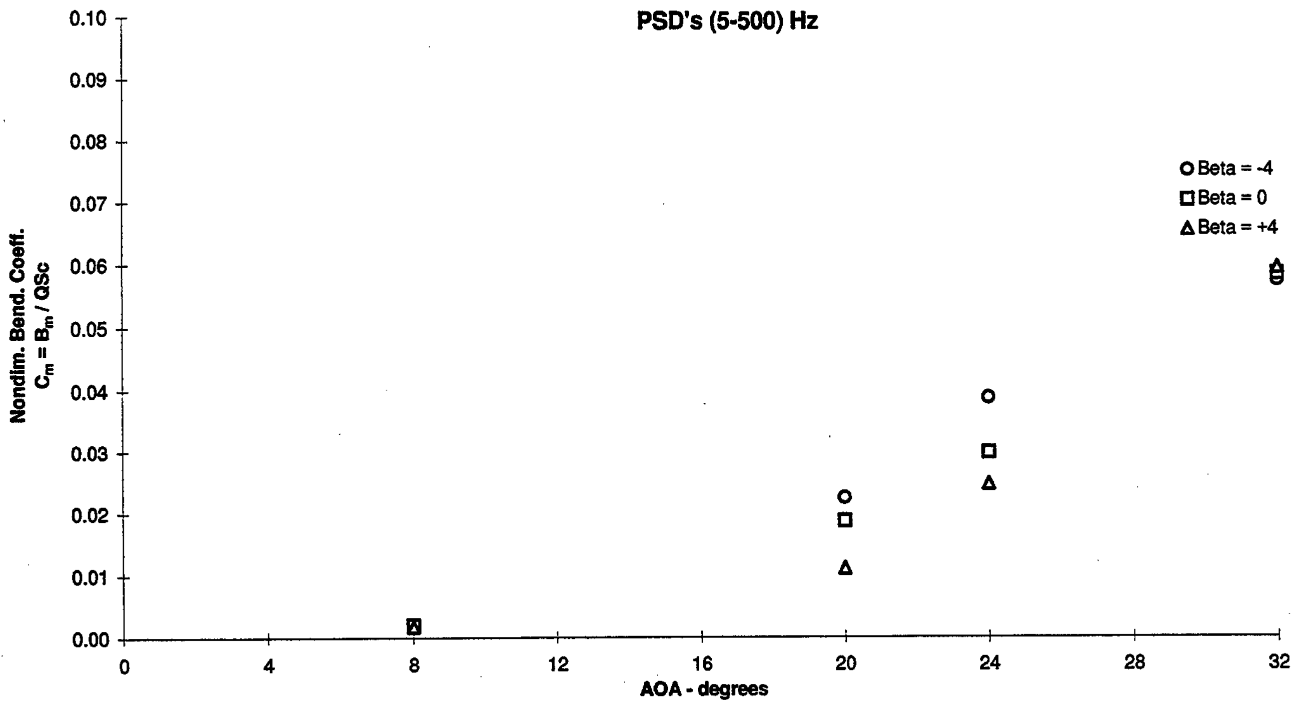

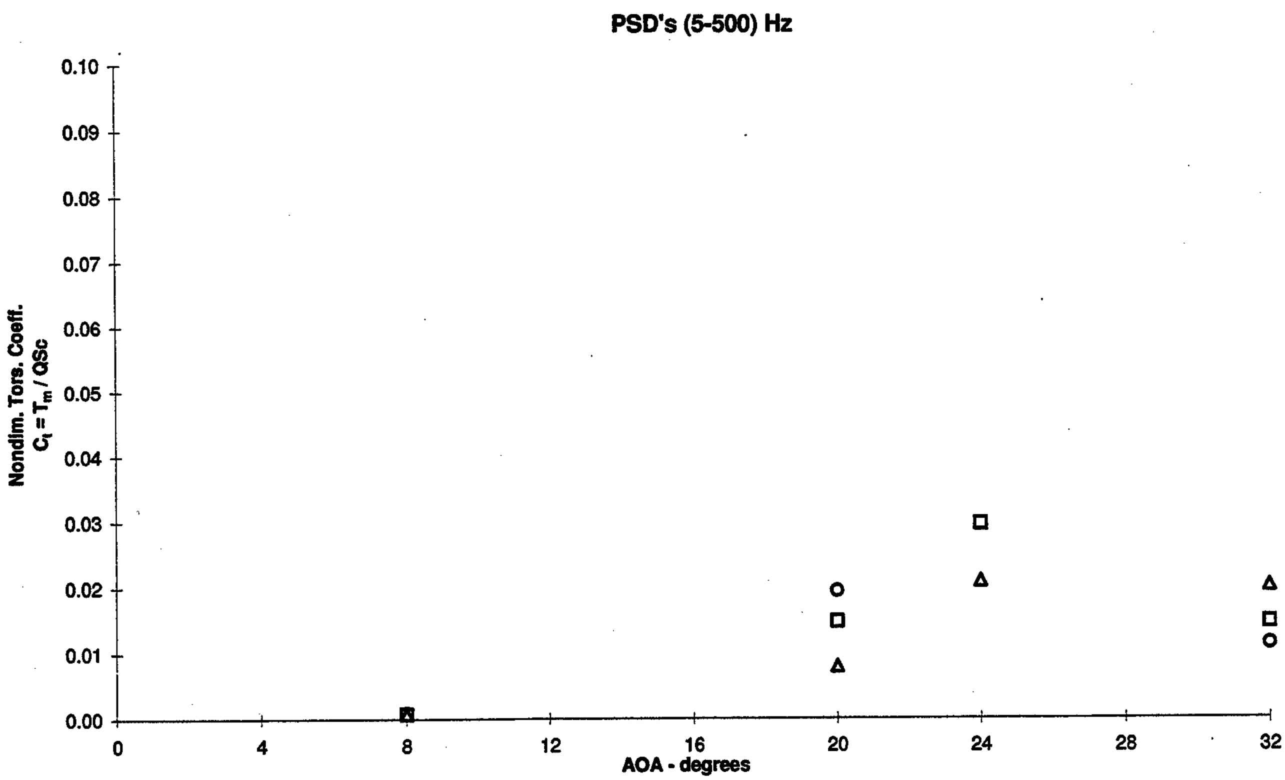

Figure 3.4.7 - Flex Tail Response vs Angle of Attack
Nondimensional Bending and Torsion, Q = 56 psf, Wing Blowing, p = 45 psi

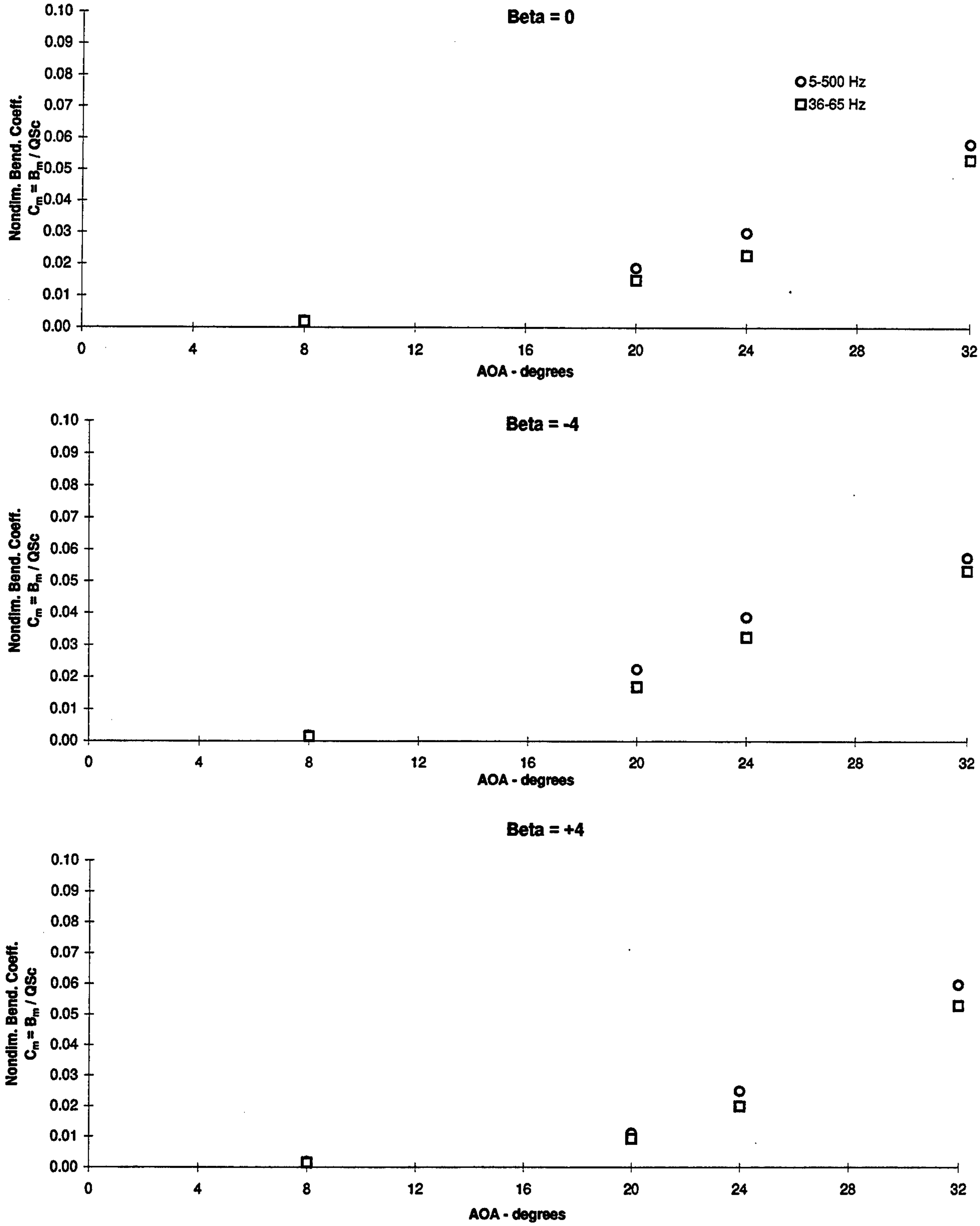

Figure 3.4.8 - Flex Tail Response vs Angle of Attack
Nondimensional Bending, Q = 56 psf, Wing Blowing, p = 45 psi

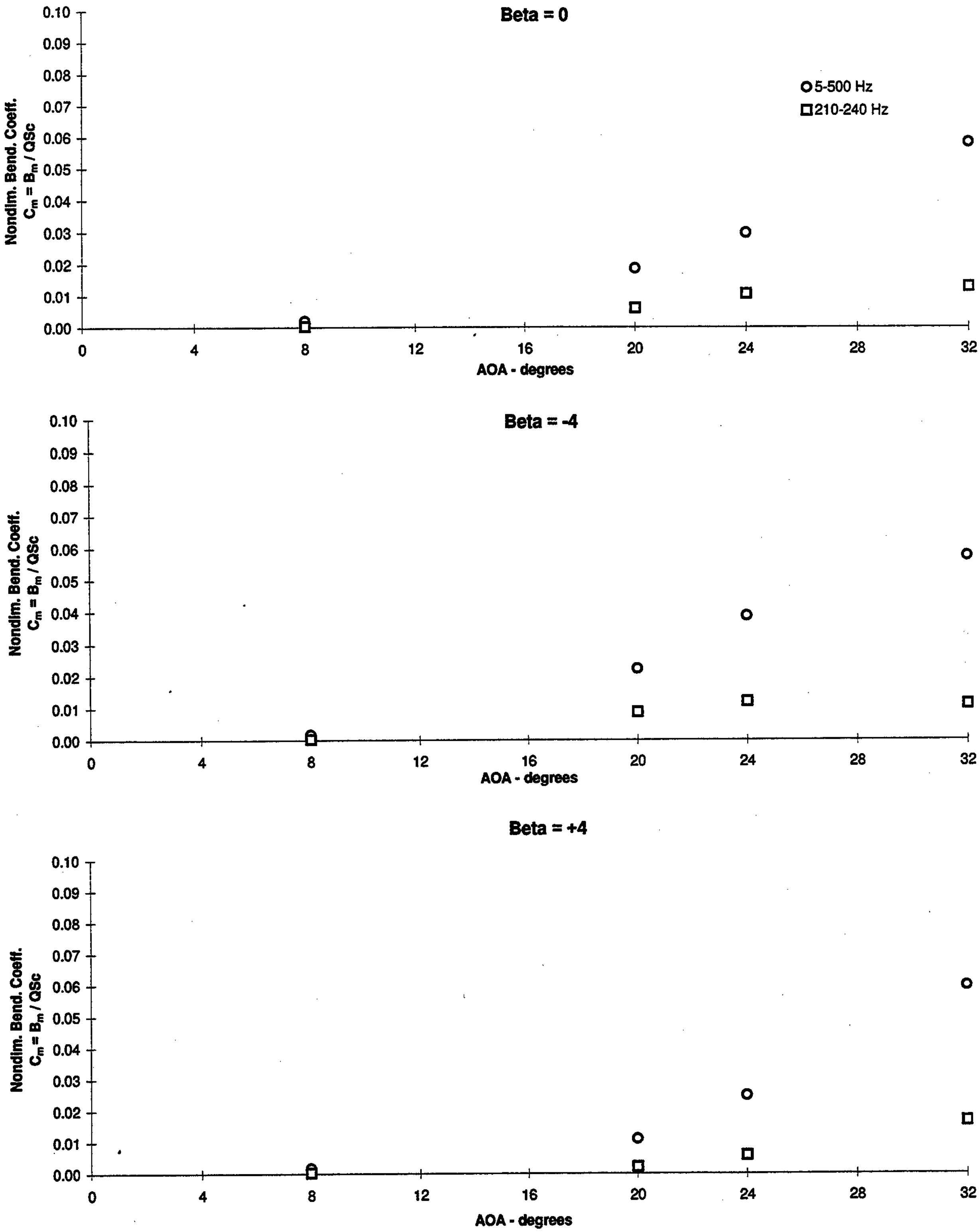

Figure 3.4.9 - Flex Tail Response vs Angle of Attack
Nondimensional Bending, Q = 56 psf, Wing Blowing, p = 45 psi

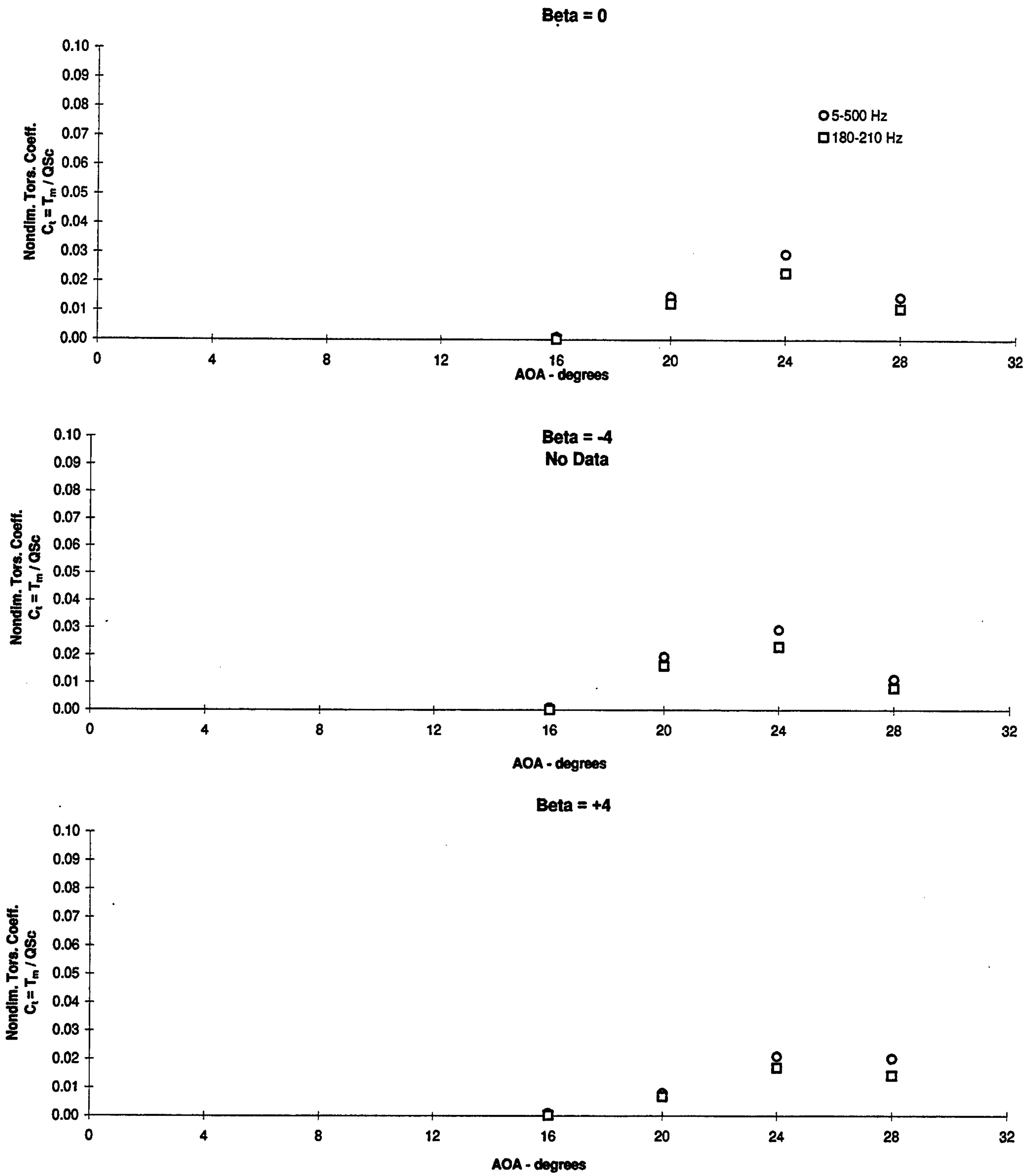

Figure 3.4.10 - Flex Tail Response vs Angle of Attack
Nondimensional Torsion, Q = 56 psf, Wing Blowing p = 45 psi

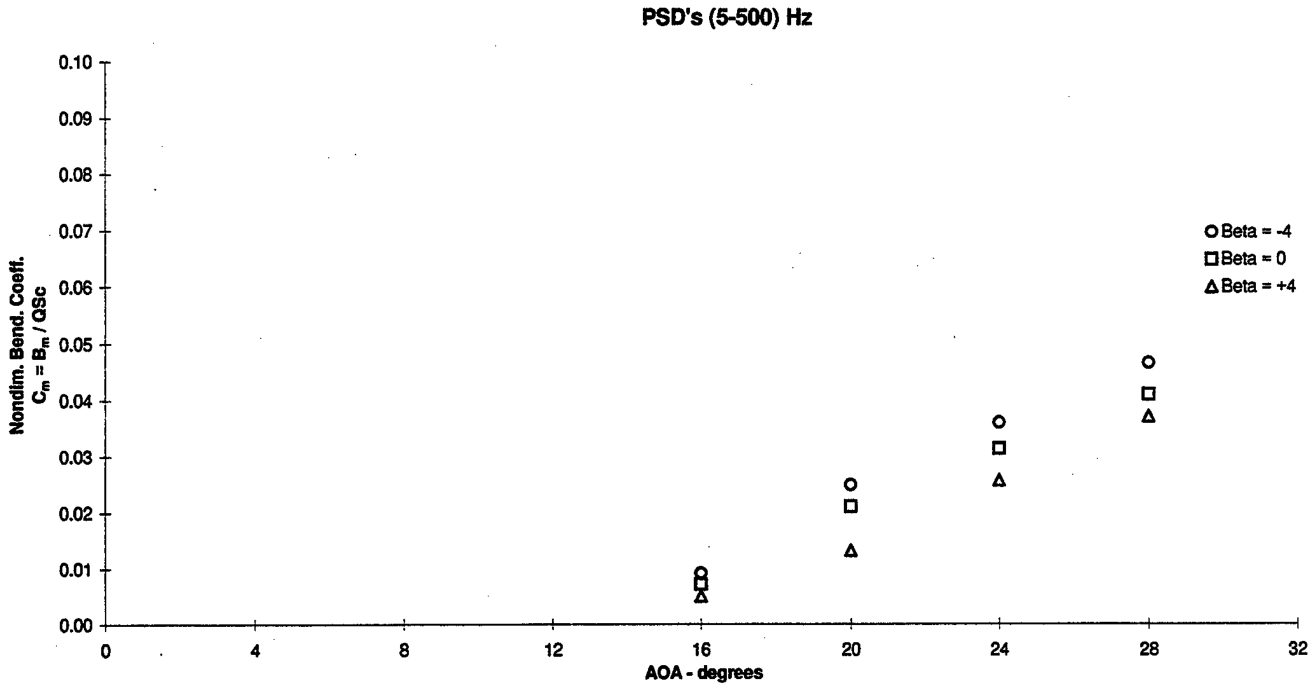

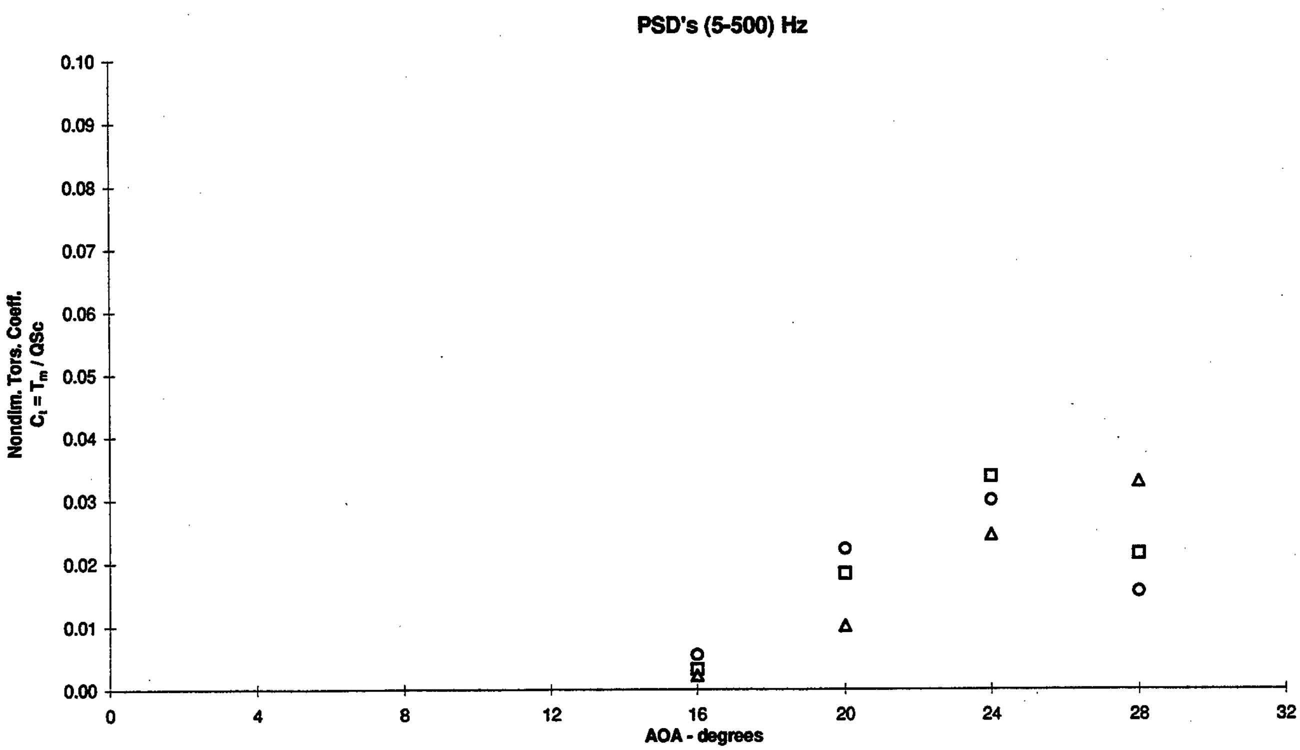

Figure 3.4.11 - Flex Tail Response vs Angle of Attack
Nondimensional Bending and Torsion, Q = 56 psf, Wing Blowing, p = 65 psi

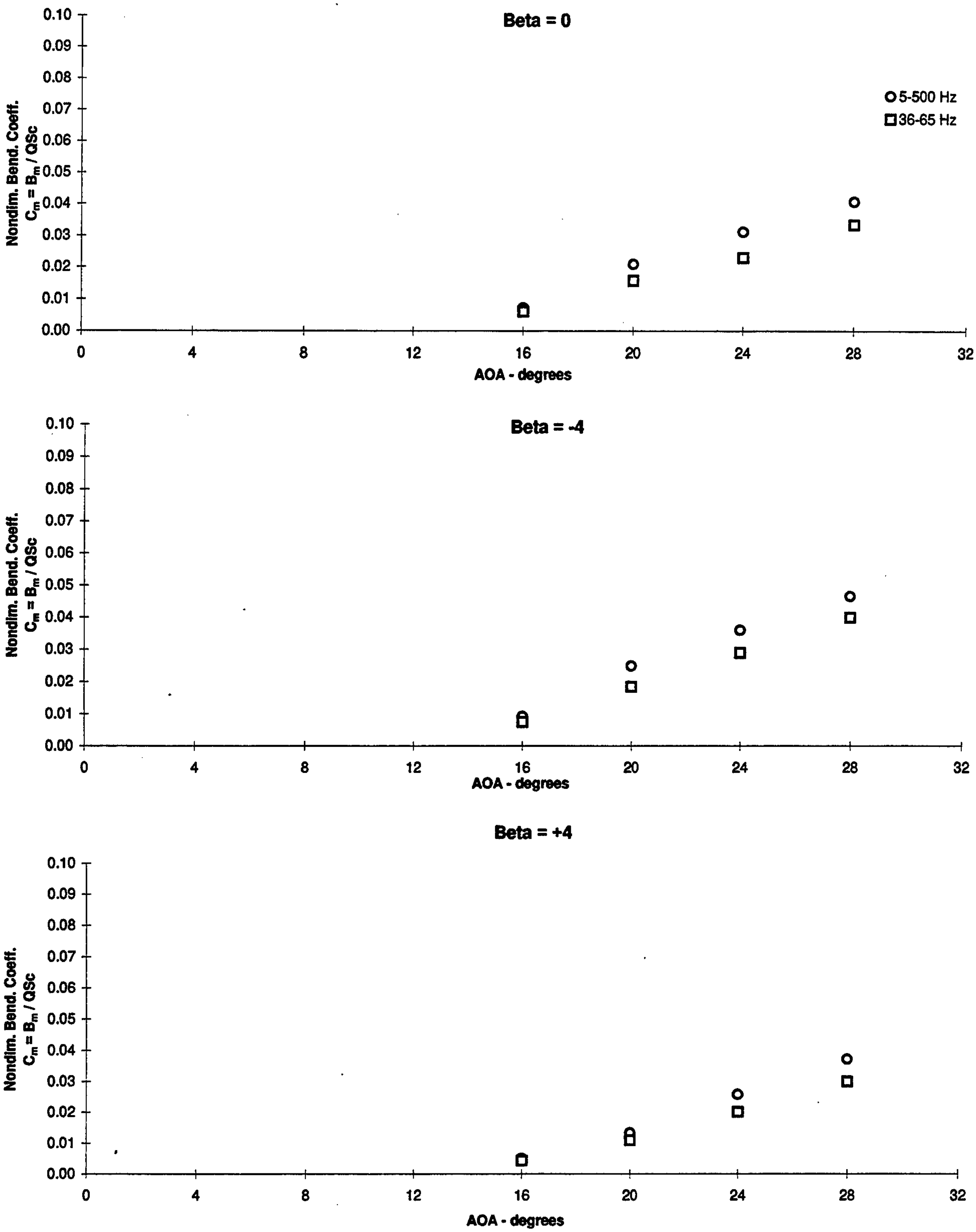

Figure 3.4.12 - Flex Tail Response vs Angle of Attack
Nondimensional Bending, Q = 56 psf, Wing Blowing, p = 65 psi

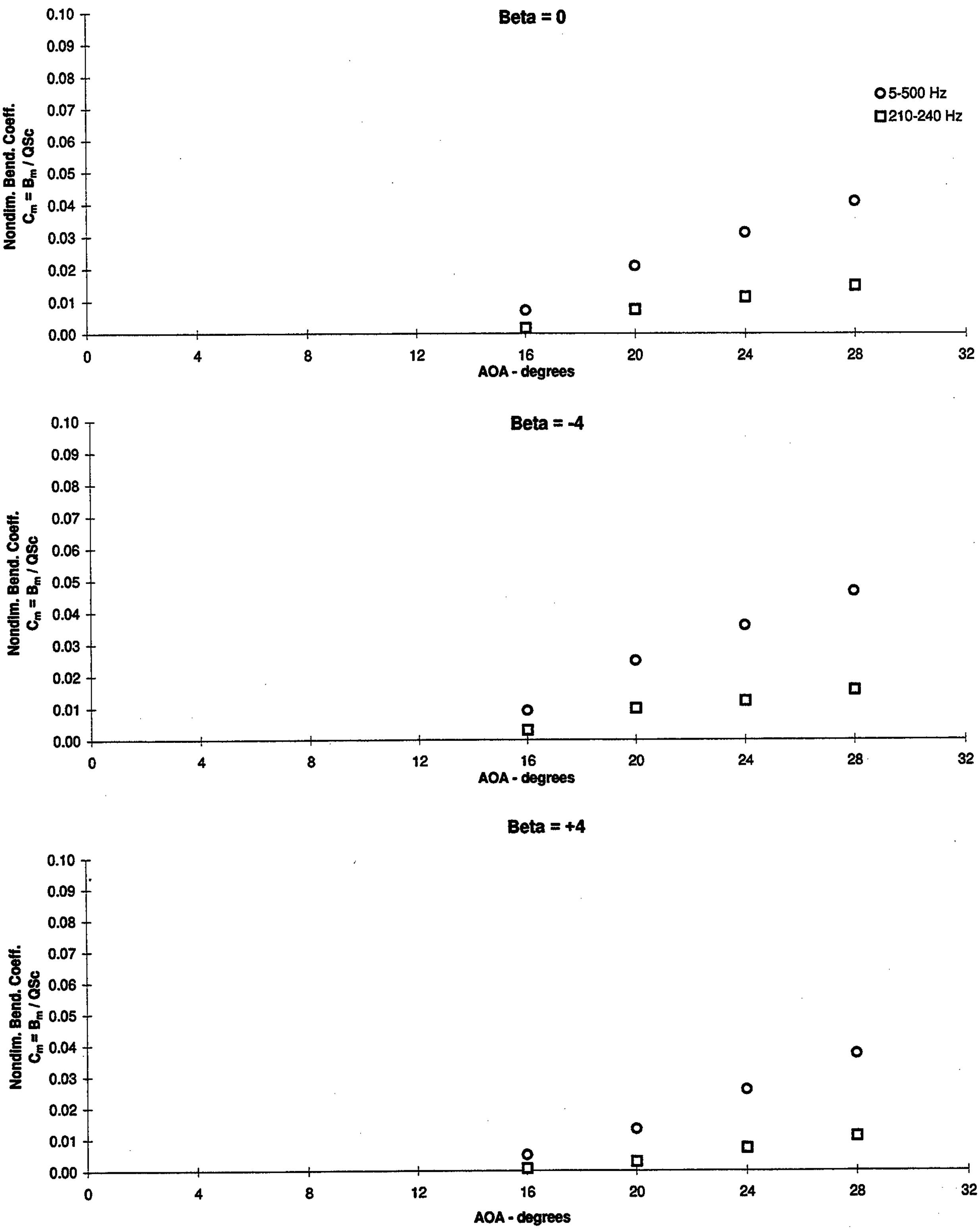

Figure 3.4.13 - Flex Tail Response vs Angle of Attack
Nondimensional Bending, Q = 56 psf, Wing Blowing, p = 65 psi

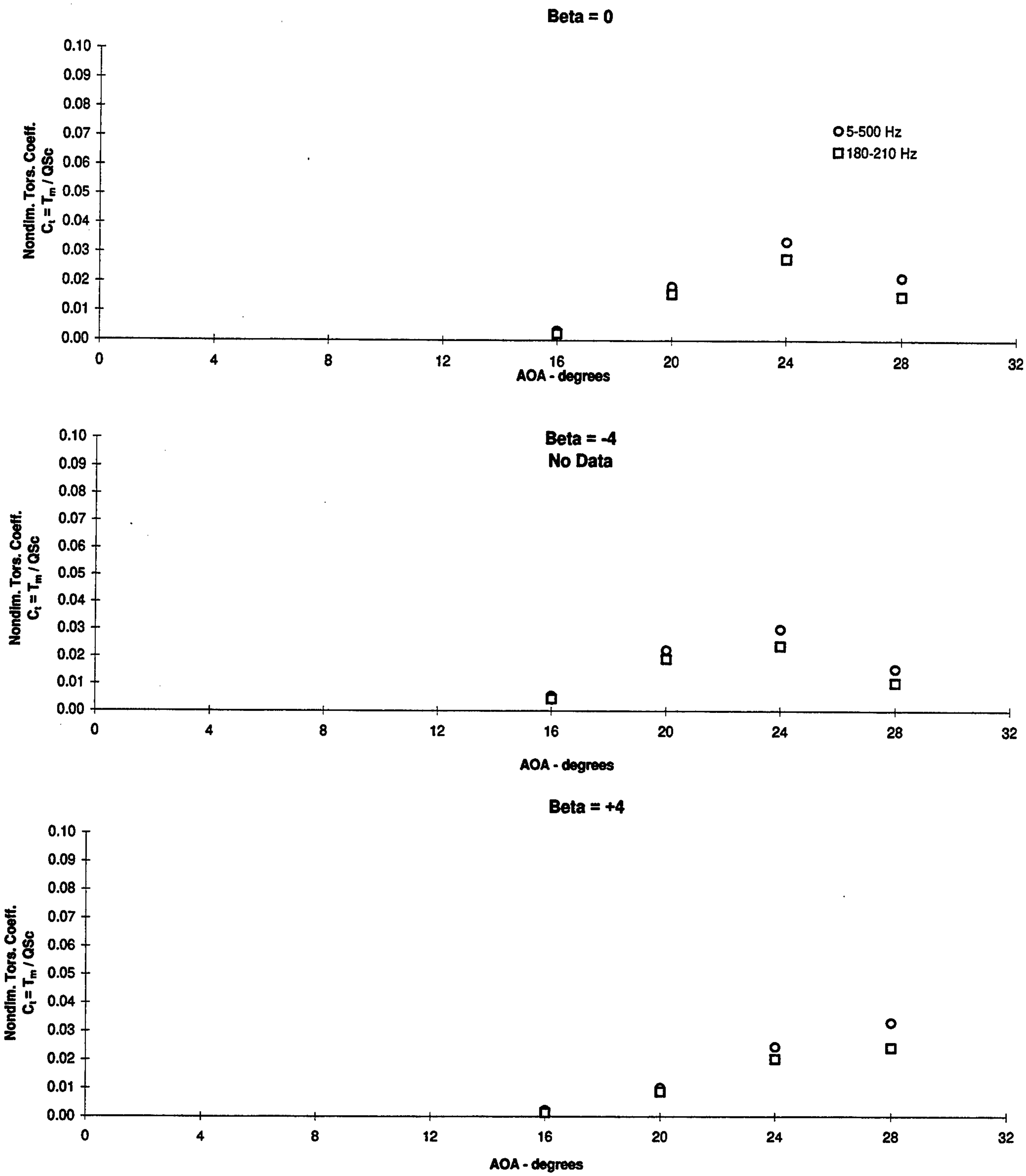

Figure 3.4.14 - Flex Tail Response vs Angle of Attack
Nondimensional Torsion, Q = 56 psf, Wing Blowing p = 65 psi

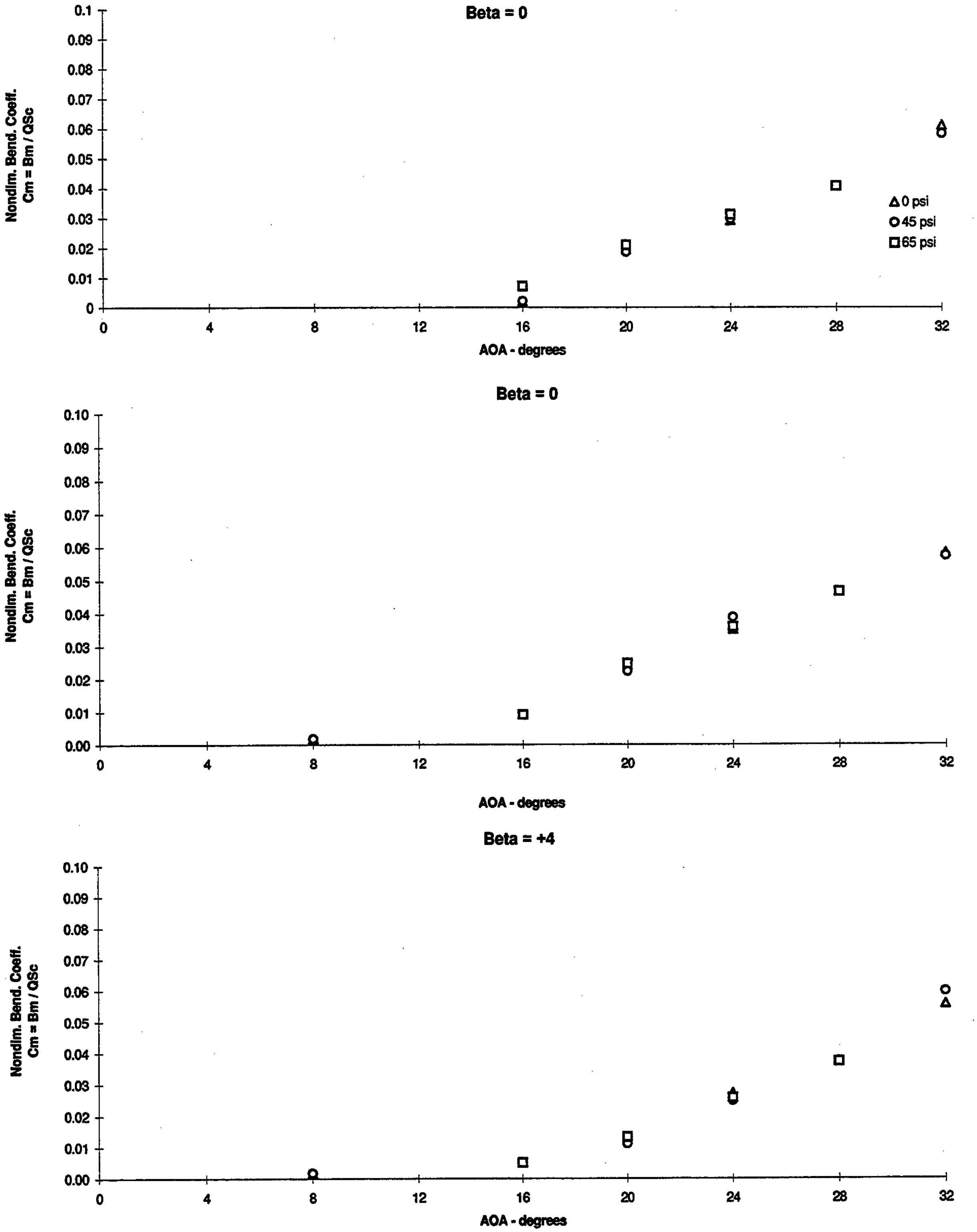

Figure 3.4.15 - Flex Tail Response vs Angle of Attack
Nondimensional Bending, Q = 56 psf, PSD's (5-500) Hz, Wing Blowing Summary

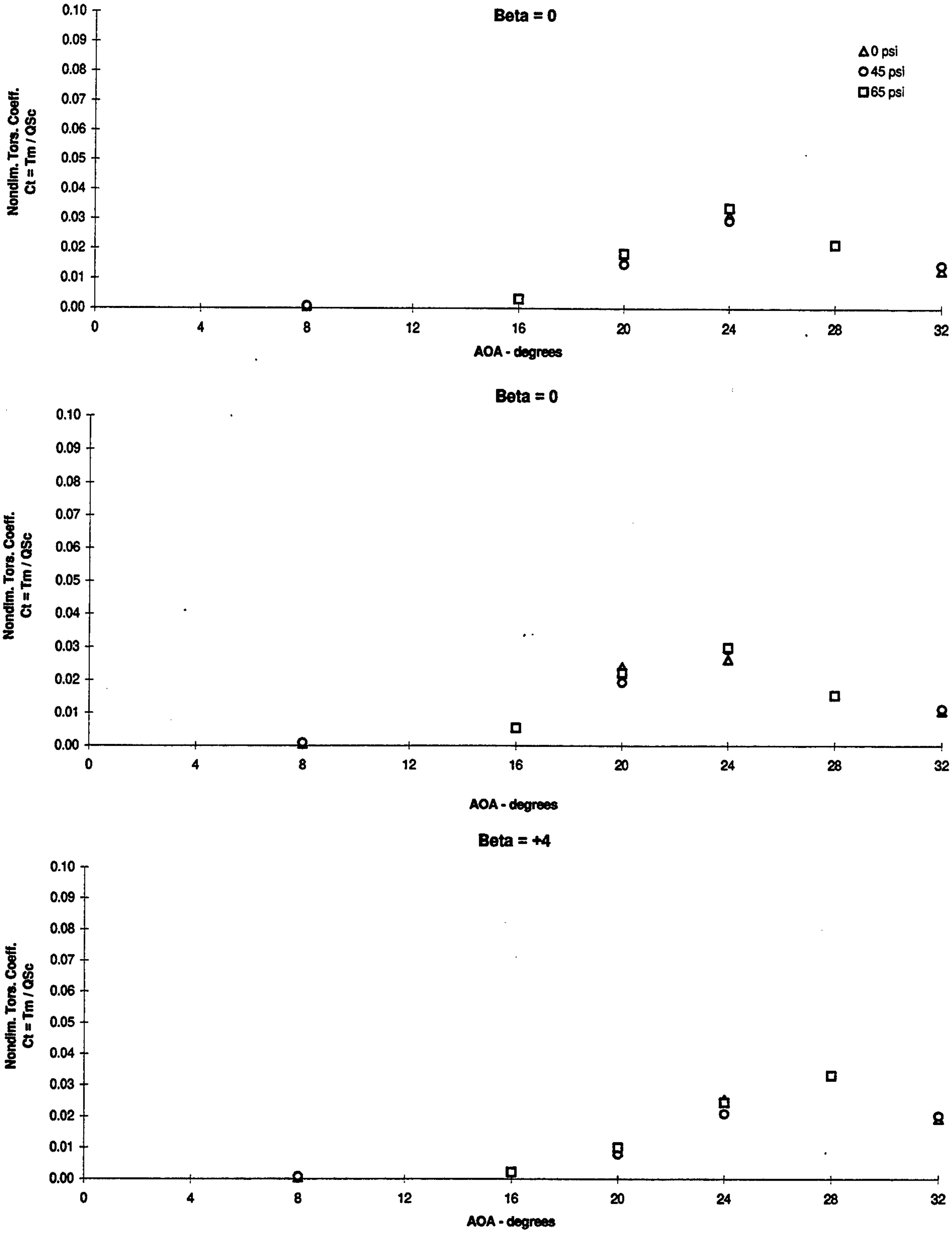

Figure 3.4.16 - Flex Tail Response vs Angle of Attack
Nondimensional Torsion, Q = 56 psf, PSD's (5-500) Hz, Wing Blowing Summary

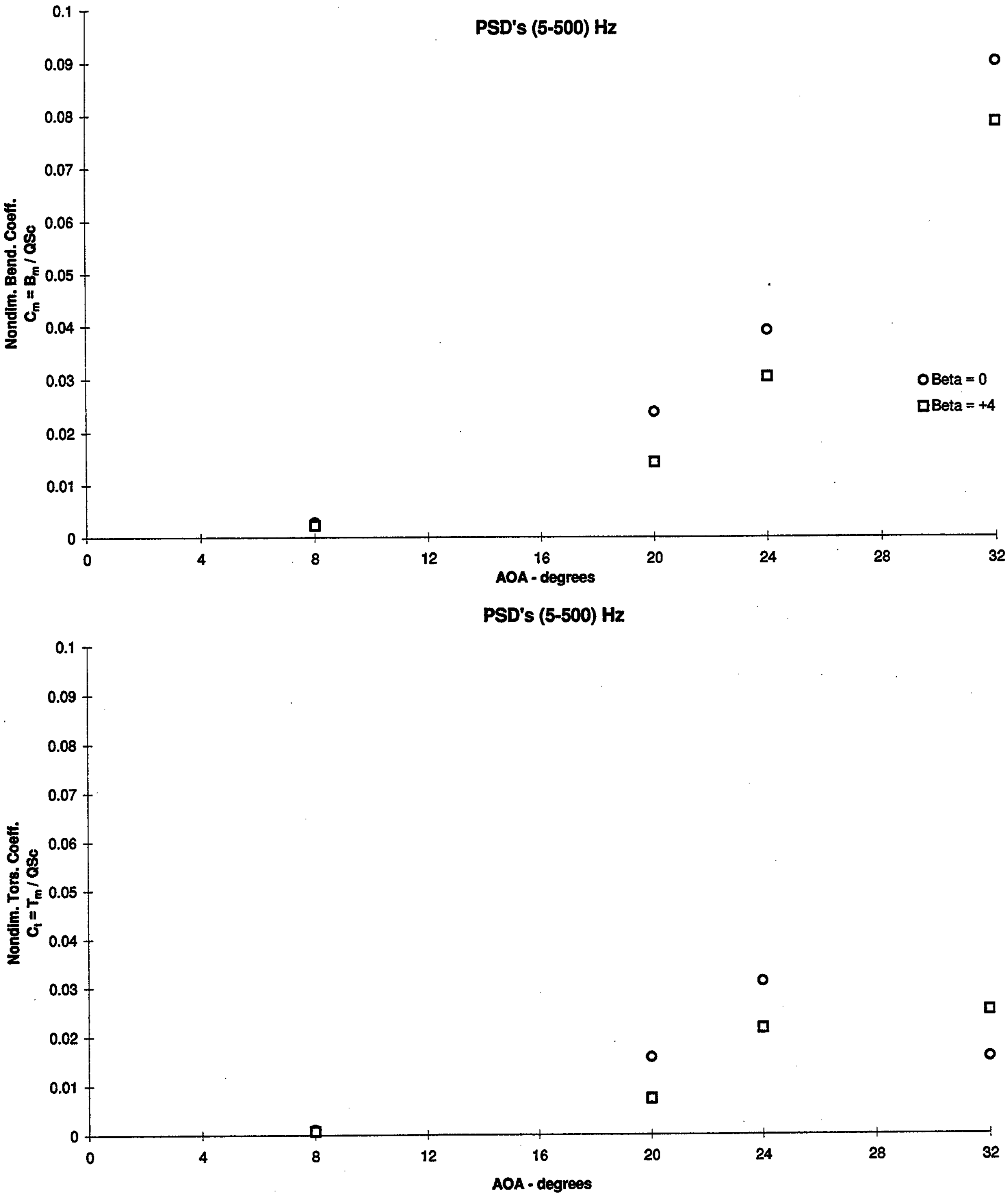

Figure 3.4.17 - Flex Tail Response vs Angle of Attack
Nondimensional Bending and Torsion, Q = 30 psf, No Blowing

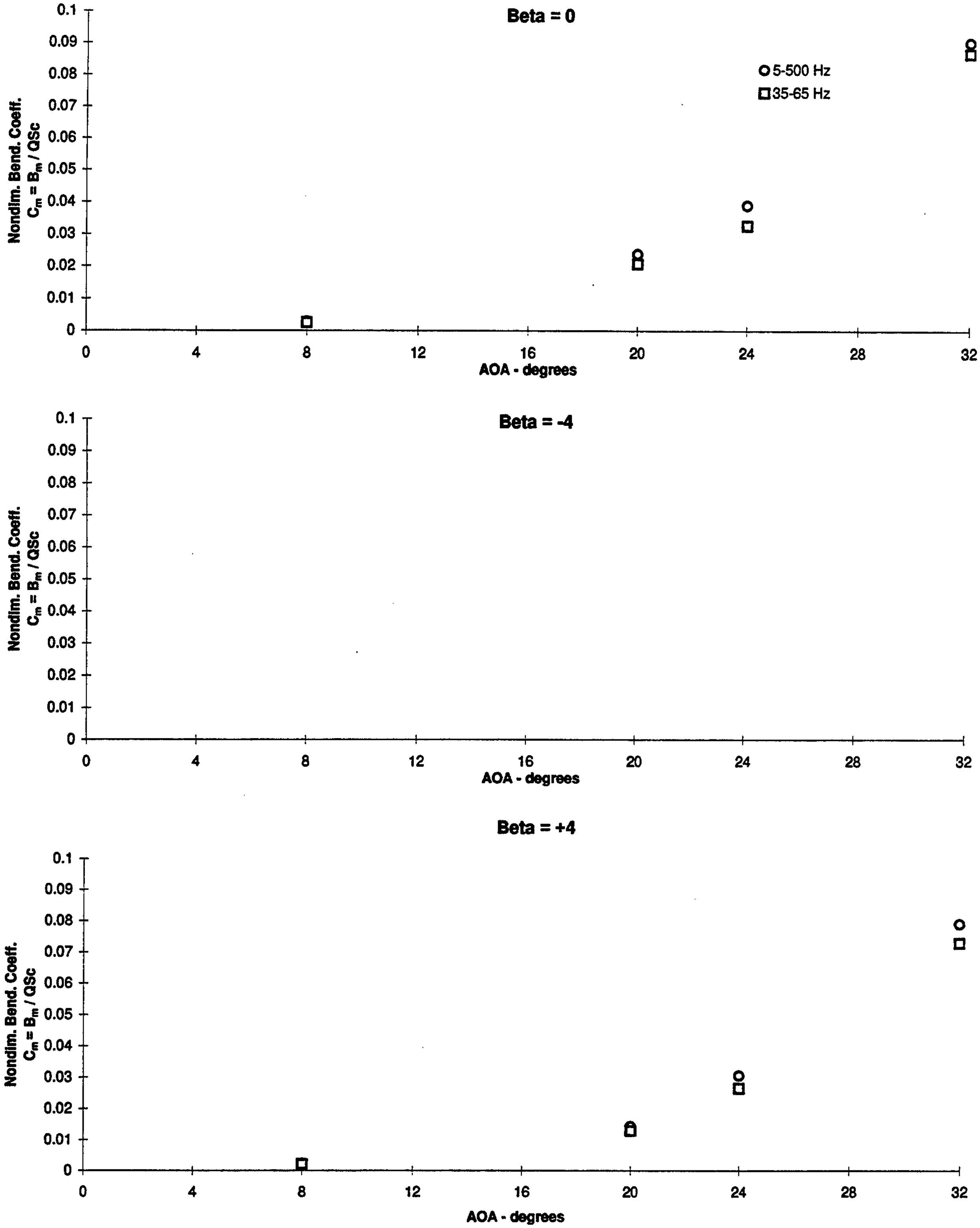

Figure 3.4.18 - Flex Tail Response vs Angle of Attack
Nondimensional Bending, Q = 30 psf, No Blowing

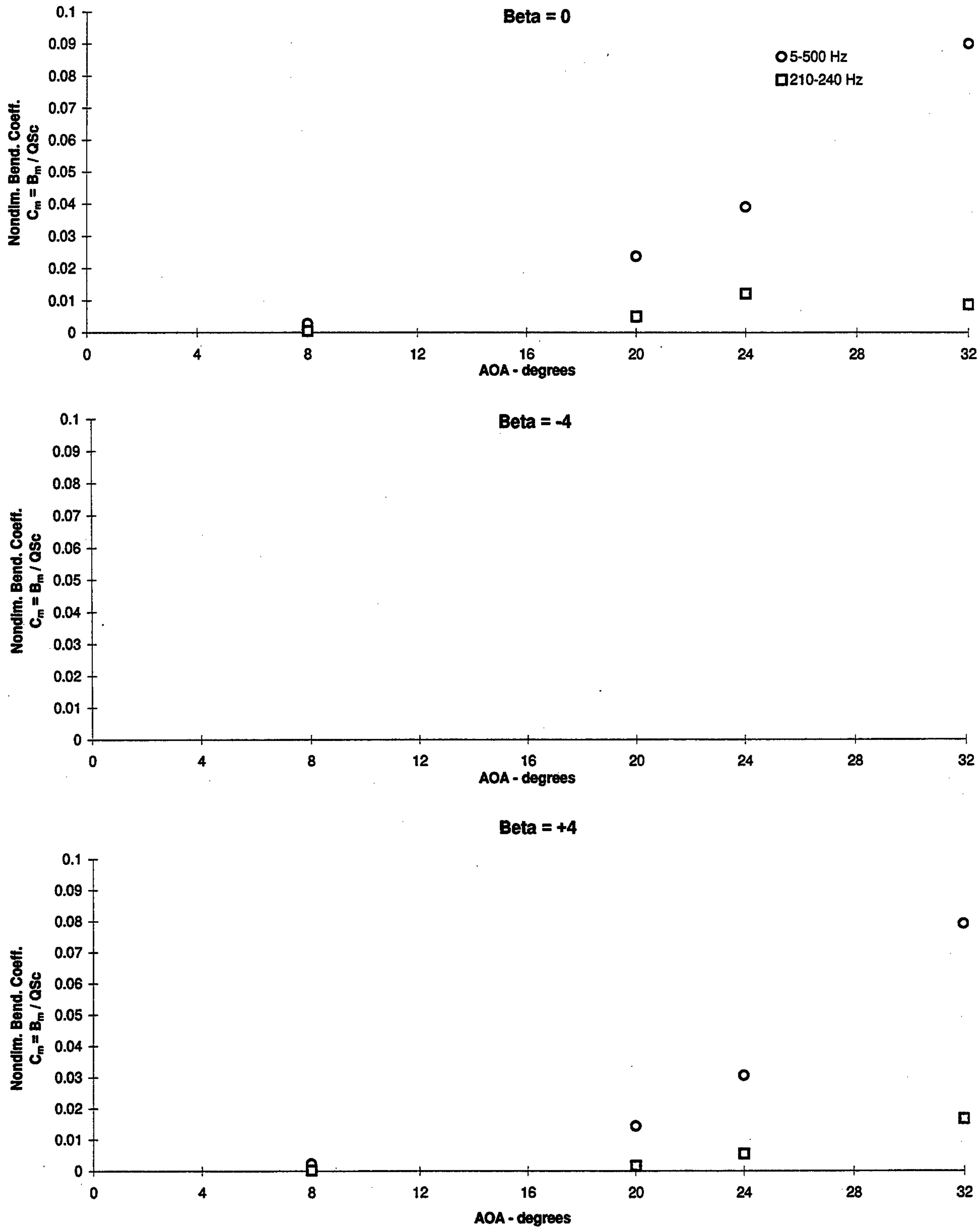

Figure 3.4.19 - Flex Tail Response vs Angle of Attack
Nondimensional Bending, Q = 30 psf, No Blowing

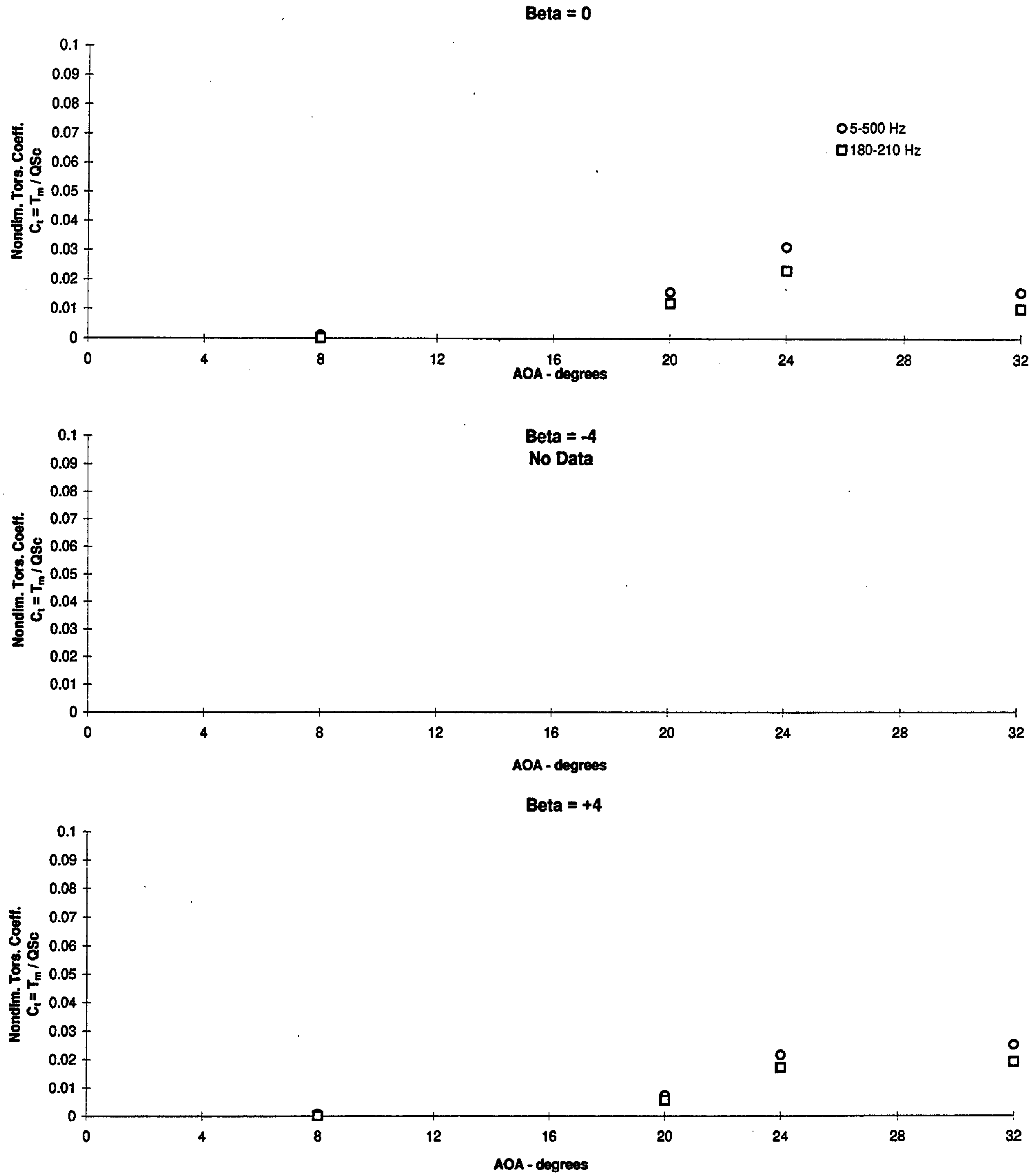

Figure 3.4.20 - Flex Tail Response vs Angle of Attack
Nondimensional Torsion, Q = 30 psf, No Blowing

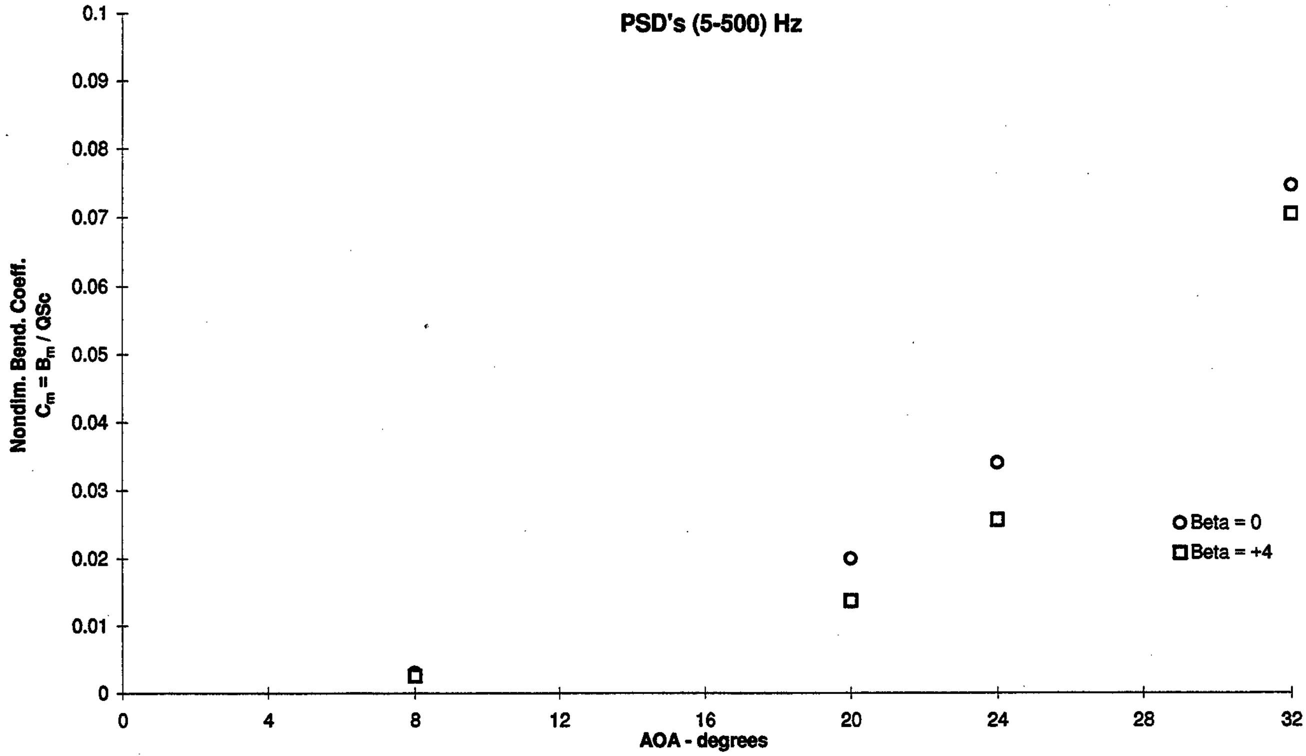

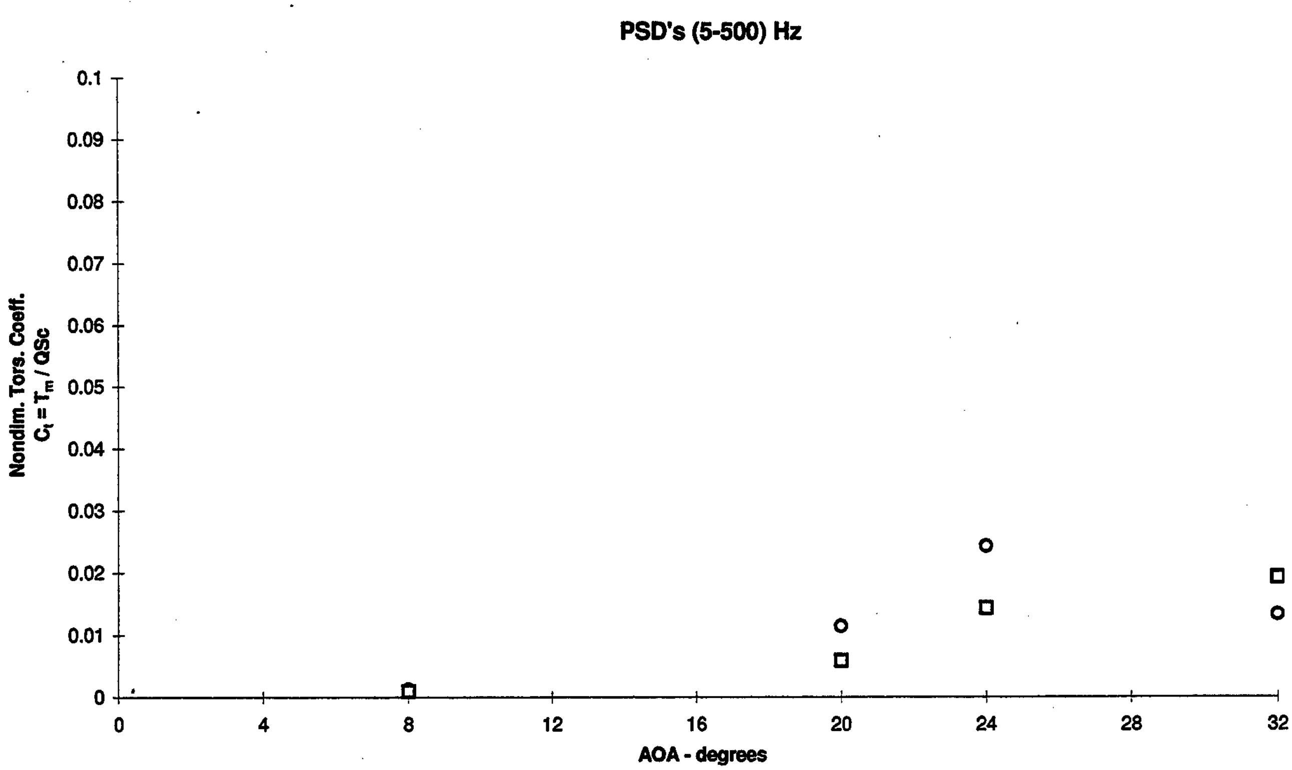

Figure 3.4.21 - Flex Tail Response vs Angle of Attack
Nondimensional Bending and Torsion, Q = 30 psf, Wing Blowing p = 45 psi

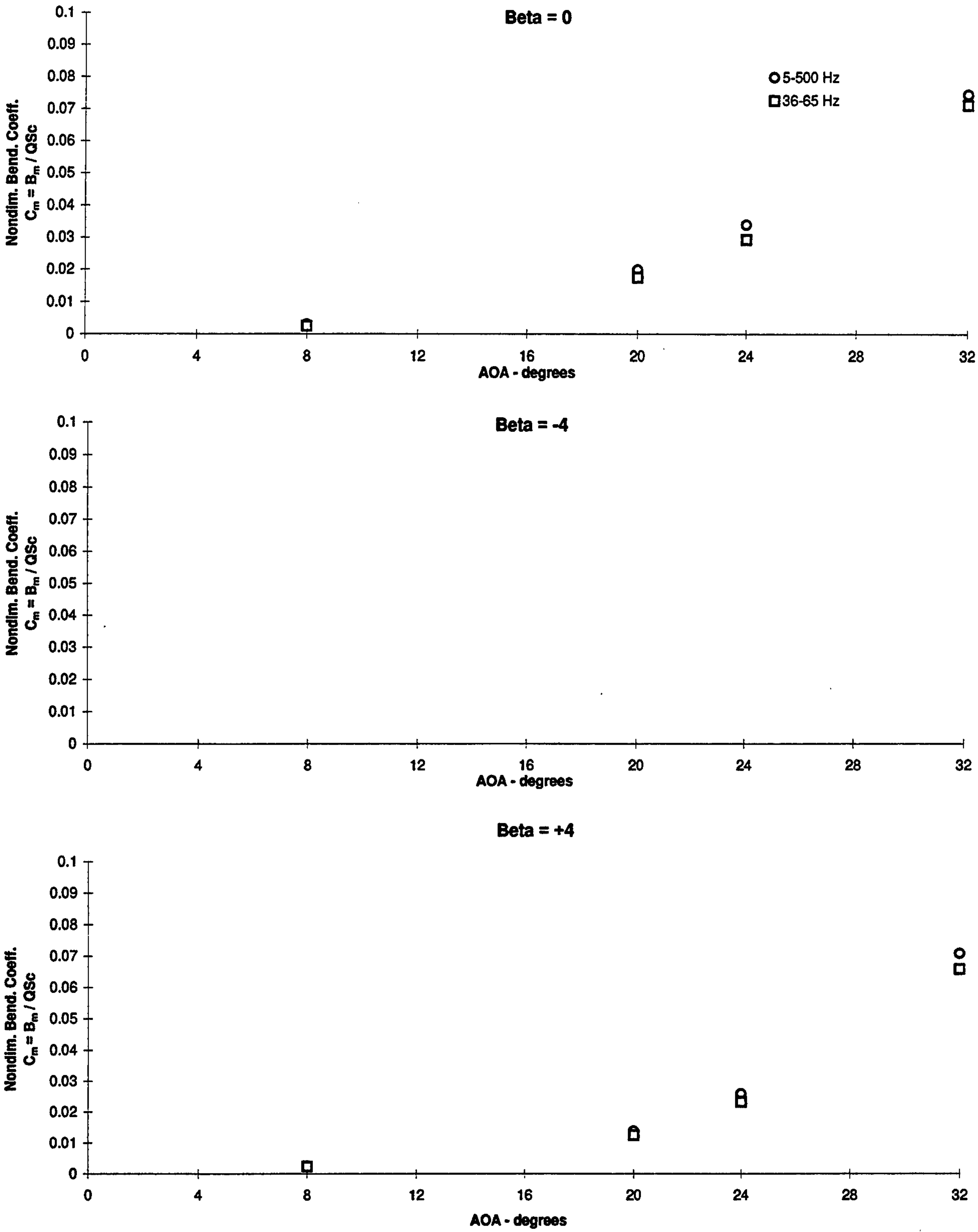

Figure 3.4.22 - Flex Tail Response vs Angle of Attack
Nondimensional Bending, Q = 30 psf, Wing Blowing, p = 45 psi

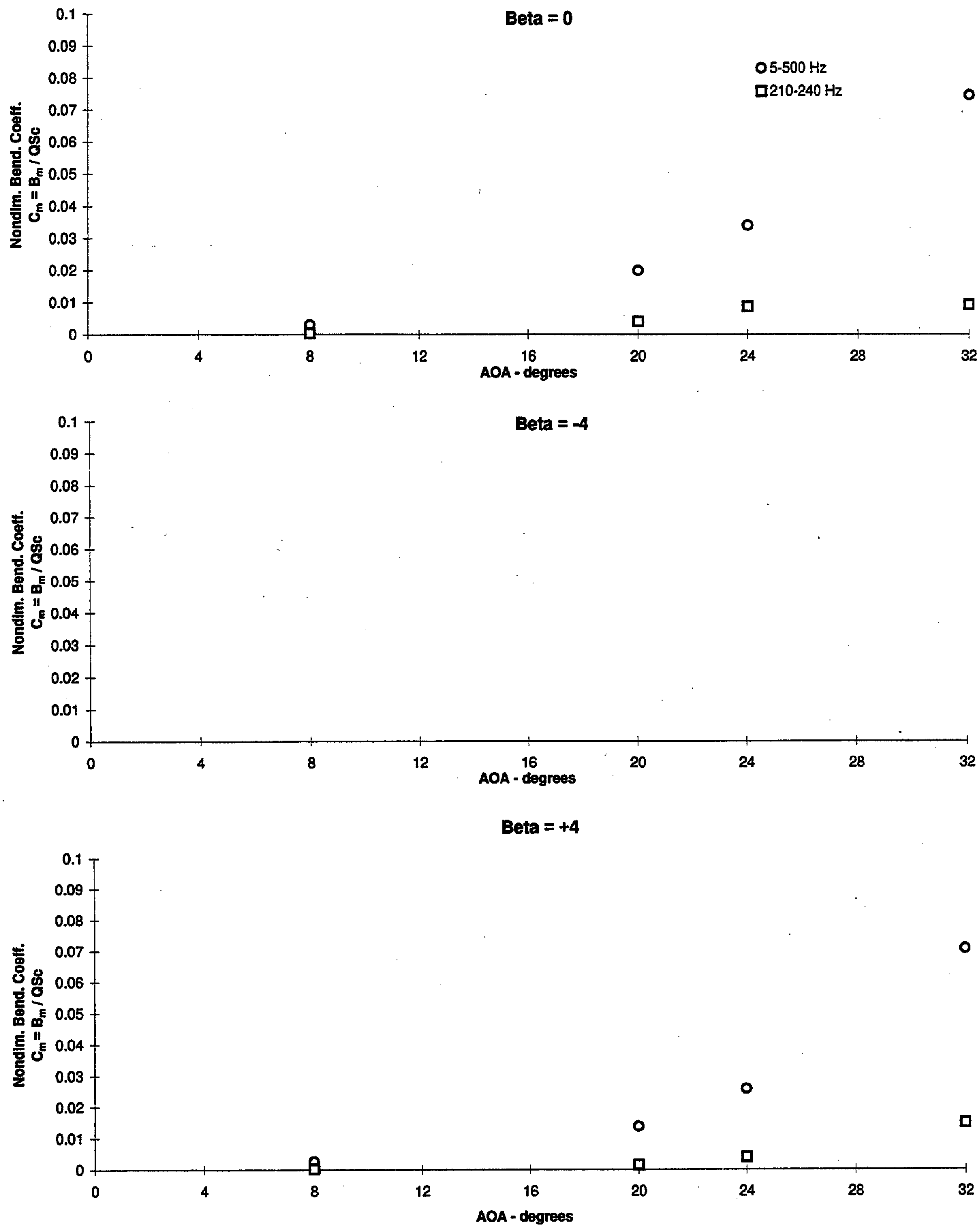

Figure 3.4.23 - Flex Tail Response vs Angle of Attack
Nondimensional Bending, Q = 30 psf, Wing Blowing, p = 45 psi

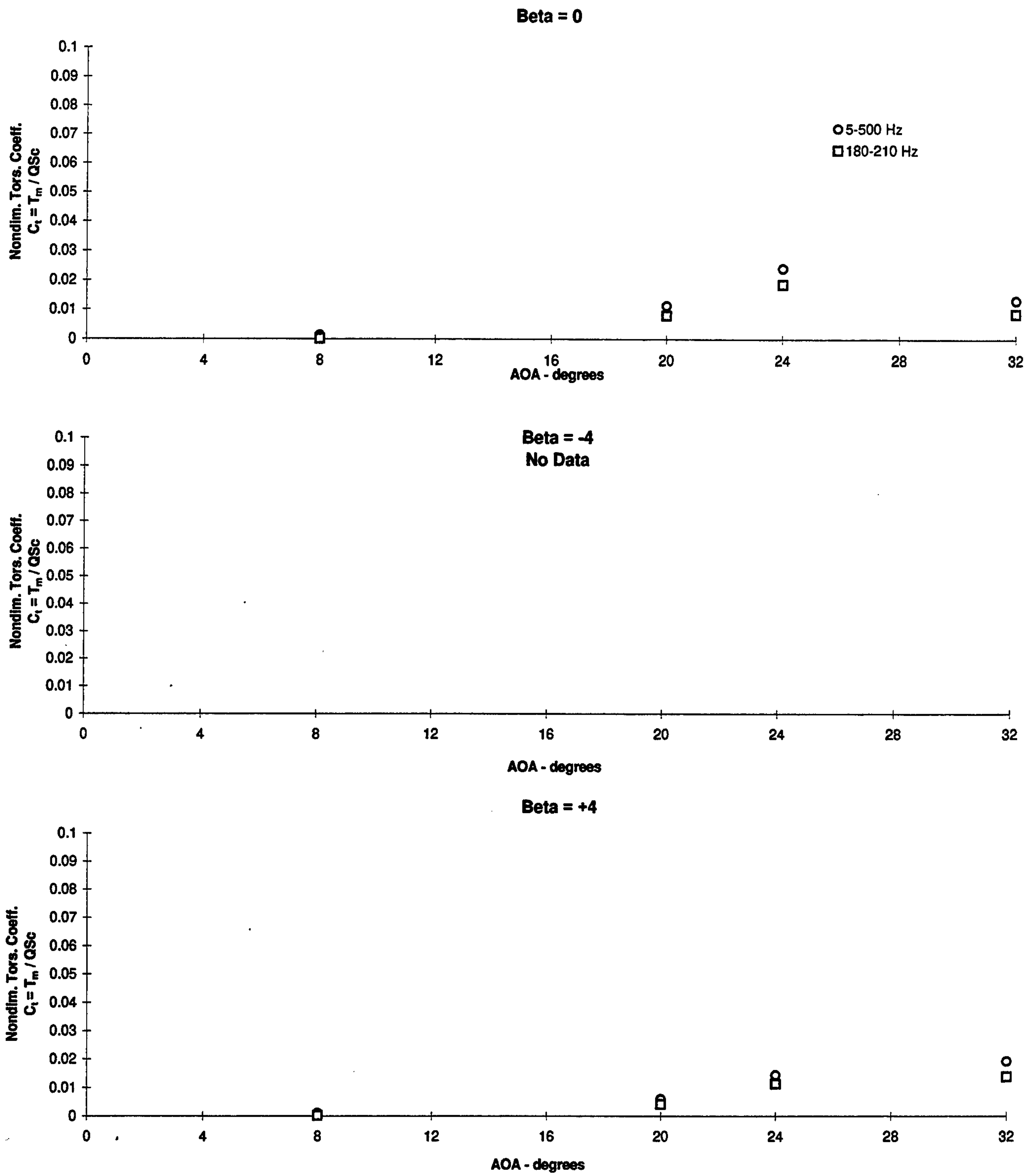

Figure 3.4.24 - Flex Tail Response vs Angle of Attack
Nondimensional Torsion, Q = 30 psf, Wing Blowing p = 45 psi

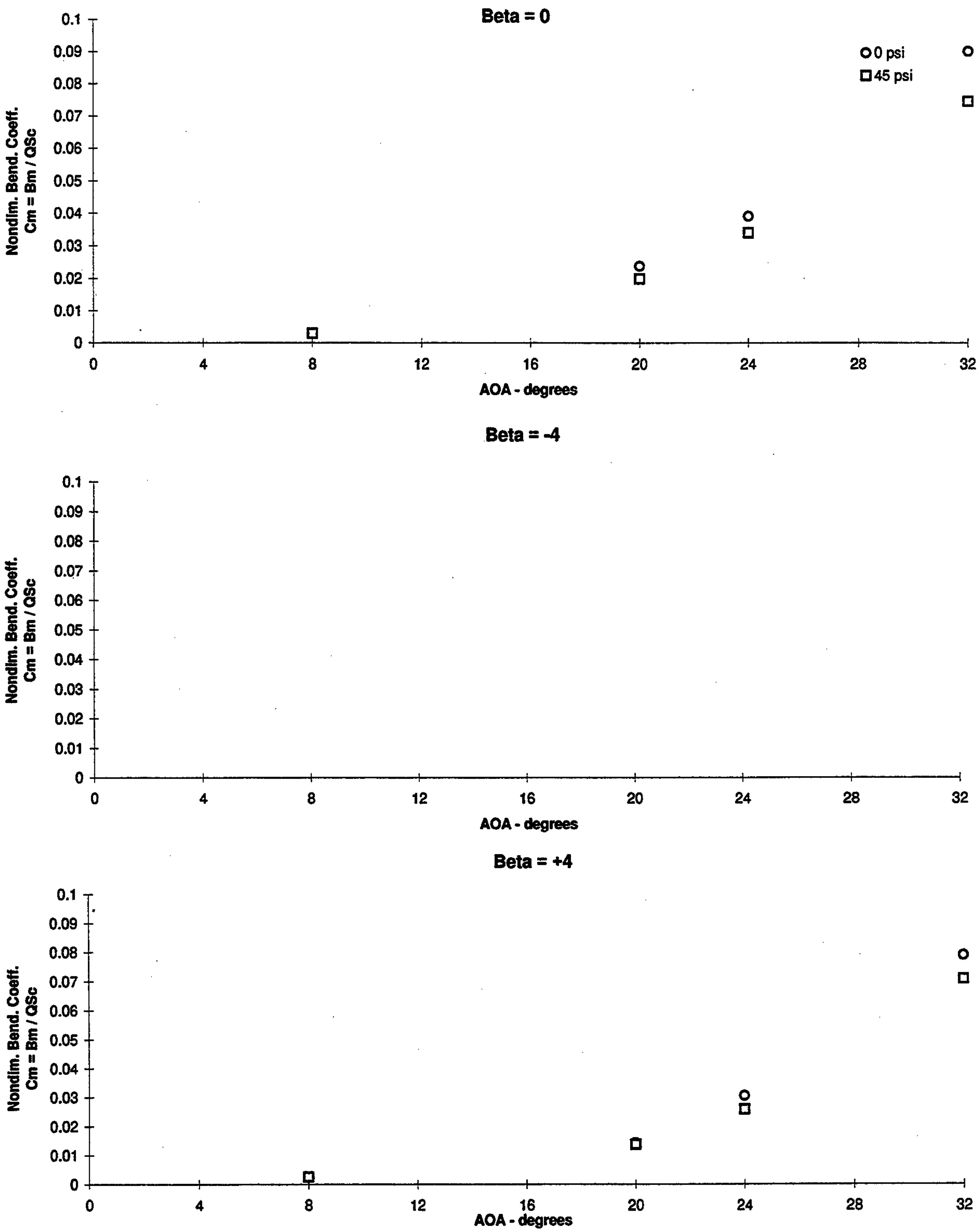

Figure 3.4.25 - Flex Tail Response vs Angle of Attack
Nondimensional Bending, Q = 30 psf, PSD's (5-500) Hz, Wing Blowing Summary

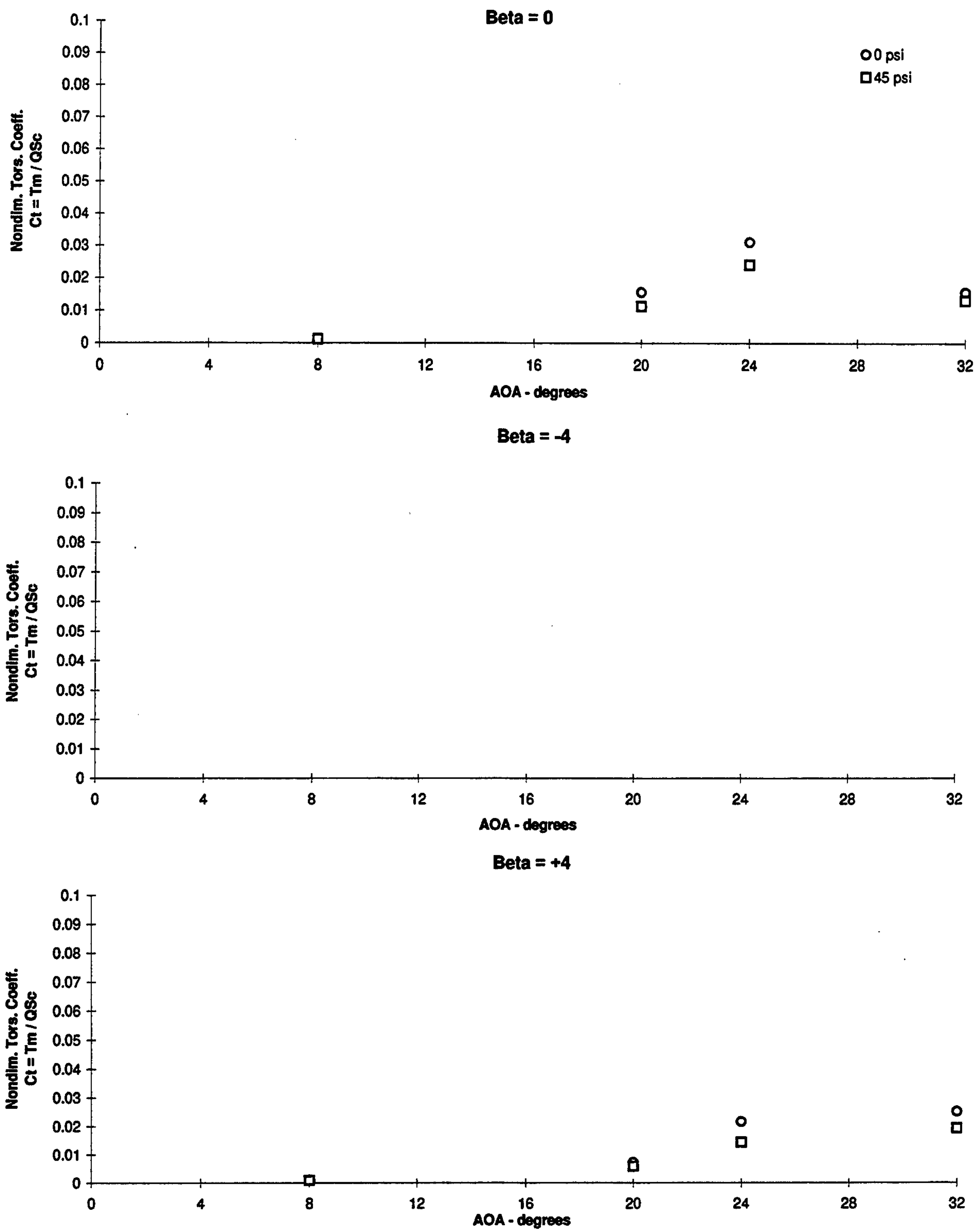

Figure 3.4.26 - Flex Tail Response vs Angle of Attack
Nondimensional Torsion, Q = 30 psf, PSD's (5-500) Hz, Wing Blowing Summary

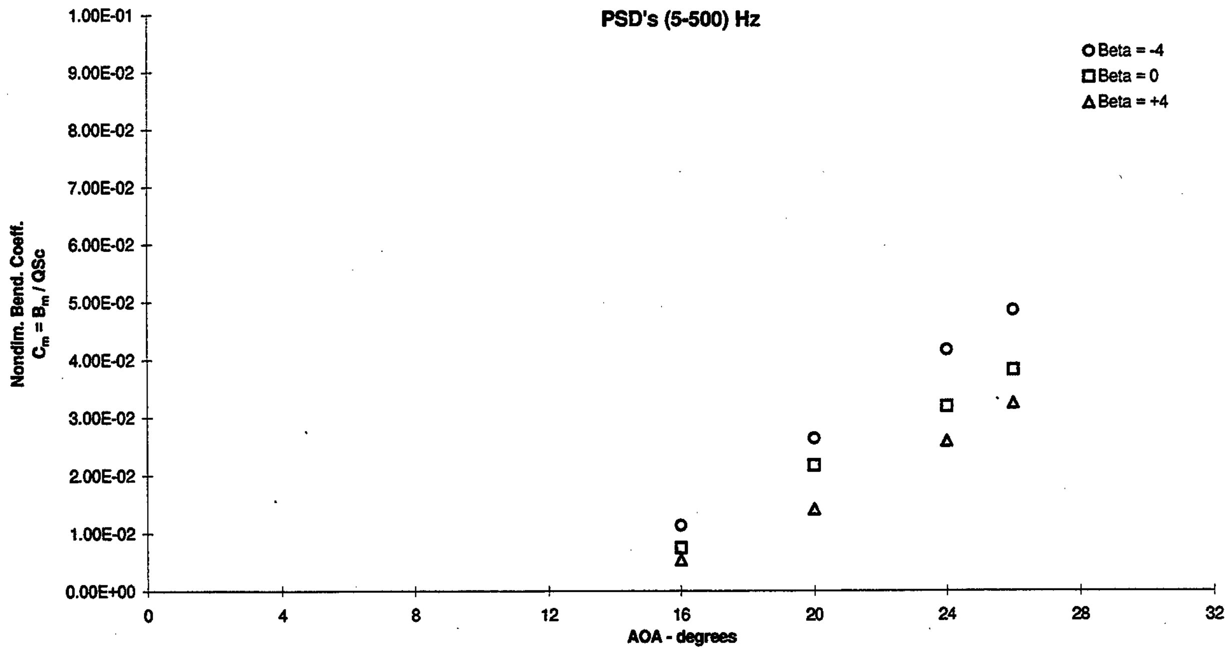

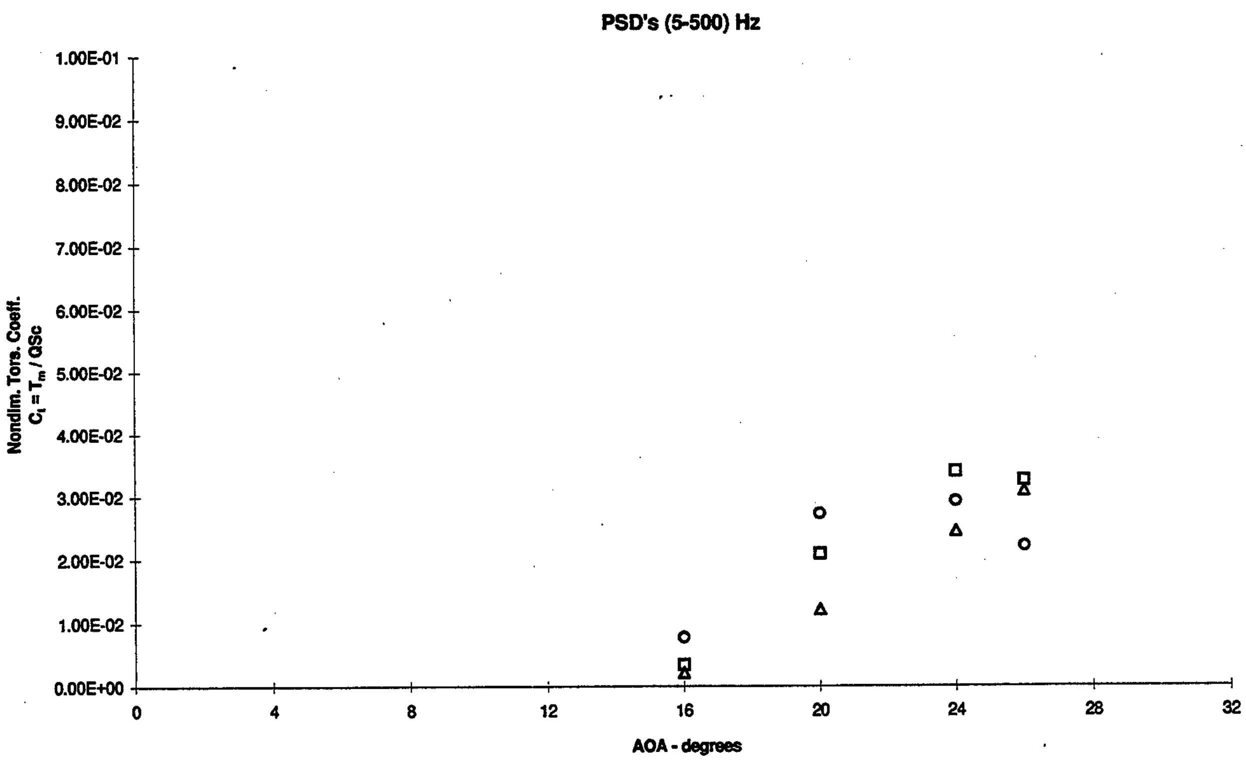

Figure 3.4.27 - Flex Tail Response vs Angle of Attack
Nondimensional Bending and Torsion, Q = 56 psf, Gun Blowing p = 65 psi

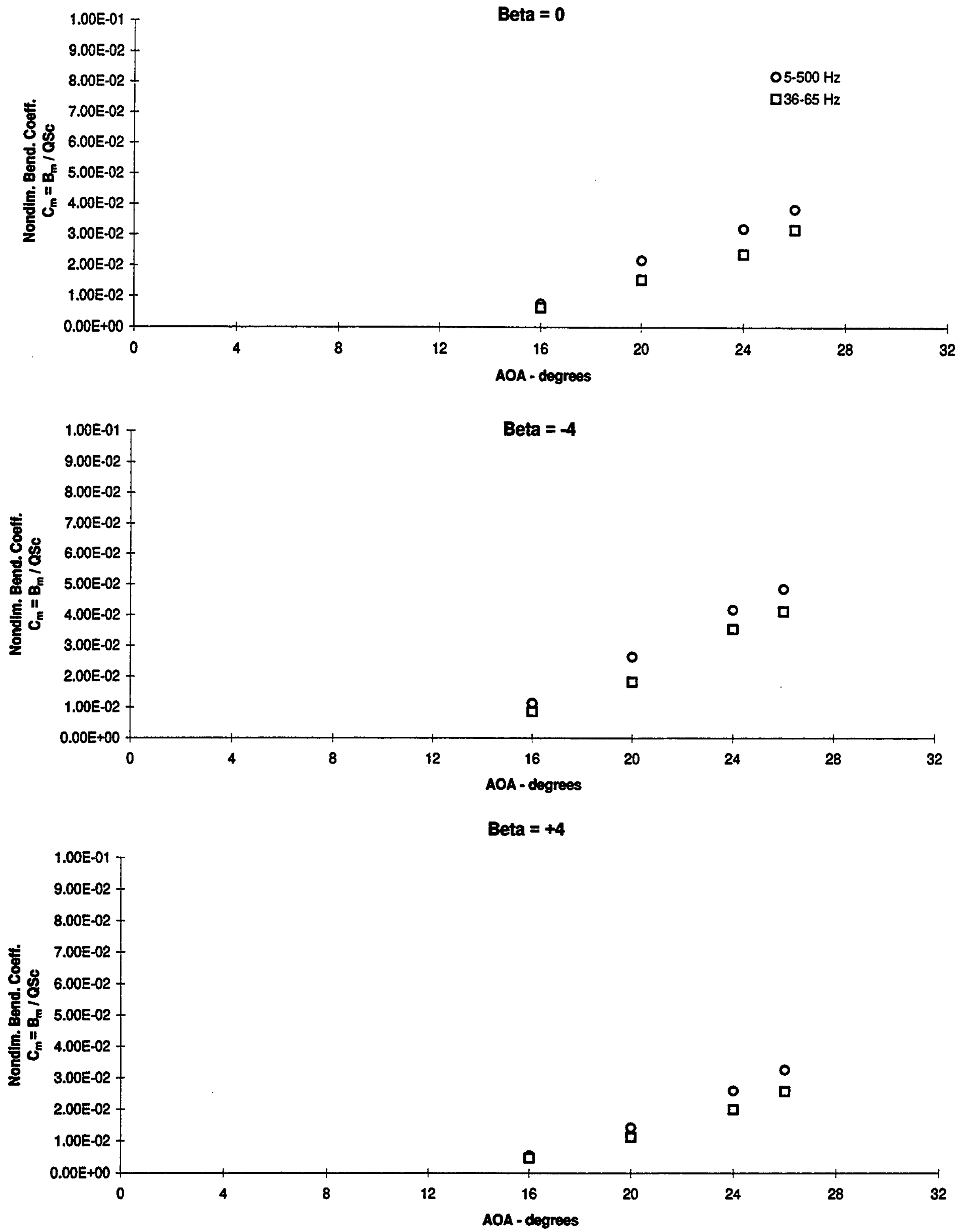

Figure 3.4.28 - Flex Tail Response vs Angle of Attack
Nondimensional Bending, Q = 56 psf, Gun Blowing Pressure = 65 psi

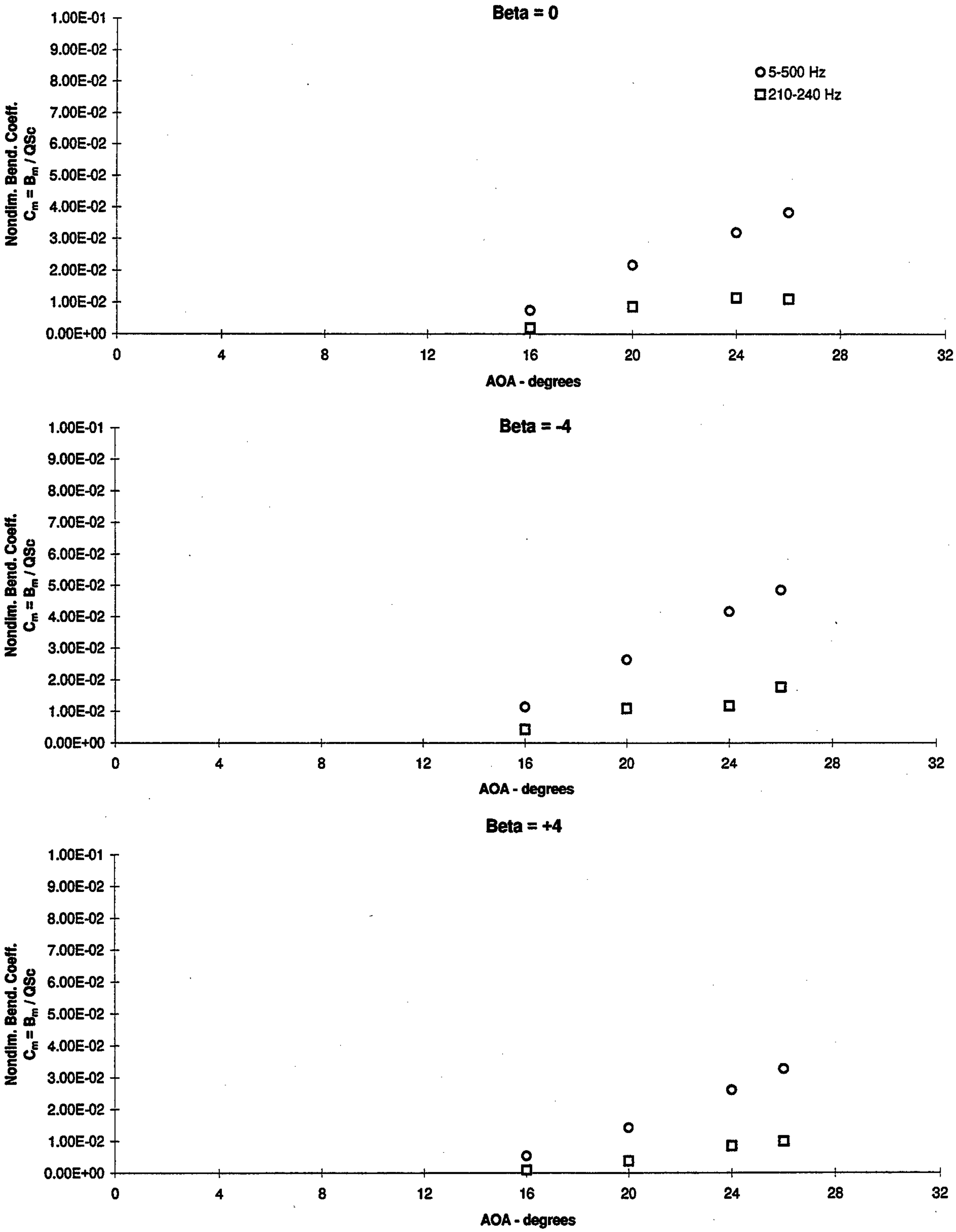

Figure 3.4.29 - Flex Tail Response vs Angle of Attack
Nondimensional Bending, Q = 56 psf, Gun Blowing Pressure = 65 psi

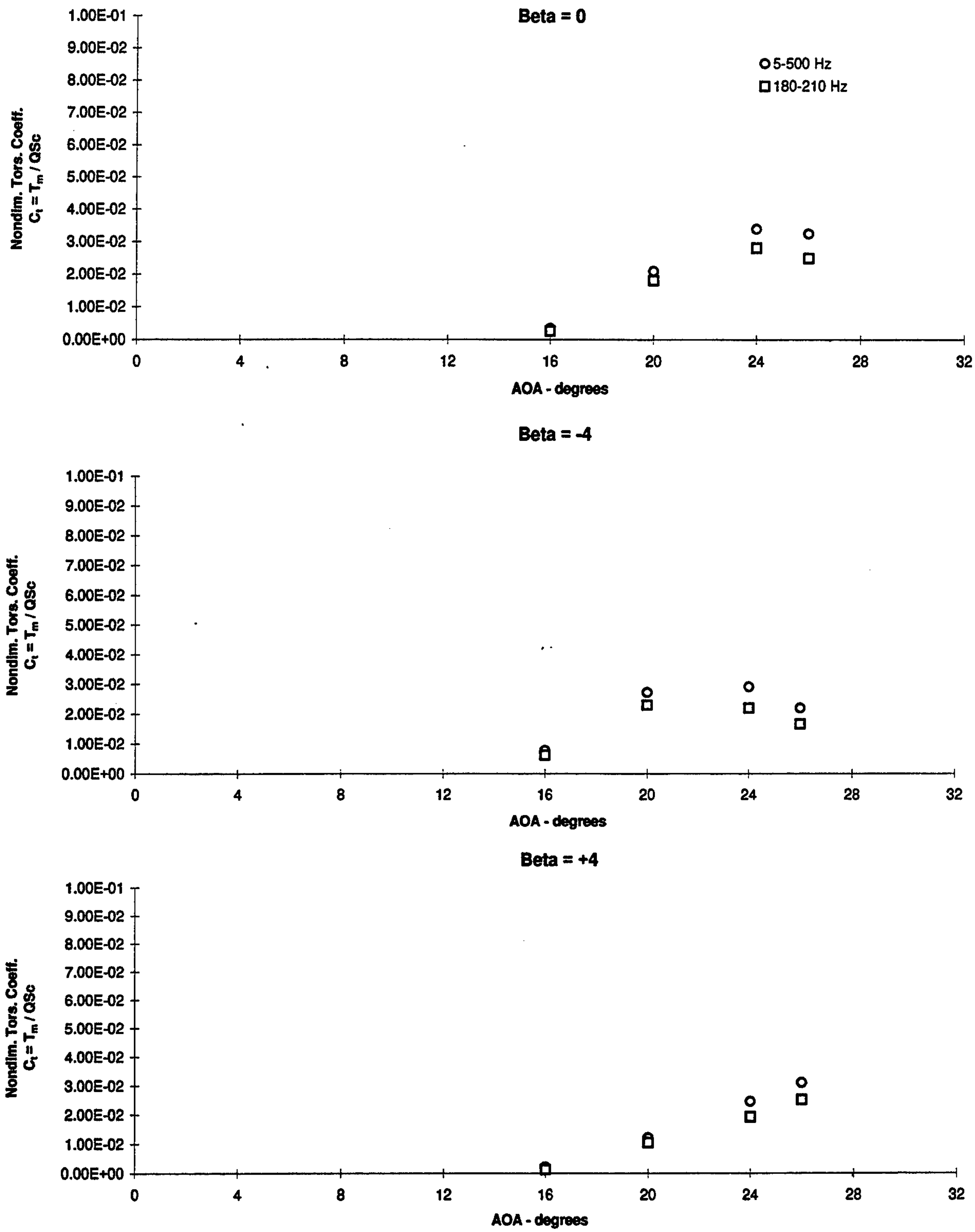

Figure 3.4.30 - Flex Tail Response vs Angle of Attack
Nondimensional Torsion, Q = 56 psf, Gun Blowing p = 65 psi

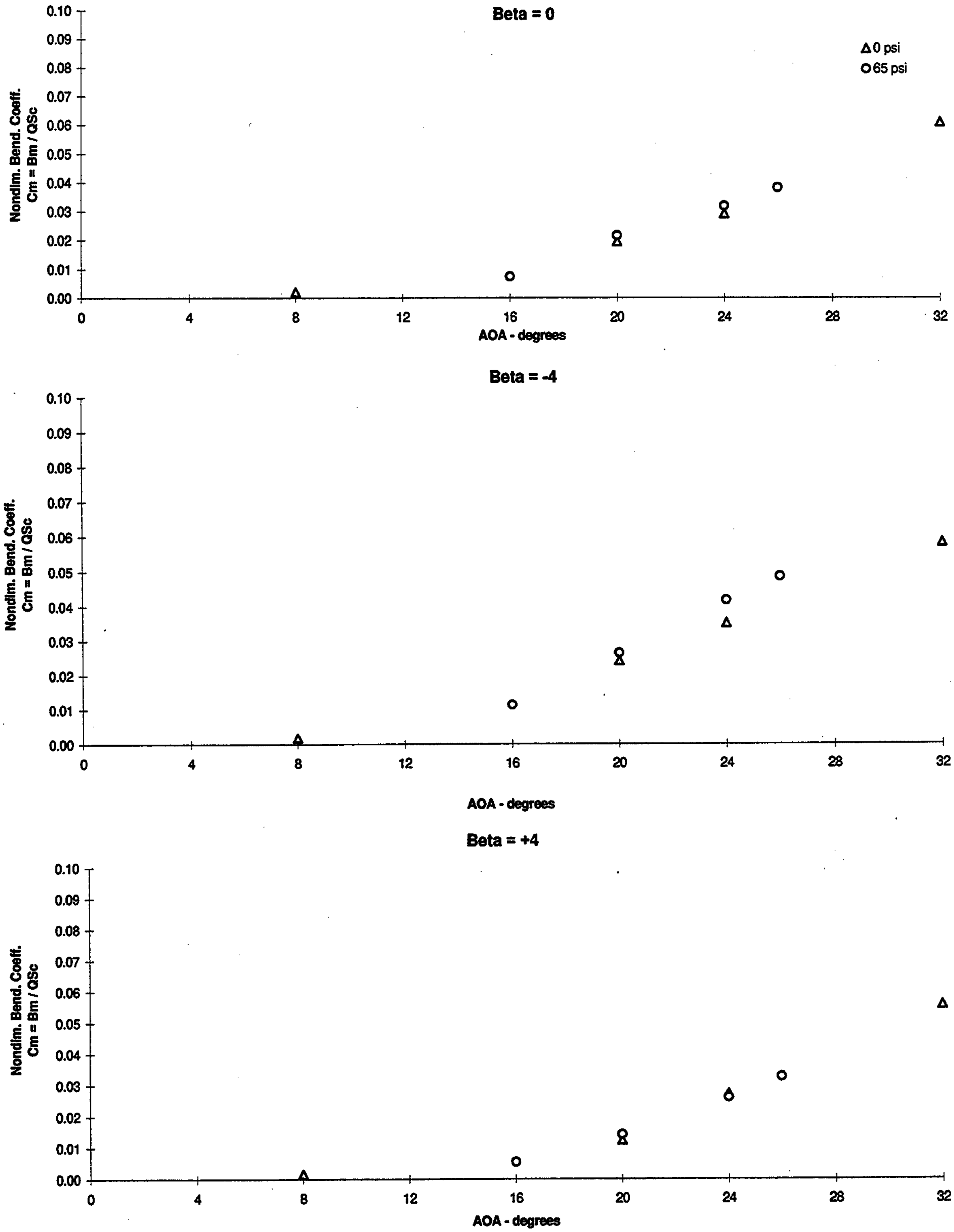

Figure 3.4.31 - Flex Tail Response vs Angle of Attack
Nondimensional Bending, Q = 56 psf, PSD's (5-500) Hz, Gun Blowing

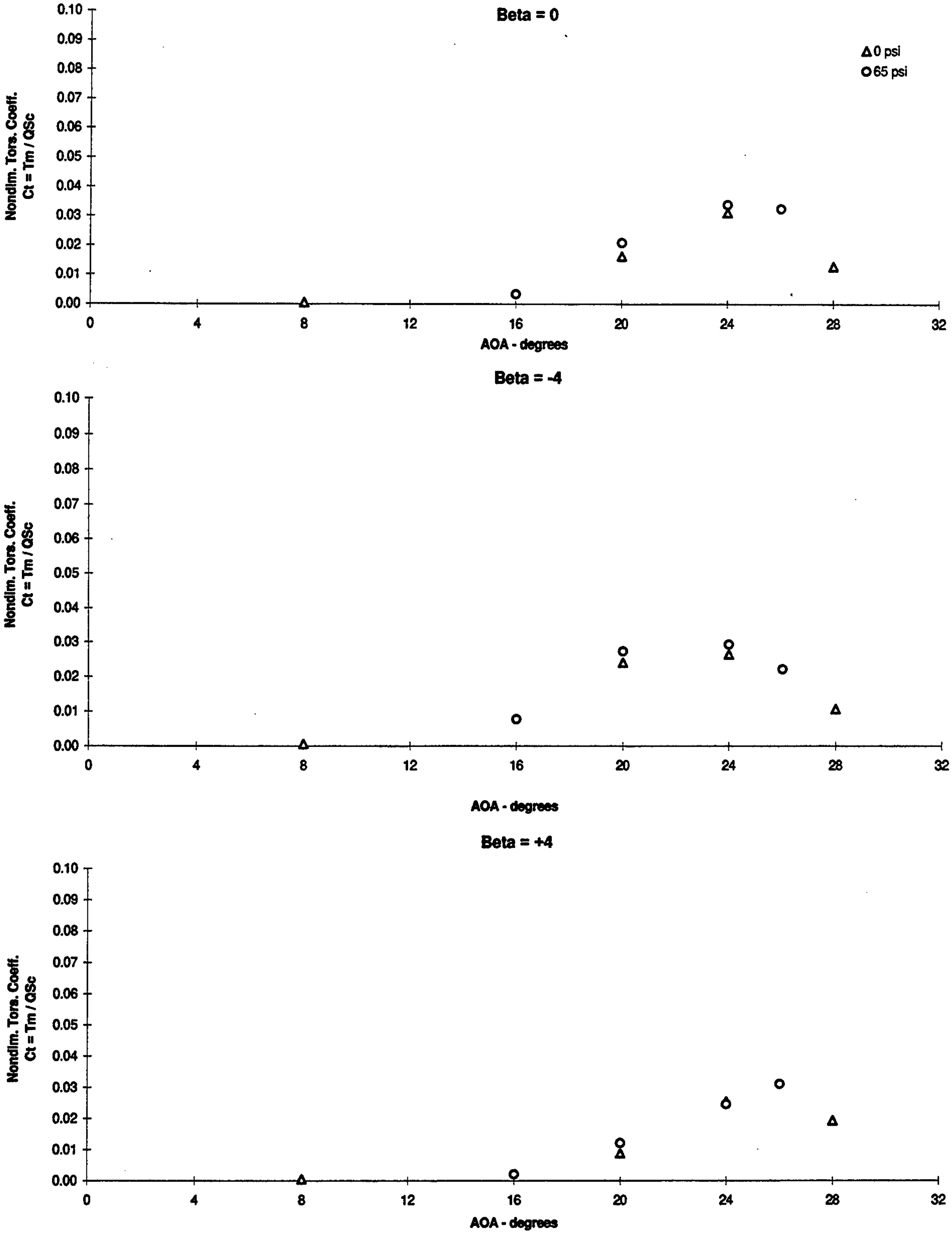

Figure 3.4.32 - Flex Tail Response vs Angle of Attack
Nondimensional Torsion, Q = 56 psf, PSD's (5-500) Hz, Gun Blowing

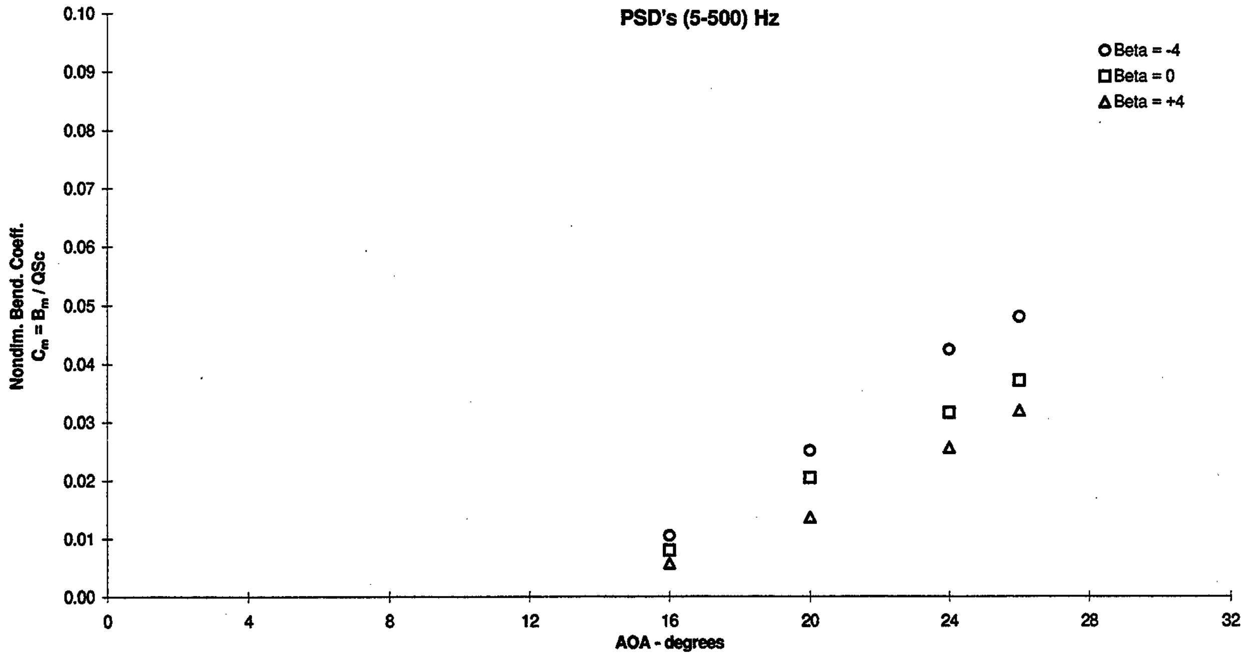

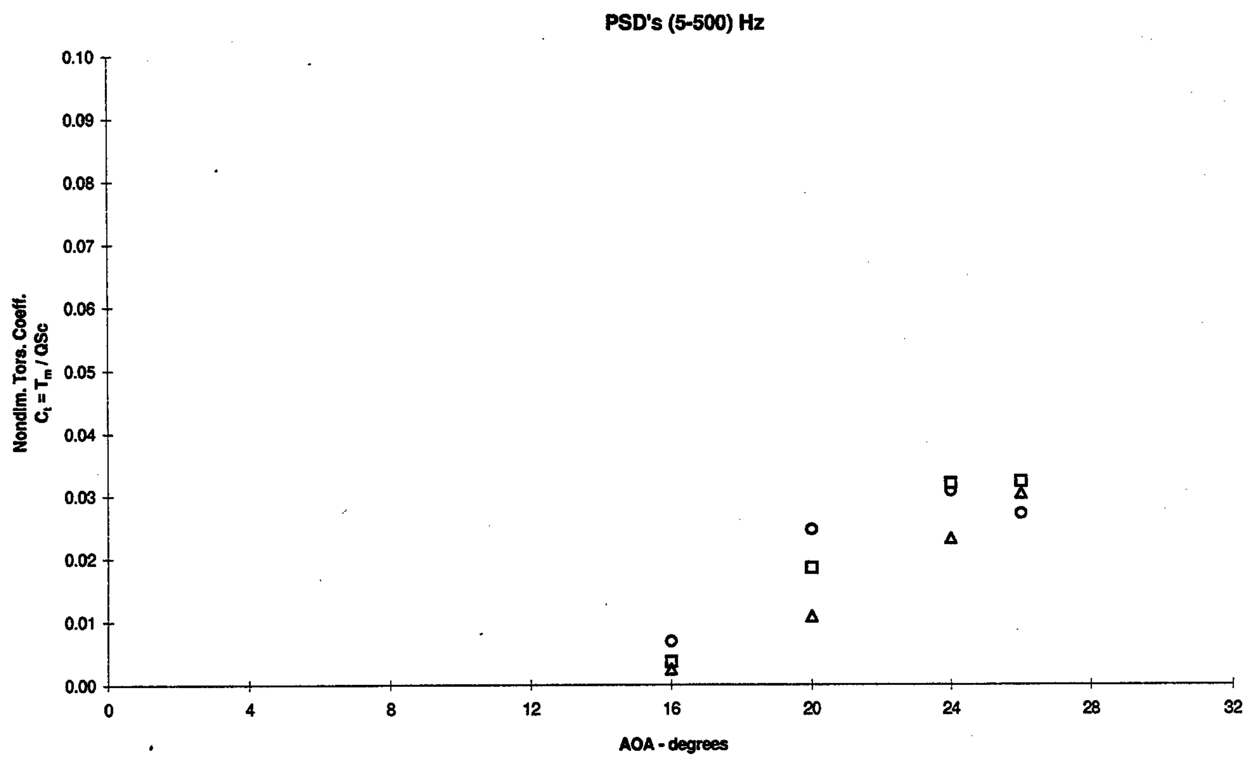

Figure 3.4.33 - Flex Tail Response vs Angle of Attack
Nondimensional Bending and Torsion, Q = 56 psf, Gun and Wing L.E. Blowing p = 65 psi

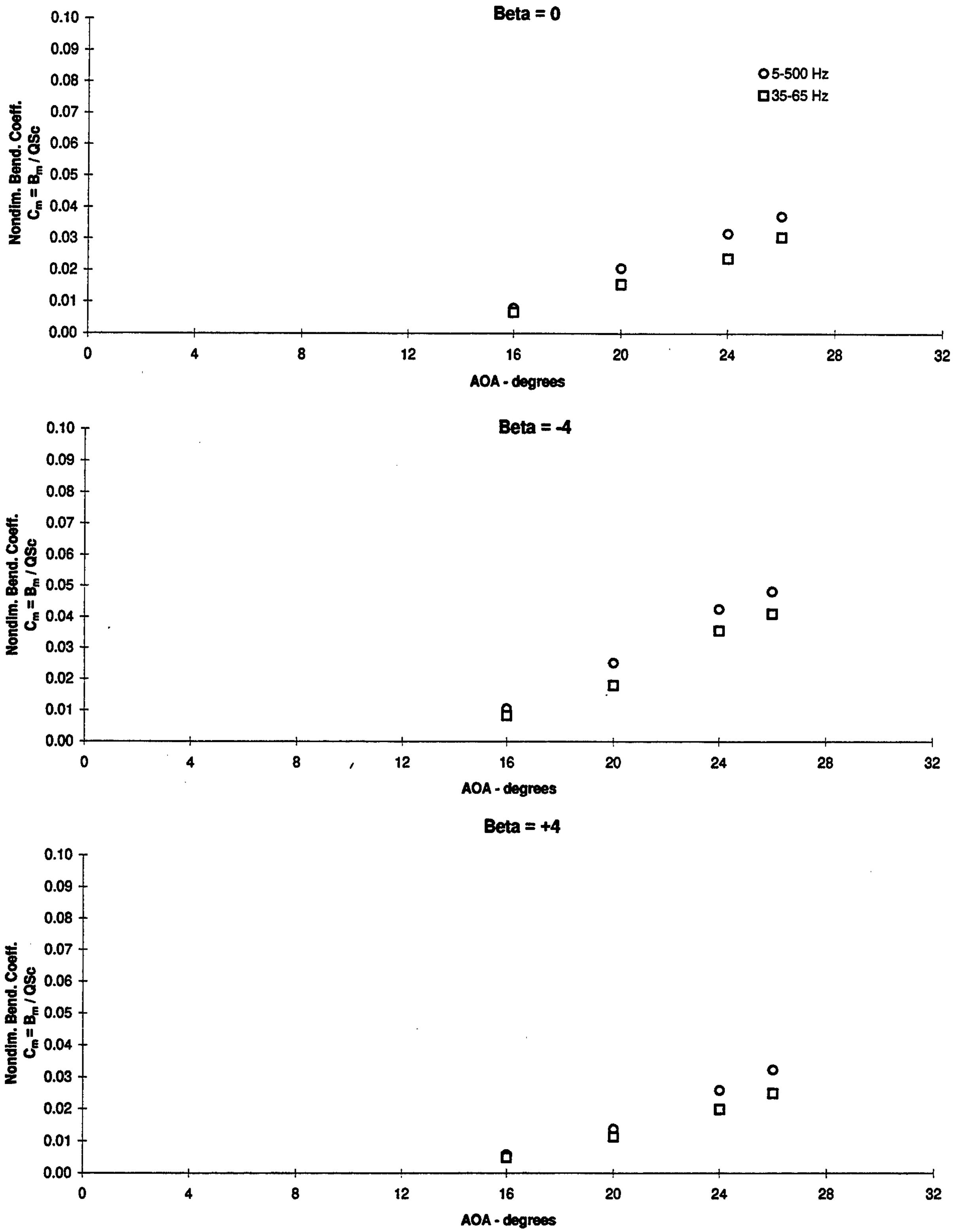

Figure 3.4.34 - Flex Tail Response vs Angle of Attack
Nondimensional Bending, Q = 56 psf, Gun and Wing L.E. Blowing p = 65 psi

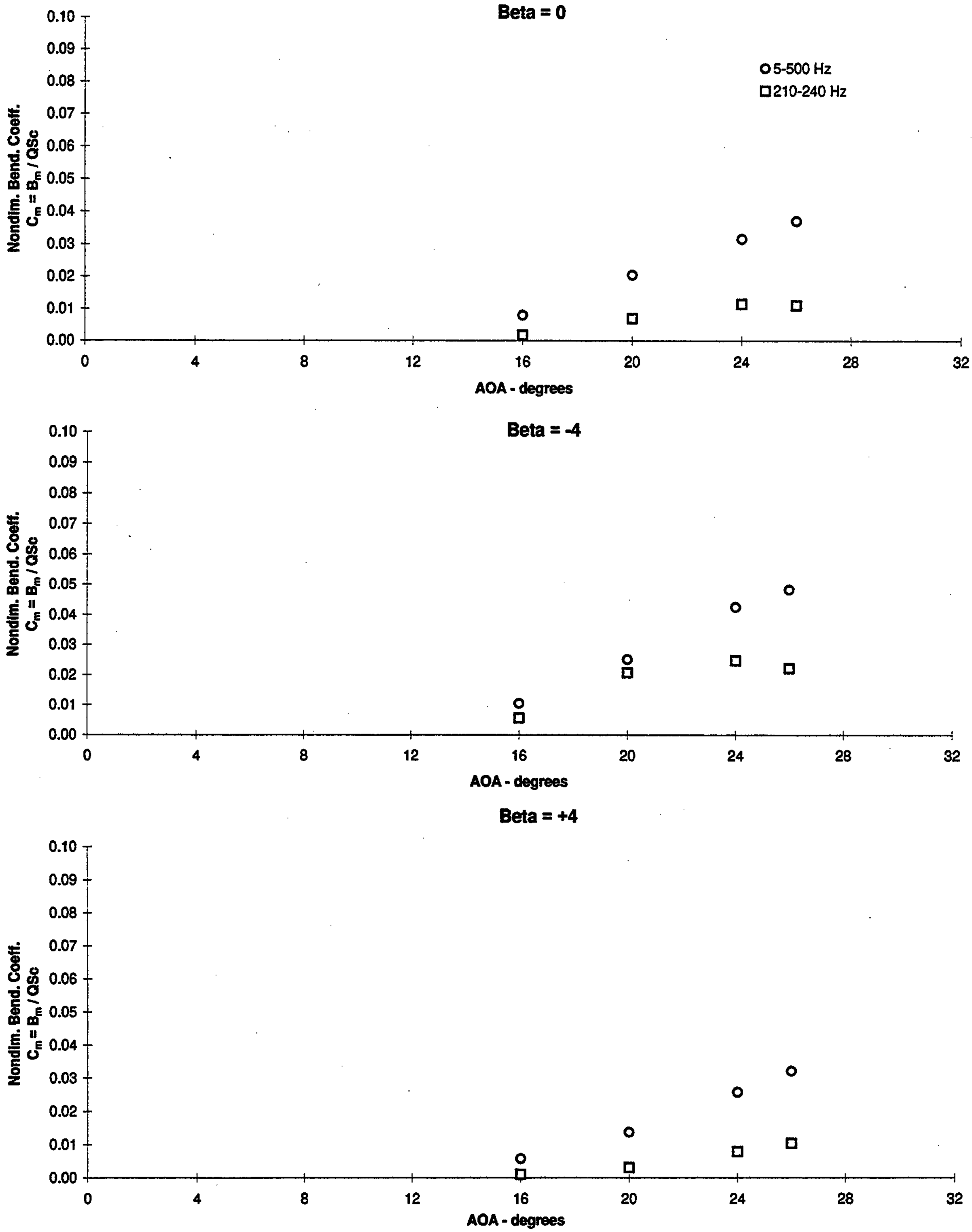

Figure 3.4.35 - Flex Tail Response vs Angle of Attack
Nondimensional Bending, Q = 56 psf, Gun and Wing L.E. Blowing p = 65 psi

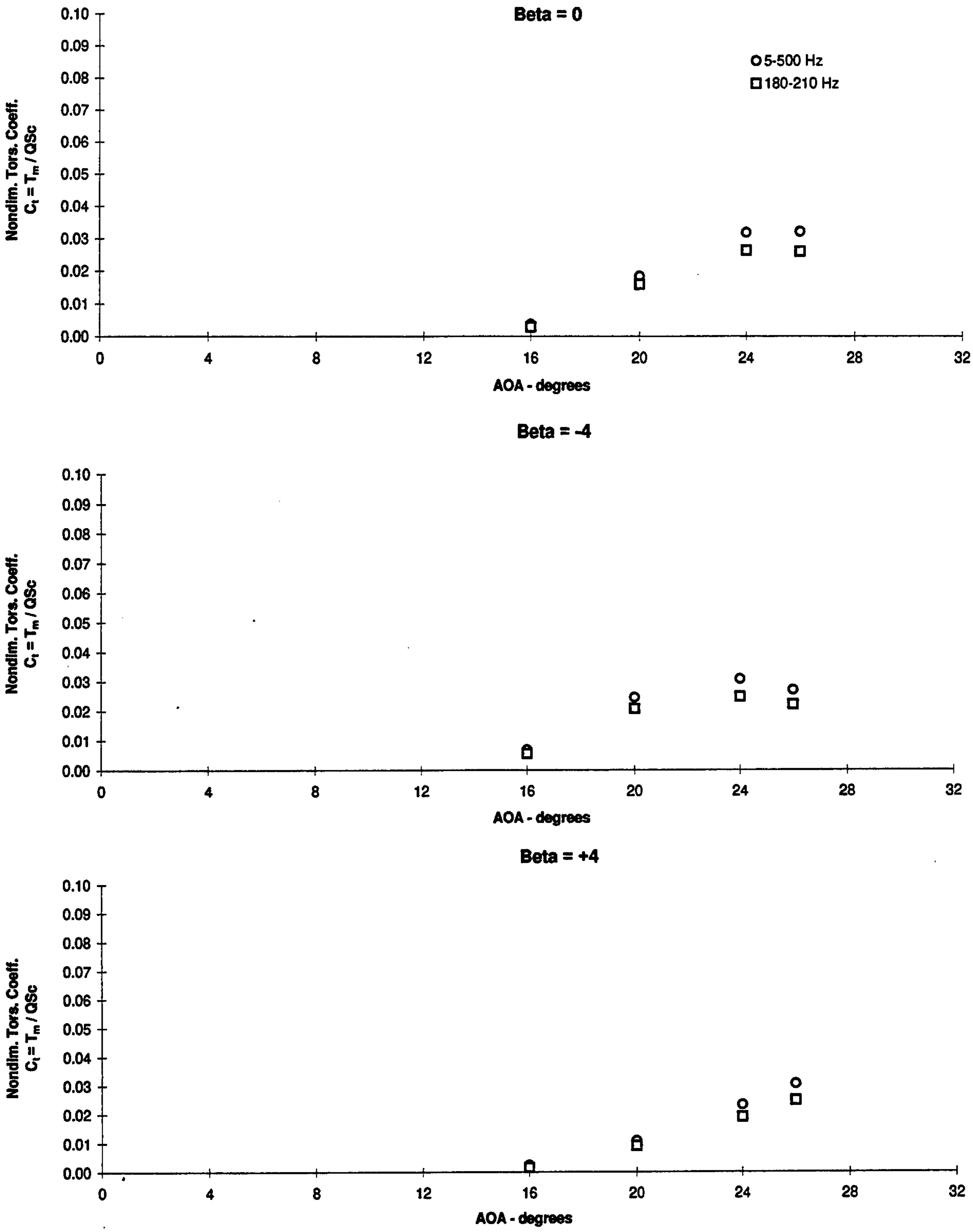

Figure 3.4.36 - Flex Tail Response vs Angle of Attack
Nondimensional Torsion, Q = 56 psf, Gun and Wing L.E. Blowing p = 65 psi

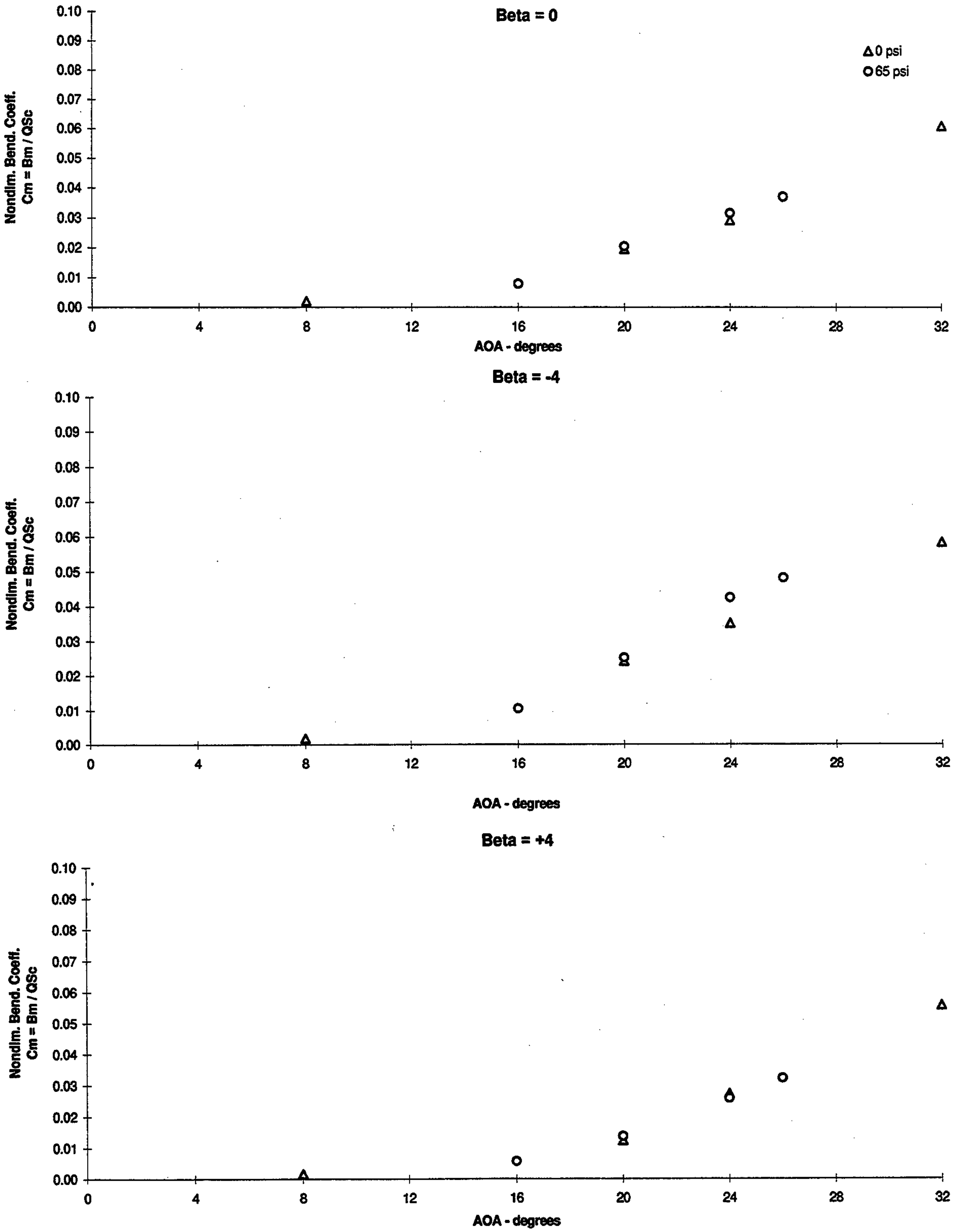

Figure 3.4.37 - Flex Tail Response vs Angle of Attack
Nondimensional Bending, Q = 56 psf, PSD's (5-500) Hz
Gun and Wing LE Blowing Summary

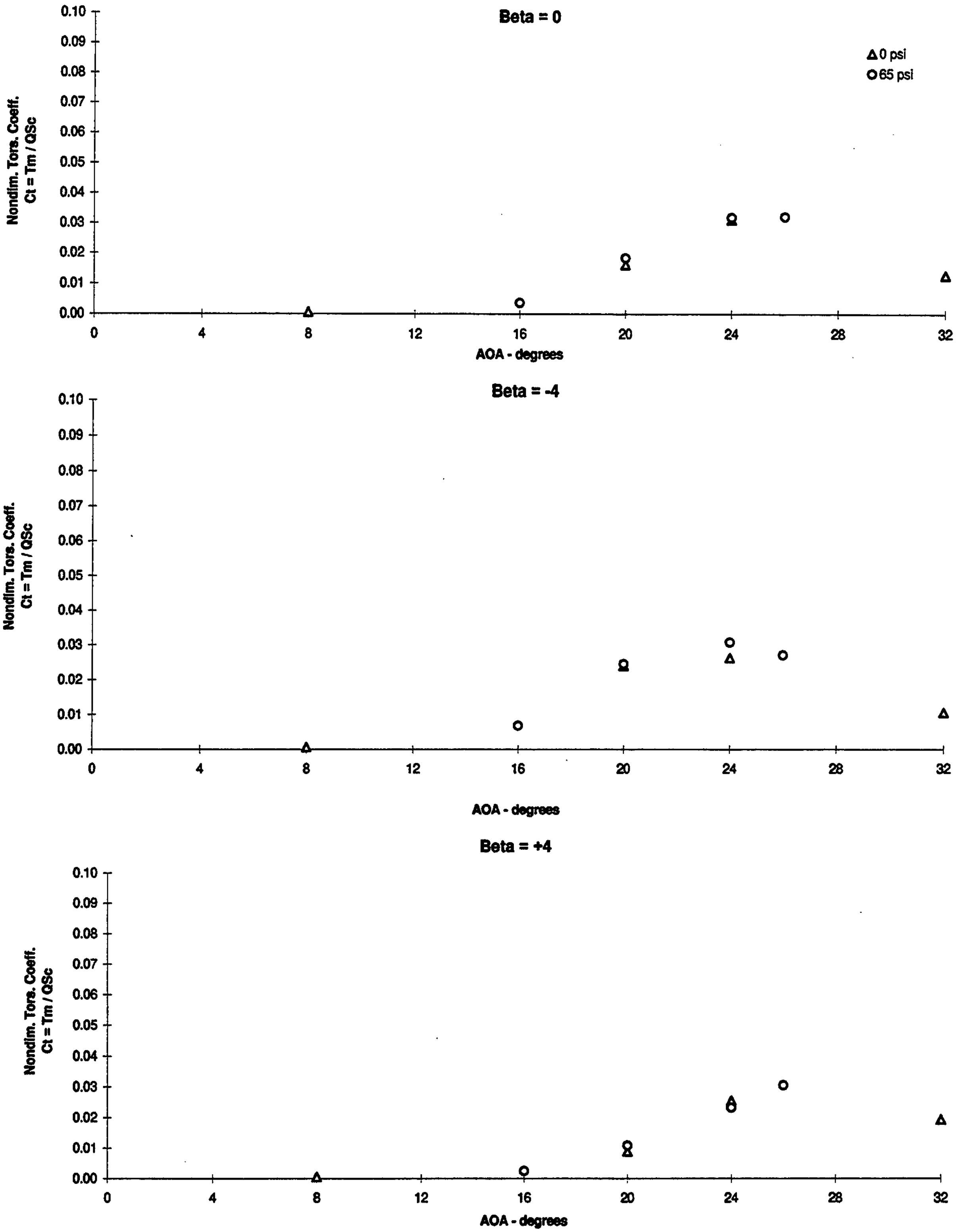

Figure 3.4.38 - Flex Tail Response vs Angle of Attack
Nondimensional Torsion, Q = 56 psf, PSD's (5-500) Hz
Gun and Wing LE Blowing Summary

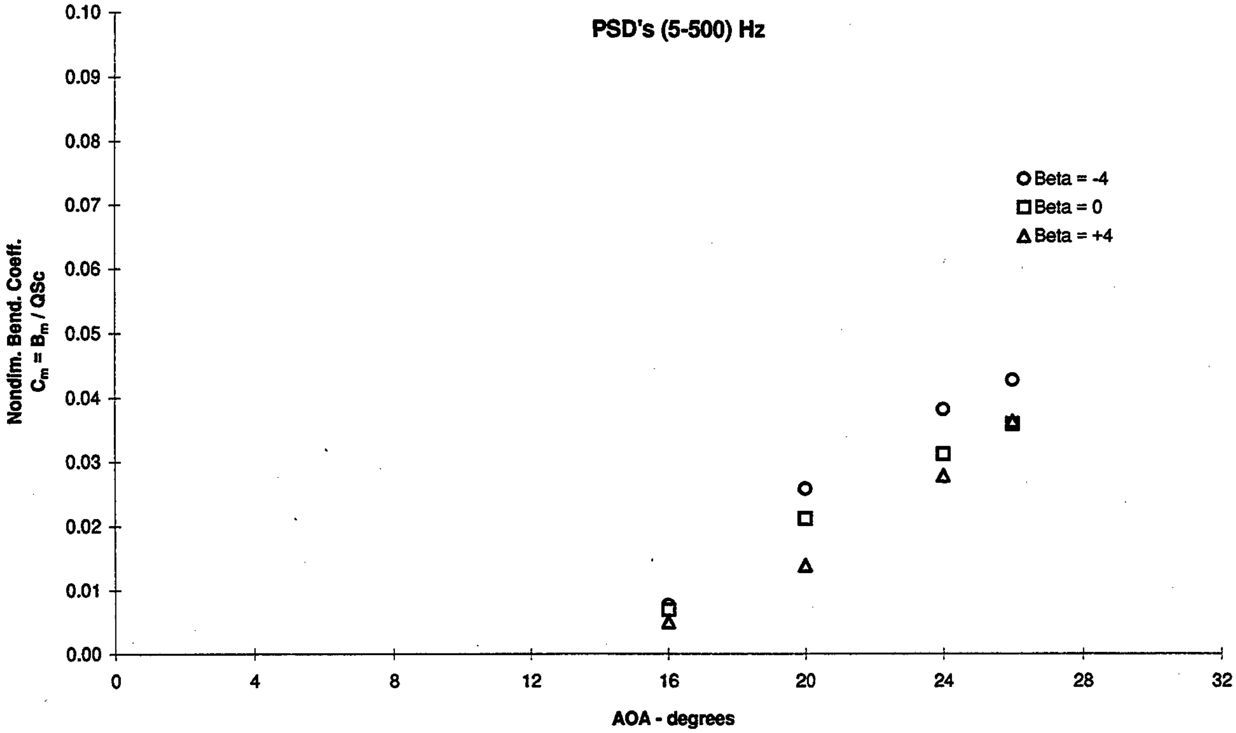

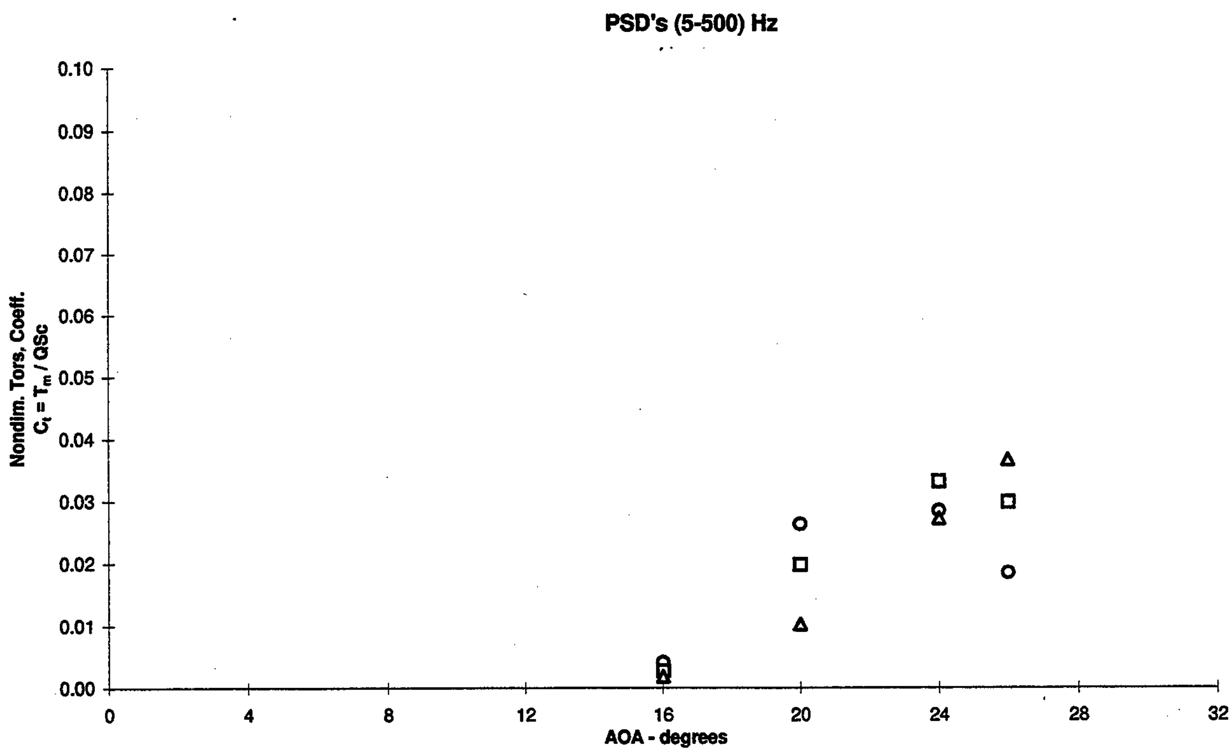

Figure 3.4.39 - Flex Tail Response vs Angle of Attack
Nondimensional Bending and Torsion, Q = 56 psf, Nose Blowing p = 87 psi

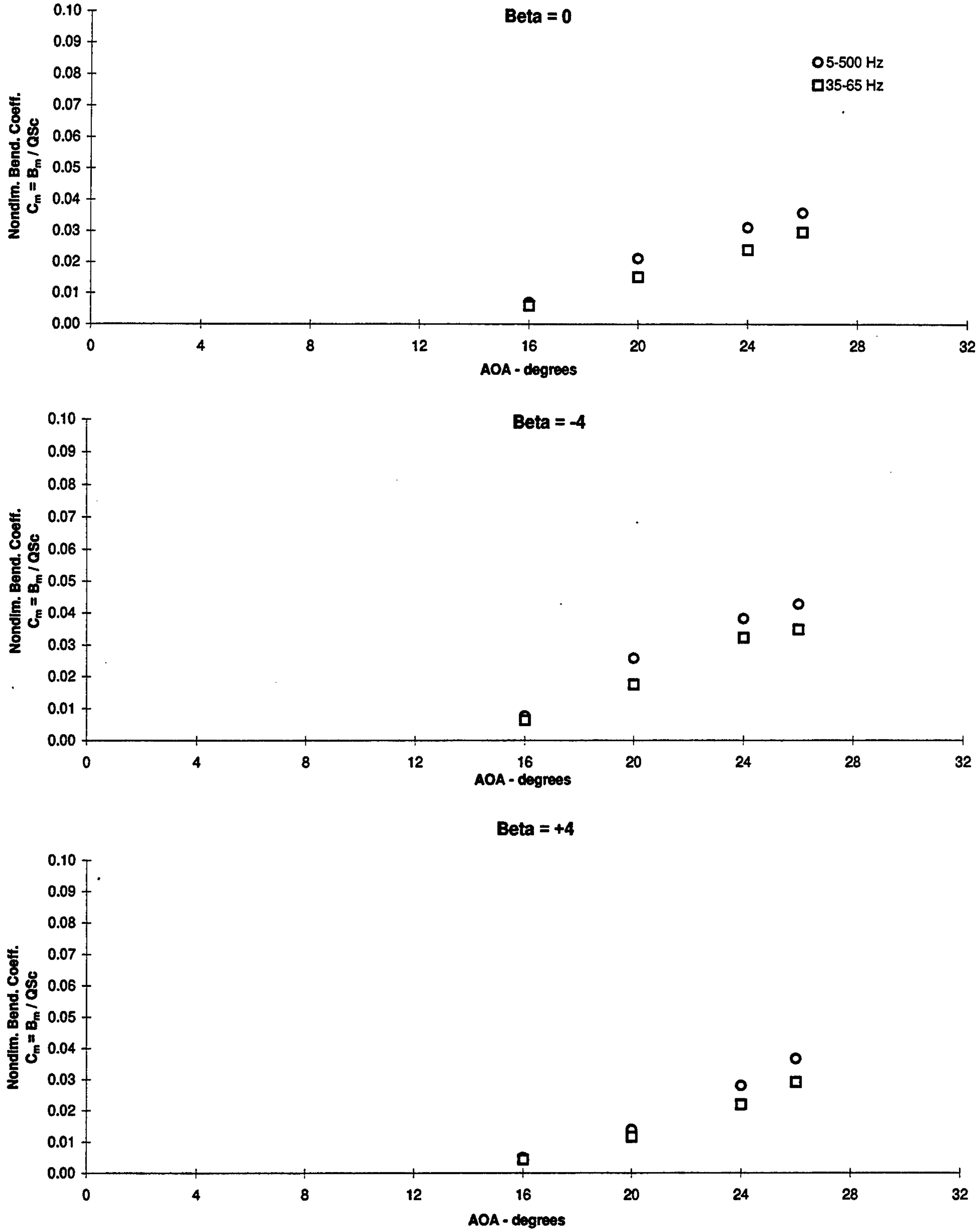

Figure 3.4.40 - Flex Tail Response vs Angle of Attack
Nondimensional Bending, Q = 56 psf, Nose Blowing p = 87 psi

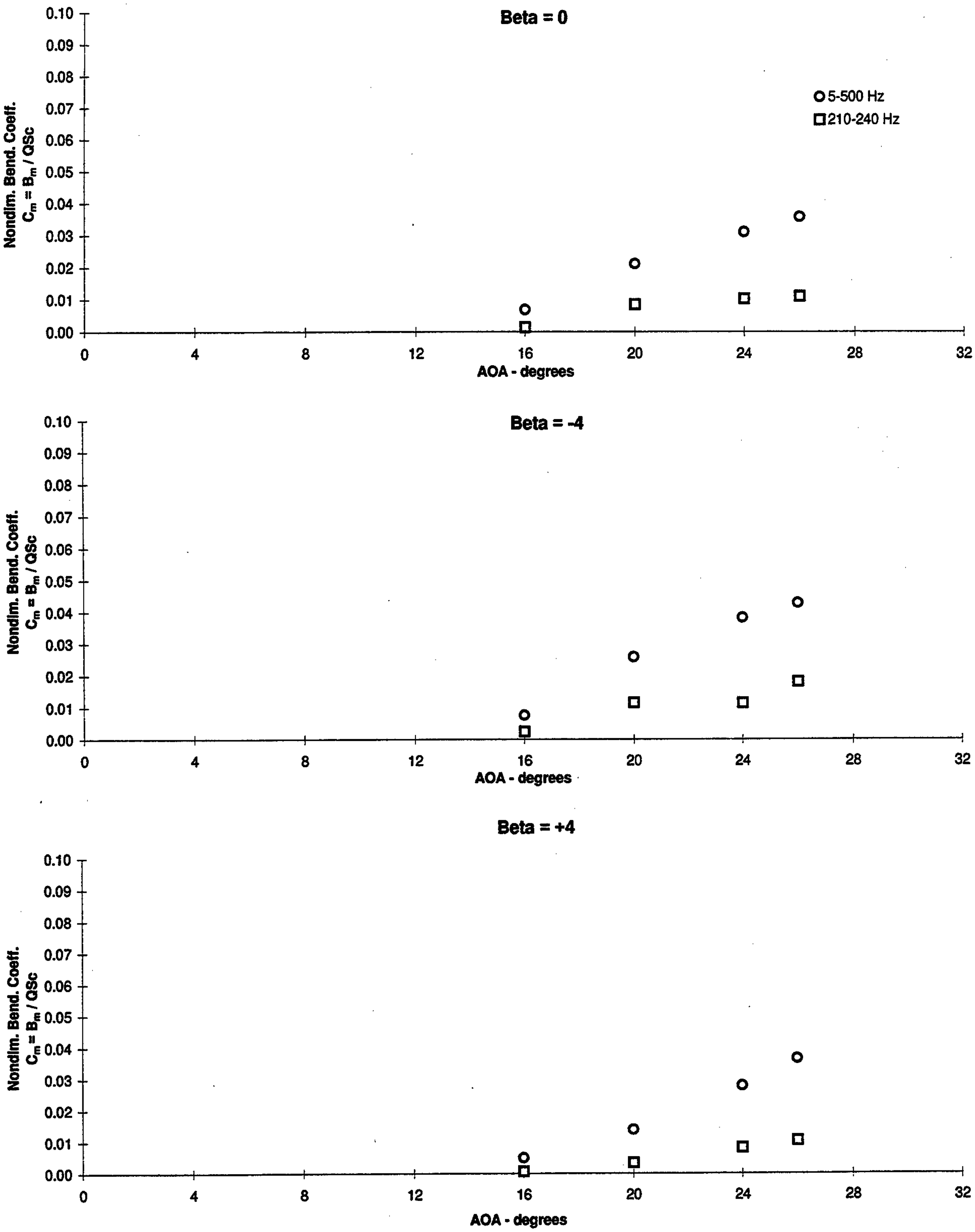

Figure 3.4.41 - Flex Tail Response vs Angle of Attack
Nondimensional Bending, Q = 56 psf, Nose Blowing p = 87 psi

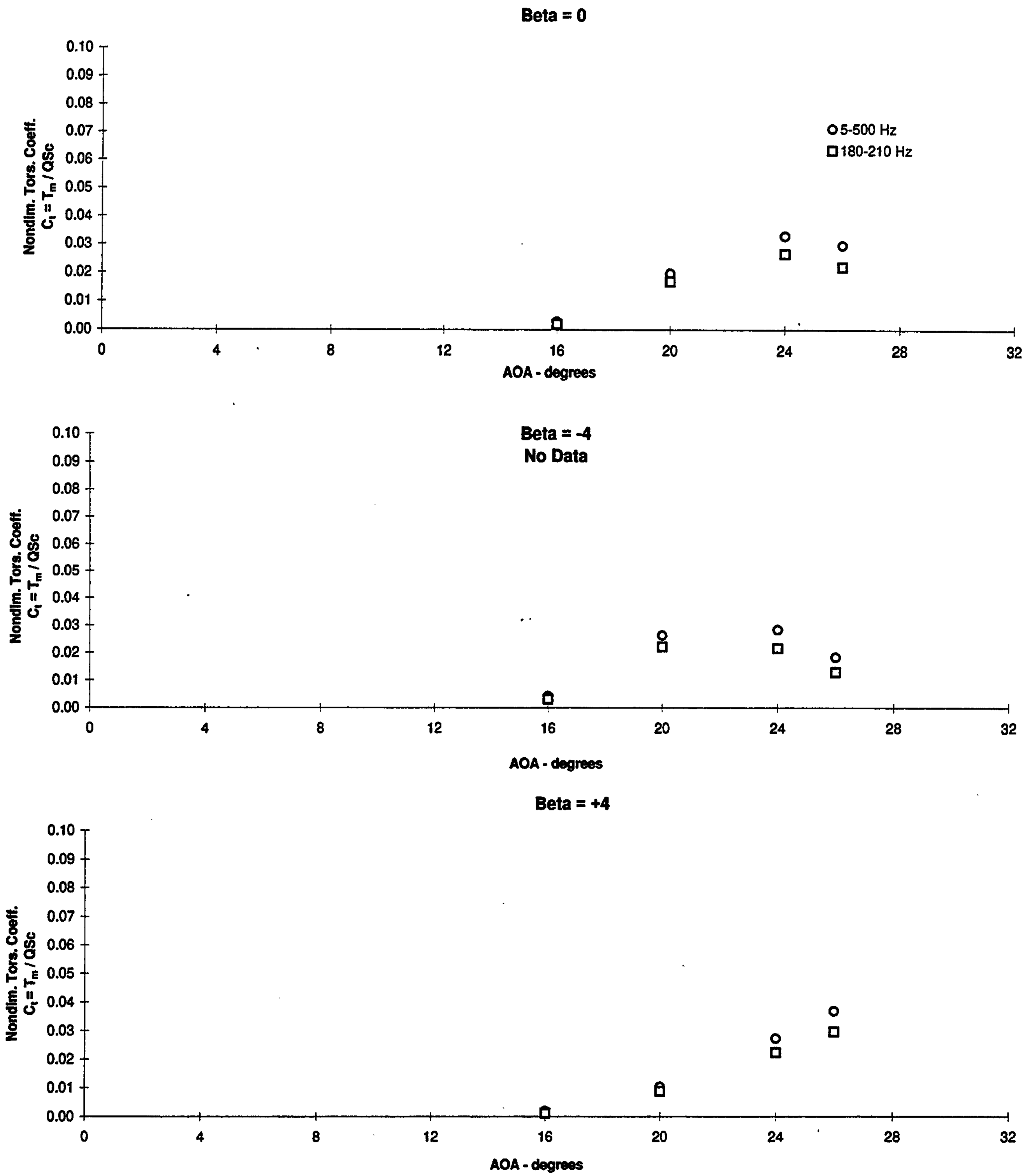

Figure 3.4.42 - Flex Tail Response vs Angle of Attack
Nondimensional Torsion, Q = 56 psf, Nose Blowing p = 87 psi

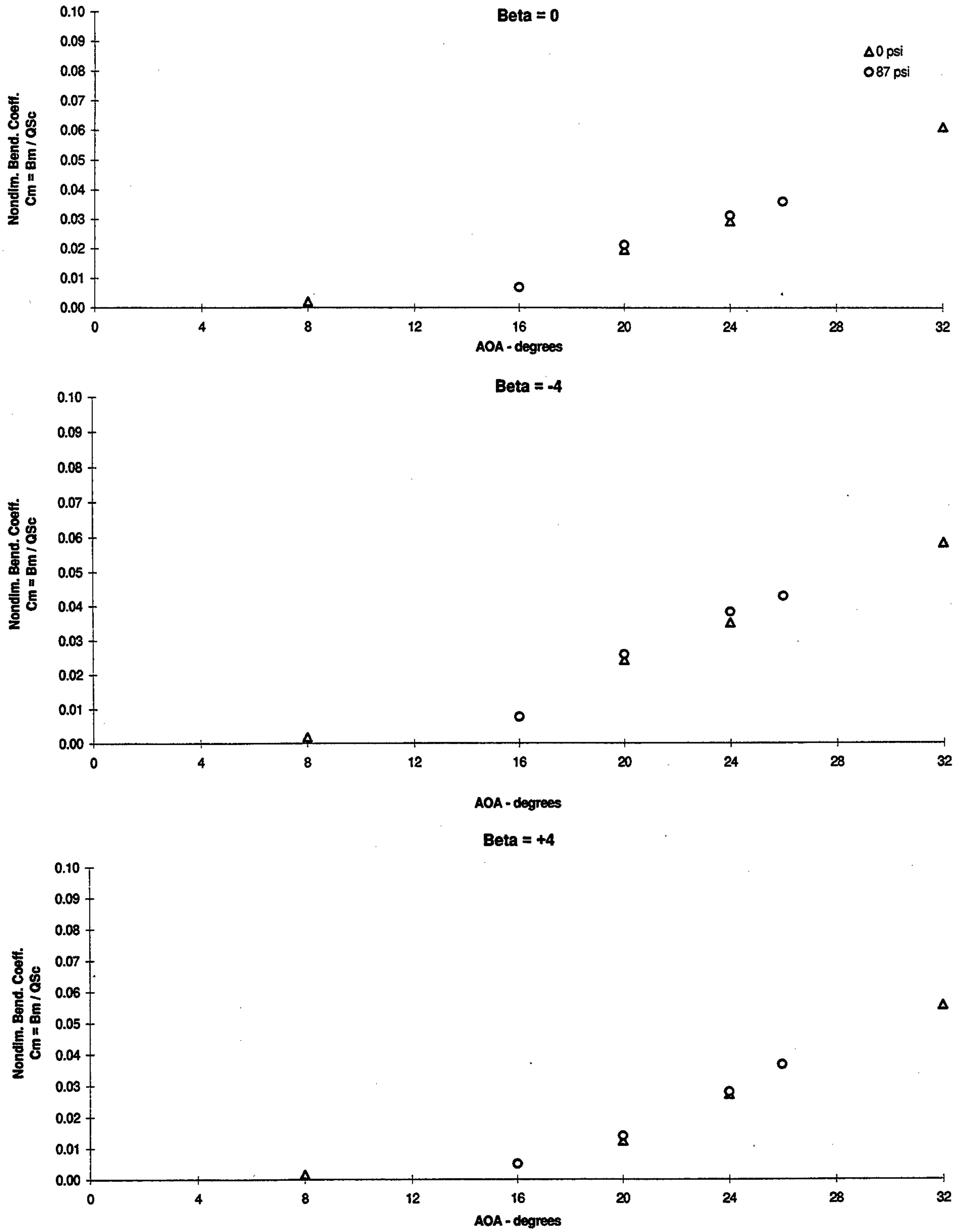

Figure 3.4.43 - Flex Tail Response vs Angle of Attack
Nondimensional Bending, Q = 56 psf, PSD's (5-500) Hz, Nose Blowing Summary

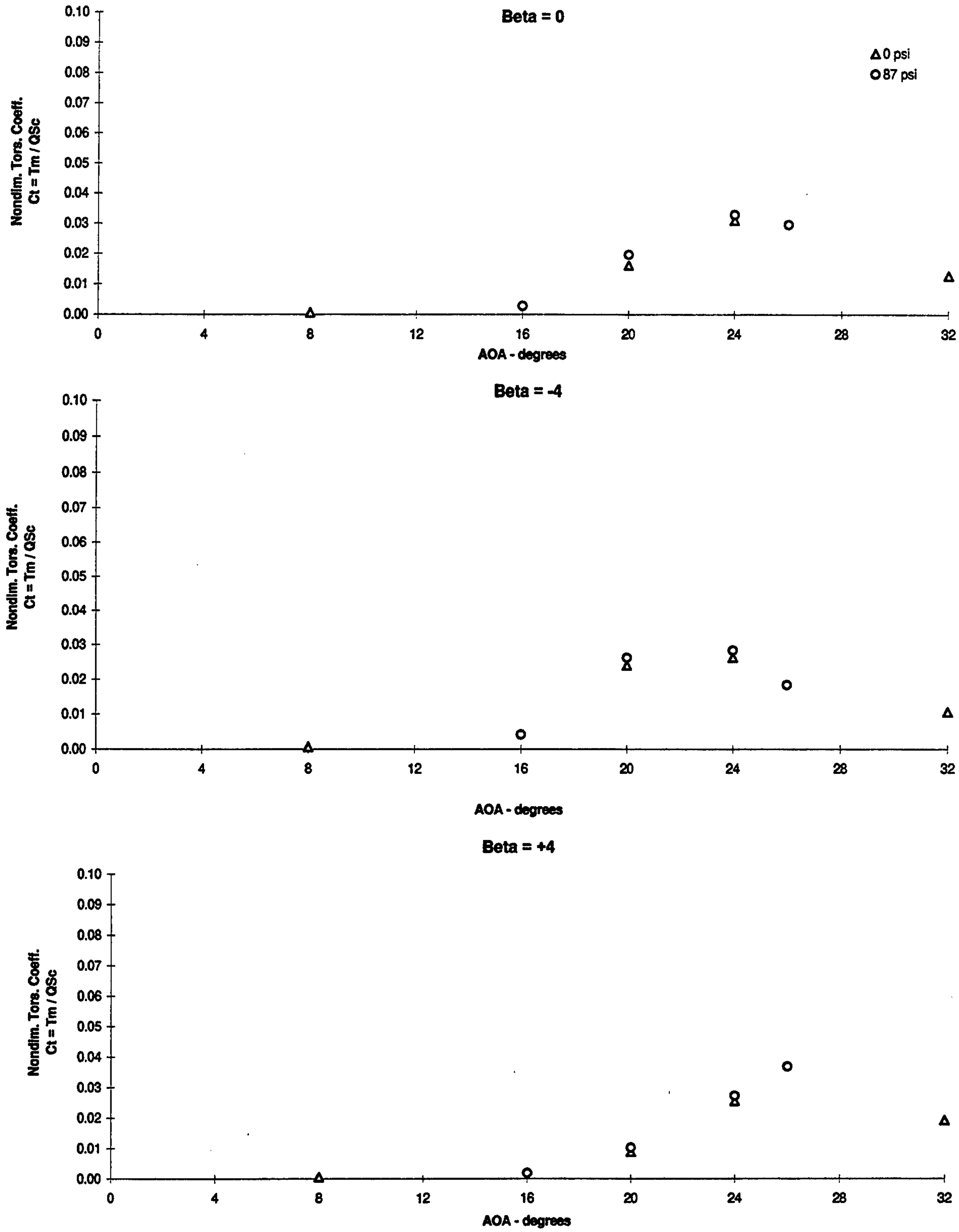

Figure 3.4.44 - Flex Tail Response vs Angle of Attack
Nondimensional Torsion, Q = 56 psf, PSD's (5-500) Hz, Nose Blowing Summary

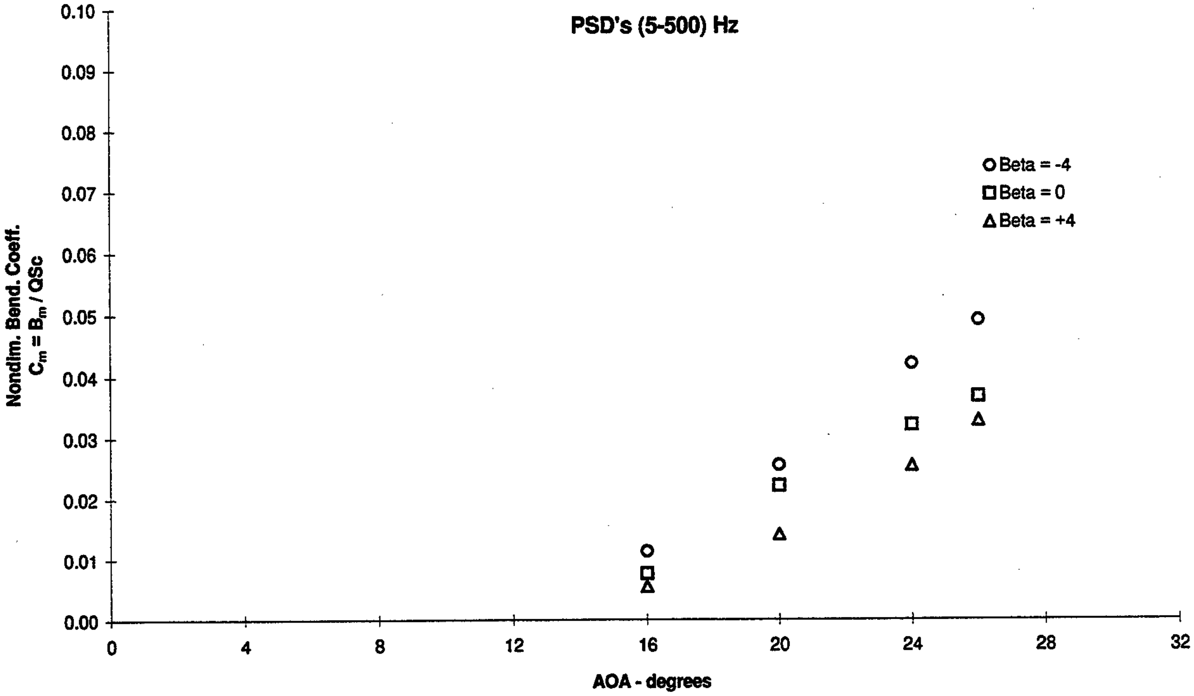

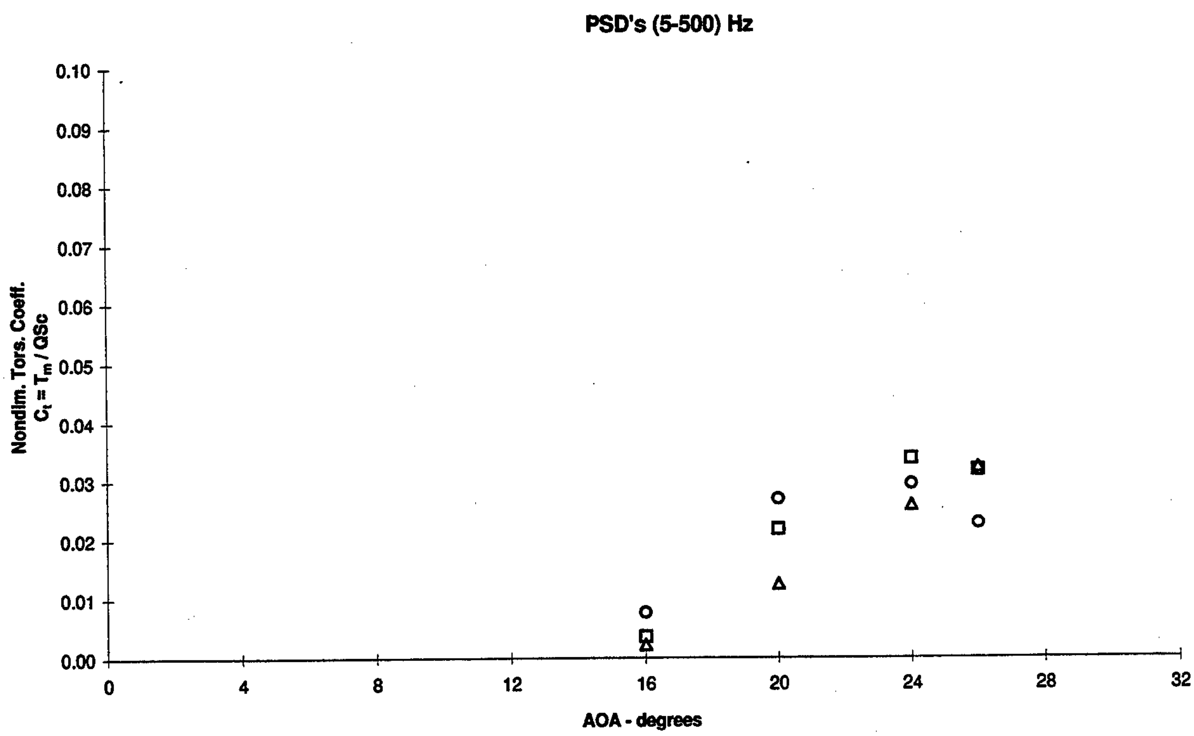

Figure 3.4.45 - Flex Tail Response vs Angle of Attack
Nondimensional Bending and Torsion, Q = 56 psf
Nose Blowing p = 87 psi, Gun p = 65 psi

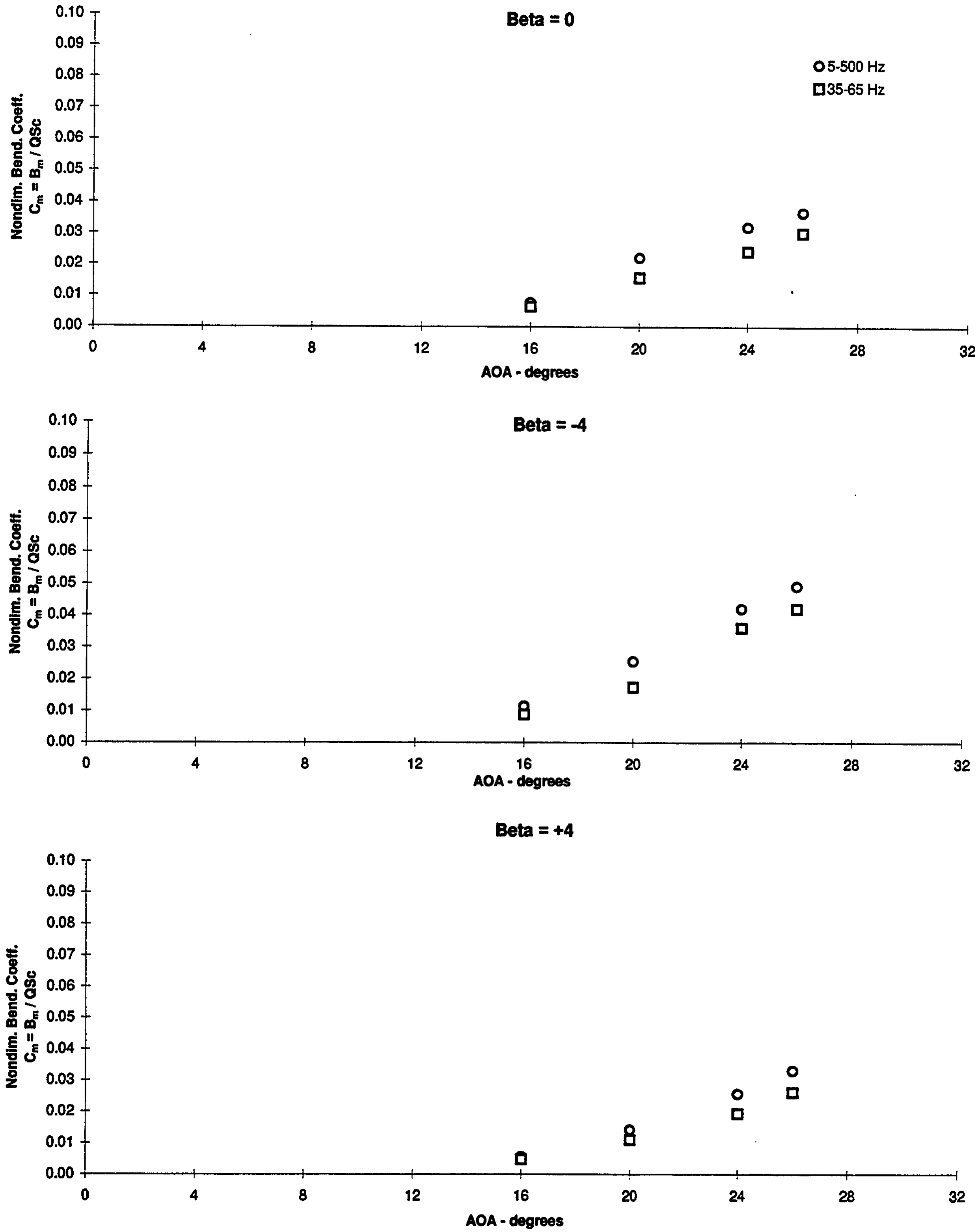

Figure 3.4.46 - Flex Tail Response vs Angle of Attack
Nondimensional Bending, Q = 56 psf
Nose Blowing p = 87 psi, Gun p = 65 psi

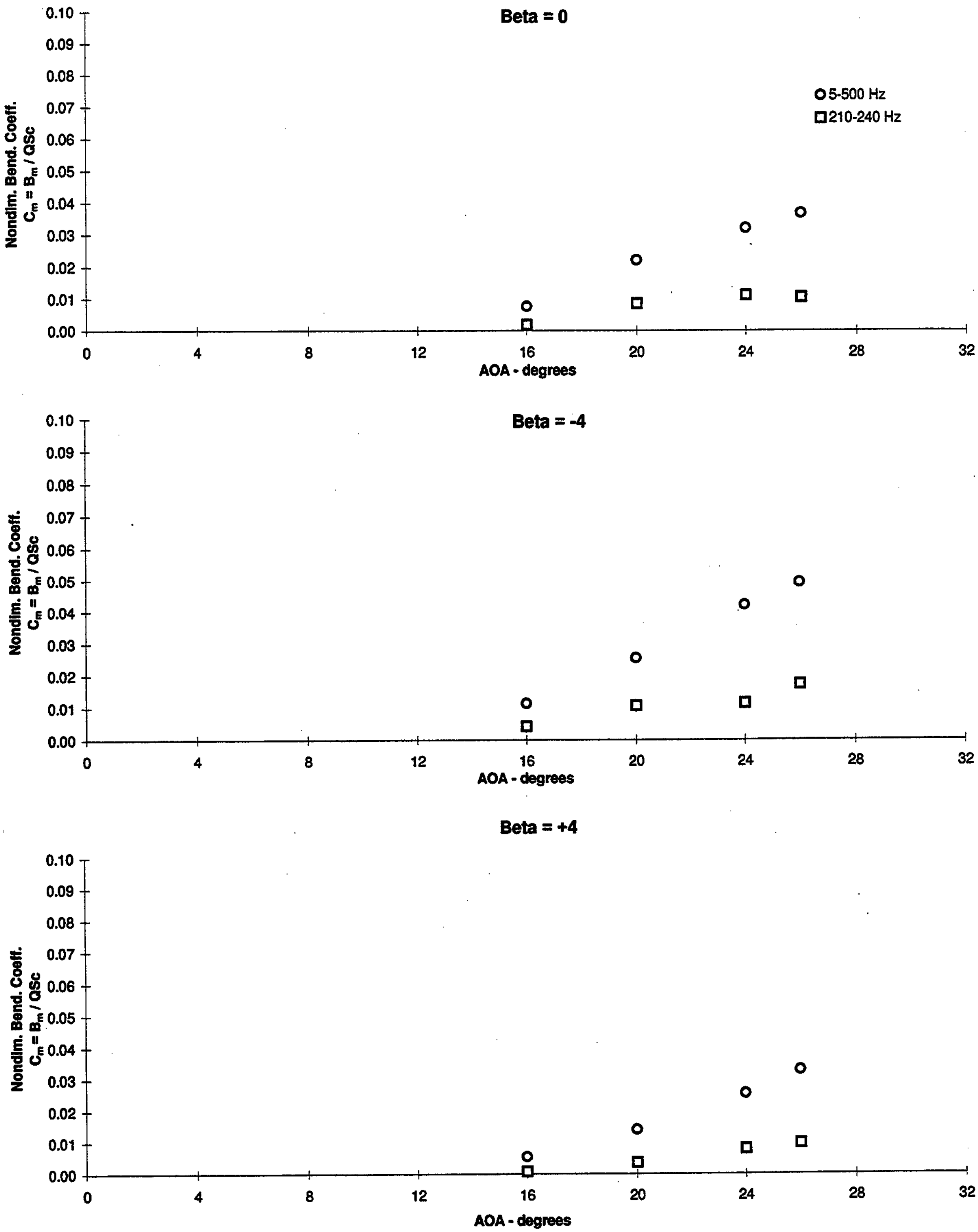

Figure 3.4.47 - Flex Tail Response vs Angle of Attack
Nondimensional Bending, Q = 56 psf
Nose Blowing p = 87 psi, Gun p = 65 psi

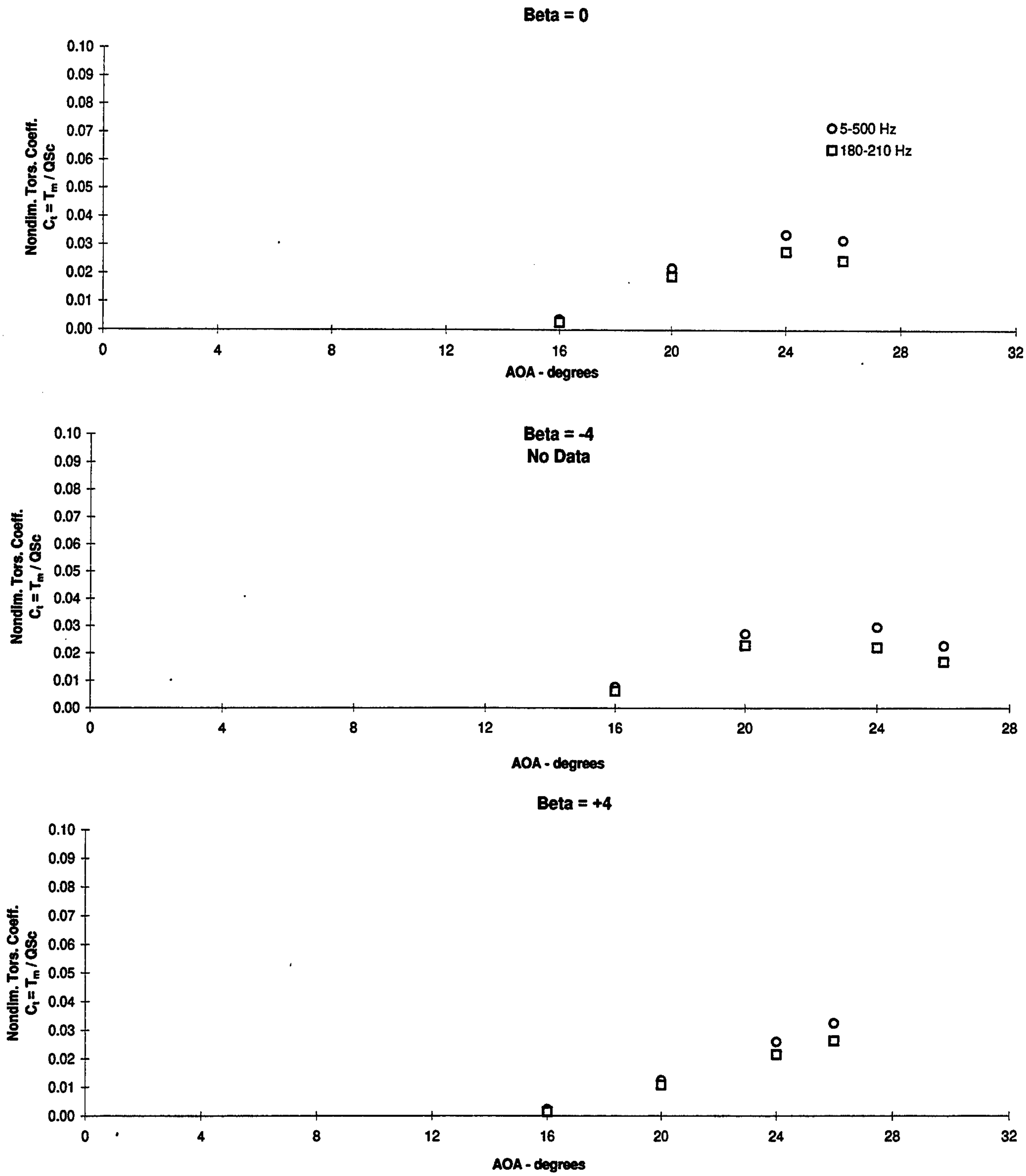

Figure 3.4.48 - Flex Tail Response vs Angle of Attack
Nondimensional Torsion, Q = 56 psf
Nose Blowing p = 87 psi, Gun p = 65 psi

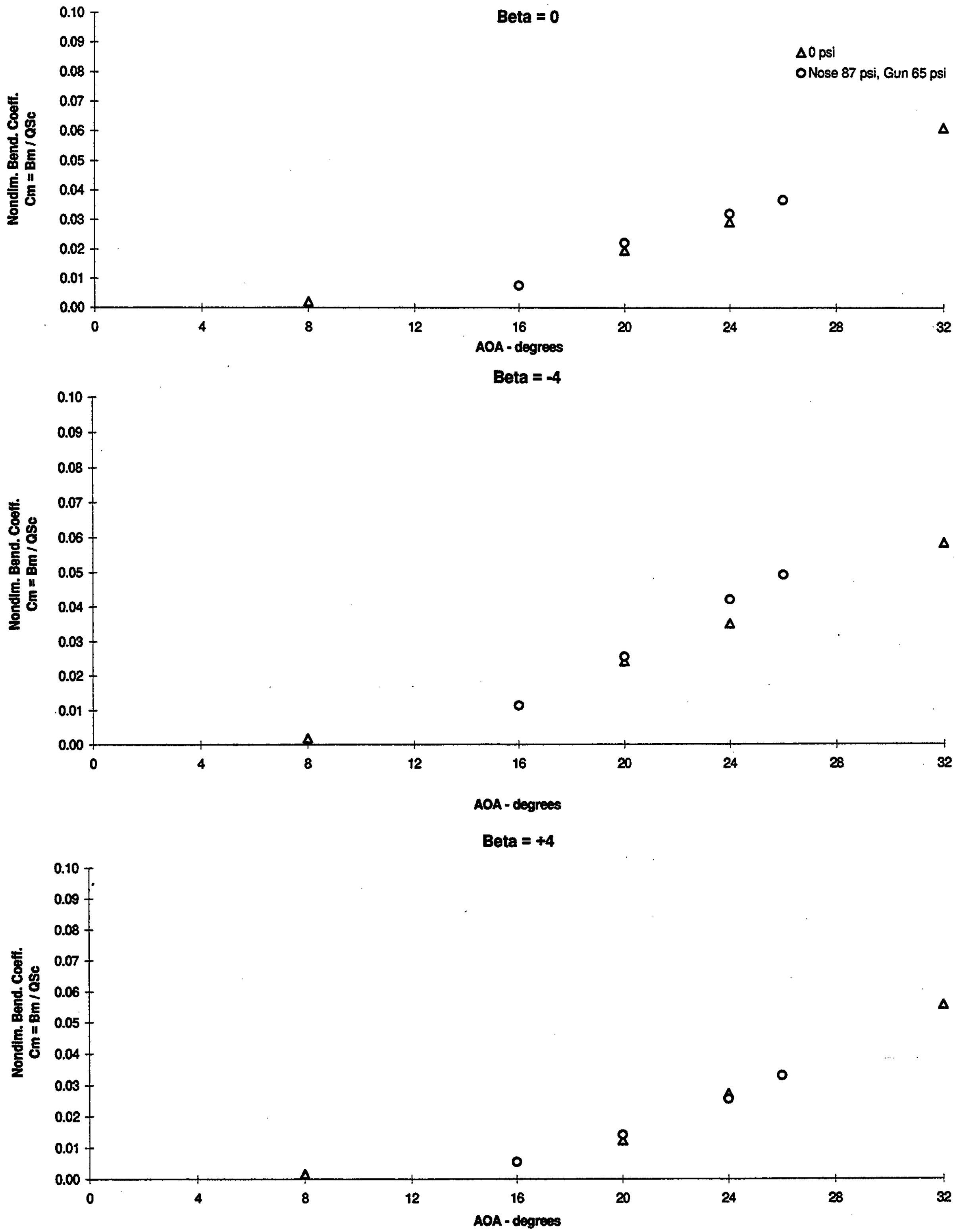

Figure 3.4.49 - Flex Tail Response vs Angle of Attack
Nondimensional Bending, Q = 56 psf, PSD's (5-500) Hz
Nose and Gun Blowing Summary

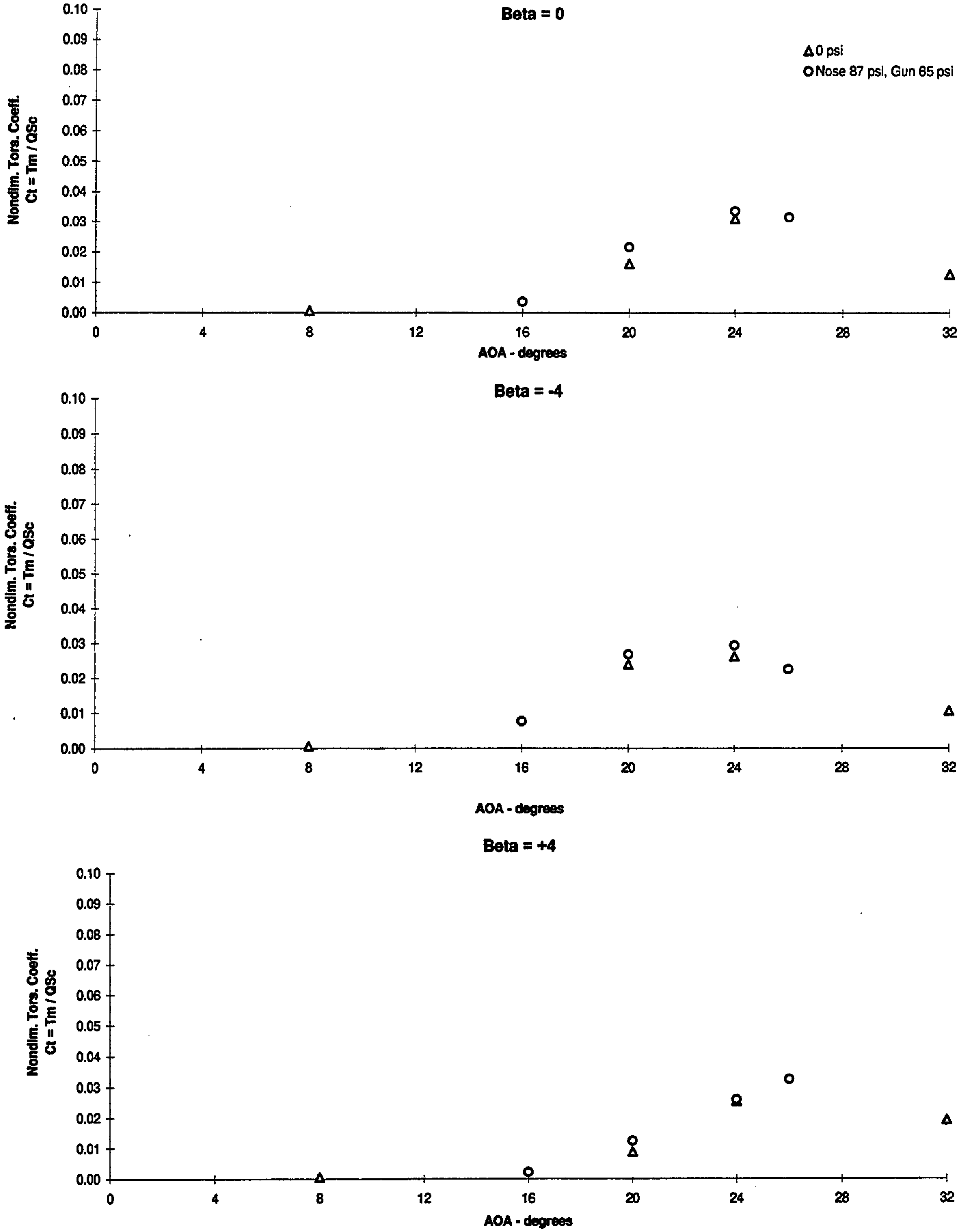

Figure 3.4.50 - Flex Tail Response vs Angle of Attack
Nondimensional Torsion, Q = 56 psf, PSD's (5-500) Hz
Nose and Gun Blowing Summary

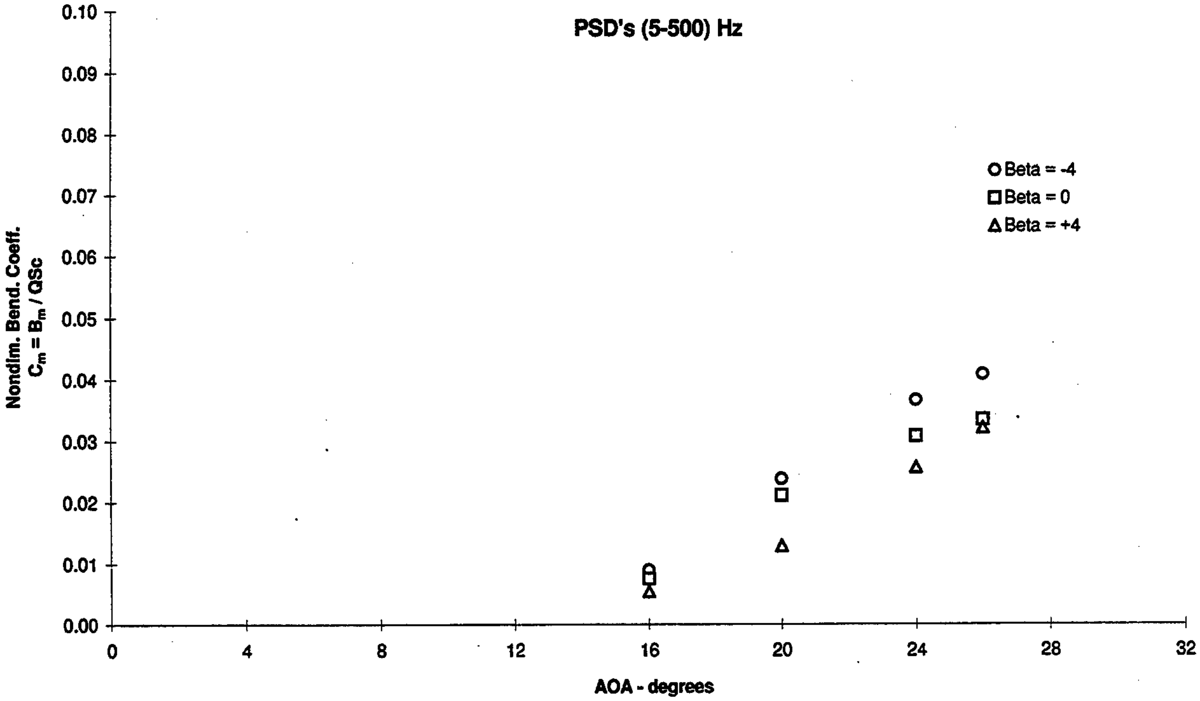

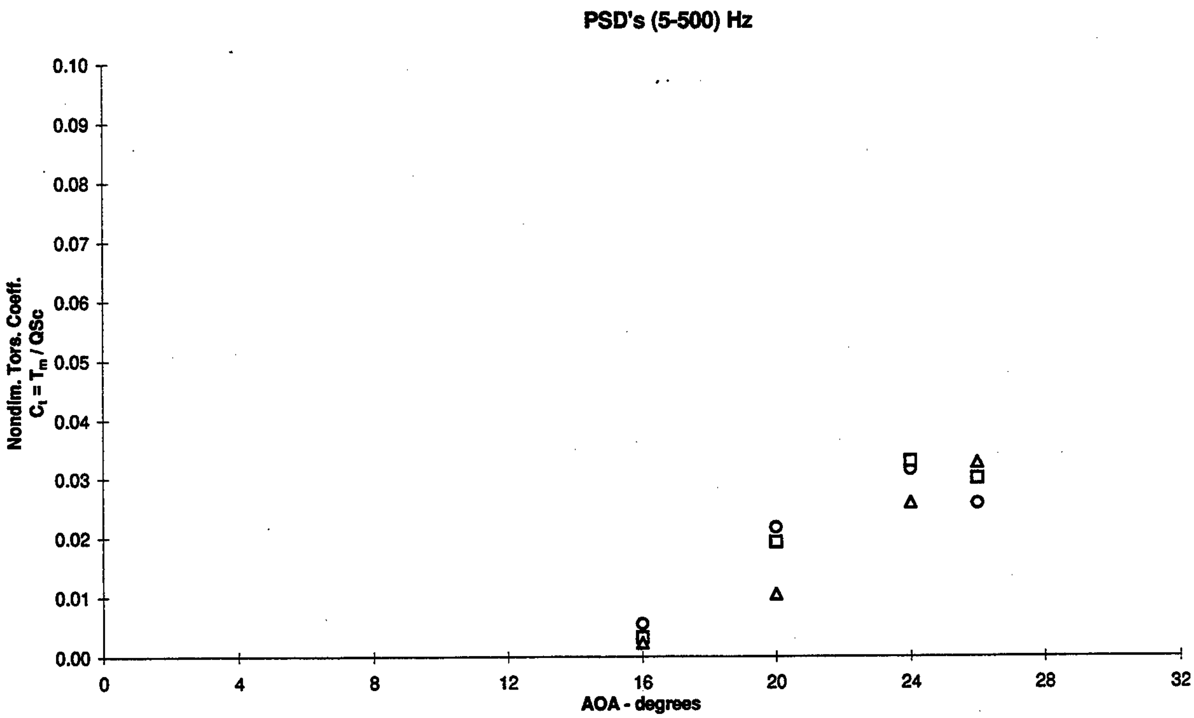

Figure 3.4.51 - Flex Tail Response vs Angle of Attack
Nondimensional Bending and Torsion, Q = 56 psf
Nose Blowing p = 87 psi, Wing L.E. p = 65 psi

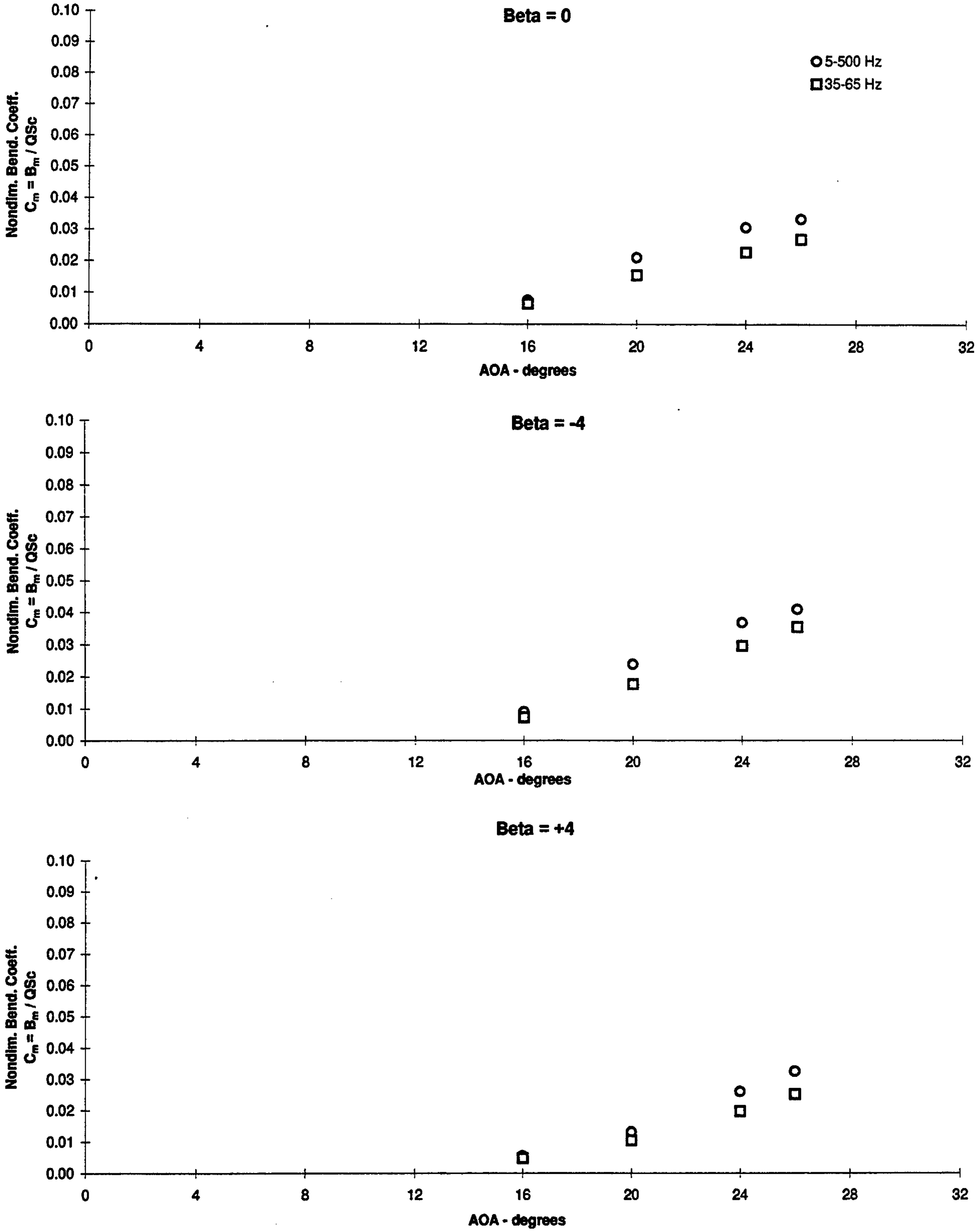

Figure 3.4.52 - Flex Tail Response vs Angle of Attack
Nondimensional Bending, Q = 56 psf
Nose Blowing p = 87 psi, Wing L.E. p = 65 psi

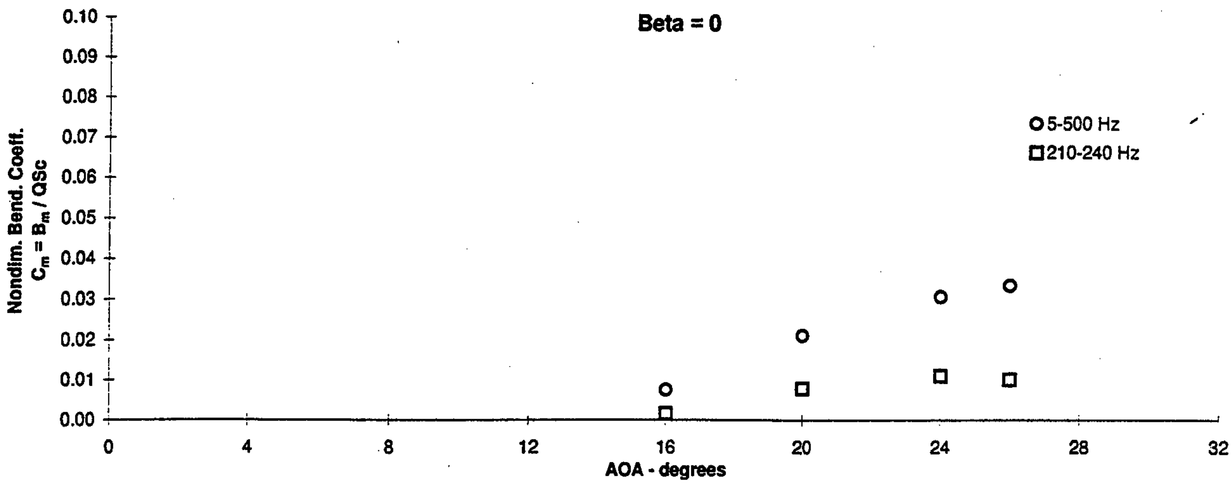

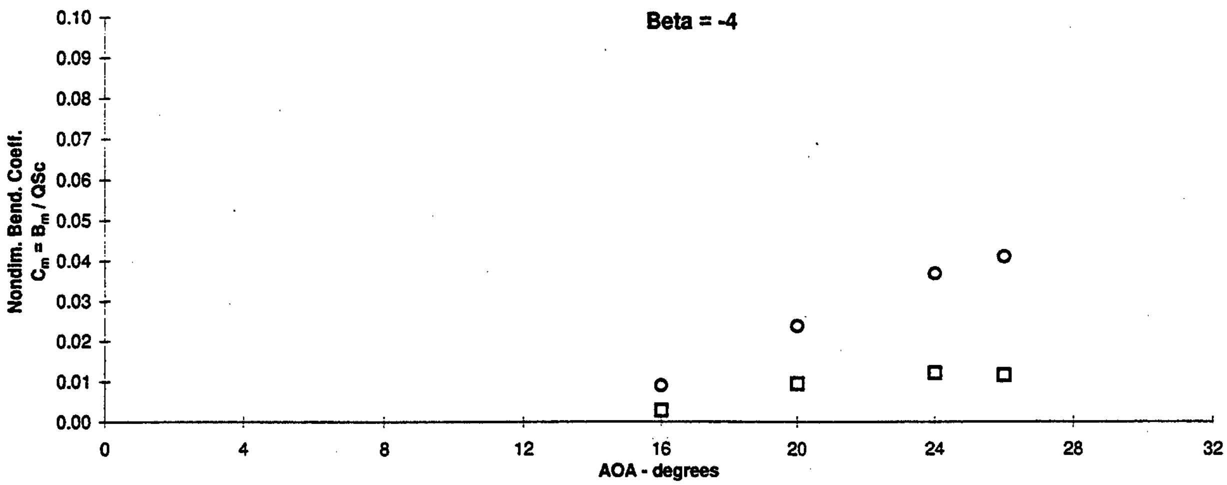

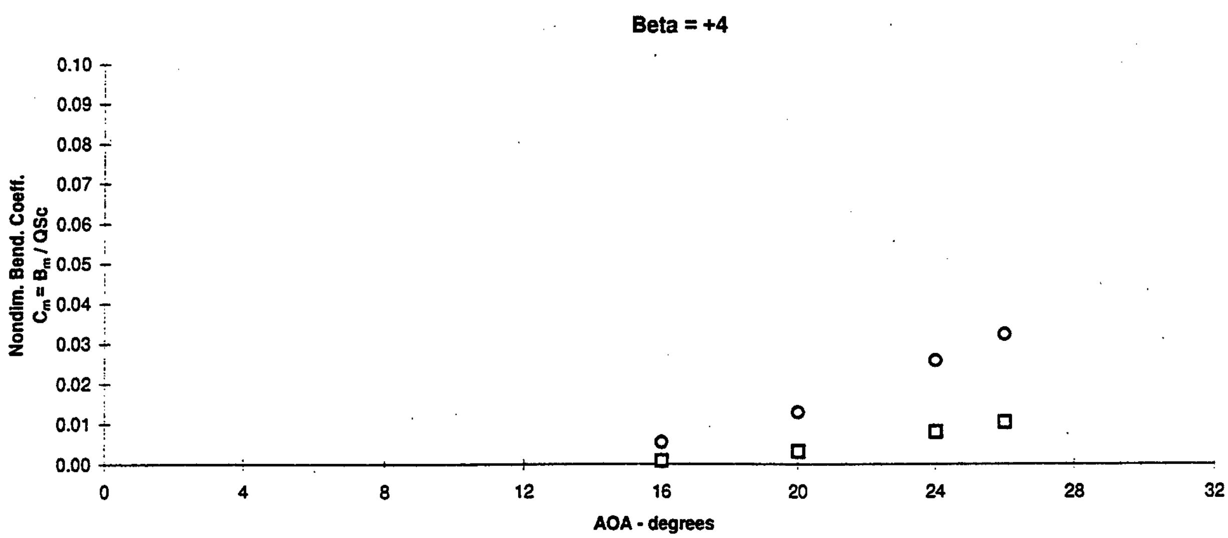

Figure 3.4.53 - Flex Tail Response vs Angle of Attack
Nondimensional Bending, Q = 56 psf
Nose Blowing p = 87 psi, Wing L.E. p = 65 psi

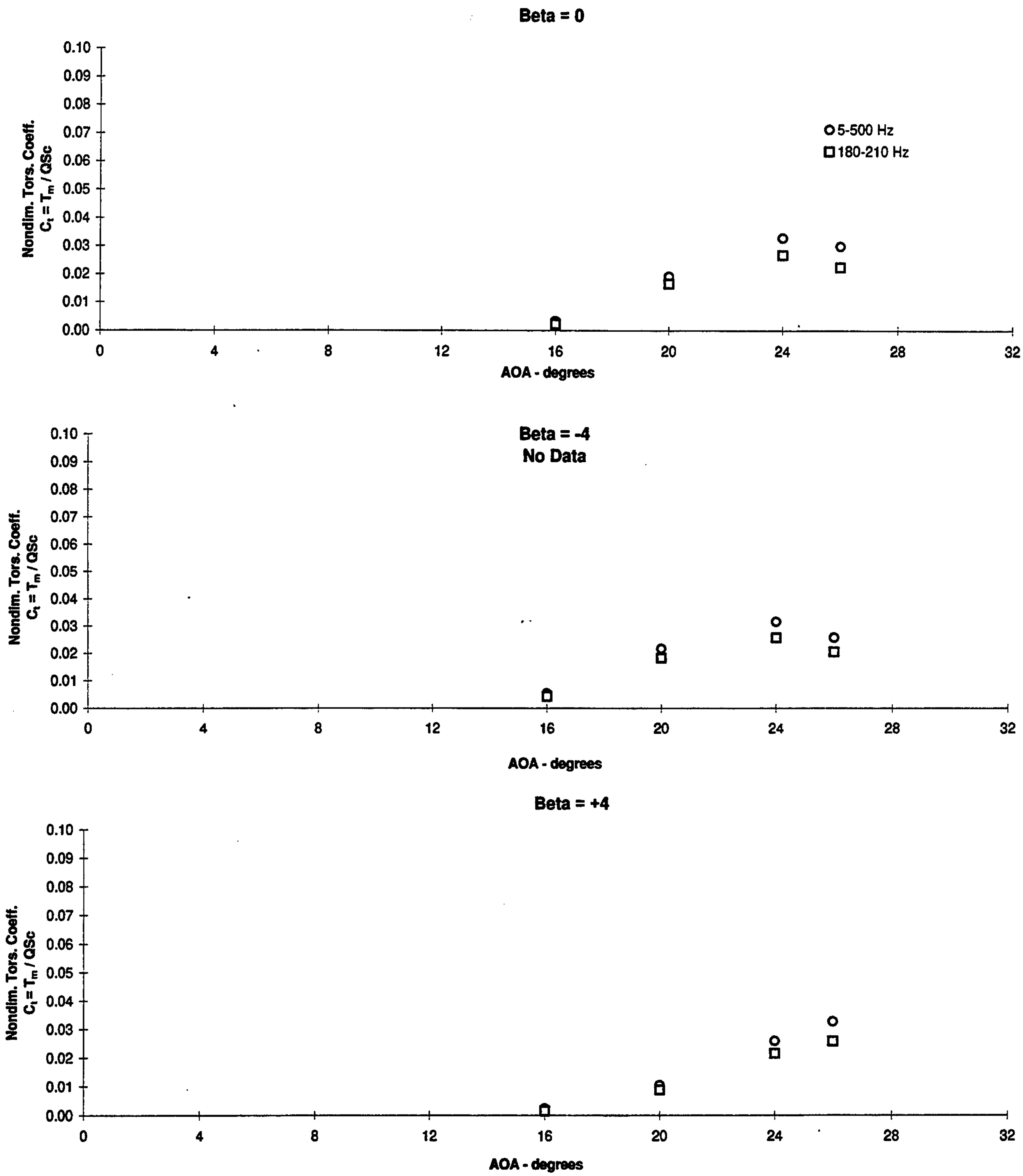

Figure 3.4.54 - Flex Tail Response vs Angle of Attack
Nondimensional Torsion, Q = 56 psf
Nose Blowing p = 87 psi, Wing L.E. p = 65 psi

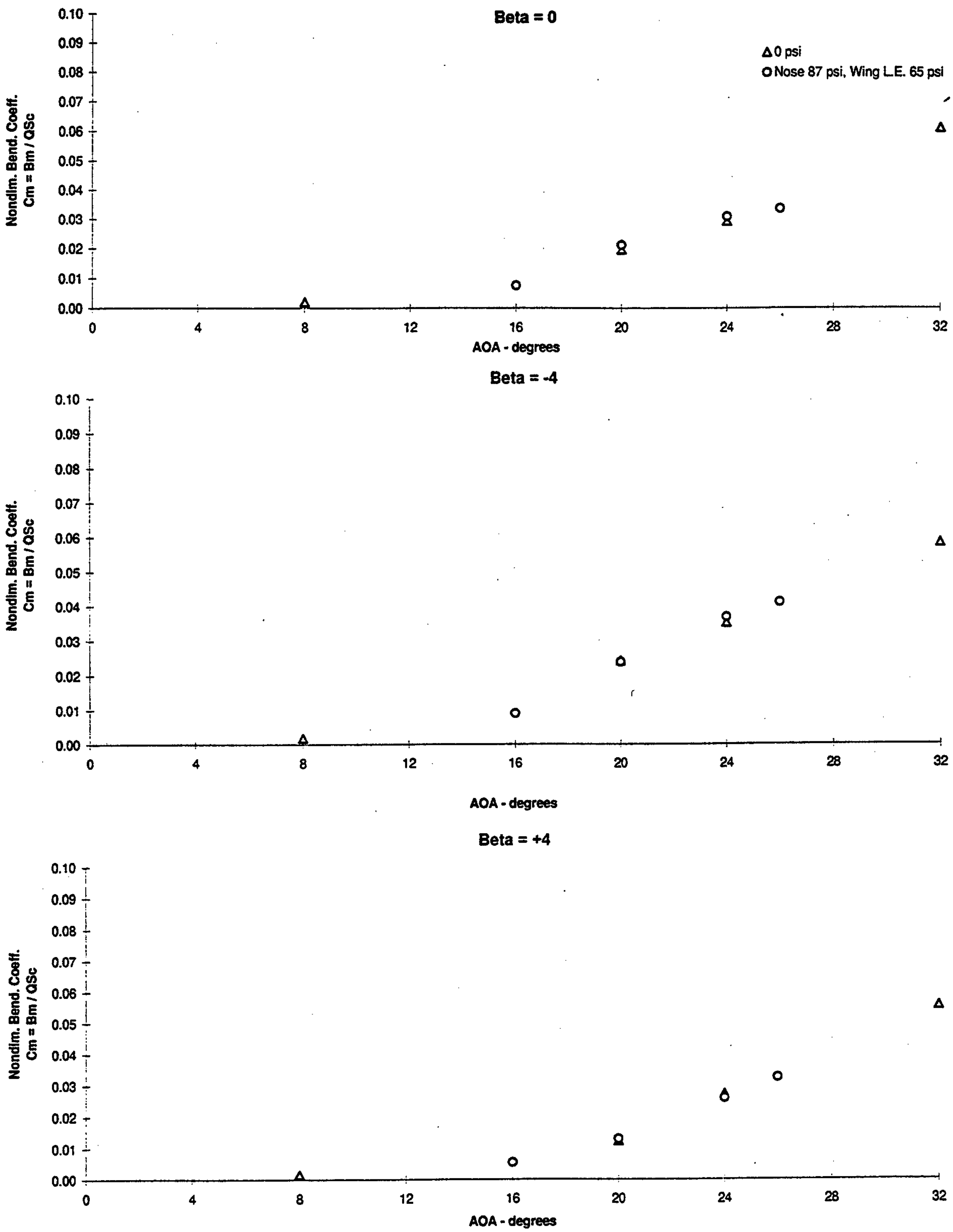

Figure 3.4.55 - Flex Tail Response vs Angle of Attack
Nondimensional Bending, Q = 56 psf, PSD's (5-500) Hz
Nose and Wing L.E. Blowing Summary

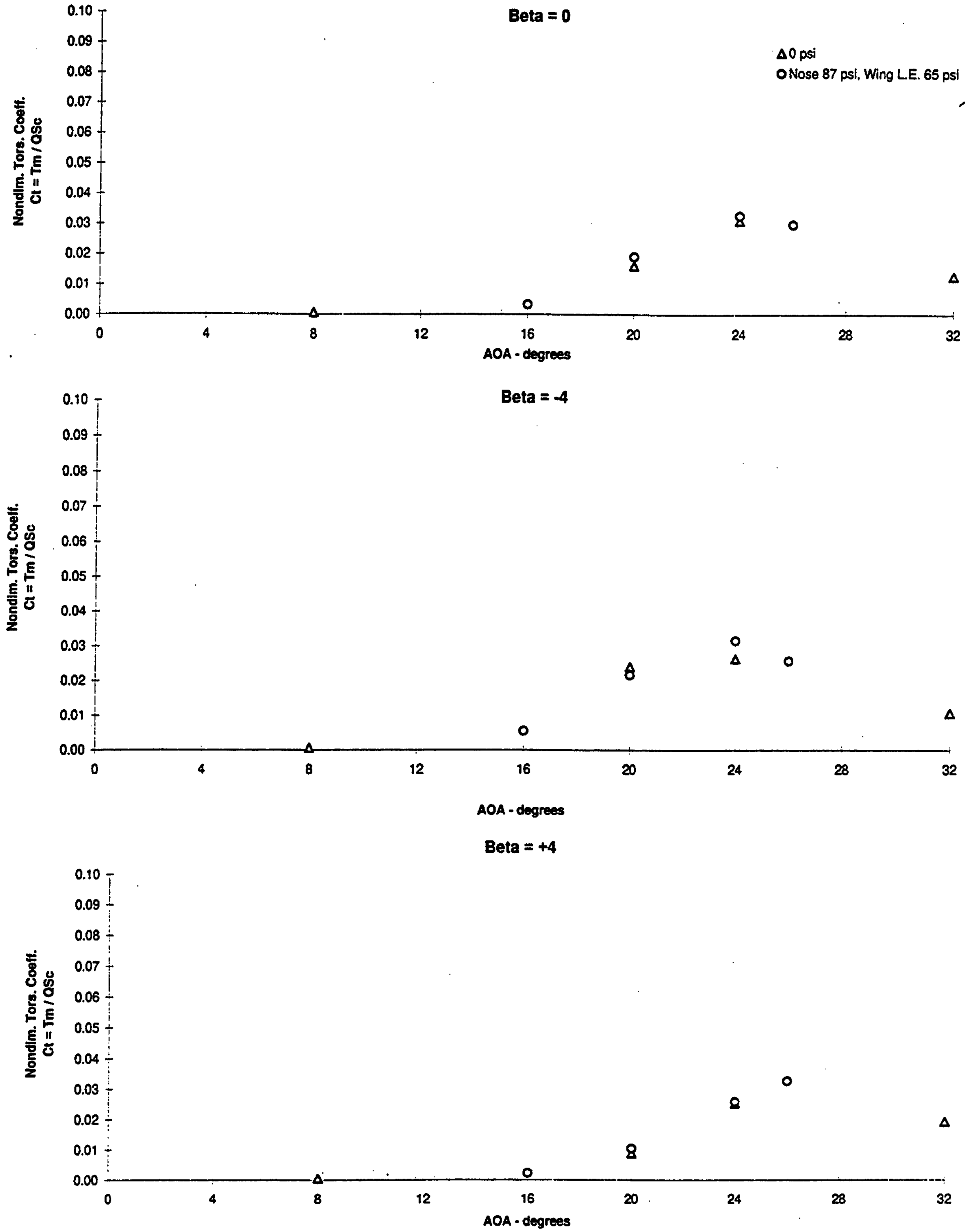

Figure 3.4.56 - Flex Tail Response vs Angle of Attack
Nondimensional Torsion, Q = 56 psf, PSD's (5-500) Hz
Nose and Wing L.E. Blowing Summary

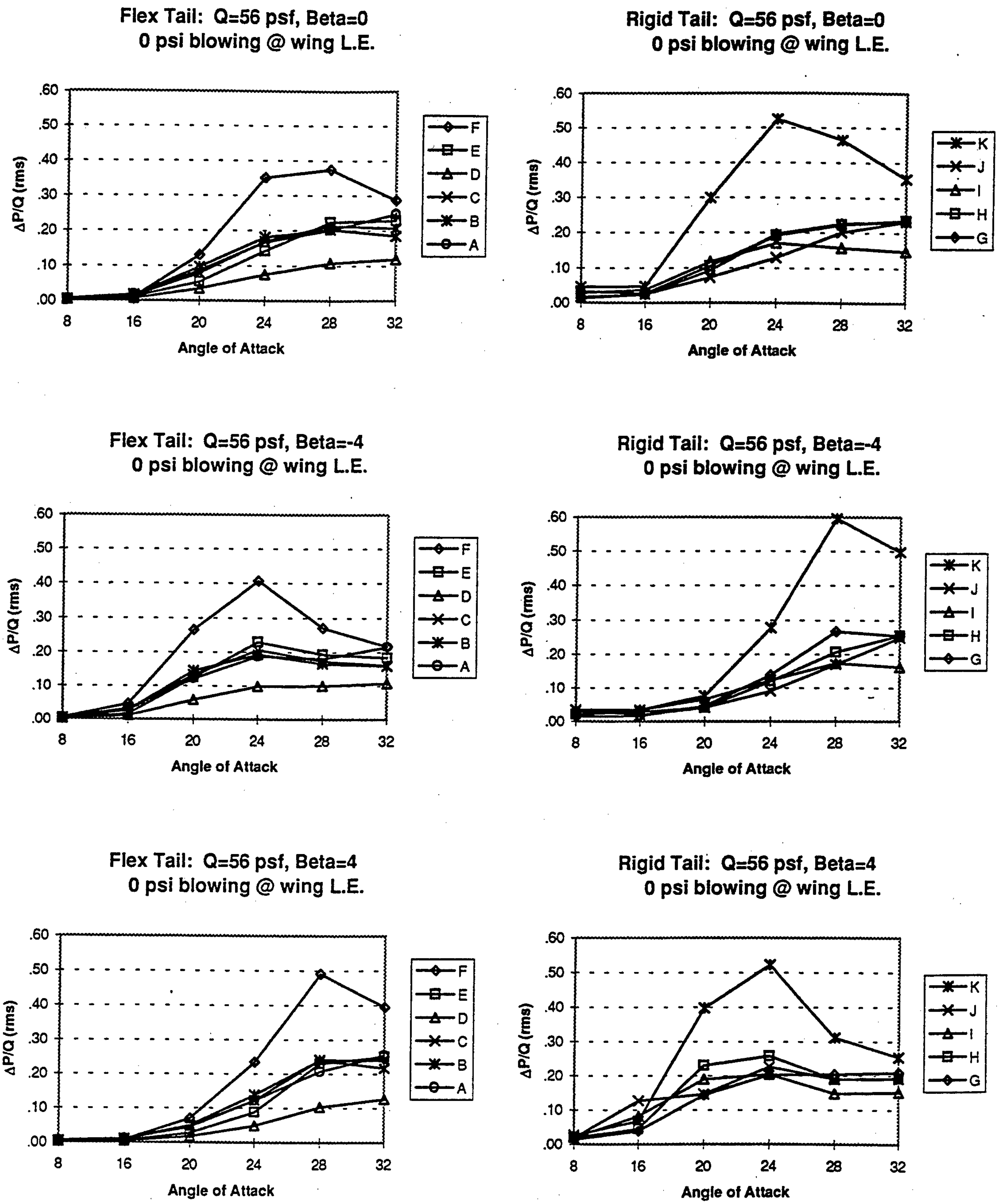

Figure 3.5.1 Flex. And Rigid Tails - RMS Pressures Vs Alpha, Q= 56 PSF, Beta=0, -4, 4

WBP =0

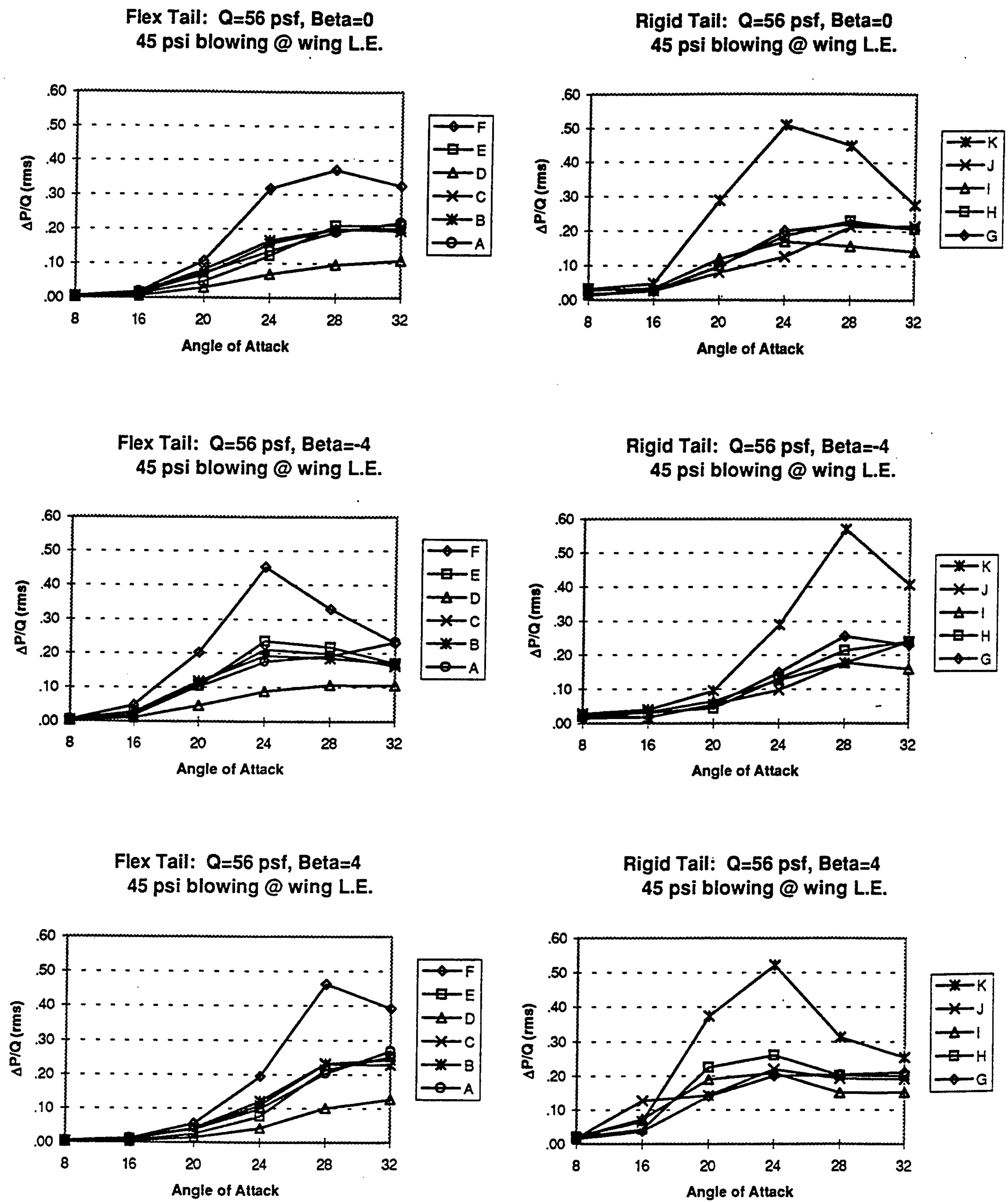

Figure 3.5.2 Flex. And Rigid Tails - RMS Pressures Vs Alpha, Q= 56 PSF, Beta=0, -4, 4

WBP =45 psi

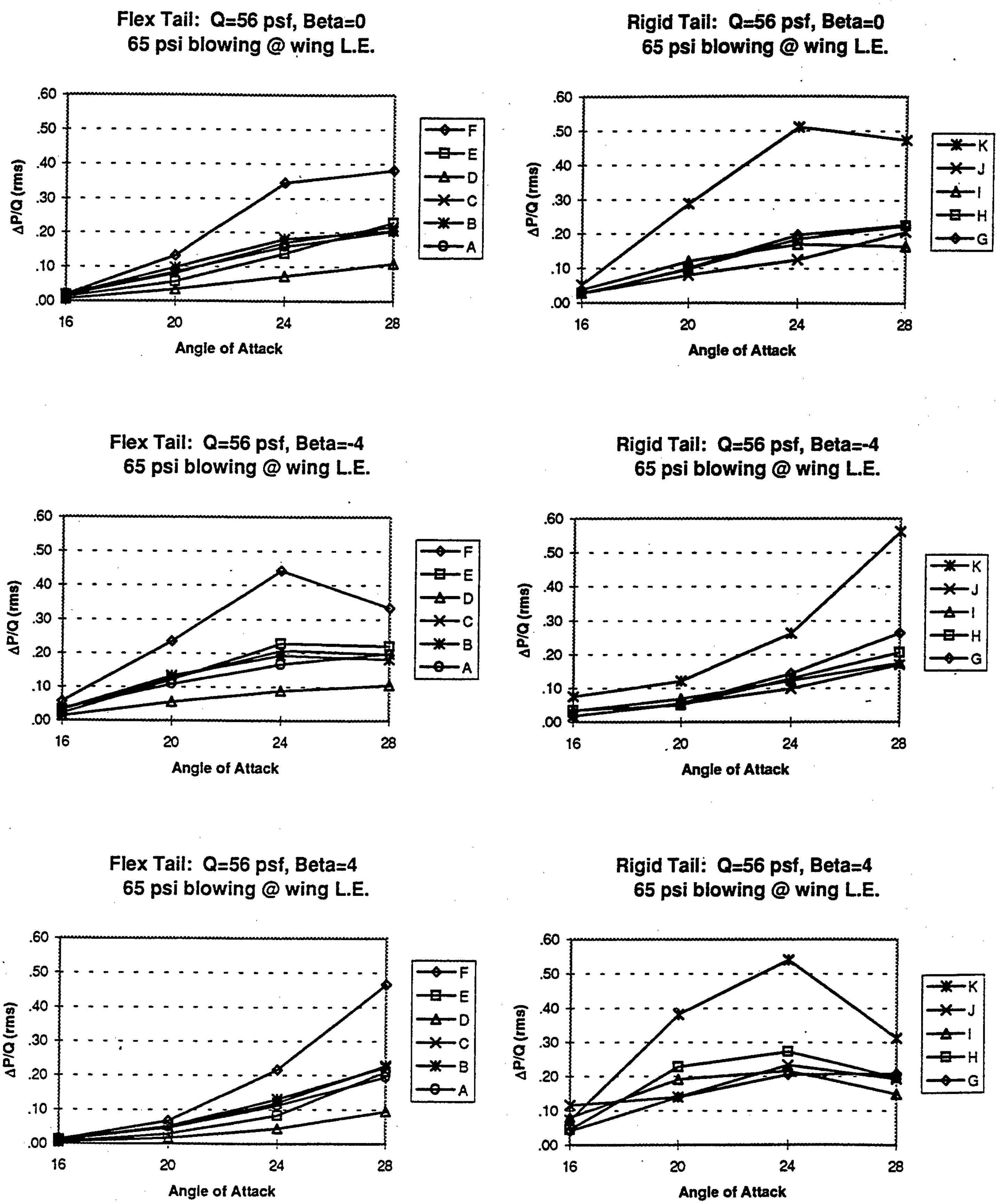

Figure 3.5.3 Flex. And Rigid Tails - RMS Pressures Vs Alpha, Q= 56 PSF, Beta=0, -4, 4

WBP =65 psi

Flex Tail: Q=56 psf, Beta=0
65 psi blowing @ gun only

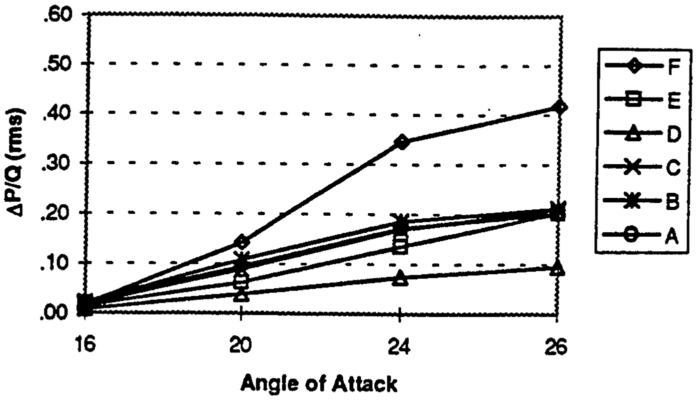

Rigid Tail: Q=56 psf, Beta=0
65 psi blowing @ gun only

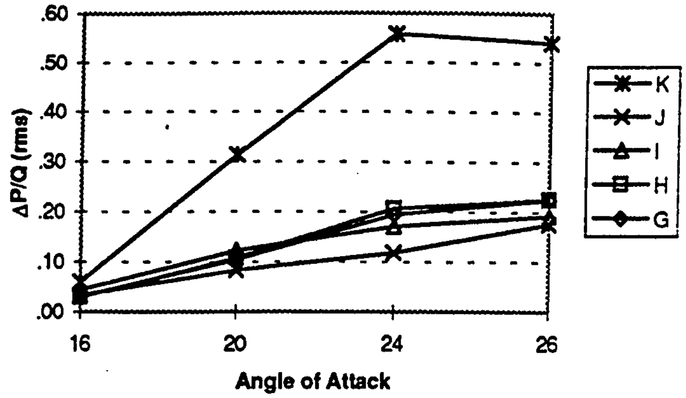

Flex Tail: Q=56 psf, Beta=-4
65 psi blowing @ gun only

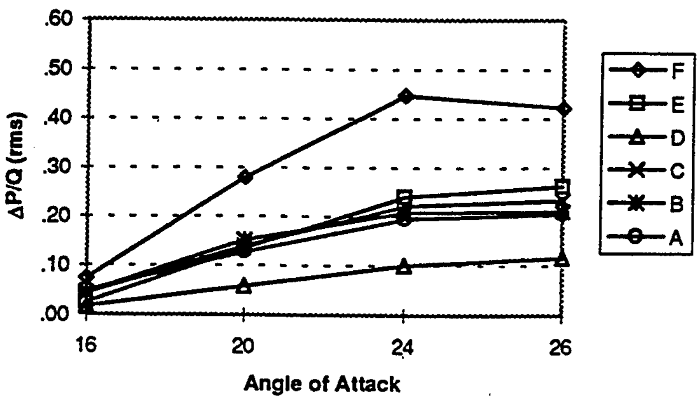

Rigid Tail: Q=56 psf, Beta=-4
65 psi blowing @ gun only

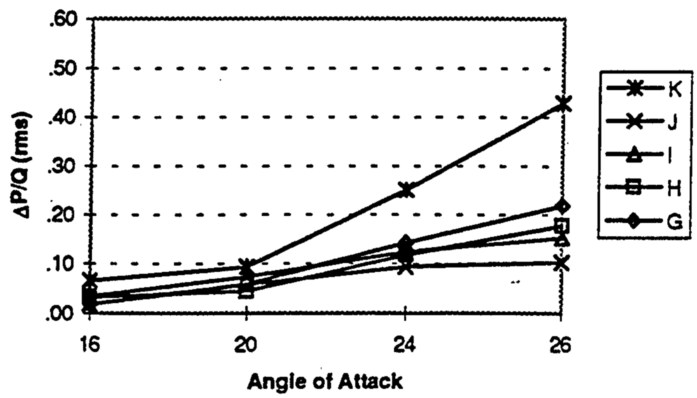

Flex Tail: Q=56 psf, Beta=4
65 psi blowing @ gun only

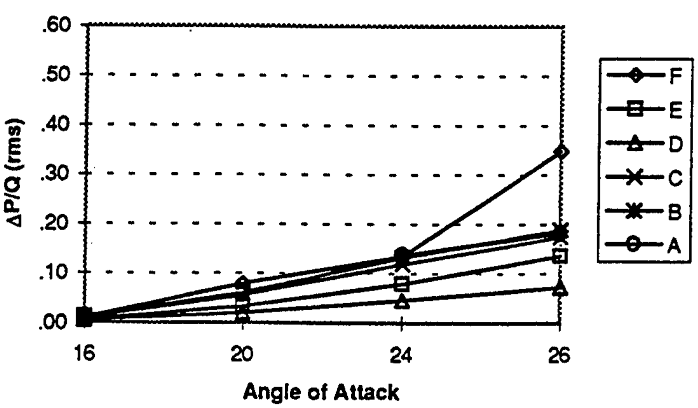

Rigid Tail: Q=56 psf, Beta=4
65 psi blowing @ gun only

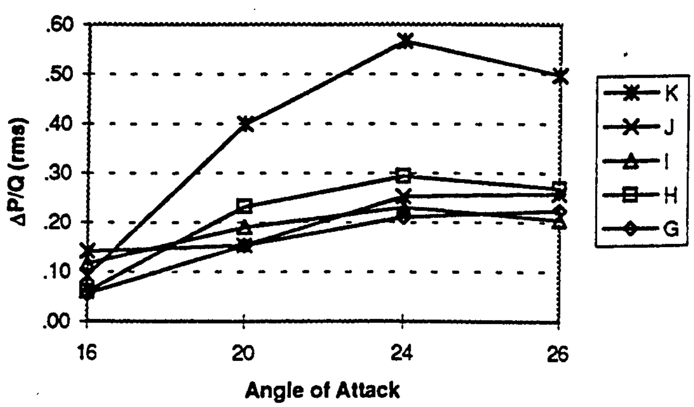

Figure 3.5.4 Flex. And Rigid Tails - RMS Pressures Vs Alpha, Q= 56 PSF, Beta=0, -4, 4
GBP = 65 psi

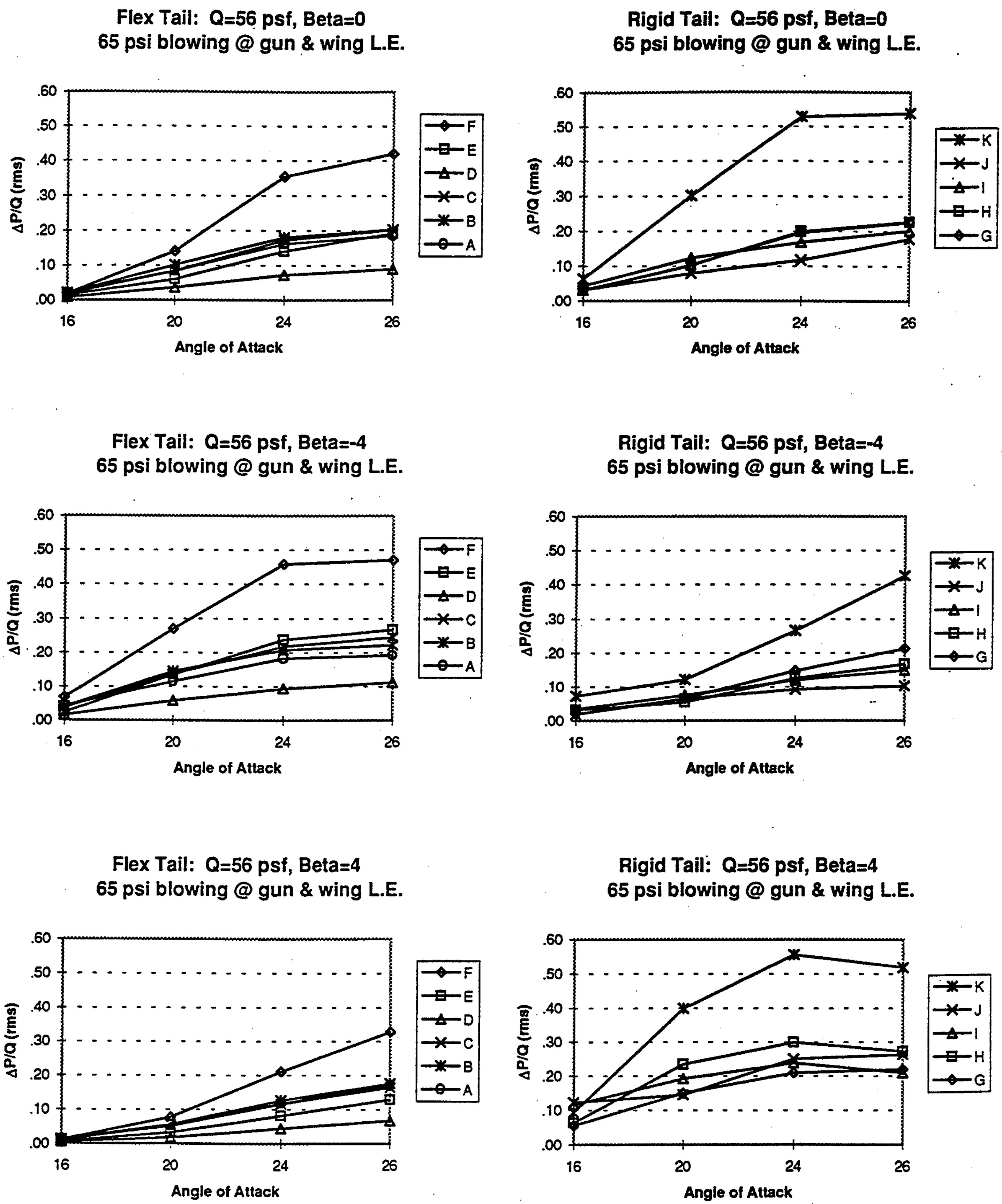

Figure 3.5.5 Flex. And Rigid Tails - RMS Pressures Vs Alpha, Q= 56 PSF, Beta=0, -4, 4

WBP = 65 psi, GBP = 65 psi

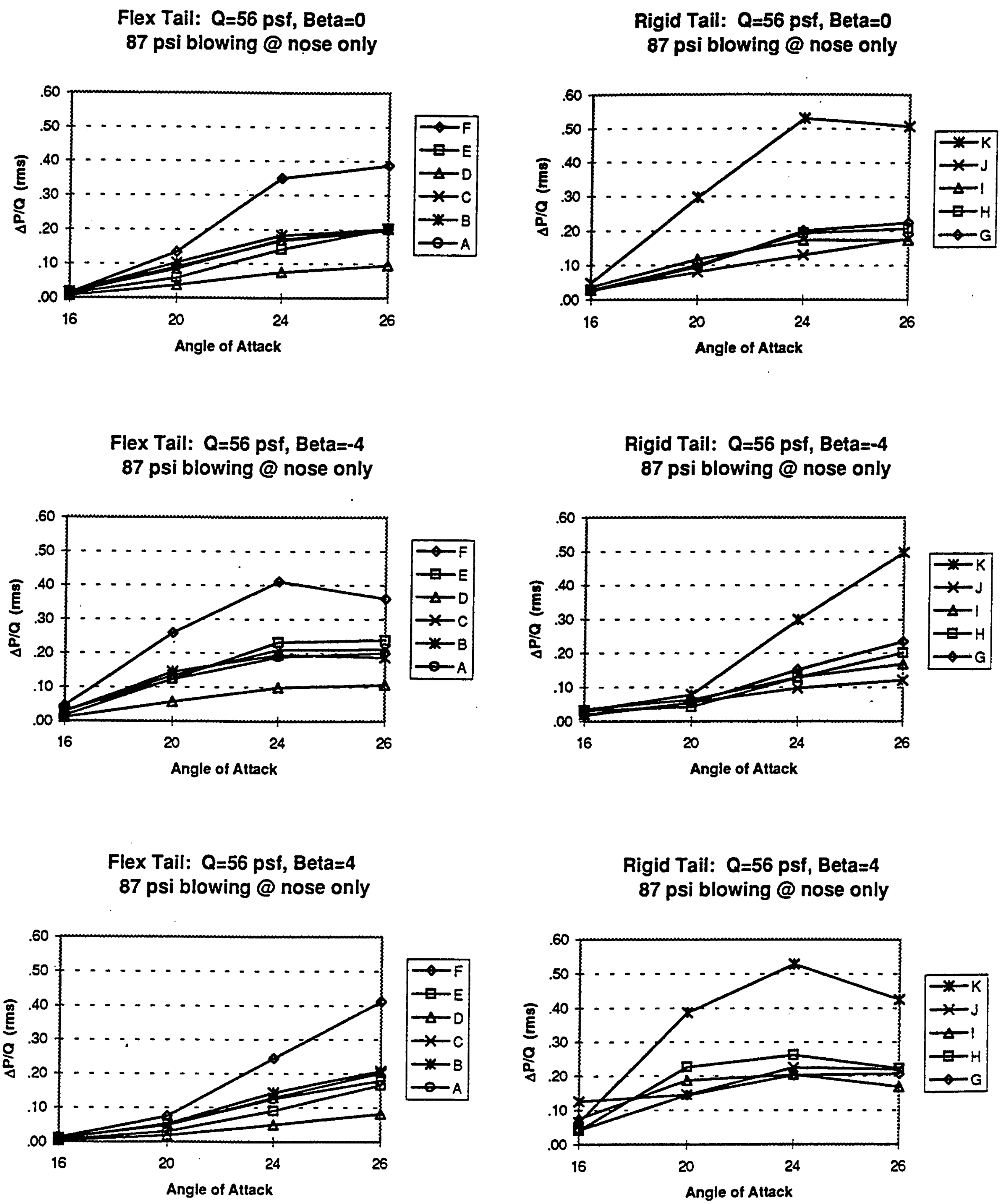

Figure 3.5.6 Flex. And Rigid Tails - RMS Pressures Vs Alpha, Q= 56 PSF, Beta=0, -4, 4, NBP = 87 psi

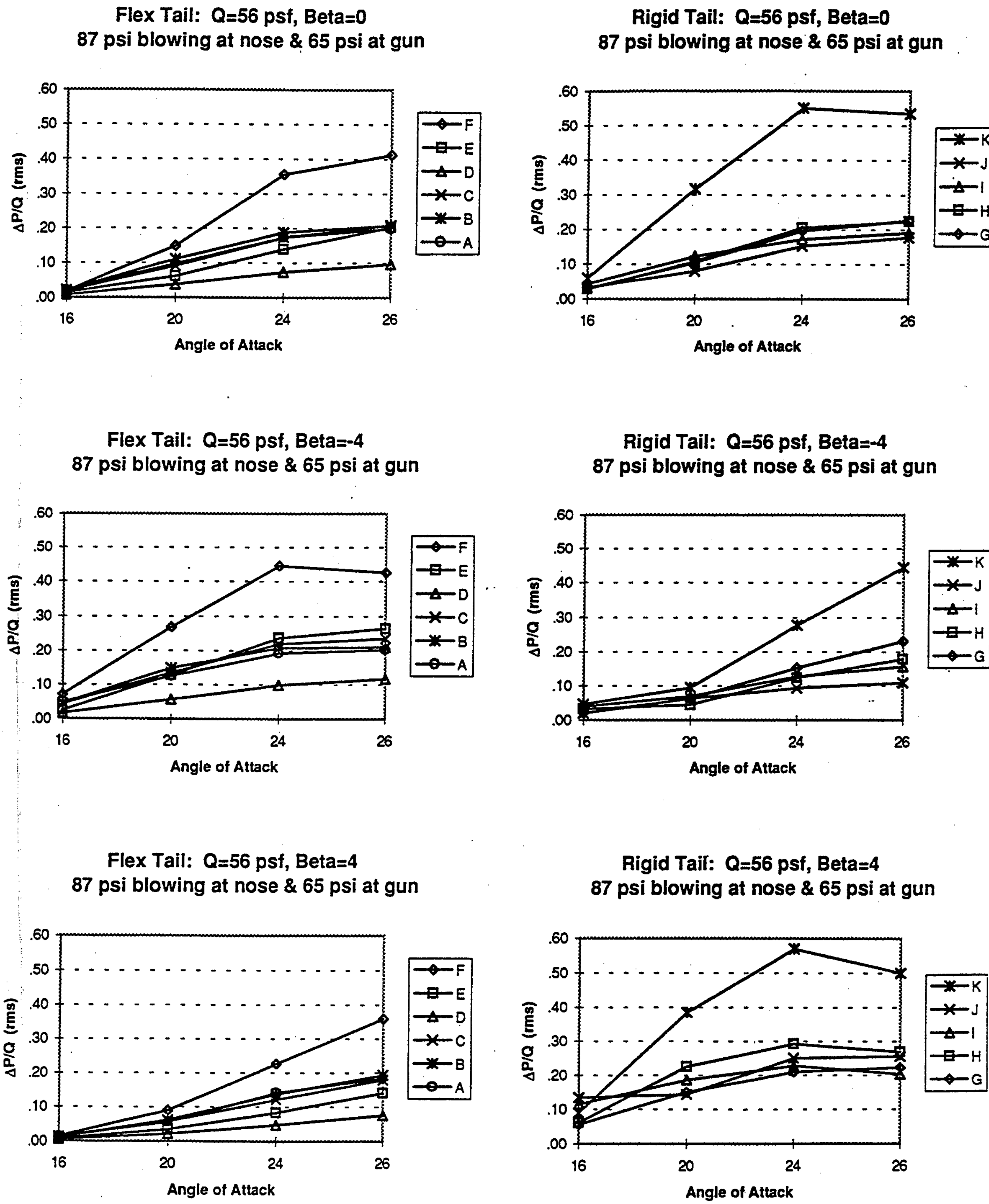

Figure 3.5.7 Flex. And Rigid Tails - RMS Pressures Vs Alpha, Q= 56 PSF, Beta=0, -4, 4, NBP = 87 psi, GBP = 65 psi

Flex Tail: Q=56 psf, Beta=0
87 psi blowing at nose &
65 psi at wing L.E.

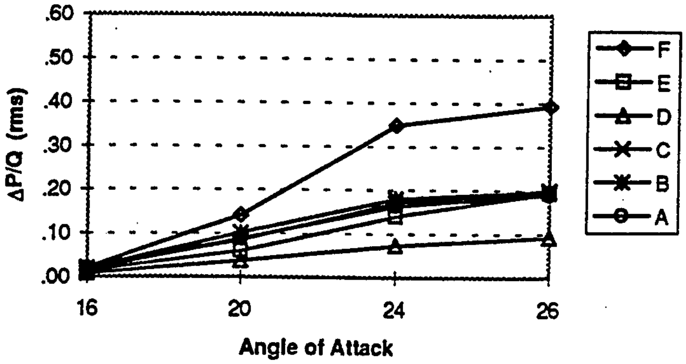

Rigid Tail: Q=56 psf, Beta=0
87 psi blowing at nose &
65 psi at wing L.E.

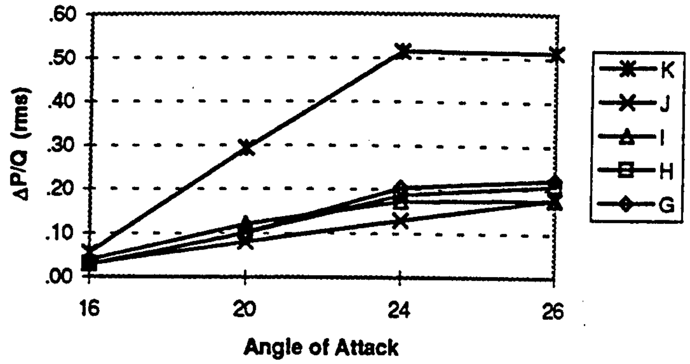

Flex Tail: Q=56 psf, Beta=-4
87 psi blowing at nose &
65 psi at wing L.E.

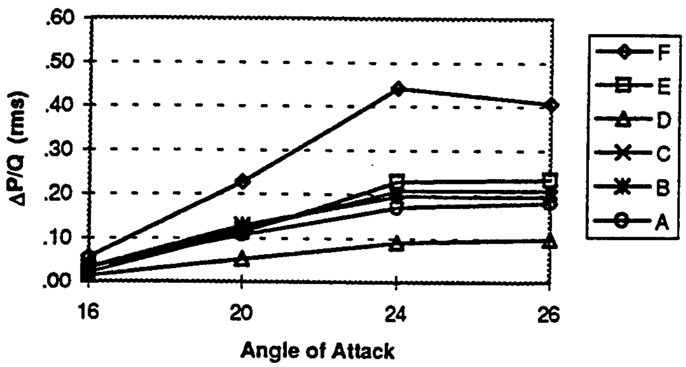

Rigid Tail: Q=56 psf, Beta=-4
87 psi blowing at nose &
65 psi at wing L.E.

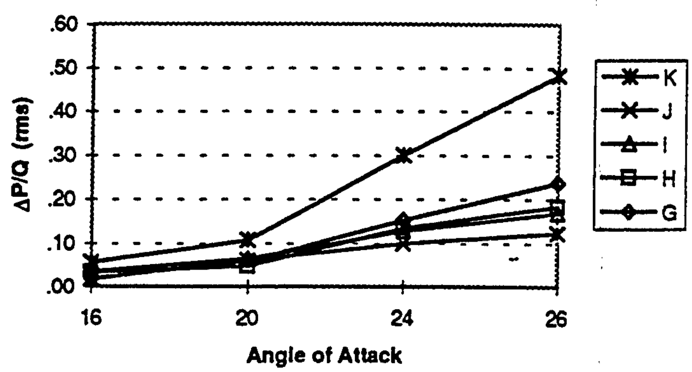

Flex Tail: Q=56 psf, Beta=4
87 psi blowing at nose &
65 psi at wing L.E.

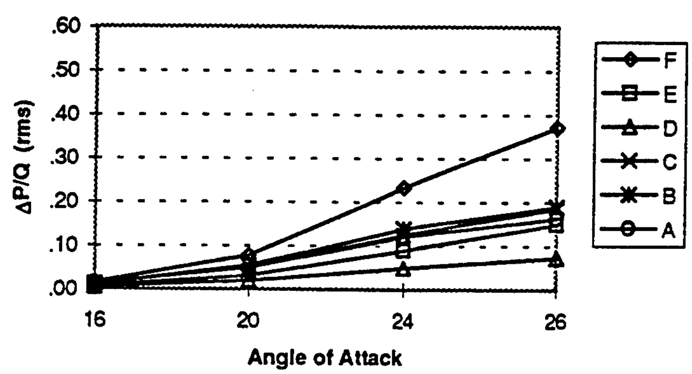

Rigid Tail: Q=56 psf, Beta=4
87 psi blowing at nose &
65 psi at wing L.E.

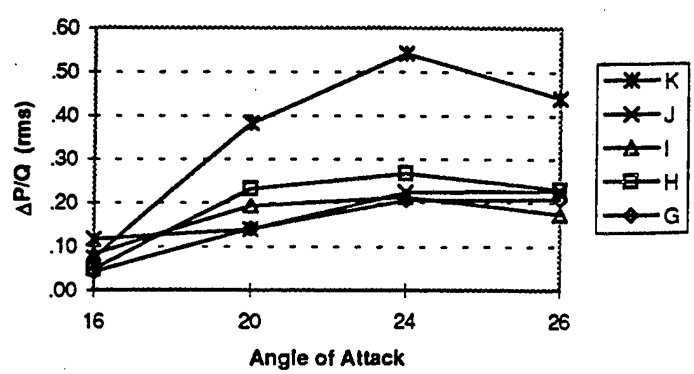

Figure 3.5.8 Flex. And Rigid Tails - RMS Pressures Vs Alpha, Q= 56 PSF, Beta=0, -4, 4, NBP = 87 psi, WBP = 65 psi

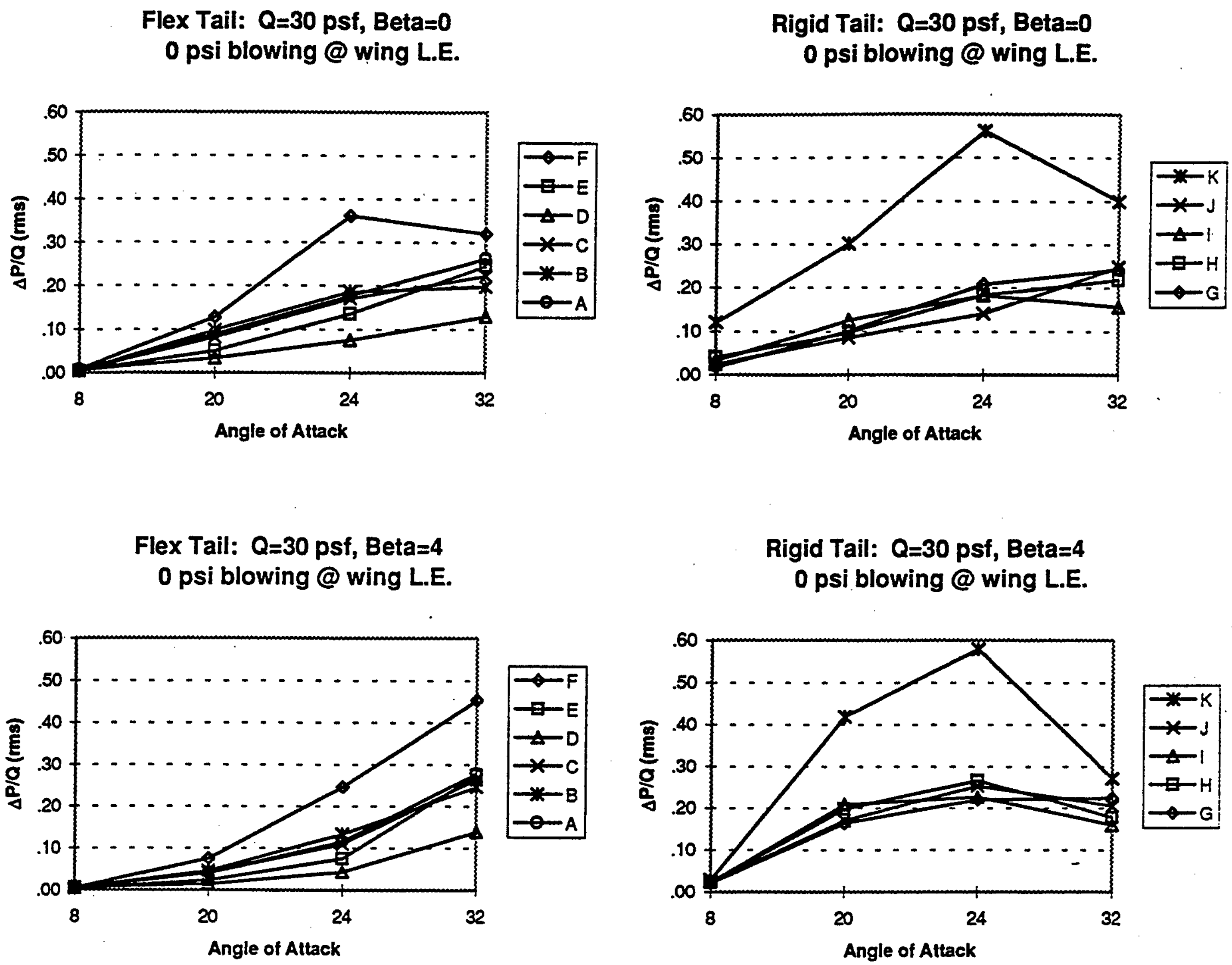

Figure 3.5.9 Flex. And Rigid Tails - RMS Pressures Vs Alpha, Q= 30 PSF, Beta=0, -4, 4, WBP =0

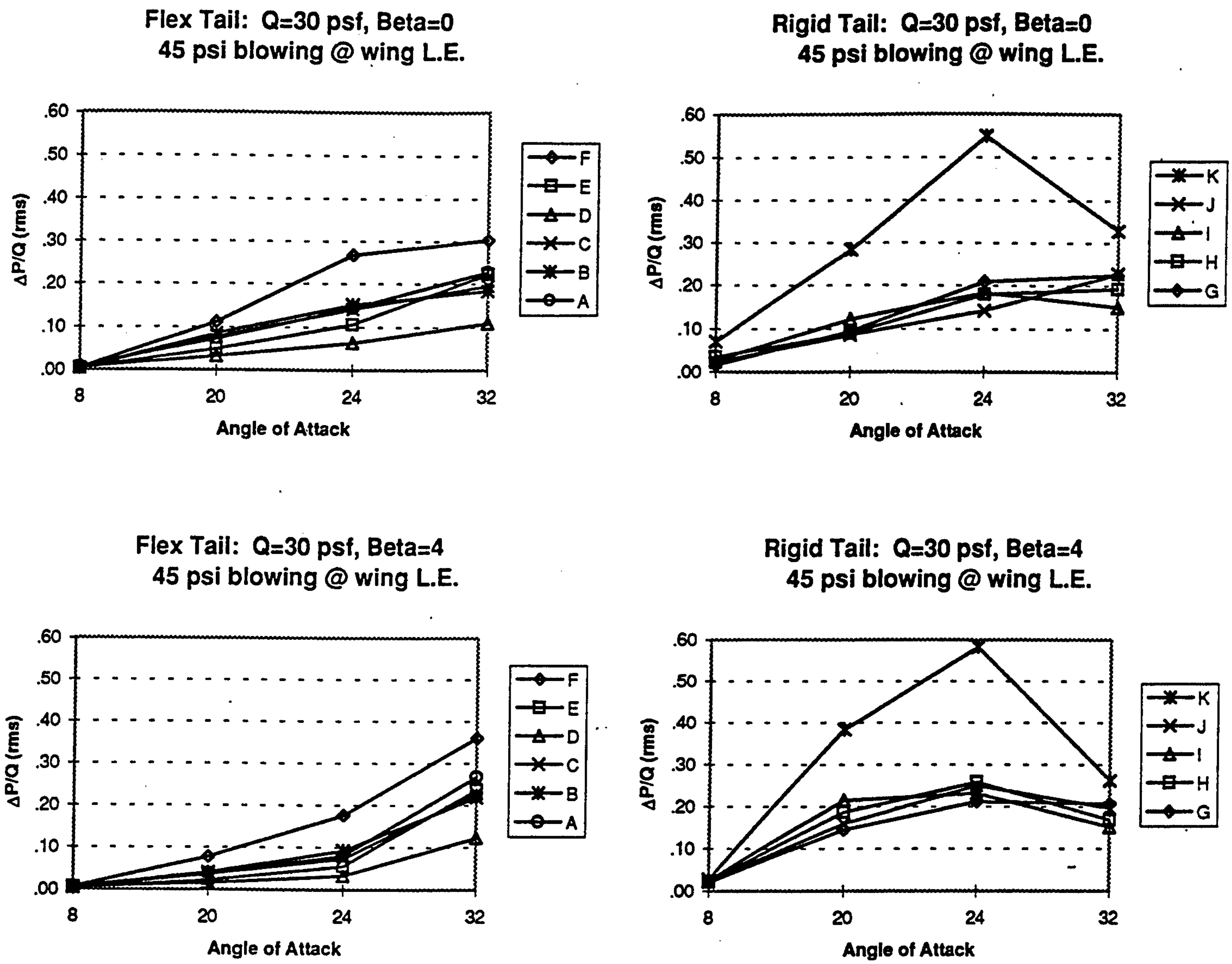

Figure 3.5.10 Flex. And Rigid Tails - RMS Pressures Vs Alpha, Q= 30 PSF, Beta=0, -4, 4, WBP =45 psi

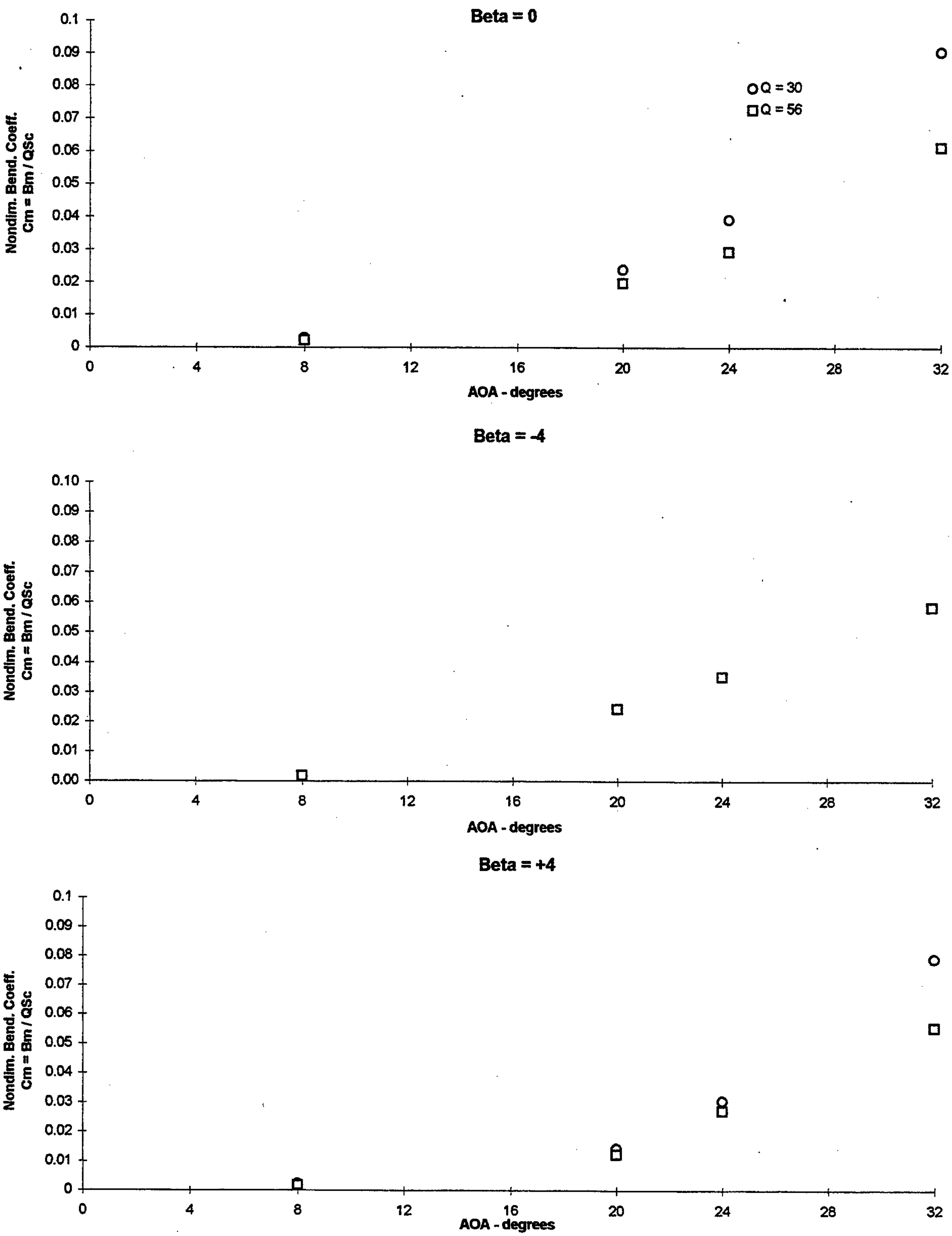

3.6.1 Flex Tail Response vs Angle of Attack, Q= 30, 56 PSF, No Blowing, PSD's (5- 500HZ), Nondimensional Bending

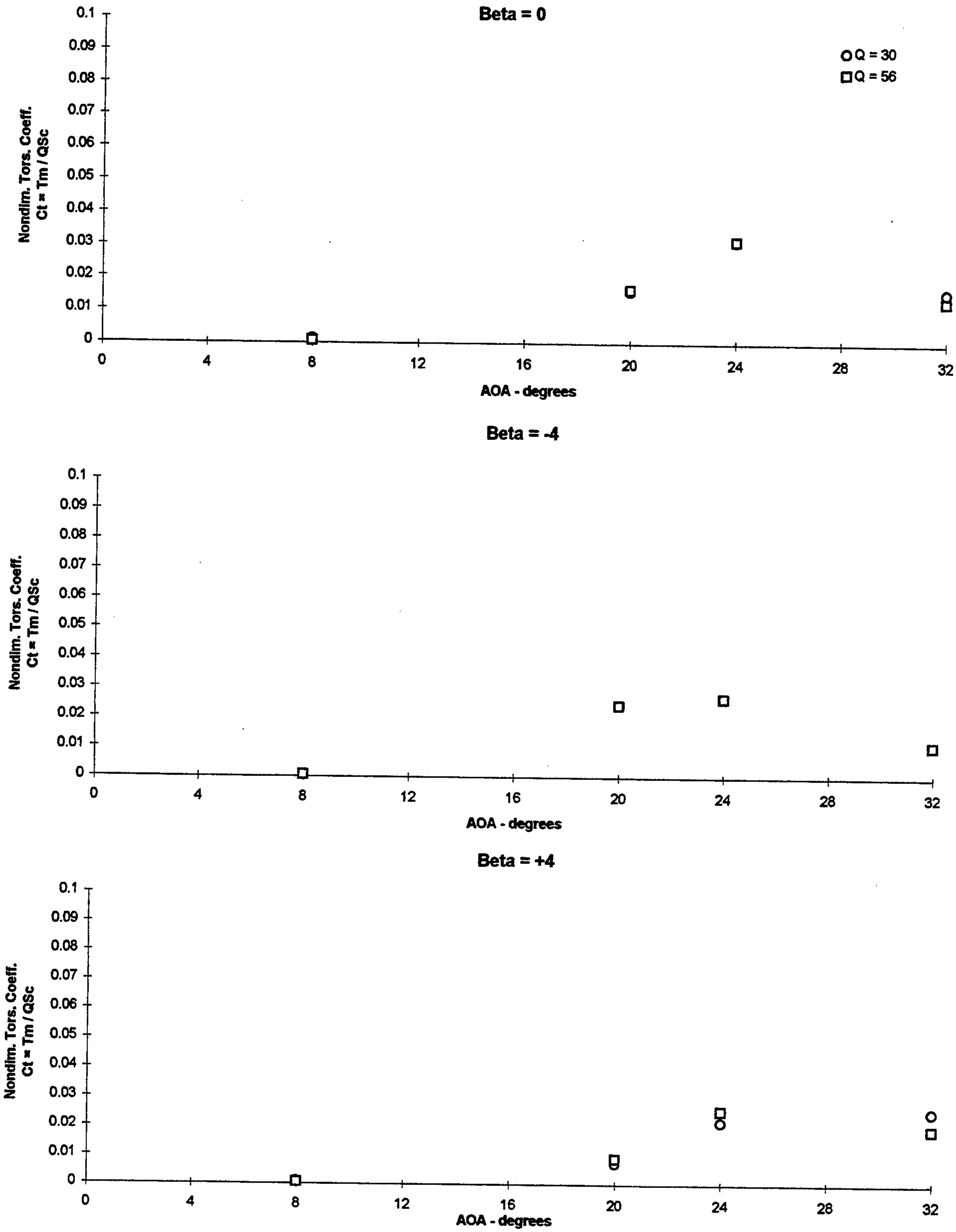

3.6.2 Flex Tail Response vs Angle of Attack, Q= 30, 56 PSF, No Blowing, PSD's (5- 500HZ), Nondimensional Torsion

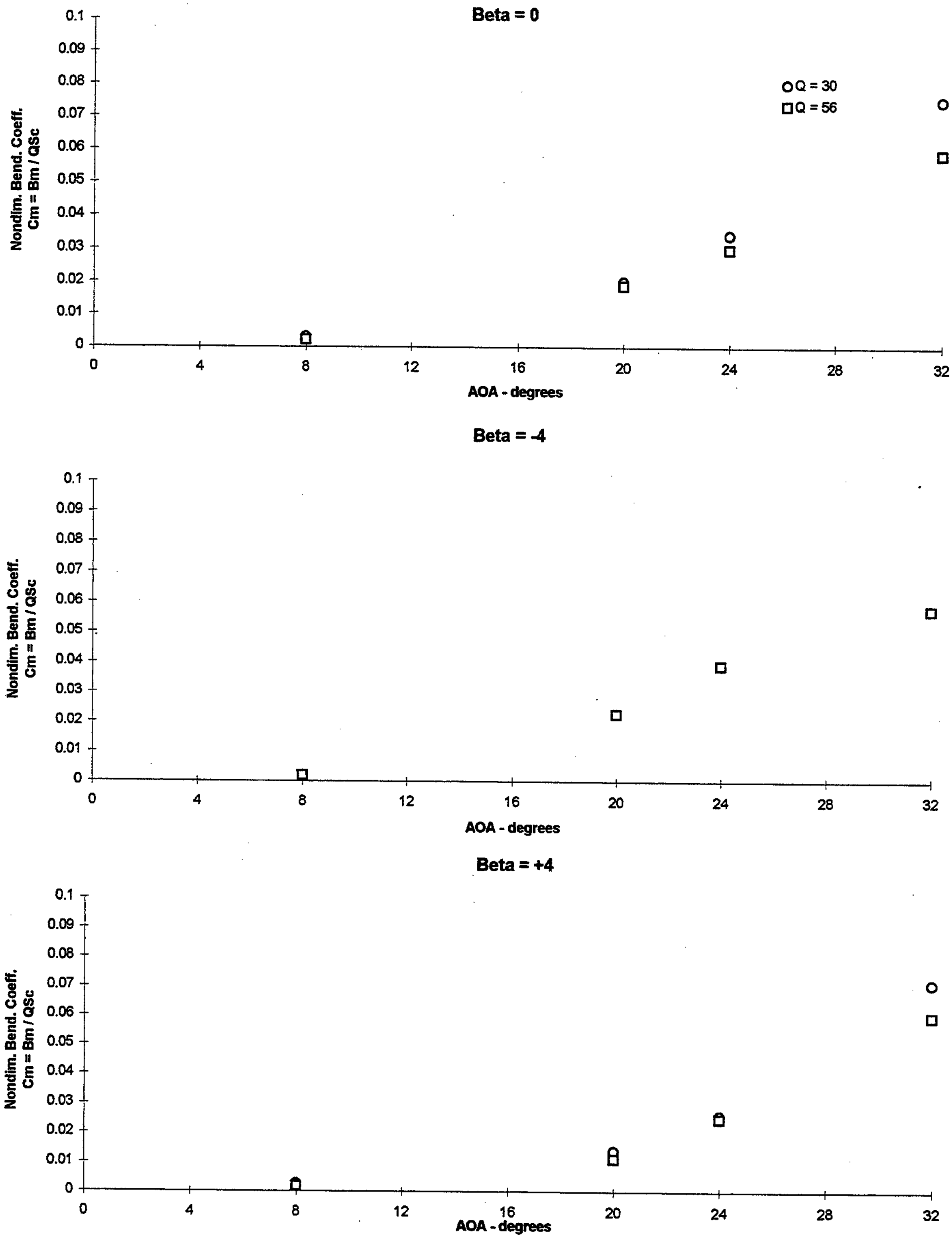

3.6.3 Flex Tail Response vs Angle of Attack, Q= 30, 56 PSF,Wing Blowing= 45 psi, PSD's(5- 500HZ), Nondimensional Bending

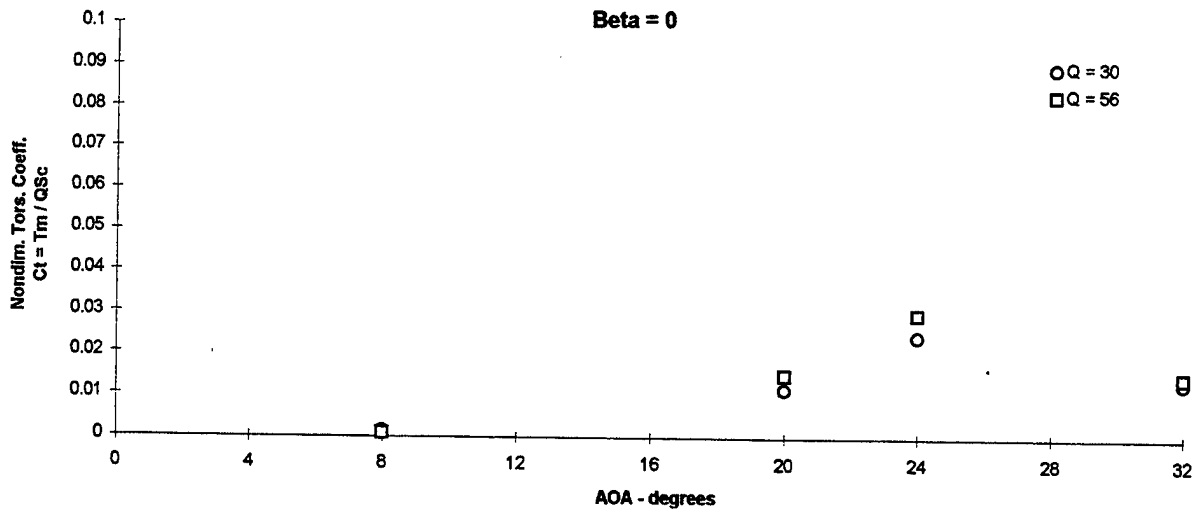

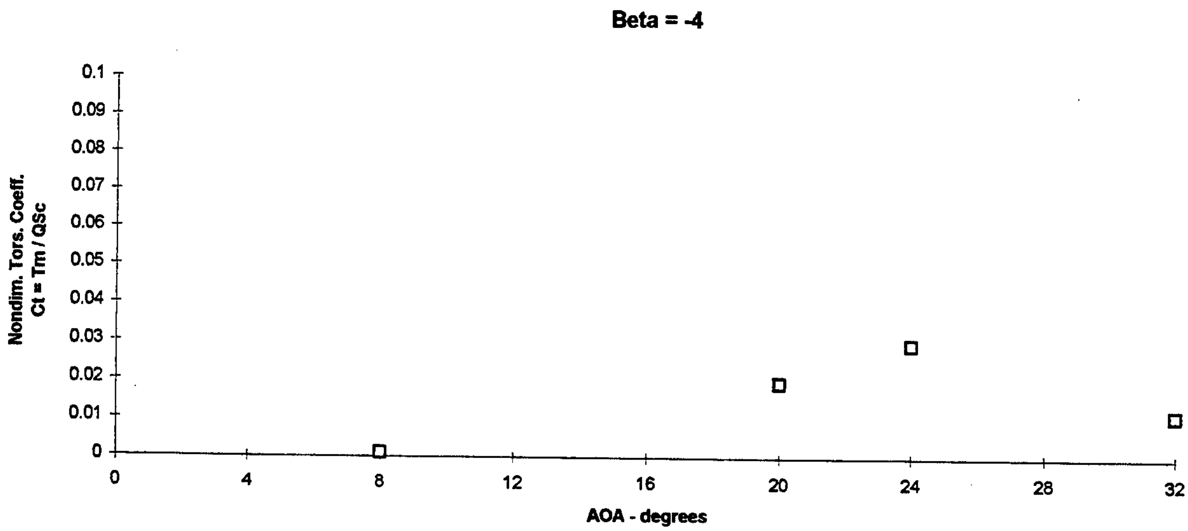

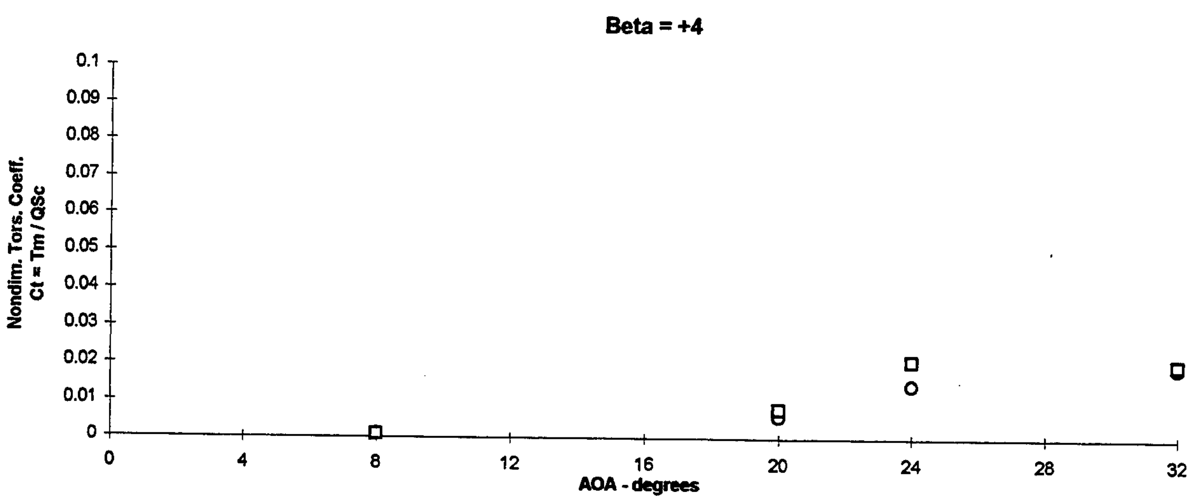

Figure 3.6.4 Flex Tail Response vs Angle of Attack, Q= 30, 56 PSF,Wing Blowing= 45 psi, PSD's(5- 500HZ), Nondimensional Torsion

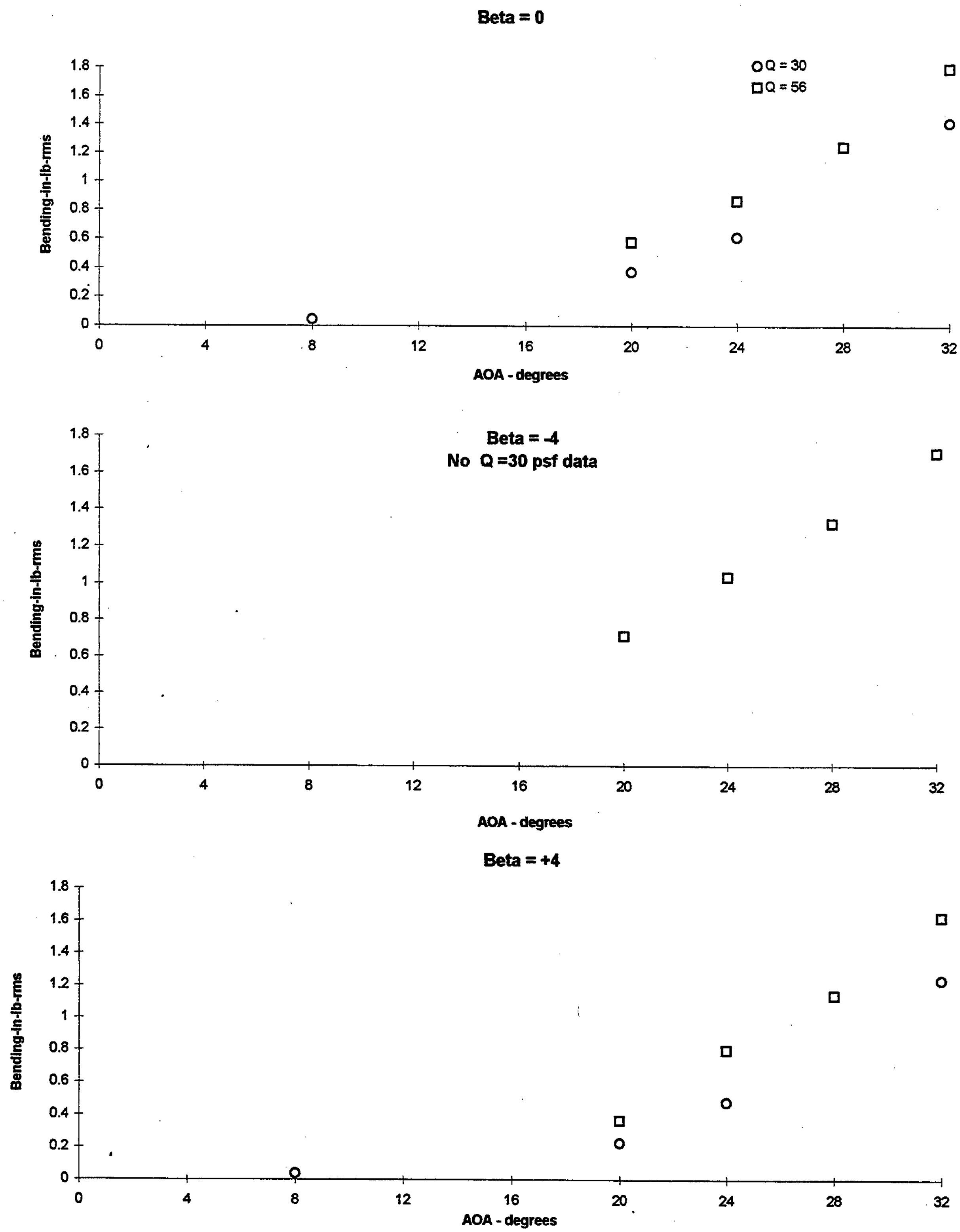

Figure 3.6.5 Flex Tail Response vs Angle of Attack, Q= 30, 56 PSF,No Blowing, PSD's(5- 500HZ), Bending

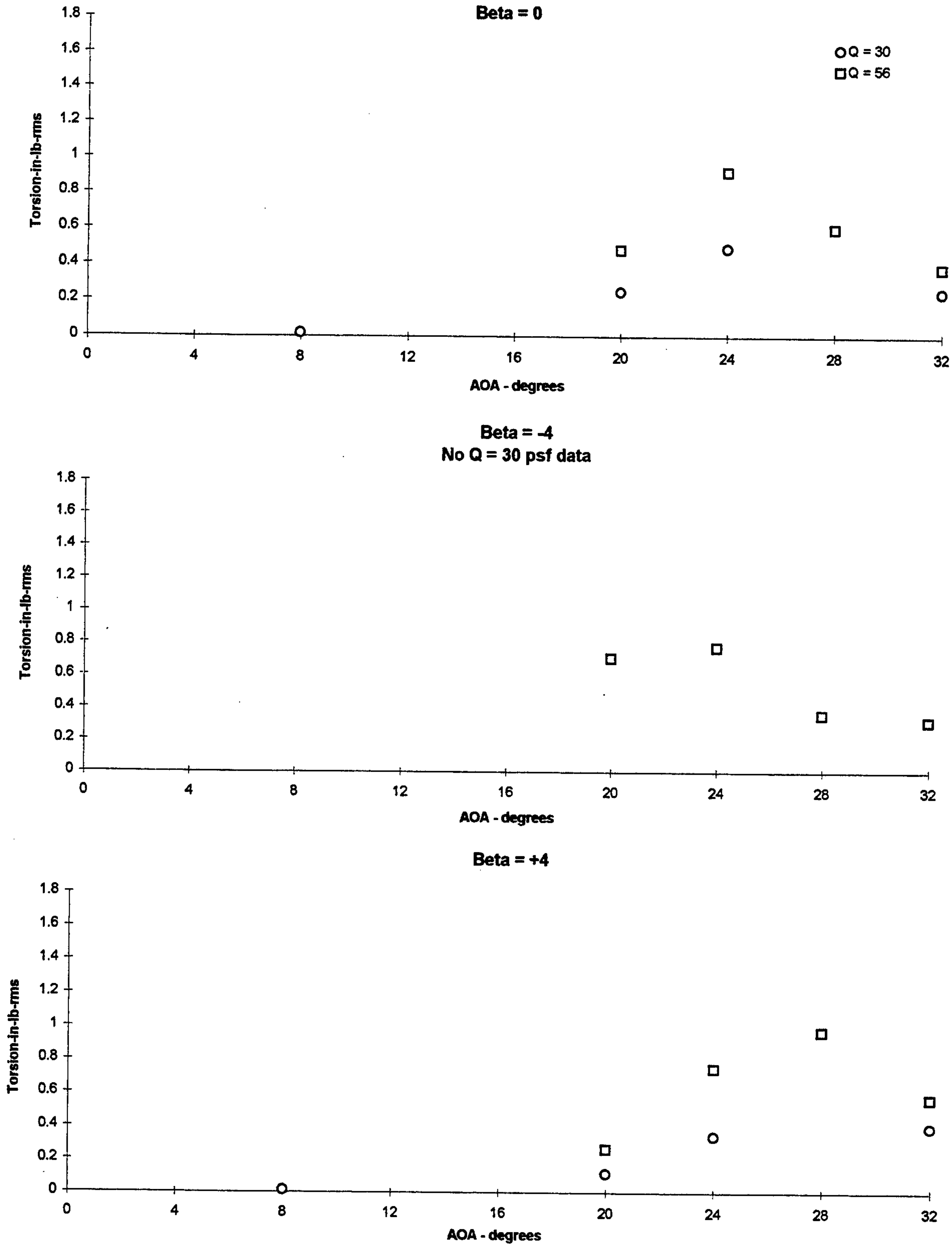

Figure 3.6.6 Flex Tail Response vs Angle of Attack, Q= 30, 56 PSF, No Blowing, PSD's(5- 500HZ), Torsion

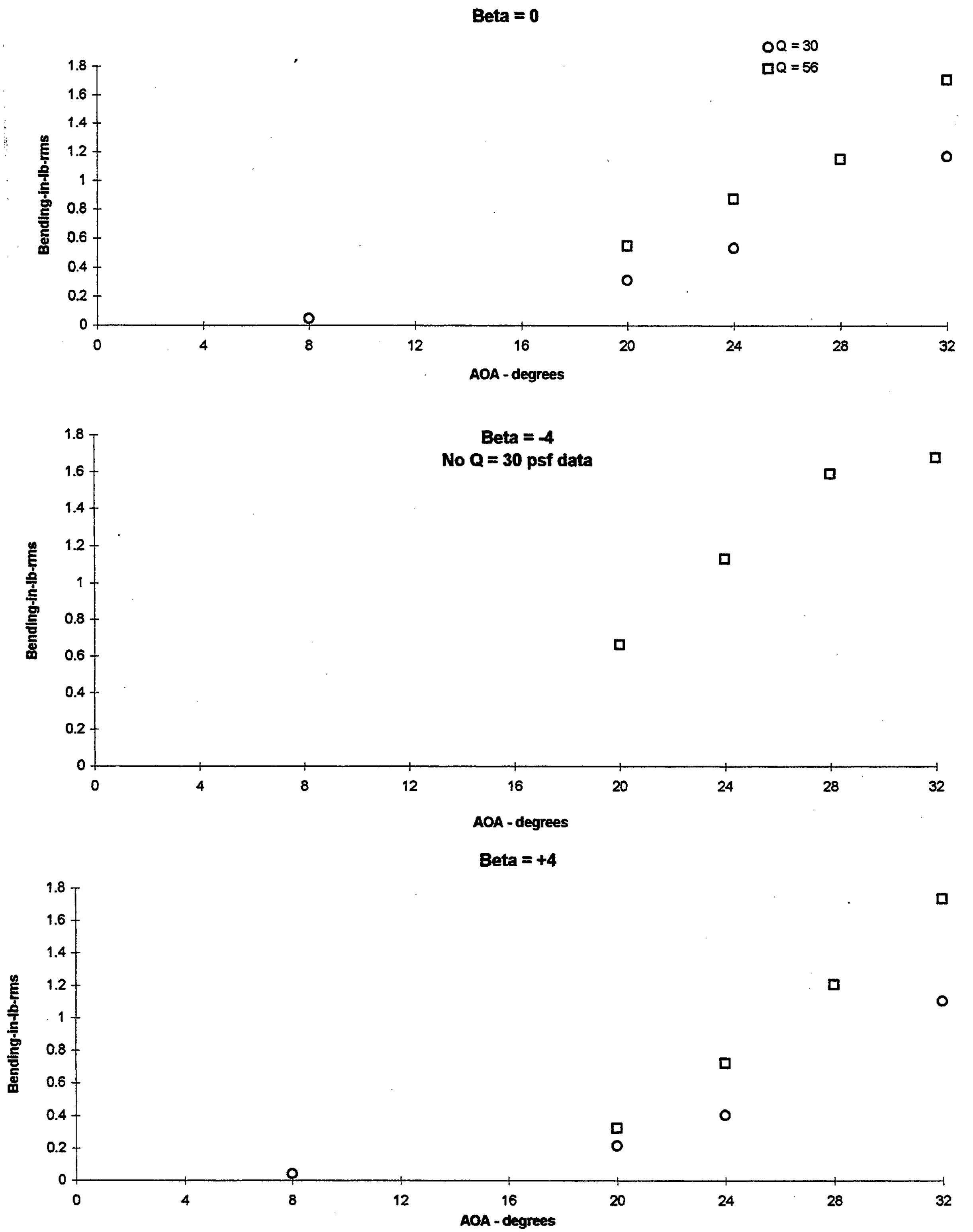

Figure 3.6.7 Flex Tail Response vs Angle of Attack, Q= 30, 56 PSF,Wing Blowing = 45 psi, PSD's(5- 500HZ), Bending

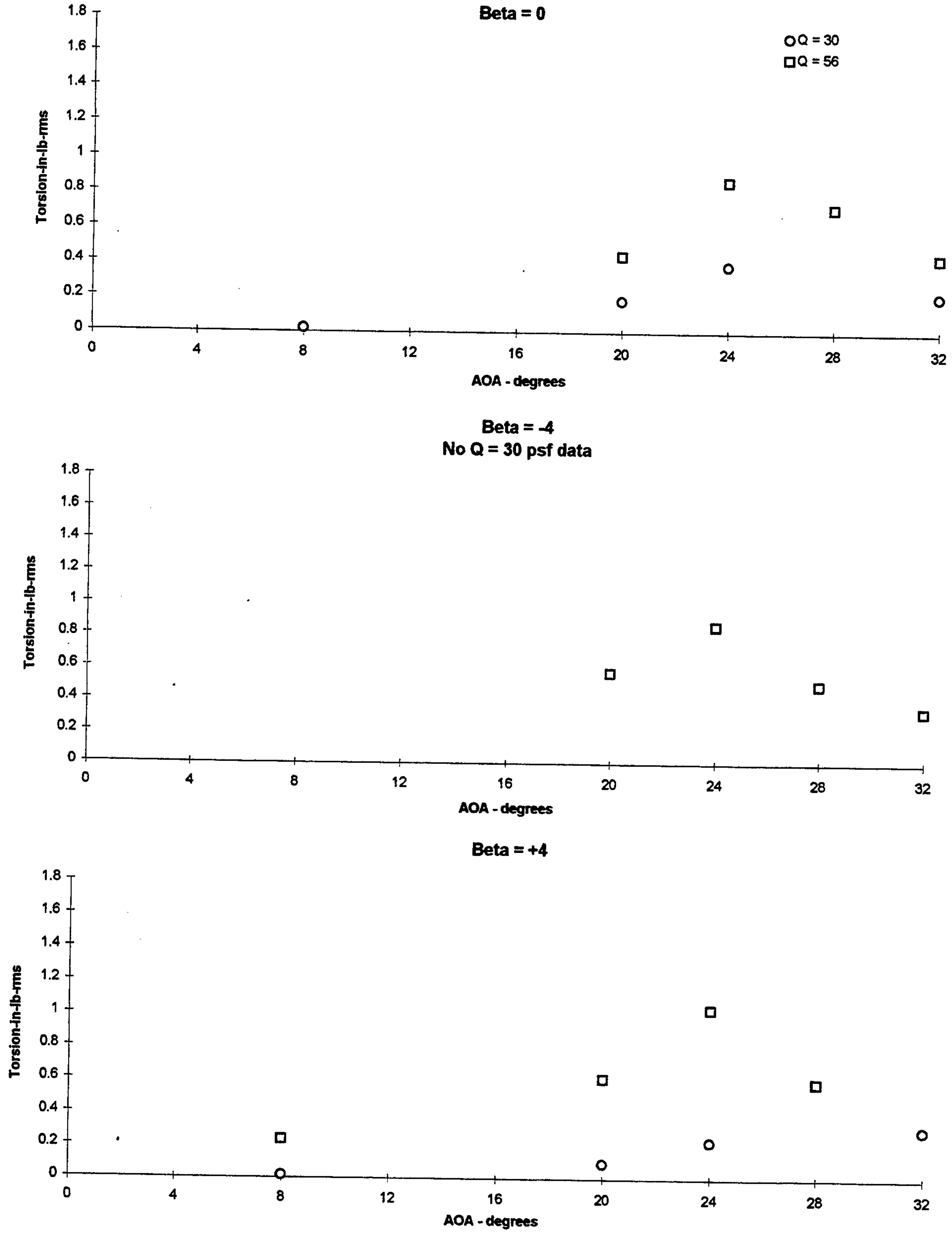

Figure 3.6.8 Flex Tail Response vs Angle of Attack, Q= 30, 56 PSF, Wing Blowing = 45 psi, PSD's(5- 500HZ), Torsion

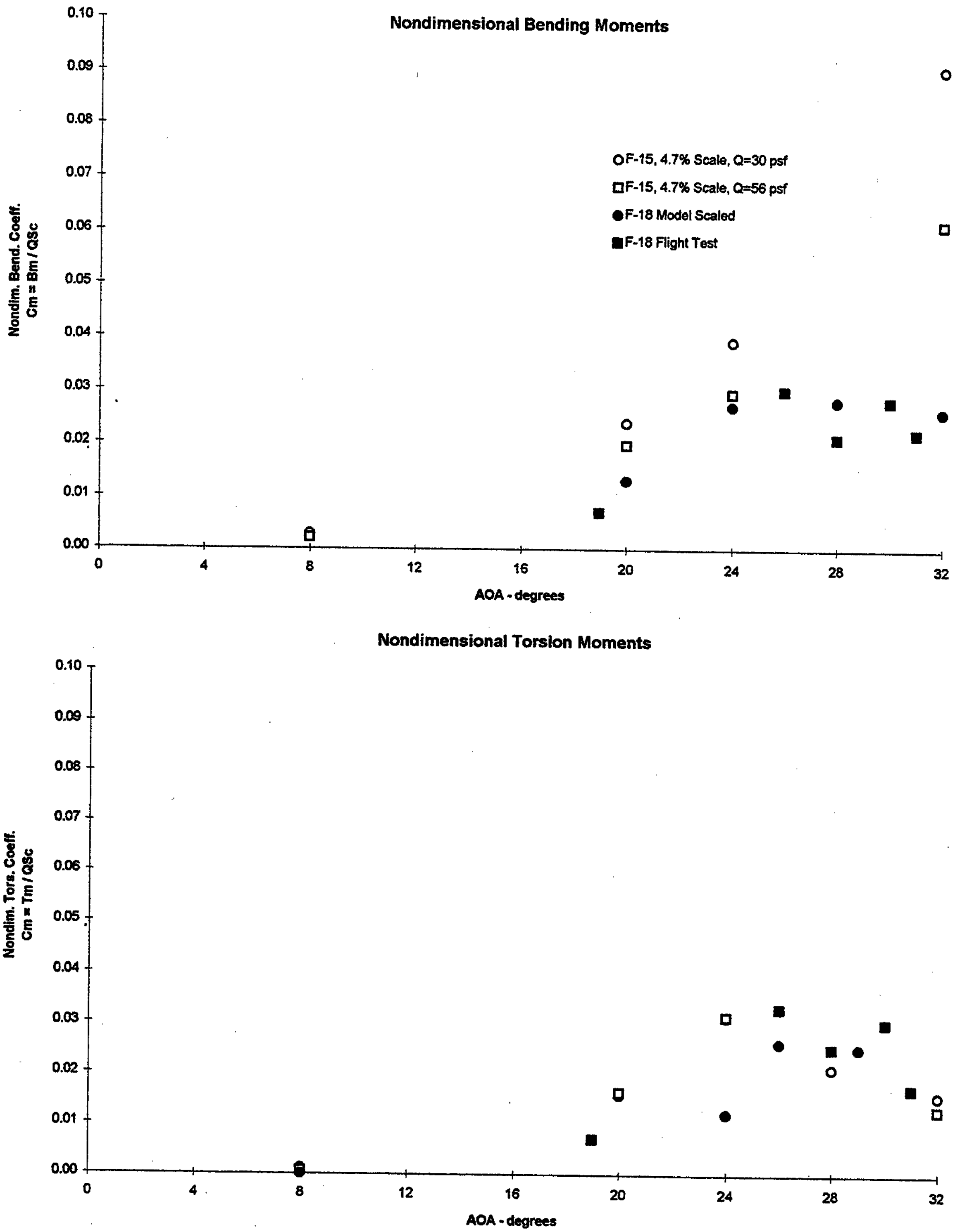

Figure 3.6.9 Correlation Between 4.7% Scale F-15 Vertical Tail and and F-18 Vert Tail Part 1- F-18 Vertical Tail Outboard Bending and Torsion

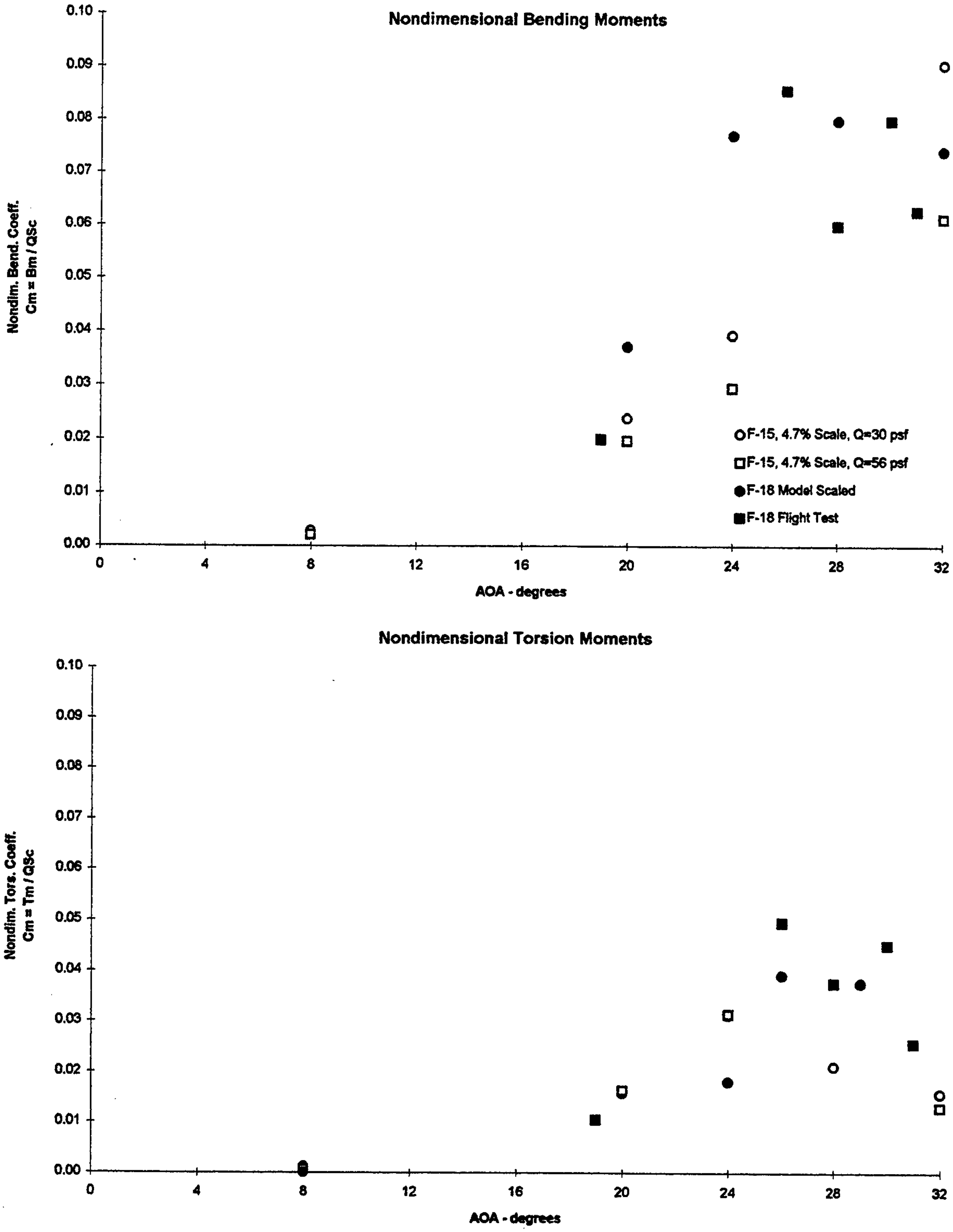

Figure 3.6.9 Correlation Between 4.7% Scale F-15 Vertical Tail and and F-18 Vert Tail
Part 2 - F-18 Vertical Tail Inboard Bending and Torsion -(Ratioed)

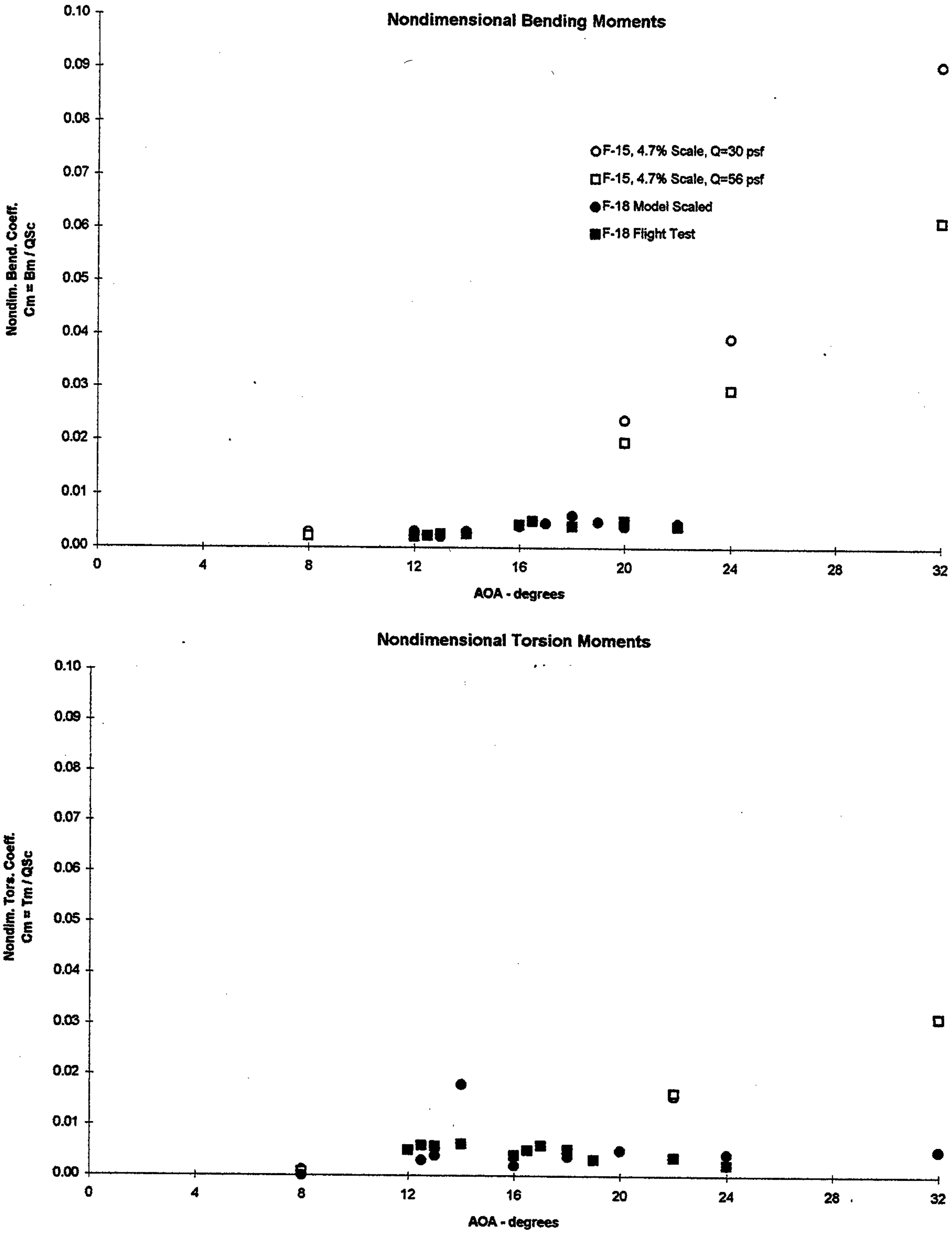

Figure 3.6.10 Correlation Between 4.7% Scale F-15 Vertical Tail and and F-18 Stabilator
Part 1 - F-18 Stabilator Outboard Bending and Torsion

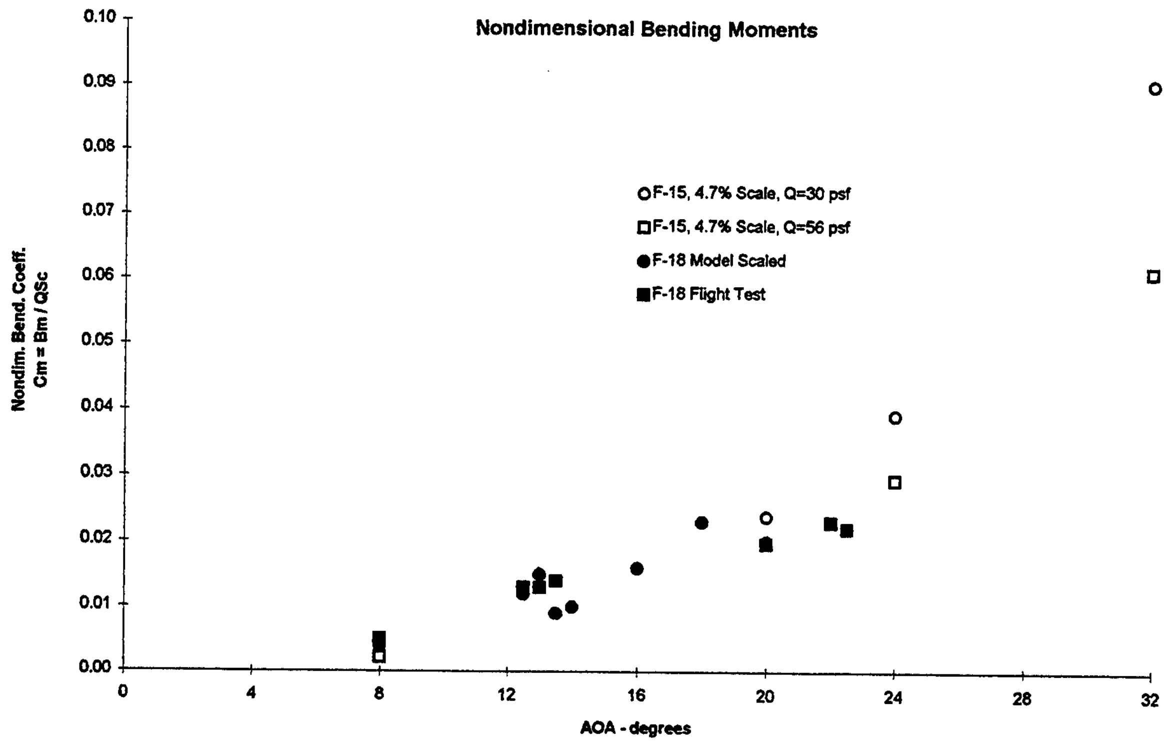

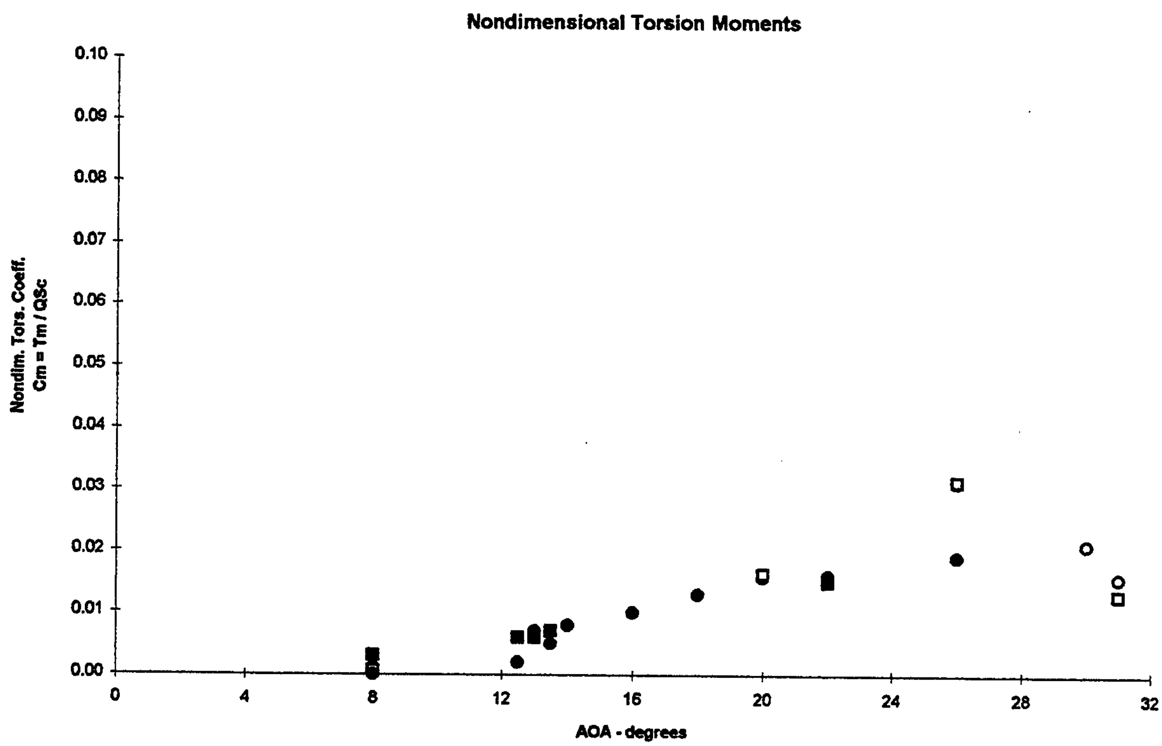

Figure 3.6.10 Correlation Between 4.7% Scale F-15 Vertical Tail and and F-18 Stabilator
Part 2 - F-18 Stabilator Inboard Bending and Torsion

8. BIBLIOGRAPHY

HUTTSELL, L.J., TINAPPLE, J. A., AND WEYER,R. M., "AN EXPERIMENTAL INVESTIGATION OF BUFFET LOAD ALLEVIATION ON A SCALED F-15 TWIN TAILED MODEL,"AGARD REPORT-R-822, AGARD SMP, AALBERG, DENMARK, 14-15 OCT 1997

ZIMMERMAN, N. H., AND FERMAN, M. A., "PREDICTION OF TAIL BUFFET LAODS FOR DESIGN APPLICATIONS," USN REPORT, NADC88043-60, JULY 1987

ZIMMERMAN, N. H. FERMAN. MA A., YURKOVICH, R.N., AND GERSTERNKORN, G.,"PREDICTION OF TAIL BUFFET LOADS FOR DESIGN APPLICATIONS," AIAA 30TH SDM, MOBILE, AL, 3-5 APRIL 1989

FERMAN, M. A. PATEL, S., ZIMMERMAN, N. H., AND GERSTENKORN, G., "A UNIFIED APPROACH TO BUFFET RESPONSE OF FIGHTER AIRCRAFT EMPENNAGE," AGARD/NATO, 70TH SMP, SORRENTO, ITALY, 2-4 APRIL 1990

FERMAN, M. A., AND LIGUORE, S.L., "BUFFET COUPLED RESPONSE OF THE HARV THRUST VECTORING VANE SYSTEM," NASA HIGH ANGLE OF ATTACK CONFERENCE,HAMPTON, VA, OCT 1990

WASHBURN, A.E.,JENKINS, L.N., AND FERMAN, M. A., "EXPERIMENTAL INVESTIGATION OF VORTEX-FIN INTERACTION," 31ST AEROSPACESCIENCS MEETING, RENO, NV, 11-14 JAN 1993

FERMAN, M.A.,LIGOURE, S. L., COLVIN, B.J., AND SMITH, C.M., "COMPOSITE EXOSKIN DOUBLER EXTENDS FATIGUE F-15 VERTICAL TAIL FATIGUE LIFE," AIAA/ASME 34TH SDM, LA JOLLA, CA 19-21 APRIL 1993

DIMA, C., "THE EFFECTS OF TIME VARYING MANEUVER CONDITIONS ON EMPENNAGE BUFFET RESPONSE," MS THESIS, PARKS COLLEGE OF ST. LOUIS UNIVERSITY, DEC 1994

FINDLAY, D., "NUMERICAL ANALYSIS OF VERTICAL TAIL BUFFET," AIAA PAPER, 97-06721, 35TH AERROSPACE SCIENCES MEETING, RENO, NV, 6-10 JANUARY 1997

BEAN, DAVID E. AND WOOD, NORMAN J., "AN EXPERIMENTAL INVESTIGATION OF TWIN FIN BUFFETING AND SUPPRESSION," AIAA PAPER NO 93-0054 JANUARY 1993

MURRI, DANIEL G. AND SHAH, GAUTAM H. AND DICARLO, DANIEL J.,"ACTUATED FOREBODY STRAKE CONTROLS FOR THE F-18 HIGH-ALPHA RESEARCH VEHICLE."

CORNELIUS, KENNETH C., "ANALYSIS OF VORTEX BURSTING UTILLING THREE-DIMENSIONAL LASER MEASUREMENTS," JOURNAL OF AIRCRAFT VOL.32 NO., MARCH-APRIL,1995

EDWARDS, JOHN W., "ASSESSMENT OF COMPUTATIONAL PREDICTION OF TAIL BUFFETING," NASA TECHNICAL MEMORANDUM 101613 JANUARY,1990

LAZARUS, KENNETH B., "AN ACTIVE SMART MATERIAL SYSTEM FOR BUFFET LOAD ALLEVIATION," 95 SPIE CONFERENCE

CANBAZOGLU,S. AND LIN,J C AND WOLFE.AND ROCKWELL,D., "BUFFETING OF FIN: DISTORTION OF INCIDENT VORTEX," AIAA JOURNAL VOLUME 33 NO. 11 NOVEMBER, 1995

CANBAZOGLU,S.,AND LIN,JC AND WOLFE AND ROCKWELL,D."BUFFETING OF A FIN: STEAMWISE EVOLUTION OF FLOW STRUCTURE."JOURNAL OF AIRCRAFT VOL.33 NO.1 JAN.-FEB.,1995

WOLFE,S.AND CANBAZOGLU,S. AND LIN,J. C. AND ROCKWELL,D., "BUFFETING OF FINS: AN ASSEMENT OF SURFACE PRESSURE LOADING." AIAA VOL.33,NO.11

MABEY,DENNIS G. AND PYNE,CLIVE R., "BUFFETING ON THE SINGLE FIN OF A COMBAT AIRCRAFT CONFIGURATION AT HIGH ANGLES OF INCIDENCE."

MABEY,D.G. AND PYNE,C.R., "BUFFETING ON THE SINGLE FIN OF A COMBAT AIRCRAFT CONFIGURATION AT HIGH ANGLES OF INCIDENCE." TR 91006, JANUARY, 1991

MABEY,D.G. AND BOYDEN R. P. AND JOHNSON W.N.,"BUFFETING TEST IN A CRYOGENIC WINDTUNNEL."AERONAUTICAL JOURNAL JANUARY,1995

ZAN,STEVEN J. AND MAULL, DAVID J., "BUFFET EXCITATION OF WINGS AT LOW SPEEDS." JOURNAL OF AIRCRAFT VOL.29, NO.6, NOV.-DEC. 1992

VORACEK, DAVID F. AND CLARKE, ROBERT, "BUFFET INDUCED STRUCTURAL/FLIGHT-CONTROL SYSTEM INTERACTION OF THE X-29A AIRCRAFT." AIAA-91-1053-CP 1991

LEE, B. H. K. AND TANG, F.C., "BUFFET LOAD MEASUREMENTS ON AN F/A-18 VERTICAL FIN AT HIGH-ANGLE-OF-ATTACK," FIBRL C-7689 1992

LEE, B. H. K. AND TANG, F.C., "CHARACTERISTICS OF THE SURFACE PRESSURES ON A F/A-18 VERTICAL FIN DUE TO BUFFET," JOURNAL OF AIRCRAFT VOL.31 NO.1, JAN.-FEB.1994

BEAN, D. E. AND LEE, B.H.K., "CORRELATION OF WIND TUNNEL AND FLIGHT TEST DATA FOR F/A-18 VERTICAL TAIL BUFFET," AIAA-94-1800-CP 1994

HEBBAR, SHESHAGIRI K. AND PLATZER, MAX F.AND FRANK, WILLIAM D., "EFFECT OF LEADING-EDGE EXTENSION FENCES ON THE VORTEX WAKE OF AN F/A-18 MODEL," JAN-11, 1993

MABEY, D.G., "ELIMINATION OF BUFFETING ON THE REAR FUSELAGE OF THE HERCULES TANKER," THE AERONAUTICAL JOURNAL NOVEMBER 1985

GRAHAM, A. D. AND MADLEY, C.K. AND WALDMAN, W., "FATIGUE ANALYSIS AND TESTING OF AIRCRAFT SUBJECTED TO MANOEUVRE AND BUFFET LOADS OF COMPARABLE MAGNITUDE," ICAF CONF.PAPER 1995

LEE, B.H.K. AND BROWN, D. AND TANG, F.C. AND PLOSENSKI, M., "FLOWFIELD IN THE VICINITY OF AN F/A-18 VERTICAL FIN AT HIGH ANGLES OF ATTACK," JOURNAL OF AIRCRAFT VOL.30, .NO.1, JAN.-FEB.1993

KOMERATH, N.M. AND SCHWART, R. J. AND KIM, J.M., "FLOW OVER A TWIN-TAILED AIRCRAFT AT ANGLE OF ATTACK, PART II: TEMPORAL CHARACTERISTICS," JOURNAL OF AIRCRAFT VOL.29, NO.4, JULY-AUG.1992

KOMERATH, N.M. AND MCMAHON, H.M. AND SCHWART, R. J. AND LIOU, S.G. AND KIM, J.M., "FLOW FIELD MEASUREMENTS NEAR A FIGHTER MODLE AT HIGH ANGLES OF ATTACK," AIAA AERODYNAMIC GROUND TEST CONFERENCE JUNE 18-20 1990

MENY, LARRY A. AND JAMES, KEVIN,A, "FULL-SCALE WIND TUNNEL STUDIES OF F/A-18 TAIL BUFFET," JOURNQL OF AIRCRAFT VOL.33, NO.3, MAY-JUNE 1996

BARRETT, DAVID J. AND RAY, HERMAN AND AROCHO, ANNETTE, "HIGHLY DAMPED STRUCTURE," NAWCADWAR-94126-60 OCT.1993

SHEN-JWU SU AND CHUEN-YEN CHOW, "IMPROVEMENT OF TRANSONIC WING BUFFET BY GEOMETRIC MODIFICATIONS," J. AIRCRAFT. VOL. 32, NO.4

BEYERS, MARTIN E., "INTERPRETATION OF EXPERIMENTAL HIGH ALPHA AERODYNAMICS-IMPLICATIONS FOR FLIGHT PREDICTION," JOURNAL OF AIRCRAFT, VOL. 32, NO.2, MARCH-APRIL 1995

ZAN, S.J., "MEASUREMENTS OF SINGLE-FIN BUFFETING GENERIC FIGHTER AIRCRAFT CONFIGURATION," INTERNATIONAL FORM AEROIARTISITY, 1993

ZAN, S.J., "MEASUREMENTS OF WING AND FIN BUFFETING ON THE STANDARD DYNAMICS MODEL," NRC NO.32158, MAY, 1993

RIZK, YEHIA M. AND GURUSWAMY, GURU P. AND GEE, KEN, "NUMERICAL INVESTIGATION OF TAIL BUFFET ON F-18 AIRCRAFT," AIAA-92-2673-CP 1990

COE, CHARLES F. AND CUNINGHAM, ATLEE M., "PREDICTION OF F-111 TACT AIRCRAFT BUFFET RESPONSES AND CORRELATIONS OF FLUCTUATING PRESSURES MEASURED OF ALUMINUM AND STEEL MODELS AND THE AIRCRAFT," NASA CR-4069, MAY 1987

PETTIT, CHRIS AND BANFORD, MICHAEL AND BROWN, DANSEN AND PENDLETON, ED, "PRESSURE MEASUREMENTS ON AN F/A-18 TWIN VERTICAL TAIL IN BUFFETING FLOW," WL-TM-94-3039, AUGUST 1994

HUTTSELL, L.J., "PRESSURE MEASUREMENT ON TWIN VERTICAL TAILS IN BUFFETING FLOW," VOLUME 1, AFWAL-TR-82-3015, APRIL 1981

HAUCH,R.M. AND JACOBS,J.H. AND RAVINDRA,K. AND DIMA,C., "REDUCTION OF VERTICAL TAIL BUFFET RESPONSE USING ACTIVE CONTROL," AIAA-95-1089-CP 1995

TRIPLETT, WILLIAM E., "PRESSURE MEASUREMENTS ON TWIN VERTICAL TAILS IN BUFFETING FLOW," AFWAL-TR-82-3015, MARCH, 1982

COLE, STANLEY R. AND MOSS, STEVEN W. AND DOGGETT, ROBERT V., 'SOME BUFFET RESPONSE CHARACTERISTICS OF A TWIN-VERTICAL-TAIL CONFIGURATION," NASA-TM-102749

BECKER, J. AND GRAVELLE, A., "SOME RESULTS OF EXPERIMENTAL AND ANALYTICAL BUFFETING INVESTIGATIONS ON A DELTA WING," APRIL 1-3, 1985

KANDIL, OSAMA A. AND MASSEY, STEVEN J. AND SHETA, ESSAM F., "STRUCTURAL DYNAMICS /CFD INTERACTION FOR COMPUTATION OF VERTICAL TAIL BUFFET"

DIMA, CRIN AND JACOBS, JACK H., "THE CHARACTERIZATION OF NON-STATIONARY BUFFET ENVIRONMENTS," AIAA-95-1339-CP 1995

NIXON, DAVID, "THEORETICAL STUDY OF THE CAUSE AND CONTROL OF BUFFET," AIAA-94-0312

LEE, B.H.K. AND MURTY, H. AND JIANG, H., "THE ROLE OF KUTTA WAVES ON OSCILLATORY SHOCK MOTION ON AN AIRFOIL EXPERIENCING HEAVY BUFFETING," AIAA-93-1589-CP 1993

JACOBS, J.H. AND HEDGECOCK, C. E. AND LICHTENWALNER, P.F. PADO, L.E. AND WASHBURN, A. E., "THE USE OF ARTIFICIAL INTELLIGENCE FOR BUFFET ENVIRONMENTS," AIAA-93-1534-CP 1993

LOWSON, M. V. AND RILEY, A.J., "VORTEX BREAKDOWN CONTROL BY DELTA WING GEOMETRY," JOURNAL OF AIRCRAFT, VOL.32, NO. 4, JULY-AUGUST 1995

BEAN, DAVID E., AND GREENWELL, DOUGLAS I. AND WOOD, NORMAN J., "VORTEX CONTROL TECHNIQUE FOR THE ATTENUATION OF FIN BUFFET," JOURNAL OF AIRCRAFT, VOL.30, NO.6 NOV.-DEC. 1993

SUAREZ, CARLOS J. AND MALCOLM, GERALD N., "WATER TUNNEL FORCE AND MOMENT MEASUREMENTS ON AN F/A-18," AIAA 94-1802-CP 1994

DOGGETT, ROBERT V. AND HANSON, PERRY W.,"WIND TUNNEL BUFFET PRESSURE INVESTIGATION ON THE LOWER NOSE PORTION OF THE RF4C AIRCRAFT," LWP-227 COPY NO.39 JUNE 1966